THE EFFECT OF IMPLANTS ON THE STRUCTURAL INTEGRITY OF GRAPHITE/EPOXY LAMINATES

by

Laura Ann Kozel

B.S. Aerospace Engineering, The Ohio State University (1989)

Submitted to the Department of Aeronautics and Astronautics in Partial Fulfillment of the Requirements for the Degree of

MASTER OF SCIENCE

at the

MASSACHUSETTS INSTITUTE OF TECHNOLOGY

September 1992

Signature of Author _____
Department of Aeronautics and Astronautics
July 28, 1992

Certified by _____
Professor Michael J. Graves
Thesis Supervisor

Accepted by _____
Professor Harold Y. Wachman
Chairman, Department Graduate Committee

The Effect of Implants on the Structural Integrity of Graphite/Epoxy Laminates

by

Laura Ann Kozel

Submitted to the Department of Aeronautics and Astronautics on July 28, 1992, in partial fulfillment of the requirements for the Degree of Master of Science.

ABSTRACT

Experiments were performed to study the structural integrity of graphite/epoxy laminates with embedded optical fibers, circuit chips, piezoceramic actuators (PZA) and teflon. Embedded devices are characteristic of the smart structure concept where a structure monitors its own structural integrity and can adapt to external disturbances. The devices were embedded parallel to the loading direction into four different laminate configurations which had 10/80/10%, 25/50/25%, 40/50/10% and 0/100/0% of 0°/45°/90° plies. Uniaxial tensile testing was performed to determine the effects of the implants on the ultimate tensile stress, failure mode, and to determine at what loading damage initiated and if initial damage occurred at the implant. The implants were placed in cut out sections of the laminate with the exception of the chip and optical fiber implants, which were also placed directly into the laminate. All specimens were x-rayed and both failed and partially loaded specimens were sectioned and examined for delaminations or matrix cracking at the implant. Results indicated that the implants degraded the ultimate tensile stress up to 16% in the layup where 0° plies were cut to embed the devices. The implants had the least affect on ultimate stress when they were in layups with high percentages of ±45° plies. Implants demonstrated the ability to significantly reduce the laminate ultimate stress but were not necessarily the failure initiation site. Matrix cracking was observed in all tested specimens. Delamination at the side of the PZA implant embedded in a 100% ±45° laminate was also observed. There was no significant difference in ultimate stress for specimens with the chip implant placed in a cut area or placed directly into the laminate; however, placing the chip directly into the laminate appeared to prevent failure at the implant and had little effect on failure mode. Teflon implants degraded the ultimate stress in a manner comparable to the actual chip and PZA implants. The optical fibers degraded the ultimate stress up to 12% but did not appear to affect the failure mode of the laminates and no delamination was observed at the implant.

Thesis Supervisor: Michael J. Graves

Title: Assistant Professor, Department of Aeronautics and Astronautics, Massachusetts Institute of Technology

Acknowledgments

My work at MIT would not have been possible without the extemely generous financial support of my managers at the GE Aircraft Engine Company. I sincerely appreciate the time off for classes and the months off to work on my thesis (although some people would argue my absence was a blessing!). Thank you Paul LoPiccolo for supporting me during my time at MIT even when I was acting crazy. I appreciated the visits in the lab (especially when they were accompanied by food!) and your continued offers to help me even after you smashed your bum into the caul plate! I hope you will always treasure the picture of the geek at the milling machine. My advisor, Michael Graves, deserves a special thank you for his guidance and especially for making sure there were no spaces before the paragraph symbols in my thesis! I also enjoyed working with a great set of Professors, Administrators and Research Associates including Paul Lagace, Hugh McManus, John Dugundji, Queen Ping Lee, Debbie Bowser and Al Supple!

Good-Bye!

- My favorite car ever, the 1989 black Acura Integra with moonroof and awesome interior (Merry X-Mas)
- Late Friday night strain gaging
- Splinters in everything
- Dirt encrusted hands from the milling machine
- Spending an entire day cutting apart strips of 10 coupons that stuck together during a bond cure
- The computer mezzanine (I will never listen to 101.7!)

Hello!

- Friday and Saturday nights
- Daylight
- Learning how to play the piano
- Building the perfect body
- Life outside

Some Things Never Change (and some people take longer to graduate than others):

My friendships with Narendra, Wilson, Steve, Mak, Hiroto, Mary, Ed, Hary, Aaron, Jeff, Stacy, Malee, Elizabeth, Kerry, Kim, and Amy. All the other UROPers aren't so bad either!!!

Oh, yea, THANKS MOM!!!!

Foreword

This work was performed in the Technology Laboratory for Advanced Composites (TELAC) of the Department of Aeronautics and Astronautics at the Massachusetts Institute of Technology. This work was sponsored by the GE Aircraft Engine Company and Leaders for Manufacturing.

Table of Contents

Chapter Page

Chapter Page

List of Figures

List of Tables

Nomenclature

CHIP	Integrated Dielectric Circuit Chip
CLPT	Classical Laminated Plate Theory
C.V.	Coefficient of Variation
E_L	Longitudinal Elastic Modulus (GPa)
E_T	Transverse Elastic Modulus (GPa)
G_{LT}	Shear Modulus
GNPT	Guaranteed Non-Porous Teflon
Layup 1	$[0/(\pm 45)_2/90/(\pm 45)_2]_S$
Layup 2	$[0/(\pm 45)/90]_{2S}$
Layup 3	$[45/0/-45/0/90/-45/0/-45/0/45]_S$
Layup 4	$[\pm 45]_{4S}$
OF	Optical Fiber
PZA	Piezoceramic Actuator
TC	Teflon Chip
TPZA	Teflon PZA
v	Poisson's Ratio
Y11	Modulus in the Width or Length Direction
Y33	Modulus in the Thickness Direction

CHAPTER 1

Introduction

A smart structure is capable of sensing, evaluating and reacting to an external disturbance or monitoring its own structural integrity by using a network of embedded sensors, actuators, and controllers. Theoretically, it should be able to locate where damage occurs and determine the type of and severity of the damage to the structure. If an external disturbance affects the control of the structure, the internal sensors would adjust for it. The terms smart, intelligent, sense-able and adaptive have all been used to describe this type of structure and there is considerable debate over the proper terminology to describe this technology [1,2].

The smart structure concept is important to the aerospace industry and has received considerable attention from Boeing, McDonnell Aircraft Company, Wright Patterson Air Force Base and the US Air Force and Navy among others in the area of smart aircraft skins [3,4,5]. The Aloha Boeing 737 accident in 1988 exemplifies the complexity of predicting the amount of structural fatigue present in an aircraft [4]. The FAA requires the airframer to assess the aircraft's durability, damage tolerance, fatigue crack growth rates and to set up

inspection methods and a time schedule for the inspections which would detect cracks, corrosion and damage. Despite all of these precautions and maintenance schedules, the Aloha accident demonstrates that there is still potential for catastrophic failure of the aircraft. With the implementation of the smart skin concept, the aircraft would be able to provide real time and continual assessment of its structural integrity.

Smart skins would improve the life predictions of aircraft by addressing three important challenges with the current system. Boeing claims that the current method for individual tracking of an aircraft is expensive, often inaccurate and does not account for assessment of in-flight damage [5]. A sensing network in the structure would be capable of tracking actual flight load data for each aircraft. This aspect is also critical for survivability of combat aircraft which must assess and react to damage in real time. To accomplish this goal, McDonnell Aircraft company is investigating the use of optical fibers to sense strain and impact damage [3]. The second benefit of using the smart structure concept is the reduction of the required number of or interval between inspections to assess the structural integrity, which often prove unnecessary and result in expensive down time. Unnecessary tear down and subsequent assembly of the structure also creates an opportunity for the inspectors to damage the structure. The third problem that would be better understood with an internal sensing system is variation in manufacturing. Even with improved manufacturing techniques and industry's effort towards achieving ±6 sigma defect levels, there will always be some aircraft that incur a defect during the manufacturing process that will be undetected. An internal sensing system would be able to assess each aircraft's stiffness,

frequency and damping characteristics, and initial structural state to provide an individual signature of each aircraft prior to actual service.

The use of laminated composite materials and their potential for weight reduction, aeroelastic tailoring, improved fatigue characteristics, and corrosion resistance is often associated with the smart structure concept. Before the concept can become a reality, there are several issues that must be researched and resolved. The first major issue is interconnection of the sensing/actuating/controlling devices within the aircraft structure because aircraft are typically built in small sections. Associated with this issue is the need to develop a method for bringing the data transmission lines or leads out of the laminates and the associated connections both at the implant and outside of the laminate. The ability to repair the integrated network must also be assessed in conjunction with the need to have back-up sensors, actuators and communication to account for lost sensors during manufacturing. Although possible sensors and actuators applicable for a smart skin application have been identified [6], they must be developed and predictable before they can be effective. There are many open issues relating to the integration of the sensing network into a composite material and how to minimize the effects of the embedded devices on the host material. The embedded devices must be able to withstand the manufacturing process including the cure cycle of the composite material. The structure must also be capable of being produced efficiently and with consistent quality using automatic fabrication. The issue that is addressed in this thesis is the effect of the embedded devices on the structural integrity of the composite material.

All of the devices introduce an internal flaw in the material which must be minimized for the most effective smart structure design.

The types of implants necessary to implement a smart structure concept include sensors, actuators, controllers and a communication network. Sensors that would be capable of embedment into a composite structure include strain gages, fiber optic cables, and piezoelectric sensors. Fiber optics are capable of sensing strain, temperature, pressure, corrosion and vibration. Shape memory alloys and piezoelectric material are examples of possible actuators for this application. Shape memory alloys can be plastically deformed and embedded into the structure. They are capable of returning to their original shape if they are heated above their transition temperature. Piezoelectric actuators respond to an applied voltage. The controllers and communication network would involve a series of small microprocessors, optical fibers and data transmission lines or lead wires.

The purpose of the experiments described in this thesis was to study the structural integrity of graphite/epoxy laminates with embedded sensors, actuators or circuitry that would typically be used for a smart structure application. The testing was performed to determine the effect of implants on the ultimate tensile stress, variation in failure mode, modulus, and to determine whether the implant was the site of damage initiation and at what fraction of the ultimate stress this damage occurred. Variations in the laminate ply orientations and thicknesses were chosen to simulate real-life applications where all types of angled plies would be cut to implant the sensor/actuator or circuitry. The implants were chosen to vary in size, shape, functionality

and lead wire configuration in order to determine the effects of each and to recommend the least structurally damaging configuration.

The implants used in the experiments included silica optical fibers with a polyimide coating, rectangular integrated dielectric circuit chips which are typically used for cure monitoring, rectangular piezoceramic actuating material and teflon. They were embedded into the center of graphite/epoxy laminates which were either 16 or 20 plies thick.

A background of the current research pertinent to these investigations is reviewed in Chapter 2. Chapter 3 describes the details of the manufacture of the laminates with the embedded implants and the experimental procedure. The results of the experiments are presented in Chapter 4 and discussed in Chapter 5. Chapter 6 includes conclusions on the effects of the implants and recommendations.

CHAPTER 2

Background

The primary focus of smart structure research has been on the development of the sensors, actuators and controllers. Now that several devices are available that can be embedded into a smart structure, the effect of these devices on the structural integrity of the aircraft must be investigated. This chapter includes a review of the literature addressing the effects of embedded optical fibers, piezoceramic actuators, and circuit chips on the structural integrity of the host material.

2.1 Optical Fiber Implant Research

The primary sensor or communication device that has been researched for the last 10 years is the optical fiber. It is capable of sensing strain, temperature, magnetic and electric fields, acoustic waves, chemical concentrations and structural and vibratory mode shapes. Issues have been identified for the application of fiber optics to a smart structure application by Turner et al [7], Wood [8] and Claus et al [9]. Turner identified the criteria for optical fibers that provide a point strain measurement and also the key requirements for the optical fiber

that must be embedded into a composite material. They also reviewed current types of optical fibers that met their required criteria and compared their advantages and disadvantages. Wood more broadly defined the design and production issues associated with the use of optical fibers in a smart structure. Experimental work addressed the need to establish a fabrication and tooling technique and to establish a design database which specifies the effects of implants on the structural integrity. The design database included the effect of layup and the device placement on the sensitivity and survivability of the devices.

Placement of an optical fiber into a composite laminate creates a resin rich area around the fiber. The size of the area is dependent on the surrounding ply orientation, applied pressure during the cure, the thickness of the laminate, distance of the optical fiber from the surface and the size of the optical fiber. Sirkis et al [10] stated that the resin pocket acts like an interlaminar crack which can impair the strain transfer between the host material and optical fiber and increase the optical fiber's vulnerability to microbuckling failure modes. Wood [8] experimentally evaluated how to implant the optical fiber and obtain the smallest resin pocket. Several optical fiber placement alternatives were examined including placing it parallel or perpendicular to the surrounding plies of graphite/epoxy, flanking the optical fiber with graphite/epoxy tape and cutting the plies to make room for the optical fiber. The resin pocket was the smallest when the optical fiber was placed parallel to adjacent plies. Dasgupta et al [11] analytically predicted the size and shape of the resin pocket using an energy method. Finite element methods were used to determine the stress/strain relationship in the pocket and surrounding composite material. Their

results agreed with Wood and showed that the size of the resin pocket increases with an increasing angle between the optical fiber and surrounding plies. The finite element analysis verified that a larger pocket creates a larger stress concentration at the optical fiber/matrix interface.

The stress concentration at the optical fiber has been evaluated analytically and experimentally by Salehi et al [12] using moiré interferometry and finite element modeling. Their experiments involved implanting an optical fiber with a .142 mm outer diameter perpendicular to the uniaxial loading direction in unidirectional and [0/90] type layups. Their results verified those of Wood and Dasgupta and determined that the resin pocket caused by the optical fiber was a function of the surrounding ply angle and that the stress concentration was a function of the resin pocket size. The moiré interferometry technique did not produce the same magnitudes of strain concentration as the results of the finite element modeling because the size of the fringe pattern allowed only a few data points across the actual fiber and the peak strain values were difficult to determine. The finite element analysis predicted a stress concentration of up to 18 when the optical fiber was placed perpendicular to surrounding plies and up to 5 when it was placed parallel to surrounding plies. The model included material properties of the optical fiber cladding, core and coating and showed that the largest strain occurred in the coating of the optical fiber.

During their research into the stress concentrations at the optical fiber, both Wood [8] and Salehi [12] found that the optical fiber was cracked prior to testing when it was placed between 45° and 90° plies. Salehi [12] also noted that when a laminate has 90° plies perpendicular

to the loading direction similarly to the optical fiber, the microcracking that will occur may crack the coating of the optical fiber.

The effect of the coating on the stress concentration around the optical fiber was analytically evaluated by Dasgupta et al [13]. Using finite element analysis and a closed form elasticity solution, they showed an optimum coating and coating diameter can minimize the stress concentration in the host material. Their analytic model was of a transversely isotropic host material with the embedded optical fiber placed parallel to the surrounding plies and loaded uniaxially. There were identified several coatings available today including acrylates, polyimides and metals which can be used in a variety of environments.

Experimental work on the effect of embedded optical fibers on the tensile and compressive strengths of composite laminates has been performed by Jensen et al [14] and Measures et al [15]. Jensen implanted multiple optical fibers with a .250 mm outer diameter into graphite/bismaleimide laminates with a $[0_3/90_2/0]_S$ layup. Their experiments included variations where the optical fiber was placed parallel and perpendicular to the applied load, parallel and perpendicular to the surrounding plies and symmetrically and unsymmetrically about the midplane of the laminate. The laminates were tested under uniaxial tension. Results indicated that the optical fiber degraded the ultimate tensile stress the most (9%) when it was placed perpendicular to the plies and perpendicular to the applied load. All of the other cases had an impact of 4% or less on ultimate tensile stress. Five to nine specimens were tested for each case and the spread of data was large enough that the 9% decrease was possibly within the standard deviation of the samples tested.

Measures implanted an optical fiber with a .125 mm outer diameter into six Kevlar/epoxy panels. The panel consisted of four 0° plies and the optical fiber was placed perpendicular to the plies and loading direction. Results indicated that the optical fiber had a negligible effect on the tensile and compressive strengths of the material.

2.2 Piezoceramic Implant Research

Crawley et al [16] has created an analytic model to predict the response of piezoceramic actuators to an applied voltage. They experimentally verified their model by exciting the actuators and measuring the induced vibrations. They also performed static testing on four glass/epoxy test specimens to determine the effect of the implant on ultimate stress. Two of the specimens did not include any implants and were used as controls. Each of the remaining two had one 38.1 by 15.2 by .25 mm piezoceramic actuator embedded into the center of a $[0/90/0/90/0]_S$ laminate. The implants reduced the ultimate tensile stress by 20%.

2.3 Circuit Chip Implant Research

Warkentin [17] performed experiments to determine the effect of embedding a low conductivity integrated circuit dielectric sensor chip into a graphite/epoxy laminate on the structural integrity of the host material and on the functionality of the devices. The $[0/90/0_2]_S$ coupons were subjected to quasi-static and cyclic loading and also to a

temperature/humidity/bias environment. Five specimens were tested to failure with a resulting 15% decrease in ultimate stress.

Chow [18] performed a finite element analysis based on the Hellinger-Reissner variational principle on the same sensor chip used by Warkentin embedded into a graphite/epoxy laminate with 0°/90° layups. Results indicated that the worst stress concentration around the embedded chip occurred when 0° plies were cut to embed the device with a decreasing stress concentration as the angle of the cut plies increased to 90°. It was also shown that the lead wire connection to the main sensor chip could be ignored as a significant stress concentration site.

CHAPTER 3

Experimental Procedure

The experiments were designed to determine the effect of implants on the structural integrity of graphite/epoxy composite laminates. X-rays were made of the specimens during and after tensile testing in conjunction with sectioning of tested and untested specimens to determine where damage initiation occurred. The type, shape and size of implants are presented and the rationale for their selection and laminate layups are described for all specimens.

3.1 Experimental Approach

The purpose of the experiments was to study the structural integrity of graphite/epoxy with embedded sensors, actuators or circuitry that would typically be used for a smart structure application. The testing was performed to determine the effect of implants on the ultimate tensile stress, variation in failure mode, modulus, and to determine whether the implant was the site of damage initiation and at what fraction of the ultimate stress this damage occurred. Variations in the laminate ply orientations and thicknesses were chosen to

simulate real-life applications where all types of angled plies would be cut to implant the sensor/actuator or circuitry. The different percentages of 0°, 90° or 45° plies also reflect the various applications composite materials might be used for depending on the type of load carrying capability desired. The implants were chosen to vary in size, shape, functionality and lead wire configuration in order to determine the effects of each and to recommend the least structurally damaging configuration.

All 50 by 356 mm tensile specimens were made using prepreg with Hercules AS4 graphite fibers in 3501-6 resin. The material properties are given in Table 3.1. A graphite/epoxy system was chosen because of its applicability to aircraft and spacecraft structures. Because the purpose of the experiments was to determine the effect of implants in real-life applications, 16-20 ply laminates were chosen to simulate "smart" skins which typically vary between 30-141 plies thick. Four different layups were chosen with different percentages of 0°/45°/90° plies as shown in Table 3.1. The four layups demonstrate variance in the angular orientation of plies cut for and surrounding the implant. Layup 1, which had 10/80/10% of 0°/45°/90° plies respectively, is indicative of a layup used for a skin structure or shear web which must be shear resistant with minimal longitudinal reinforcement. Layup 2, which had 25/50/25% of 0°/45°/90° plies respectively, is a standard quasi-isotropic layup used in industry where the longitudinal and transverse moduli are identical. Layup 3, which had 40/50/10% of 0°/45°/90° plies respectively, is dominated by 0° plies and was expected to behave the most linearly of all four layups. This configuration might be used as an

Table 3.1 Material and Calculated Laminate Properties

Material or Laminate	E_L (GPa)	E_T (GPa)	V_{LT}	G_{LT} (GPa)	% [0/45/90]
AS4/3501-6	142.0	9.8	0.3	6.0	——
Layup 1 $[0/(\pm 45)_2/90/(\pm 45)_2]_s$	37.18	37.18	.5313	30.57	10/80/10
Layup 2 $[0/\pm 45/90]_{2s}$	55.51	55.51	.300	21.35	25/50/25
Layup 3 [45/0/-45/0/90/-45/0/-45/0/45]s	72.59	36.62	.439	21.04	40/50/10
Layup 4 $[\pm 45]_{4s}$	20.80	20.8	.737	36.7	0/100/0

E_L = Longitudinal Modulus

E_T = Transverse Modulus

V_{LT} = Poisson's Ratio

G_{LT} = Shear Modulus

integral stringer or stiffener in a smart skin application. Layup 4, which had all ±45° plies, is matrix dominated and was expected to behave nonlinearly with applied longitudinal load. This configuration would be used for a structure which is dominated by shear loading.

Optical fibers, piezoceramic material, a low conductivity integrated dielectric circuit chip and teflon rectangles, which approximated the size and shape of the PZA and chip, were the implants chosen for the experiments. The effects of laying over versus cutting out an area for the implant was investigated by testing the chip placed directly into the center of layup 2 and by testing the optical fiber placed in two cut-out plies also in layup 2.

Cylindrical fused silica optical fibers with a polyimide coating were manufactured by Radiant Communications. They had a core diameter of 200 micrometers and an outer diameter of 266 micrometers which is roughly equivalent to two plies of graphite/epoxy material. The polyimide coating allows the optical fiber to withstand temperatures from -190° to 385°C.

The 8.9 by 11.1 by .5 mm rectangular integrated dielectric circuit chip manufactured by Micromet Industries and typically used for cure monitoring is shown in Figure 3.1. It was encased by a polyimide coating to protect the electronics from the graphite fibers. This circuit chip was used in previous studies to determine the feasibility of implanting sensitive electronic devices in graphite/epoxy [16]. The circuit chip had lead wires .13 mm thick equal to the width of the chip that extend halfway along the tensile coupon.

A G1195 piezoceramic material manufactured by Piezo Systems was implanted as an example of a strain actuator. This piezoceramic

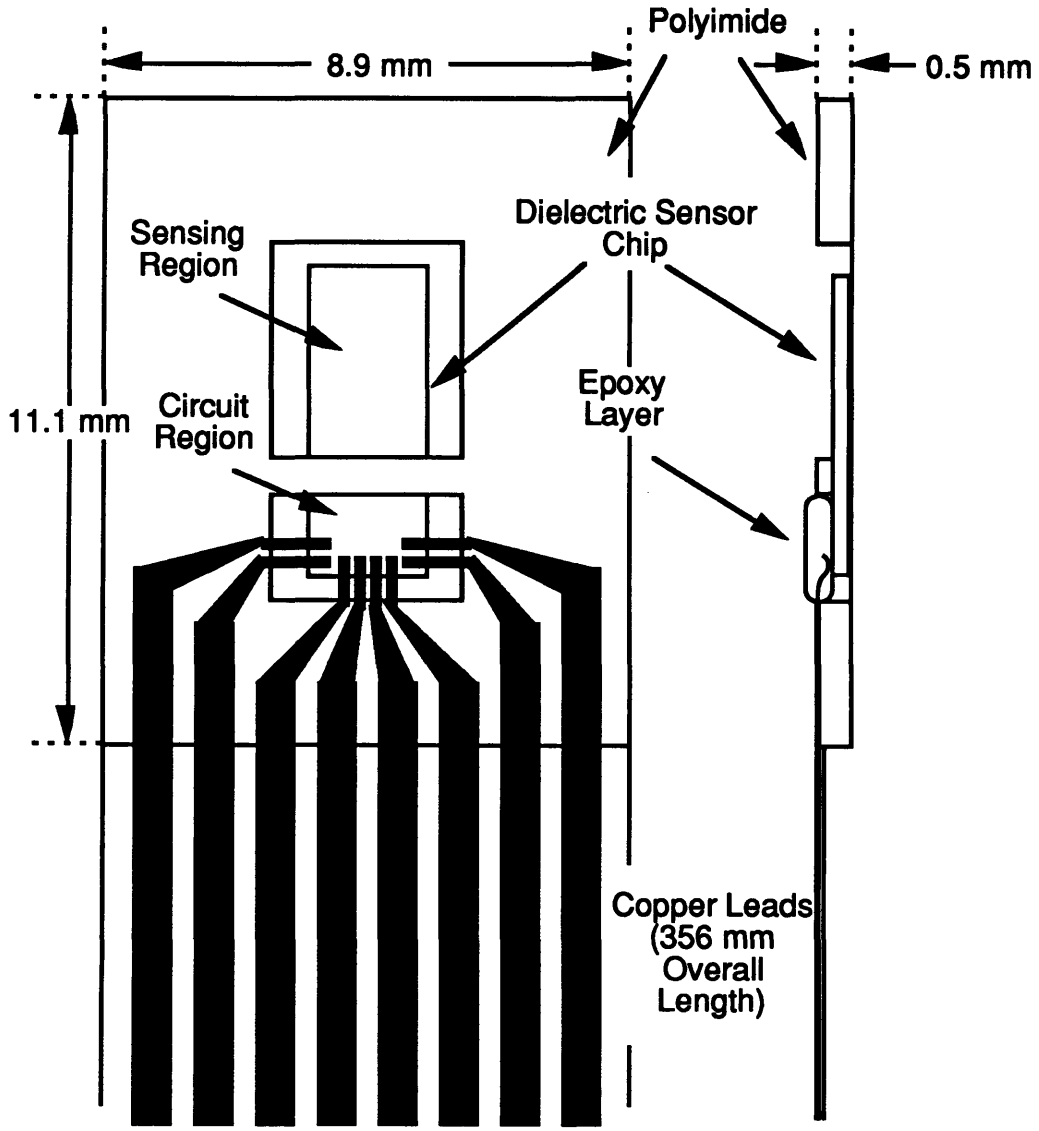

Figure 3.1 Enlarged View of Micromet Integrated Dielectric Circuit Chip and Lead Attachment

material had a high modulus and curie temperature. The high modulus allows the PZA to carry loads within the graphite/epoxy and the high curie temperature protects the material during the cure cycle. Piezoceramic material will cause a bending moment when two piezoelectrics are bonded or embedded at opposite but equal distances from the neutral axis of the composite material and a voltage is applied across the PZA. The properties of the piezoceramic are shown in Table 3.2. Y11 is the modulus in the length or width direction. Y33 is the modulus in the .25 mm thickness direction. Because these experiments were not focused on the operation of the embedded sensors, actuators, or circuitry, only a single PZA with two lead wires was embedded instead of the pair normally required for actuation.

The PZA material was purchased in 64 by 38 by .25 mm sheets. Each sheet was cut with a sharp razor and straight edge into four 16 by 38 by .25 mm pieces. The lead wires were easily cut with a razor from the leads of integrated dielectric circuit chips and consisted of two of the eight copper wires. 1.5 mm of polyimide coating on one end of the lead wires had to be scraped off with a razor to allow soldering of the wires to the PZA. The lead wires were placed on opposite edges of the PZA, one on the top and one on the lower surface, halfway along its length as shown in Figure 3.2. M-FLUX AR manufactured by Measurements Group helps the solder adhere to different surfaces and was put on the PZA where the end of the lead would be attached and also on the bare copper wires on the leads. Both the PZA and the lead wires were painted with solder which minimized the size of the finished solder joint. The lead wire tips were straightened after the solder was painted on. Methanol was used to clean up the M-FLUX around the painted solder

Table 3.2 Material Properties of Piezoceramic Material

Moduli:	Y33 = 4.9×10^{10} N/m^2
	Y11 = 6.3×10^{10} N/m^2
Density:	7600 kg/m^3
Curie Temperature:	360°C
Tensile Static Strength:	6.3×10^{7} N/m^2
Tensile Dynamic Strength:	2.1×10^{7} N/m^2
Thermal Expansion Coefficient:	5×10^{-6} m/m C
Compressive Strength:	5.2×10^{8} N/m^2

Y33 = Modulus through Thickness

Y11 = Transverse and Longitudinal Modulus

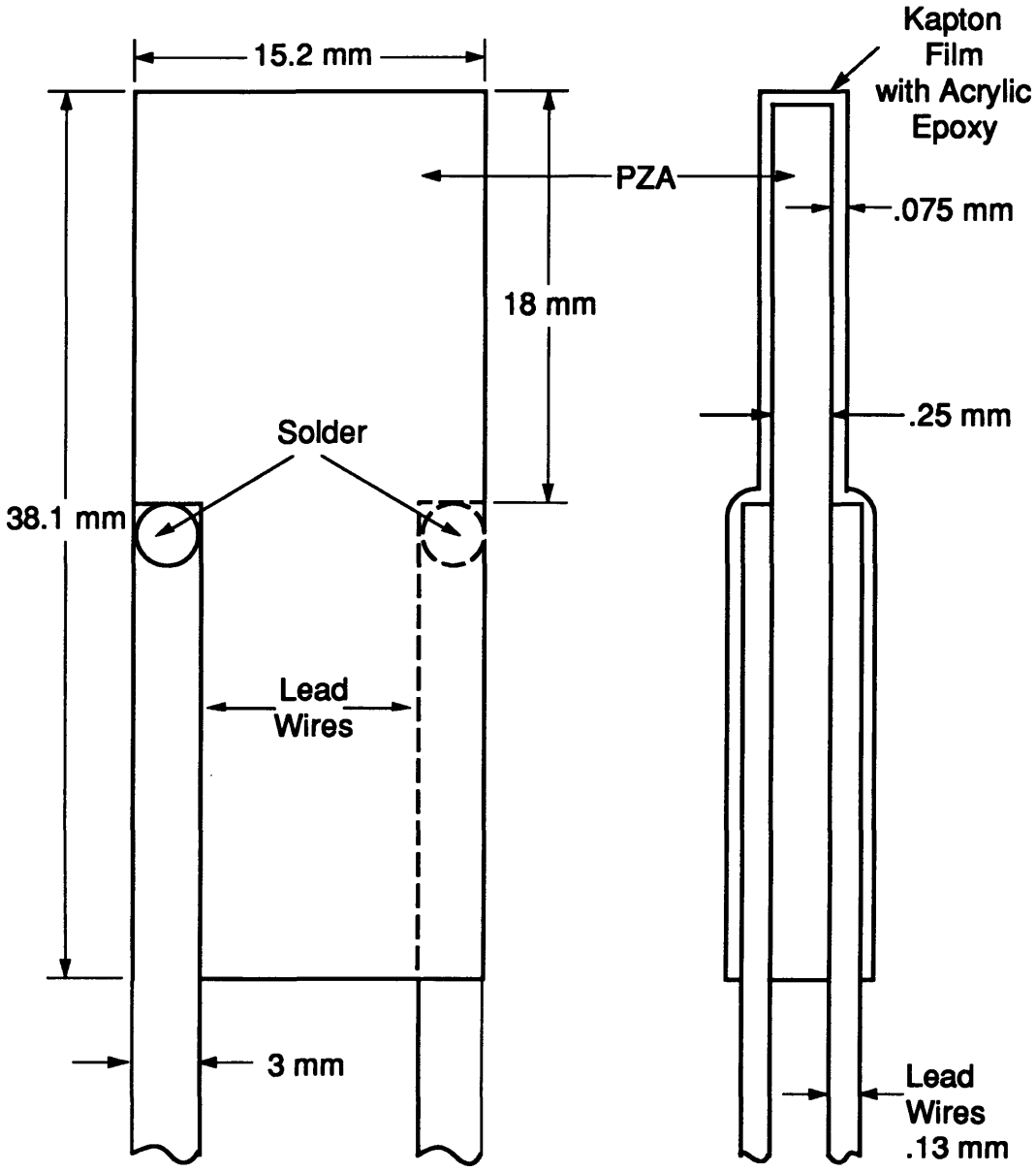

Figure 3.2 Schematic of Piezoceramic Implant with Lead Wires Attached

on both the PZA and leads. The leads were then soldered to the PZA such that the lead wires were aligned with the sides of the implant. The PZA and the portion of the leads along the PZA were encased in .075 mm thick Kapton film with pressure sensitive acrylic epoxy manufactured by 3M which electrically insulated the PZA from the graphite fibers. The acrylic adhesive had a lamination temperature of 135-150°C and a maximum operating temperature of 105°C for short-term exposures. Piezoceramic material is extremely brittle and caution had to be exercised to avoid cracking it during this process.

The teflon implants were manufactured by Altec Plastics. A 305 by 305 by 0.5 mm thick teflon sheet was cut into 9 by 11 mm rectangles to simulate the size of the circuit chip. A 305 by 305 by 0.25 mm thick teflon sheet was cut into 16 by 38 mm rectangles to simulate the size of the PZA. The thickness of the teflon chip was equivalent to the actual chip implant thickness. The thickness of the teflon PZA was equal to the thickness of the PZA material but was only one half the thickness of the combined PZA, film coating and lead wires. These teflon pieces were used to investigate how the material properties of the implant affected the tensile strength of the coupons and also to compare how well the actual implants versus teflon bonded to the graphite/epoxy. The material properties of teflon are shown in Table 3.3. Because of the difficulty in attaching anything to teflon, there were no lead wires attached to the teflon pieces. The teflon, chip, PZA and optical fibers were placed directly into the composite with no additional bonding material. Figure 3.3 shows a comparison of the chip, PZA and teflon implants' relative sizes and shapes.

Table 3.3 Material Properties of Teflon

Tensile Strength	6.9 GPa - 27.6 GPa
Melting Point	326.67 °C
Specific Gravity	2.16
Coefficient of Linear Thermal Expansion (CTE)	13.33 in/in °C x 10^{-6}

Note: Properties as quoted by Altec Plastics

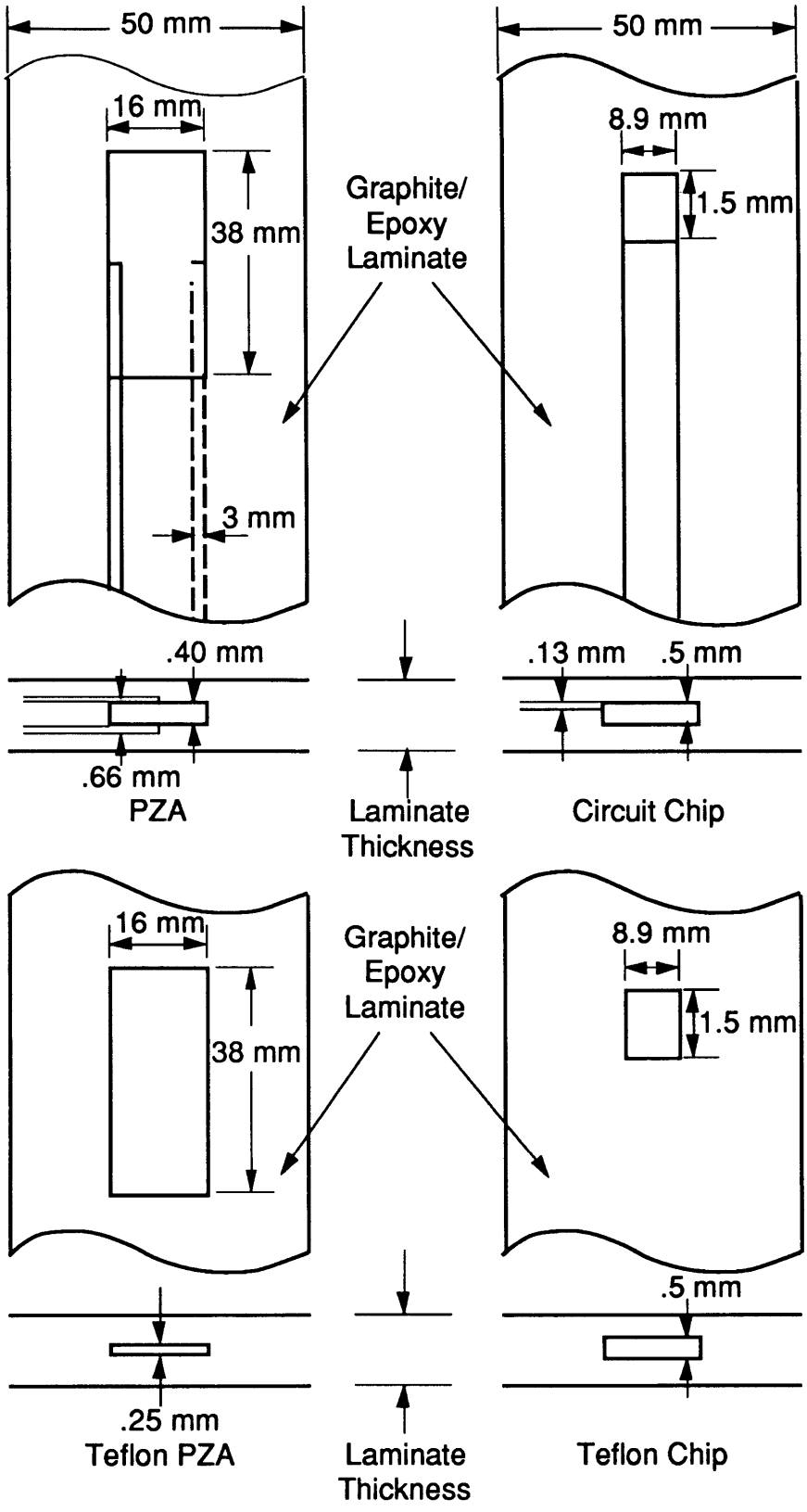

Figure 3.3 Comparison of Implant Sizes

The matrix showing all the combinations of implants and layups that were manufactured is shown in Table 3.4. A total of 5 tensile coupons were manufactured for each variation of layup and implant. A set of "virgin" specimens without implants was made and tested to validate theoretical mechanical properties of the laminate and to have an experimental comparison to the specimens with implants. A common type of layup used in industry is the quasi-isotropic laminate layup 2. This was the primary layup used to study the effect of laying over the implant vs. cutting out plies and to make a comparison between the effects of using teflon versus the chip and PZA implants. The tensile specimen configuration is shown in Figure 3.4.

3.2 Manufacturing Procedure of Tensile Coupons

All experimental work was performed in the Technology Laboratory for Advanced Composites. Manufacturing, instrumenting and testing was performed using procedures described in the TELAC Manufacturing Class Notes [19]. Special procedures described in the following sections 3.2.1-3.2.4 were developed for inserting the implants into the laminates.

The individual plies were cut from a 305 mm wide roll of unidirectional AS4/3501-6 prepreg manufactured by Hercules. The tensile coupons were manufactured from a 305 by 356 mm plate. Cutting 0 degree plies was straightforward. The cutting of ± 45 degree and 90 degree plies from unidirectional tape was slightly more complicated and is illustrated in Figure 3.5. The plies were laid up by

Table 3.4 Number of Coupons Manufactured

Implant	Layup			
	1 $[0/(\pm45)_2/90/(\pm45)_2]_s$	2 $[0/\pm45/90]_{2s}$	3 $[45/0/-45/0/90/-45/0/-45/0/45]_s$	4 $[\pm45]_{4s}$
Virgin Specimens	5	5	5	5
Circuit Chip Implants Placed in Cut Laminate	5	5	5	5
PZA Implants Placed in Cut Laminate	5	5	5	5
Optical Fibers Placed Directly in Laminate	5	5	5	5
Teflon Circuit Chip Placed in Cut Laminate	----	5	----	----
Teflon PZA Placed in Cut Laminate	----	5	----	----
Circuit Chip Placed Directly in Laminate	----	5	----	----
Optical Fibers Placed in Cut Laminate	----	5	----	----

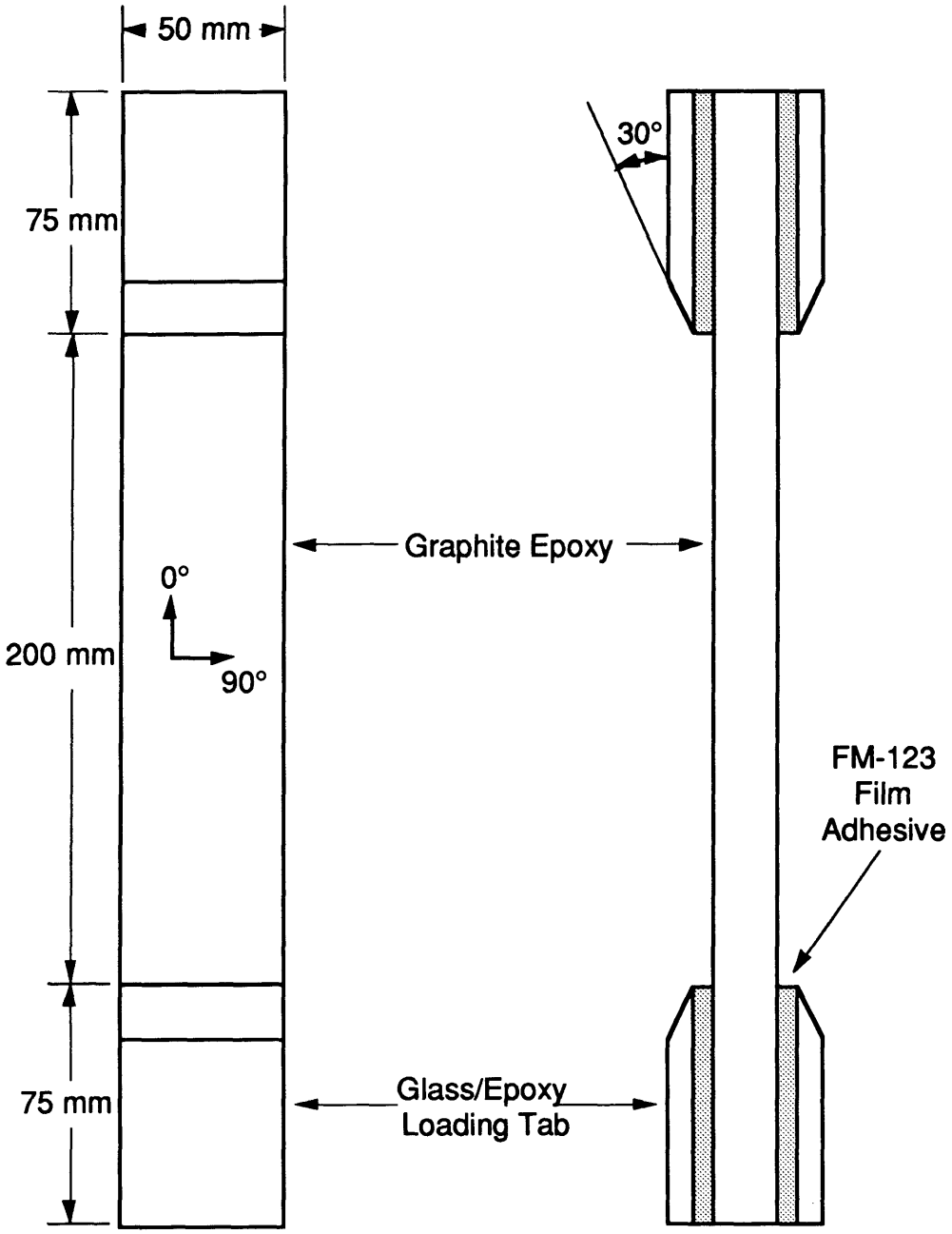

Figure 3.4 Tensile Specimen

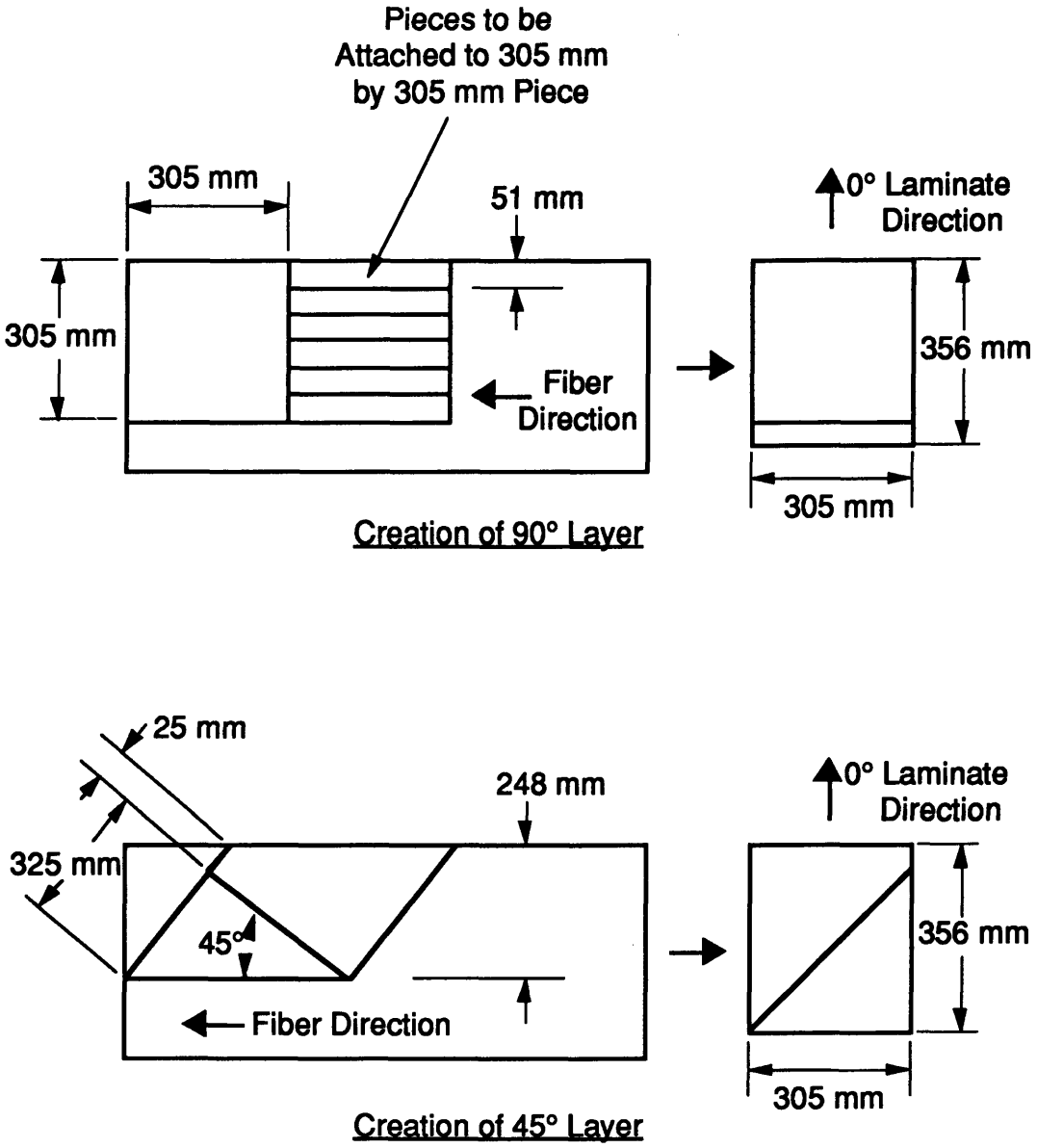

Figure 3.5 Creation of 45° and 90° Ply From Unidirectional Tape

hand against a 90 degree metal dam used to maintain consistent angular orientation of the plies and to keep two "neat" sides of the laminate that were used to align the laminate in the milling machine later.

The piezoceramic, chip and teflon implants were all placed in cut-out areas in the center of the laminate. The depth of the cutout was based on the assumption of a nominal .135 mm graphite/epoxy ply thickness. When the laminate was complete, the corner that lay in the metal frame was marked and the plate was trimmed to 305 by 356 mm. The edge where the leads extended was originally left untrimmed in an effort to help locate the position of the implants after the cure; however, the implants were successfully located using X-rays and all of the edges were later trimmed prior to the cure. When the leads were allowed to hang out of the laminate, excessive epoxy leaked out of the cure packaging. Sheets of 406 by 305 mm peel ply were placed on both sides of the laminate after they were assembled. The peel ply created a slightly roughened surface texture after the cure. The rough texture helped create a stronger bond between the graphite/epoxy and loading tabs and strain gages. The peel ply extended 50 mm past one end of the laminate to aid removal after the cure.

All laminates were placed in vacuum bags sealed with vacuum tape overnight at room temperature before being cured the following day.

3.2.1 Implanting Circuit Chips

The circuit chip thickness of .5 mm was equivalent to four cut plies of .135 mm thick graphite/epoxy and the lead wire thickness of .13 mm was equivalent to one cut ply. The lead wire ply was an extension of the fourth cut ply. A cardboard template shown in Figure 3.6 was used to cut five rectangular holes 10 by 12 mm out of a three ply sublaminate. There was a separate template for the fourth layer with the leads which is also shown in Figure 3.6. The implants were spaced 58.5 mm apart to allow an extra 8.5 mm between coupons. This machining allowance assured each 50 mm wide coupon had a centered implant.

The method used for implanting the chips was identical for all four layups. The only difference was the ply orientations in the sublaminates. The sublaminate approach to inserting the implants is shown in Figure 3.7. In order to implant the chip into layup 1, the bottom sublaminate consisting of [0/45/-45/45/-45/90/45/-45] plies was laid down and then a sublaminate consisting of [45/-45/-45] plies was put together. The three ply sublaminate had five rectangular 10 by 12 mm holes cut into it using the template shown in Figure 3.7. This sublaminate was then placed onto the existing lay-up. The last [45] ply used for the implant leads was cut using the lead wire template and then carefully placed onto the main lay-up so as to align the lead holes with the main chip cutout. Five circuit chips were then placed in the holes with the lead wires aligned with the cut-out areas in the plies. A 3 by 5 mm piece of 0.28 mm thick #34 glass filter paper manufactured by Schleicher & Schuell was put on top of the silicon chip to insulate the

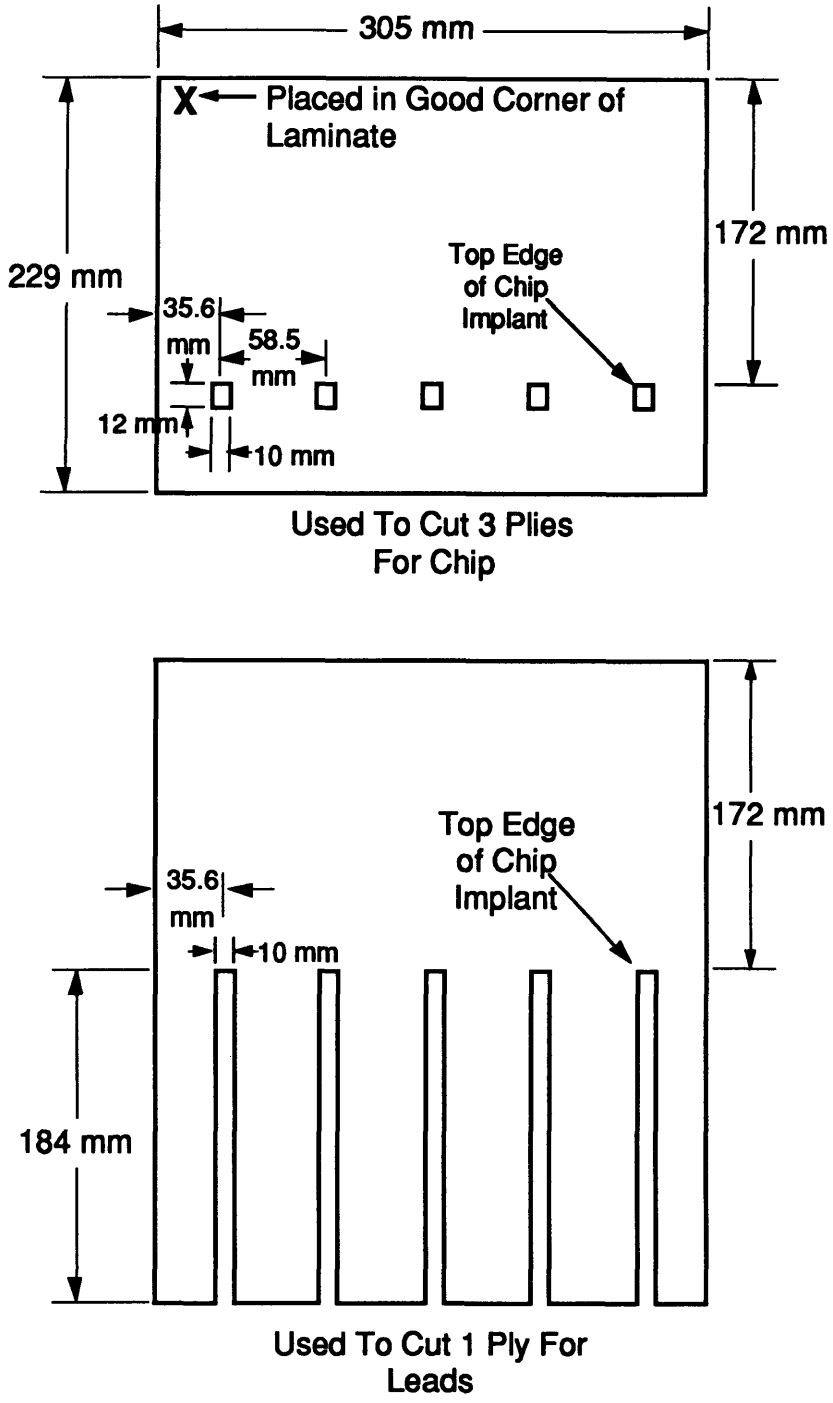

Figure 3.6 Templates Used to Cut Holes in Graphite/Epoxy for Chip Implants

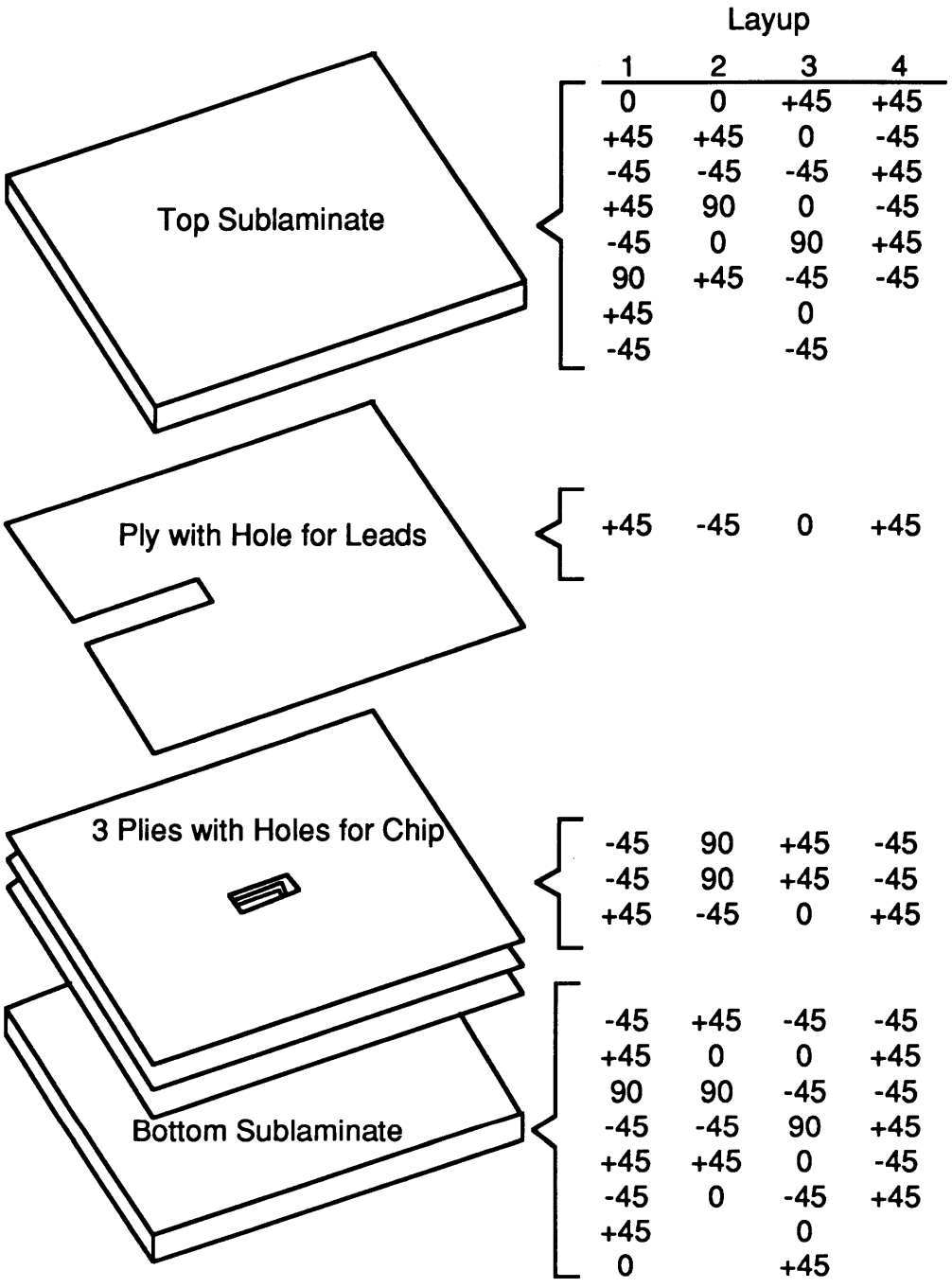

Figure 3.7 Sublaminate Approach to Implant Chips

chip from the graphite fibers. The remaining [-45/45/90/-45/45/-45/45/0] plies were than laid over the implants.

In order to place the implant in layup 2, the base laminate consisted of [0/45/-45/90/0/45] plies. The three ply sublaminate cut for the chip consisted of [-45/90/90] plies. The lead wire ply was a cut [-45]. After inserting the chip and filter paper, the remaining [45/0/90/-45/45/0] plies were assembled.

Implanting the chip into layup 3 involved laying up the [45/0/-45/0/90/-45/0/-45] plies and then creating a [0/45/45] sublaminate for the 10 by 12 mm chip cutouts. A [0] ply was cut for the lead wires and laid up on the main laminate. After the leads and filter paper were placed in the voids, the remaining [-45/0/-45/90/0/-45/0/45] plies were assembled.

Implanting the chip into layup 4 involved laying up the [45/-45/45/-45/45/-45] plies and then creating a [45/-45/-45] sublaminate for the 10 by 12 mm cut rectangular holes. The last [45] ply was cut for the lead wires and laid up on the main laminate. After the leads and filter paper were placed in the voids, the remaining [-45/45/-45/45/-45/45] plies were assembled.

There was a special case tested in which the circuit chip was placed between the center two 90° plies in layup 2. The chips were laid in the laminate using the main chip template shown in Figure 3.6.

3.2.2 Implanting the Piezoceramic

The 0.4 mm piezoceramic coated with the polyimide film required three cut graphite/epoxy plies. As shown in Figure 3.2, the 0.13 mm

thick leads were placed on opposite sides on the top and bottom of the PZA. One additional ply was cut for each lead wire. The three plies cut for the PZA and two for the leads required a total of five cut plies. Templates used to cut 40 by 17 mm holes for the PZA and 3 mm wide holes for the lead wires are shown in Figure 3.8. The lead wire template was used for both the upper and lower lead wire cutout by turning it over. The five PZAs were placed 58.5 mm apart in the laminate to allow the extra 8.5 mm between coupons.

The method used for implanting the PZA implants was identical for all four layups. The only difference was in the ply orientations in the sublaminates. The sublaminate approach to inserting the PZA implants is shown in Figure 3.9. The first uncut sublaminate for layup 1 consisted of the [0/45/-45/45/-45/90/45/-45] plies as shown in Figure 3.9. A single [45] ply was cut using the lead template and placed onto the main laminate. The PZA's were then placed such that the leads fit into the lead wire cutouts. A [-45/-45/45] sublaminate was put together and cut using the template with 17 by 40 mm holes. It was then carefully placed on top of the PZAs to line up the rectangular cut-outs with the PZA implants. The lead wire on top of the implant was pulled out through the hole in the plies and placed on top of the laminate. A [-45] ply was cut for the lead wires and carefully placed on top of the laminate such that the top lead wires lay in the cut-out slots. The remaining [45/90/-45/45/-45/45/0] plies were then assembled.

The first uncut sublaminate for layup 2 consisted of [0/45/-45/90/0/45] plies and the cut-out [-45] ply for the lead wires was placed on top of it. The PZA leads were put into the lead wire cut-outs

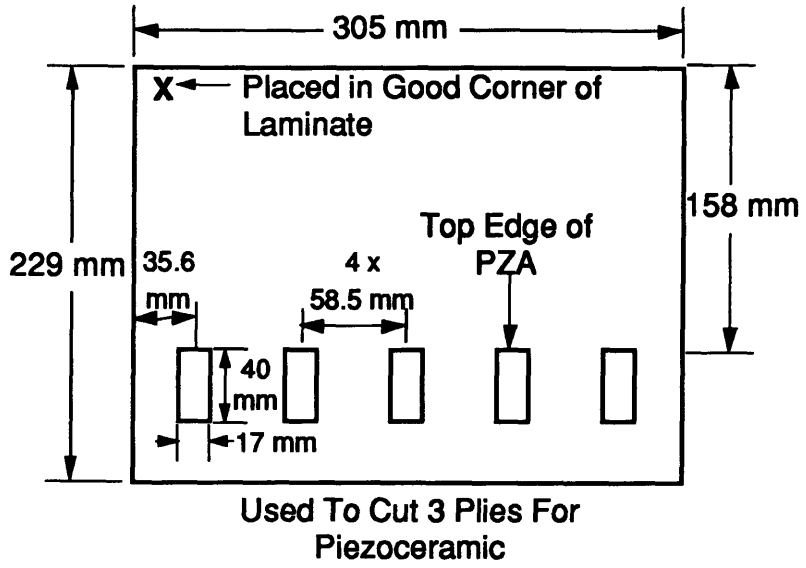

Used To Cut 3 Plies For Piezoceramic

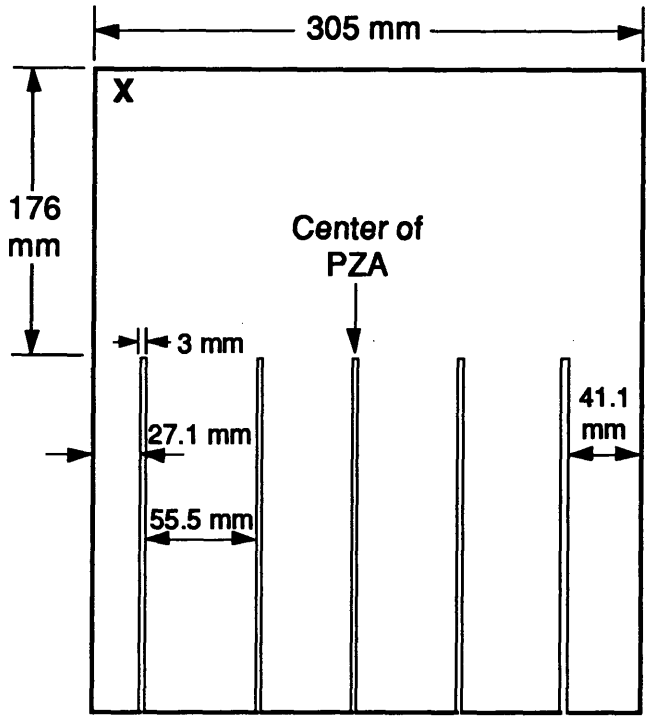

Used To Cut One Ply For Leads and Flipped Over Before Using To Cut Second Ply For Leads

Figure 3.8 Templates Used to Cut Holes in Graphite/Epoxy for PZA Implants

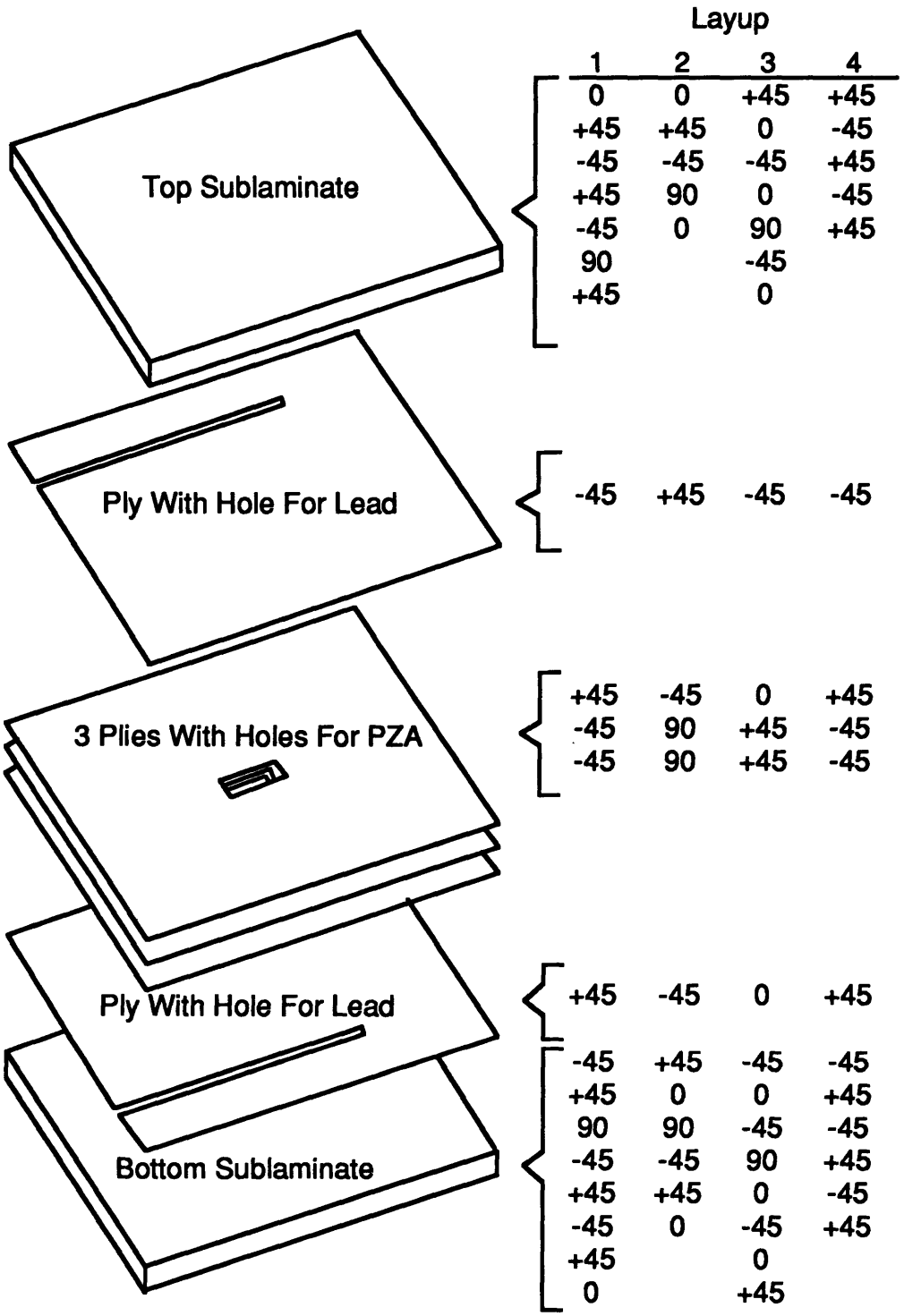

Figure 3.9 Sublaminate Approach to Implant PZA

and the templates with 17 by 40 mm holes were then used to cut holes in a [90/90/-45] sublaminate. This sublaminate was then placed on the main laminate. A [45] ply was cut for the lead wires and aligned with the leads. The remaining [0/90/-45/45/0] plies were then assembled.

The first uncut sublaminate for layup 3 consisted of [45/0/-45/0/90/-45/0/-45] plies and the first cut lead wire ply was a [0]. The next sublaminate for the main portion of the PZA consisted of [45/45/0] plies. The cut-out [-45] lead wire ply was laid up carefully over the leads. The remaining [0/-45/90/0/-45/0/45] plies were then placed on top of the implant.

The base laminate for layup 4 consisted of [45/-45/45/-45/45/-45] plies. Lead wire cut-outs were made in a [45] and rectangular cut-outs were made in a [-45/-45/45] sublaminate. The top lead wire ply consisted of one [-45] followed by the remaining [45/-45/45/-45/45] plies.

3.2.3 Implanting the Optical Fibers

The optical fibers were laid directly between the center plies in all layups in the longitudinal direction of the tensile coupon shown as 0° in Figure 3.4. They were placed 35.6, 94.1, 152.6, 211.1 and 269.6 mm from one edge as shown in Figure 3.10. A 45 degree ply surrounded the optical fiber in layups 1, 3 and 4. Layup 2 had a 90 degree ply at the center.

Five specimens were made where the optical fiber was placed in two cut 90° plies in the center of layup 2 at the same width locations shown in Figure 3.10.

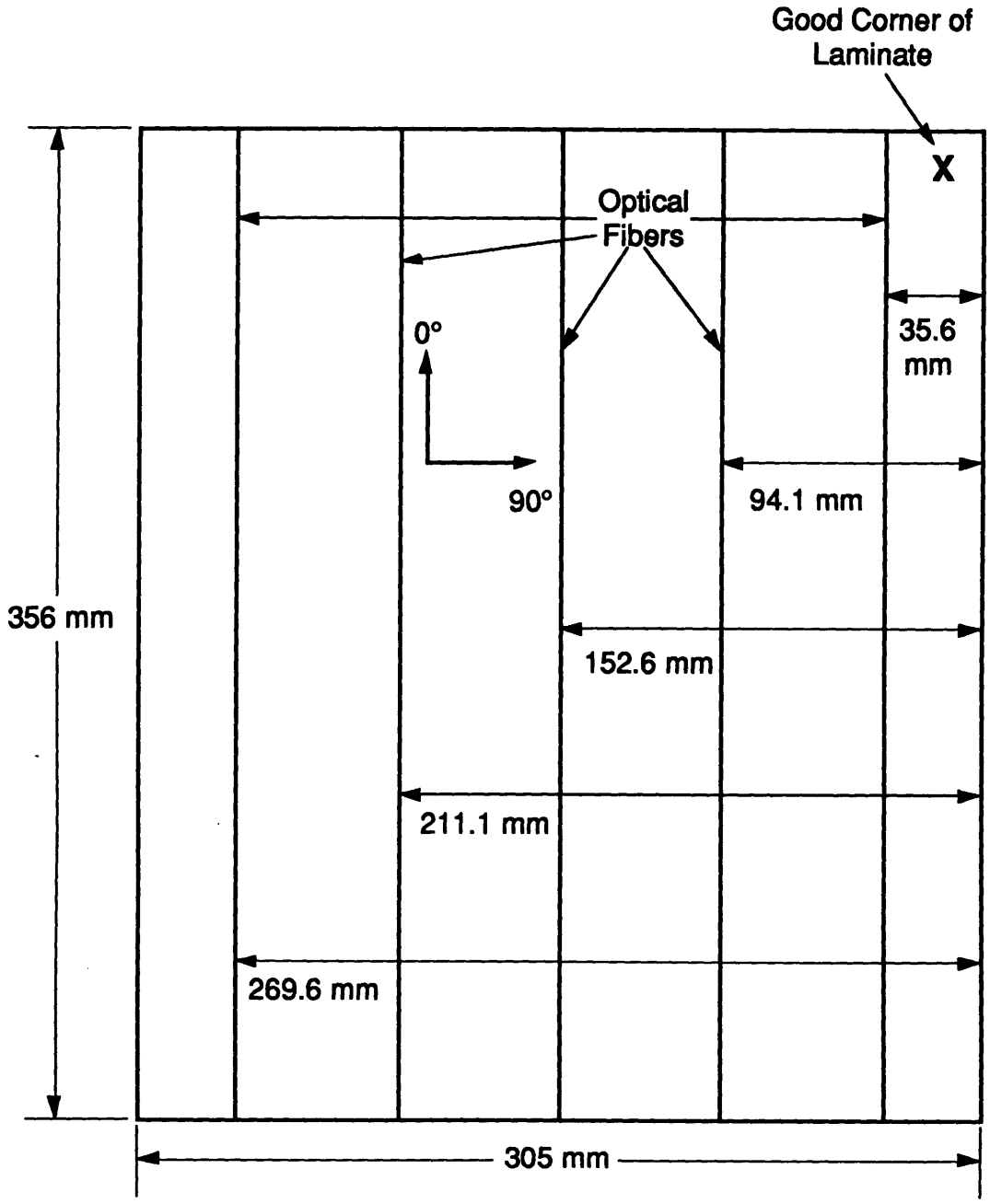

Figure 3.10 Placement of Optical Fibers in Graphite/Epoxy Laminate

3.2.4 Implanting Teflon

The teflon PZA was only implanted into layup 2 and only required that the two center 90° plies be cut. The 17 by 40 mm cutouts were made using the PZA template shown in Figure 3.8. The teflon chip required 10 by 12 mm holes be cut in the four center plies, [-45/90/90/-45], using the chip template shown in Figure 3.6. Neither of the teflon implants had lead wires or lead wire cutouts in the laminates.

3.2.5 Specimen Coding

The five coupons from each set were labeled with the appropriate layup number 1, 2, 3 or 4, the implant code names and the letters A, B, C, D or E. The implant code names for the chip, PZA, optical fiber, teflon chip and teflon PZA implants are CHIP, PZA, OF, TC and TPZA respectively. The implants were labeled OF C/O for the special case where optical fibers were placed in a cut-out area. The chip implants that were placed directly in the laminate were labeled CHIP L/O. As an example of this coding method, the coding for the five specimens in a layup 3 configuration with a chip implant was 3CHIP-A, 3CHIP-B, 3CHIP-C, 3CHIP-D and 3CHIP-E. The virgin specimens had a code name of V. For example, the virgin specimens with a layup 1 configuration were labeled 1V-A, 1V-B, 1V-C, 1V-D and 1V-E.

3.2.6 Curing Procedure

The specimens were manufactured in four batches. The first batch consisted of all the virgin specimens. The second set consisted of 2TP, 2TC, 2PZA, 1CHIP and 1OF specimens. The third set consisted of 2OF, 1PZA, 3CHIP, 3OF, 3PZA and 4CHIP. The final batch consisted of 2CHIP, 4PZA, 2CHIP L/O, 4OF, and 2OF C/O.

Laminates were cured using standard TELAC manufacturing procedures. Six 305 by 356 mm laminate plates were cured on a 1.4 by 0.8 by 9.5 mm thick aluminum baseplate covered with a layer of guaranteed nonporous teflon (GNPT). The laminates were separated by three aluminum T-dams and three layers of cork as shown in Figure 3.11. The cork and T-dams formed 305 by 355 mm rectangles. The laminates were "packaged" to keep the epoxy from flowing over all the T-dams. A piece of GNPT 355 by 406 mm was centered underneath the laminate and a sheet of 355 by 406 mm porous teflon was centered above the laminate to prevent the bleeder paper from sticking to the laminate. One sheet of 305 by 355 mm bleeder paper for every two plies of graphite/epoxy was used to soak up excess epoxy and was placed on top of the porous teflon. A second piece of GNPT was placed on top of the bleeder paper to separate the laminate from the 9.5 mm thick aluminum top plates which were the same size as the laminates. The top plates ensured an even pressure distribution on the laminates during the cure. A 305 by 355 mm piece of GNPT was placed on top of the top plates and the first sheet of GNPT was then folded over with the intermediate layers to form a protective package around the laminate and top plate. The layers were taped down using 25 mm wide flash tape. The entire

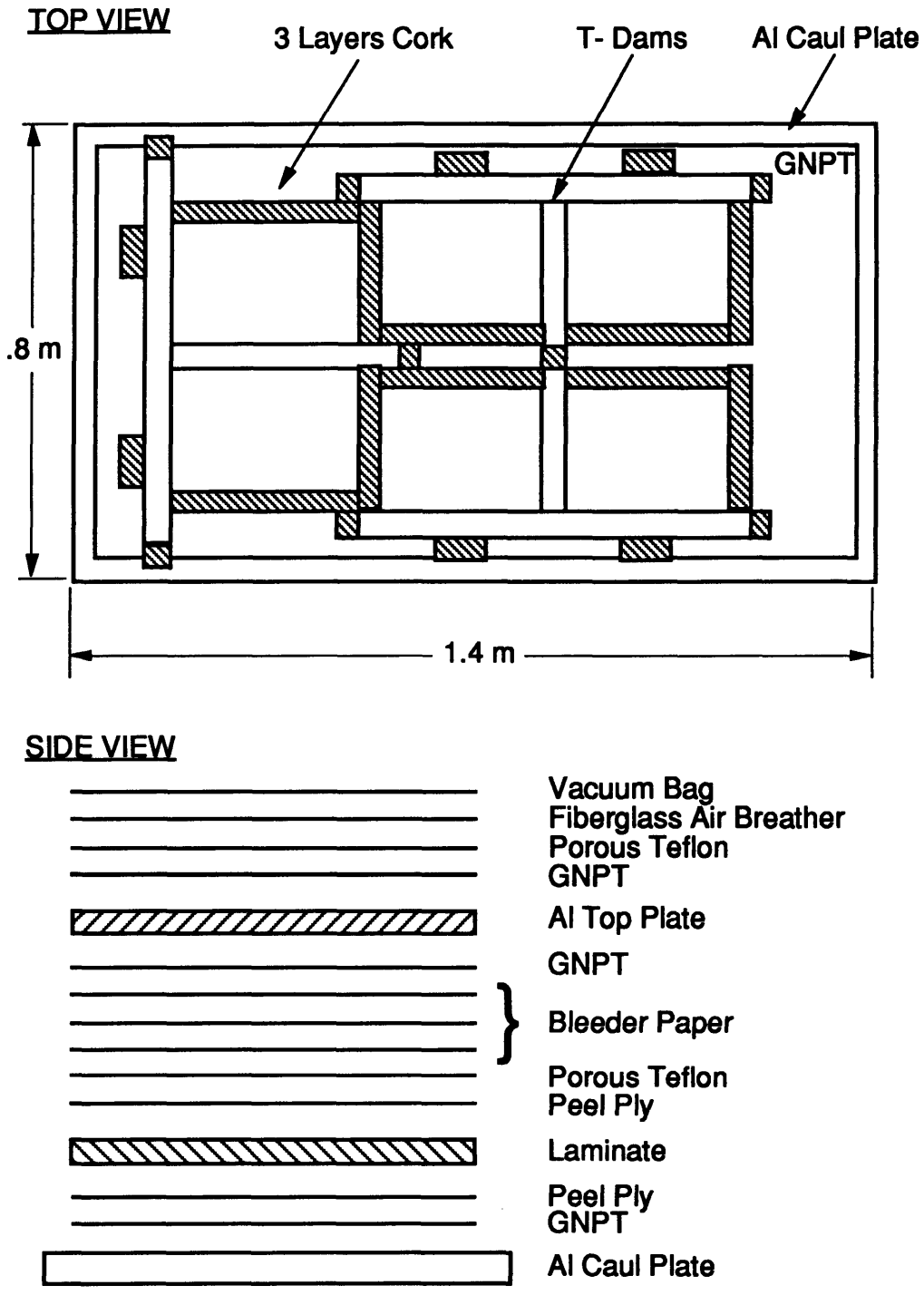

Figure 3.11 Standard Plate Cure Set-Up

assembly including T-dams and cork was covered by two sheets of fiberglass air breather. The air breather protected the outer vacuum bagging from the sharp edges of the T-dams and also helped circulate air and other fumes from the center of the plate to the vacuum holes at both ends of the cure plate. The exterior vacuum bagging was sealed to the cure plate using vacuum tape. Figure 3.11 also shows a cross-section of the cure-layup.

All laminates were cured in an autoclave under vacuum and applied pressure. An initial vacuum test was performed to ensure that the vacuum bagging was sealed correctly. A 760 mm Hg vacuum was pulled and shut off and the assembly was required to hold between 670 and 760 mm Hg for 5 minutes to ensure that vacuum could be held during the cure. If too much vacuum was lost during the test, the vacuum bagging was removed and after the bagging was resealed, the vacuum test was repeated. If the test was successful, a vacuum of 760 mm Hg was pulled and the autoclave was pressurized to .59 MPa before the temperature was raised to 115°C at a rate of 3°C per minute. After one hour at 115°C, the temperature was raised to 177°C at a rate of 2°C per minute and then held constant for an additional two hours. The autoclave was then slowly cooled to 88.5°C at a rate of 3°C per minute to minimize thermal stress effects. Figure 3.12 shows the temperature, pressure and vacuum during the cure cycle.

The laminates covered by peel ply were removed from the cure packaging and postcured for 8 hrs at 177°C with no vacuum or additional pressure.

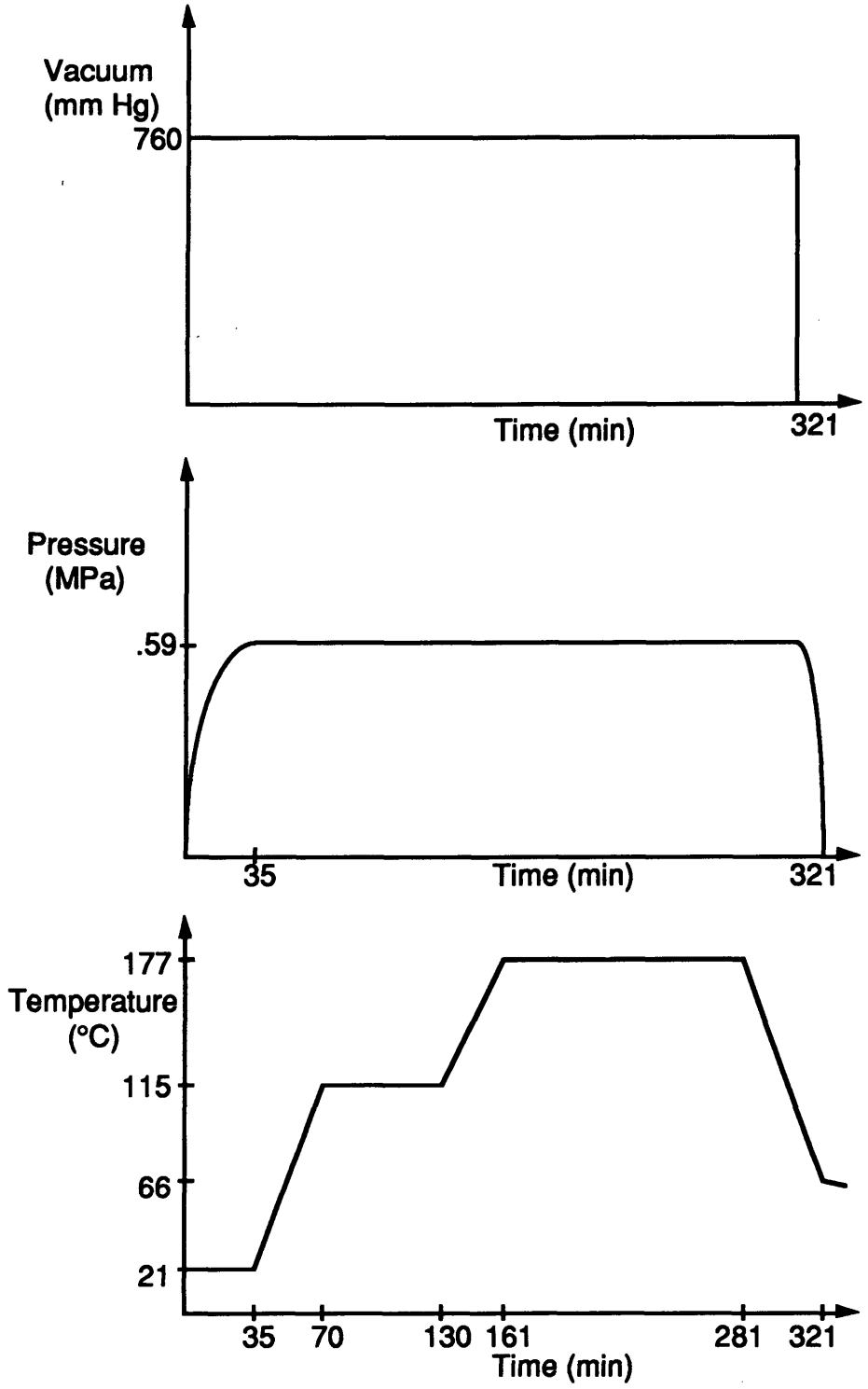

Figure 3.12 Standard Cure Cycle for AS4/3501-6 Graphite/Epoxy Laminates

3.2.7 Cutting Tensile Coupons

Five 50 by 356 mm tensile coupons with the same layup and implant were cut from the 305 by 356 mm plates. All specimens had X-rays taken prior to milling of the specimens to determine the exact location of the implants. After machining, another X-ray of one coupon from each set was made to have a comparison with the tested specimens and to see if any damage was introduced during the machining process. All X-rays were taken for 105 seconds at 30 kV with Kodak Film Type 52 using an X-Ray Inspection System Model 150D manufactured by Torrex.

The sides of the tensile coupons located 25 mm on either side of the implant center were marked at the bottom of the plate with white marker. The plates were cut on a milling table with a 155 mm diameter diamond-grit cutting wheel rotating at 1100 rpm with a table speed of 91 mm/minute. The edges adjacent to the good corner marked on the peel ply during the layup procedure were used to align the 0° axis of the laminate with the cutting wheel for the initial cuts. After the edges were trimmed, the first edge of the first coupon was cut based on the width location marked at one end of the plate. The second edge of the first coupon was cut to form a 50 mm wide specimen using spacers from the back wall of the cutting table to align the plate. Because of the 8.5 mm spacing between coupons, the wheel had to be aligned with the mark indicating the first edge of the next coupon. All coupons were rinsed with water and patted dry with paper towels after they were machined.

All of the coupons had nine thickness and three width measurements taken around the center of the coupon as shown in

Figure 3.13 to determine an actual cross-sectional area and to compare ply thicknesses with the nominal values supplied by the manufacturer. The actual thickness and width measurements for all coupons are presented in Appendix A. Average thicknesses and widths per coupon were used for all calculations and are also given in Appendix A.

3.2.8 Manufacture and Bonding of Loading Tabs

The loading tabs were made from Type 1002 cured crossply sheets of glass/epoxy manufactured by 3M. The original 380 by 600 mm sheets were cut into 50 mm by 75 mm rectangles on the milling machine using the same table and wheel speed used for the graphite/epoxy coupons. The thickness of the loading tabs were at least 1.5 times the thickness of the tensile coupons. For layups 1 and 3 which were 2.7 mm thick (20 plies), the loading tabs were 4.86 mm thick. For layups 2 and 4 which were 2.16 mm thick (16 plies), the loading tabs thickness was 4.75 mm. The end of each loading tab which would be placed closest to the coupon center was beveled to 30° using a belt sander to provide a smooth load transition into the tensile specimen. The side of the loading tab to be bonded to the specimen was sanded to enhance the bond and all of the coupons were washed with water prior to the bond cure. Four tabs were needed per tensile coupon and were placed to provide a 200 mm long test section centered around the implant.

The tabs were bonded to the coupons with American Cyanamid FM-123 film adhesive. They were placed on a sheet of the adhesive which was then cut with a sharp razor to the exact size of each tab. The

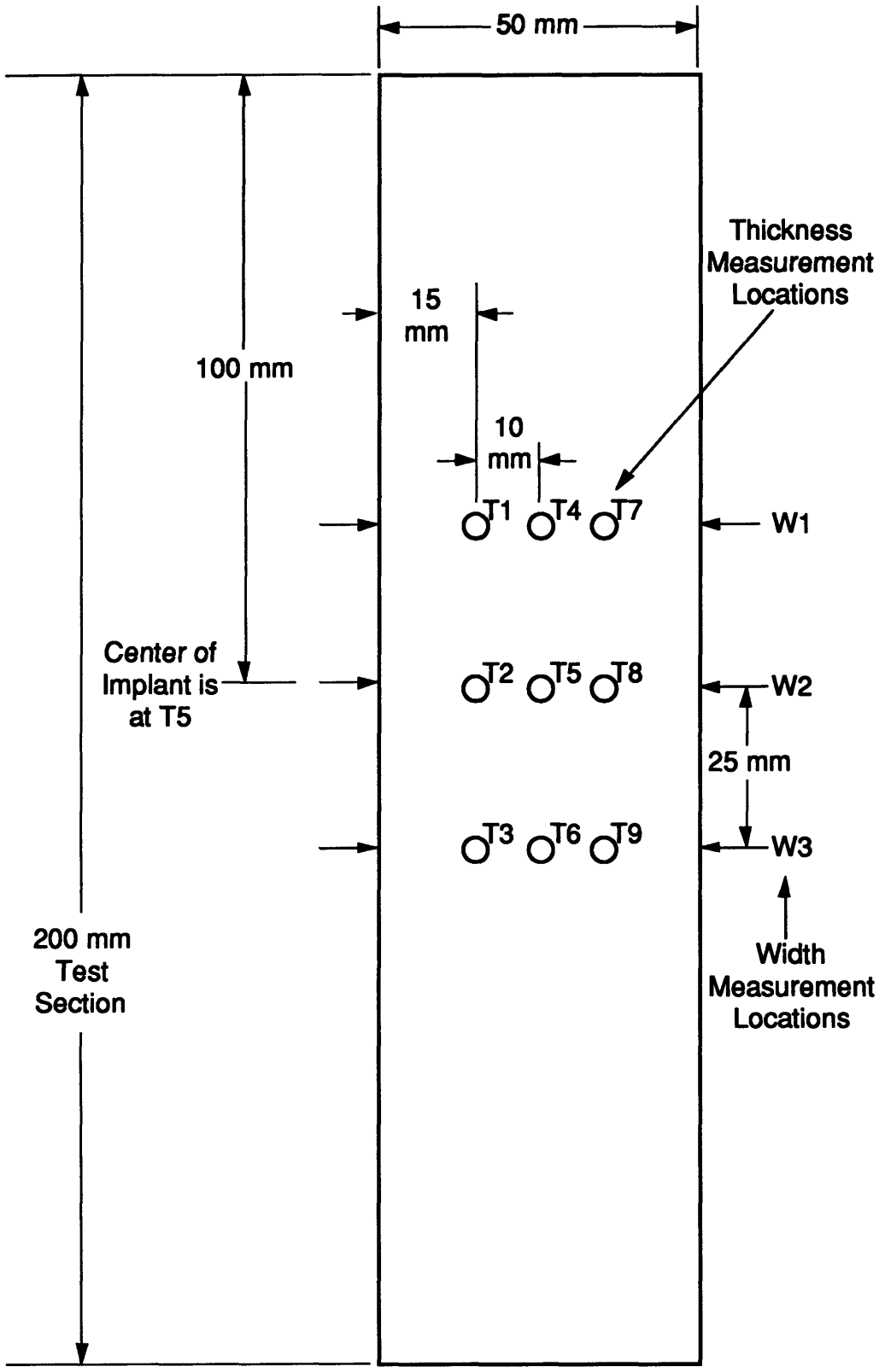

Figure 3.13 Coupon Thickness and Width Measurement Locations

film was warmed with a heat gun to increase its tackiness and was then placed on the graphite/epoxy specimen such that the beveled edge was exactly 100 mm from the center of the implant. After two tabs were bonded to one side of the coupon, the tabs for the other side were carefully placed to align the beveled edges of the tabs with the ones on the other side.

The finished tensile coupons were placed on an aluminum baseplate covered with a sheet of GNPT. The coupons were separated by at least 6 mm from one another to prevent them from bonding together. Scrap teflon was placed over the coupons to prevent the adhesive from sticking to the steel bonding plates. The steel bonding plates were placed side by side over all of the coupons to distribute the load evenly during the cure and to prevent any sideways motion of the tabs during the cure. Four layers of cork were placed around the perimeter of the specimens to transition the height from the steel plate corners which might puncture the vacuum bagging. A large sheet of porous teflon and fiberglass air breather was placed over the top plates. Vacuum bagging and vacuum tape was used to seal the assembly.

The tab cure was performed in an autoclave with a vacuum of 760 mm Hg and under a pressure of .07 MPa. After the autoclave was fully pressurized, the temperature was raised to 107°C at a rate of 3°C per minute and was held for two hours. After the bond cure, the autoclave was cooled at 3°C per minute.

3.3 Instrumentation

All tensile specimens were equipped with EA-06-125-AD-120 strain gages made by Micromeasurements Company. The gages were used to determine if the implants had any affect through the thickness on the strain above the implant and to determine the laminate elastic constants.

The virgin specimens were equipped with a longitudinal and transverse gage aligned with the midline of the coupon as shown in Figure 3.14. The transverse gage was placed 10 mm from the center of the specimen and the longitudinal gage was placed 5 mm from the center of the specimen. Comparisons of the calculated and experimentally determined elastic modulus verified the quality of the material.

All specimens with implants tested to failure had a minimum of one longitudinal strain gage directly over the center of the implant and a far-field longitudinal gage as shown in Figure 3.15. Specimens taken to a percentage of their ultimate load had a longitudinal gage at the implant and both a longitudinal and transverse far-field gage. The far-field gages for coupons with optical fiber implants were located off-center of the longitudinal axis of the coupon. Several coupons were initially equipped with an extra longitudinal gage to the side of the implant to monitor any edge effects. This gage was omitted from all future gaging after initial testing indicated its strain readings were similar to the far-field longitudinal gage.

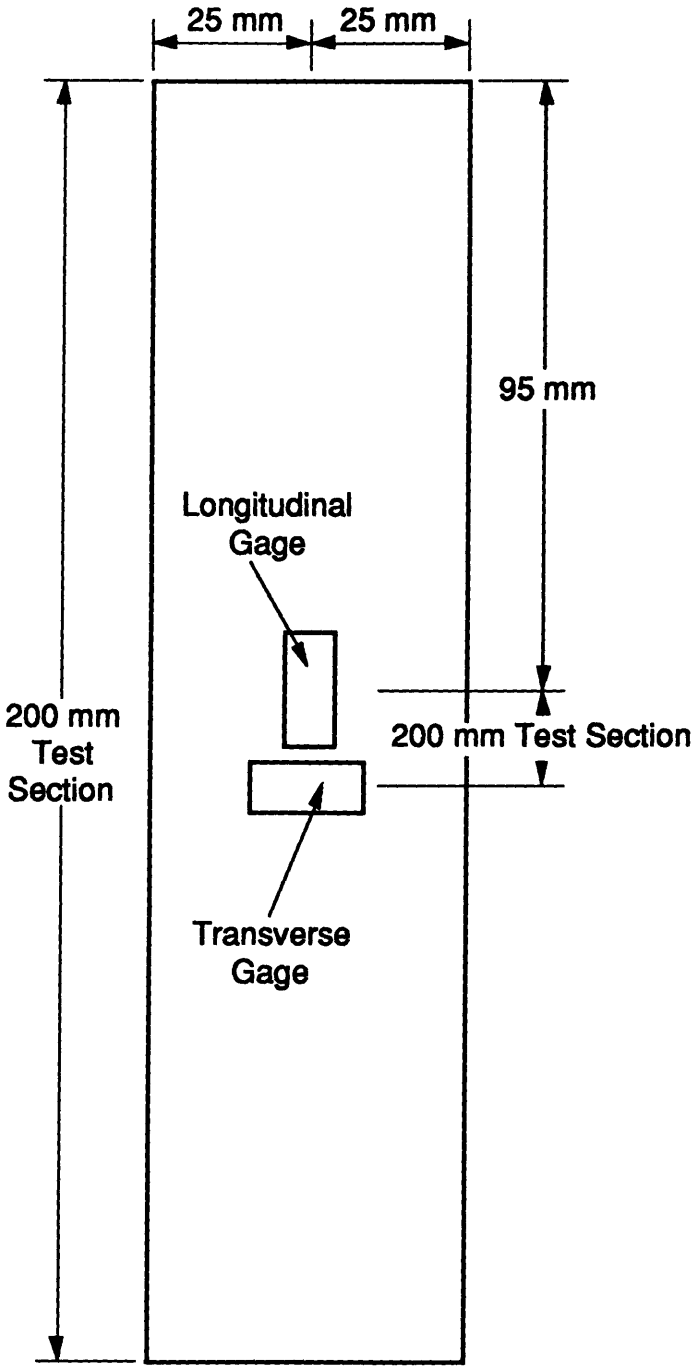

Figure 3.14 Strain Gage Placement for Virgin Specimens

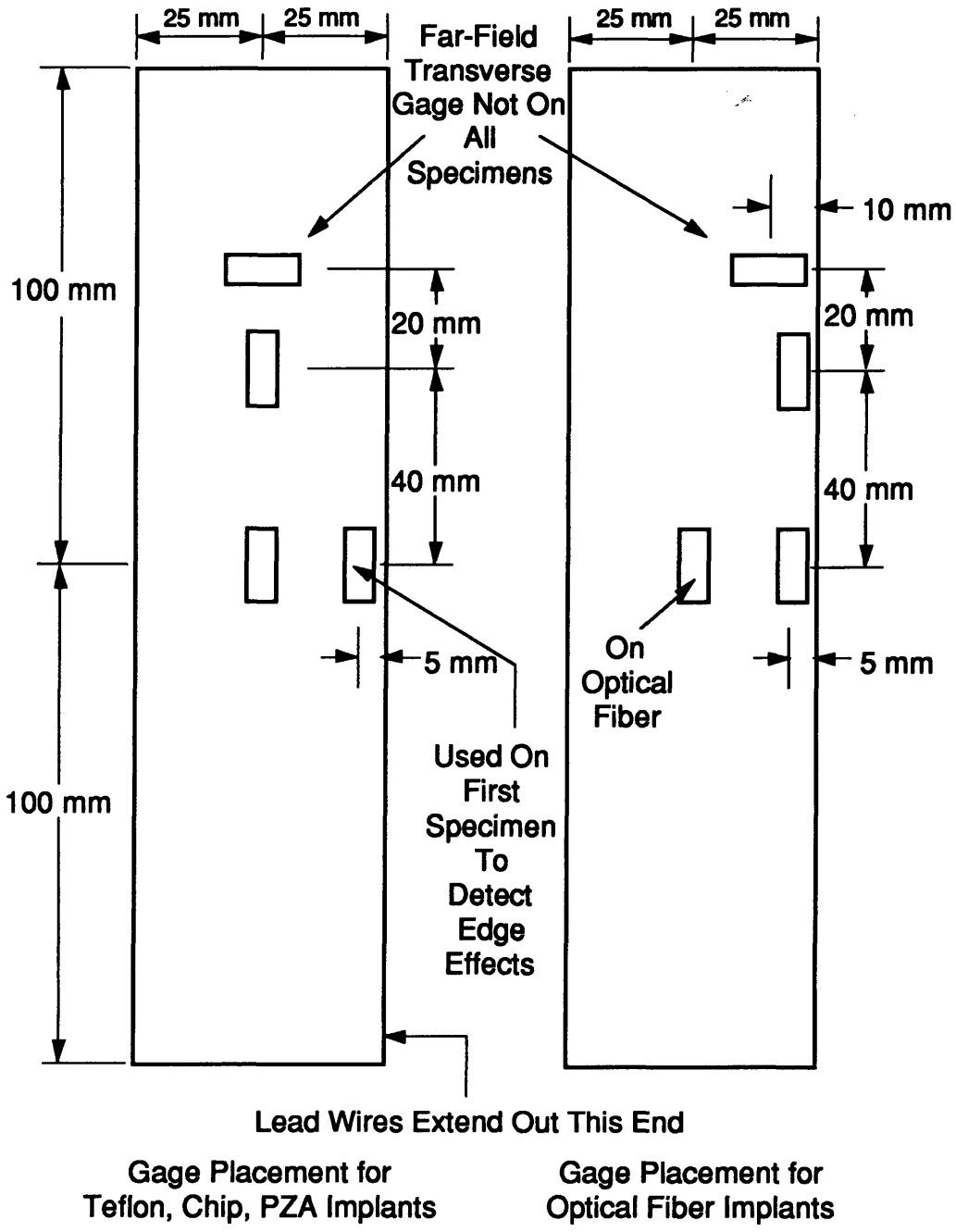

Figure 3.15 Strain Gage Placement for Specimens with Implants

3.4 Testing Procedure

All tensile testing was performed on a MTS-810 testing machine in the TELAC Laboratory. Data was taken using a Macintosh IIX computer through the LabView2 data acquisition software developed by National Instruments. The MacADIOS II Data Acquisition Board was manufactured by GW Instruments.

The coupons were placed in the upper hydraulic grips under a pressure of 566 MPa and were aligned using a triangle to ensure loading along the longitudinal axis of the specimen. The specimens were gripped over the entire surface of the loading tab to ensure even load distribution into the coupon. After one side of the coupon was gripped and the upper crosshead was lowered to align the lower loading tabs with the lower grips, the strain gages were balanced and calibrated and the load was zeroed out. The lower grip was then engaged.

All experiments were performed under stroke control. Layups 1, 2 and 3 were all performed with a stroke rate of 12.7 mm per 750 seconds. Layup 4 was tested with a stroke rate of 25.4 mm per 750 seconds. To reduce the amount of data taken, the stroke rate was increased for layup 4 which strained extensively but did not experience two piece failure.

All of the virgin specimens were tested to failure. The experimental procedure was to first fail two out of the five specimens from each layup/implant set. Of the remaining three coupons, one was left untested and one was tested to 90% of the ultimate stress determined by the two previously failed coupons. This specimen was examined after

testing by X-raying or sectioning with microscopic evaluation to detect any cracking or delamination around the implant. If any damage was detected, the last specimen was tested to 80% of the ultimate stress. In most cases, no damage was found at this level and the remaining specimen was loaded to 95% of the ultimate stress. Table 3.5 shows the number of specimens tested to failure for all of the virgin specimens made to each of the four layup configurations, and for each of the implant/layup combinations. Many of the coupons failed that were intended to be loaded to 95% of the ultimate stress. This is evident in Table 3.5 wherever three specimens were failed versus the intended two. Table 3.6 shows the breakdown of what testing was done for specimens loaded to a fraction of their ultimate stress. A discussion of the definition of failure versus 100% loading for layup 4 is given in Section 4.4.4. In addition to the tested coupons listed in Tables 3.5 and 3.6, there was an additional untested specimen for each implant/layup combination.

The X-ray procedure used to detect damage at the implant was not defined until after the virgin and first batch with implants was tested. The first batch with implants consisted of the 2TPZA, 2TC, 2PZA, 1CHIP and 1OF specimens. These specimens had DIB applied but the correct X-ray settings which would show the matrix cracks were not discovered until after testing and sectioning of most of these specimens. The only coupons that were still available for X-raying were 2TP-E and 2TP-B and 2PZA-E.

1,4-Diiodobutane (DIB) manufactured by Aldrich Chemical Company was applied to the edges of the coupons before or during testing for X-ray enhancement. The coupons that were tested to a

Table 3.5 Number of Failed Coupons For Each Layup/Implant Set

Implant	Layup			
	1 $[0/(\pm 45)_2/90/(\pm 45)_2]_S$	2 $[0/\pm 45/90]_{2S}$	3 $[45/0/-45/0/90/-45/0/-45/0/45]_S$	4 $[\pm 45]_{4S}$
Virgin Specimens	5	3(1)	5	5(2)
Circuit Chip Implants Placed in Cut Laminate	3	2	2	2
PZA Implants Placed in Cut Laminate	3	2	3	2
Optical Fibers Placed Directly in Laminate	2	3	3	2
Teflon Circuit Chip Placed in Cut Laminate	----	2	----	----
Teflon PZA Placed in Cut Laminate	----	2	----	----
Circuit Chip Placed Directly in Laminate	----	2	----	----
Optical Fibers Placed in Cut Laminate	----	2	----	----

(1) One coupon destroyed by accident during testing and one coupon used to experiment with techniques for detecting damage

(2) Strain data for three coupons only

Table 3.6 Testing to Partial Ultimate Strength

Implant	Layup			
	1 $[0/(\pm45)_2/90/(\pm45)_2]_s$	2 $[0/\pm45/90]_{2s}$	3 $[45/0/-45/0/90/-45/0/-45/0/45]_s$	4 $[\pm45]_{4s}$
Circuit Chip Implants Placed in Cut Laminate	1/90%	1/90% 1/95%	1/90% 1/95%	1/100% 1/80/90/100%
PZA Implants Placed in Cut Laminate	1/90%	2/90%	1/90%	1/100% 1/80/100%
Optical Fibers Placed Directly in Laminate	1/90% 1/95%	(3)	----	2/100%
Teflon Circuit Chip Placed in Cut Laminate	----	2/90%	----	----
Teflon PZA Placed in Cut Laminate	----	1/90% 1/95%	----	----
Circuit Chip Placed Directly in Laminate	----	1/90% (4)	----	----
Optical Fibers Placed in Cut Laminate	----	1/90% 1/80%	----	----

(3) Bad grips, stopped test for one coupon
(4) One coupon destroyed by accident during testing

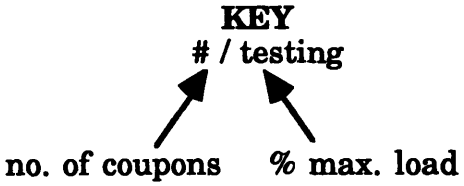

fraction of their ultimate stress were unloaded to 50% of their peak stress and then DIB was either applied or reapplied. The DIB had to be left on the coupons for a minimum of 20 minutes with several reapplications to allow it to penetrate through the entire width of the coupon through the matrix cracks. Even after the coupons were removed from the testing machine and sat for several weeks, DIB could be reapplied and would still penetrate through the matrix cracks across the width. All X-rays were taken on an X-Ray Inspection System Model 150D manufactured by Torrex. X-rays were taken at 30 kV for 105 seconds on Kodak Polaroid Film Type 52.

After all the coupons were X-rayed, some of the specimens were sectioned into 5 or 10 mm strips for microscopic examination. This examination revealed whether or not the implant was bonding well with the surrounding graphite/epoxy material and whether any damage was initiating through the thickness that would not be visible on an X-ray. X-rays were also taken of the failed specimens to determine if the failure occurred through the implant.

CHAPTER 4

Experimental Results

This chapter presents the stress-strain results, a description of the failure modes, and the results of the X-ray and sectioning investigation. The specimens that were either failed or loaded to a percentage of their ultimate stresses were evaluated to determine if and when damage initiated at the implant.

4.1 Manufacturing Results

Coupons made to layups 1 and 3 which were 20 plies thick had a nominal thickness of 2.70 mm with the assumption of a .135 mm single ply thickness. Coupons made to layups 2 and 4 which were 16 plies thick have a nominal thickness of 2.16 mm. The specimens were cut to a width as close to 50.0 mm as possible. The measured average thickness and width values for each tested specimen varied less than 3% from these values.

All of the specimens made to a layup 1 and 3 configuration had average thicknesses of 2.73 mm and 2.74 mm with coefficients of variation equal to .0318 and .043 respectively. The coefficient of variation

is the ratio of the standard deviation of the measured parameter to the mean value and is a good indication of the variability of the data. The average widths for these specimens were 50.61 mm and 50.15 mm with a coefficients of variation of .0137 and .0083 respectively. The specimens made to a layup 2 and 4 configuration had average thicknesses of 2.22 mm and 2.18 mm with coefficient of variations equal to .0263 and .0326 respectively. The average widths of these specimens were 50.30 and 50.37 mm with coefficient of variations equal to .0043 and .0032 respectively.

The elastic modulus was calculated using the applied load and strain away from the implant. The computer program LIN6 calculated the modulus from input strain and stress data [20]. The exact placement of the strain gages was described in Section 3.3. Table 4.1 shows the average moduli for each implant/layup combination. The moduli for the virgin specimens were compared to the predicted CLPT values given in Table 3.1. The moduli of the implanted specimens were compared to the moduli of the virgin specimens as noted at the bottom of the table. Experimental modulus values for coupons in batches 2TP, 2TC, 2PZA, 1CHIP and 1OF may be low by .98% because two different strain gages with gage factors that varied by 1.25% were used and placement of the gages with the higher gage factor was unknown.

4.2 Ultimate Stress Results

A comparison of the average failure stresses and coefficients of variation for each set of specimens with a particular implant and layup configuration is given in Table 4.2. Note that the values quoted for

Table 4.1 Summary of Elastic Moduli in GPa Away From Implant for all Manufactured and Tested Specimens

Implant	Layup			
	1 $[0/(\pm45)_2/90/(\pm45)_2]_S$	2 $[0/\pm45/90]_{2S}$	3 $[45/0/-45/0/90/-45/0/-45/0/45]_S$	4 $[\pm45]_{4S}$
Virgin Specimens	35.53 *-4.5%[a]*	53.62 *-3.4%[a]*	74.00 *+2.0%[a]*	21.06 *+2.6%[a]*
Circuit Chip Implants Placed in Cut Laminate	36.62* *-3.0%[b]*	52.99 *-1.1%*	71.53 *-3.4%*	20.32 *-6.5%*
PZA Implants Placed in Cut Laminate	34.06 *-3.9%*	52.53* *-1.9%*	71.90 *-2.8%*	22.49 *5.1%*
Optical Fibers Placed Directly in Laminate	35.55* *+.2%*	50.93 *-5.0%*	67.69 *-8.5%*	19.35 *-9.3%*
Teflon Circuit Chip Placed in Cut Laminate	----	53.80* *0%*	----	----
Teflon PZA Placed in Cut Laminate	----	54.54* *1.9%*	----	----
Circuit Chip Placed Directly in Laminate	----	51.50 *-3.9%*	----	----
Optical Fibers Placed in Cut Laminate	----	53.75 *+0.4%*	----	----

* Possible .98% error due to untracked strain gage gage factor

a Percentage difference from CLPT predicted values

b Percentage difference from virgin specimens

Table 4.2 Comparison of Average Failure Stresses in MPa Between Virgin and Implanted Specimens

Implant	Layup			
	1 $[0/(\pm45)_2/90/(\pm45)_2]_s$	2 $[0/\pm45/90]_{2s}$	3 $[45/0/-45/0/90/-45/0/-45/0/45]_s$	4 $[\pm45]_{4s}$
Virgin Specimens	406 C.V. = .046	682 C.V. = .014	923 C.V. = .019	157 C.V. = .068
Circuit Chip Implants Placed in Cut Laminate	405 *-0.2%* C.V. = .052	641 *-5.9%* C.V. = .090	787 *-14.8%* C.V. = .028	159 *1.2%* C.V. = .062
PZA Implants Placed in Cut Laminate	407 *0.2%* C.V. = .052	590 *-13.6%* C.V. = .0024	778 *-15.7%* C.V. = .052	166 *5.7%* C.V. = 0
Optical Fibers Placed Directly in Laminate	434 *7.0%* C.V. = .0083	604 *-11.5%* C.V. = .037	799 *-13.4%* C.V. = .073	166 *5.7%* C.V. = 0
Teflon Circuit Chip Placed in Cut Laminate	----	616 *-9.7%* C.V. = .129	----	----
Teflon PZA Placed in Cut Laminate	----	639 *-6.3%* C.V. = .0103	----	----
Circuit Chip Placed Directly in Laminate	----	622 *-8.7%* C.V. = .058	----	----
Optical Fibers Placed in Cut Laminate	----	615 *-9.8%* C.V. = .067	----	----

C.V. = Coefficient of Variation

specimens made to a layup 4 configuration are peak stress values and not the stress associated with a two-piece failure. None of these specimens were tested to two-piece failure. The stress in each coupon was based on the measured cross-sectional area given in Appendix A. The average ultimate stress values for each implant/layup combination were compared to the ultimate stresses of the virgin specimens as indicated by the percent deviation listed below the average stress value. When the specimens failed at the implant, the ultimate stress was reduced up to 12% in comparison to the specimens that failed away from the implant containing the same implant and layup configuration. Table 4.3 shows a comparison of average failure stresses with the distinction between failure at or away from the implant for specimens with a layup 1 or 2 configuration. Table 4.4 shows the same comparison for specimens with a layup 3 or 4 configuration. The percent deviation between these ultimate stress values and the virgin specimens' failure stresses is also given in Tables 4.3 and 4.4. Appendix B contains the individual ultimate stresses of each of the failed specimens. The significance of these results as regards sample size and coefficients of variation is discussed in chapter 5. The following is a brief discussion of the average ultimate stress values relative to the virgin ultimate stresses for each implant/layup combination.

Table 4.3 Comparison of Failure Stresses in MPa Between Virgin and Implanted Specimens in Layups 1 and 2 When Failure Occurred At or Away From Implant

Implant	Layup			
	1 $[0/(\pm45)_2/90/(\pm45)_2]_s$		2 $[0/\pm45/90]_{2s}$	
	Failure Away From Implant	Failure At Implant	Failure Away From Implant	Failure At Implant
Virgin Specimens	406	----	682	----
Circuit Chip Implants Placed in Cut Laminate	437 *(7.7%)* [a]	389 *(4.1%)*	682 *(.04%)*	600 *(-12.0%)*
PZA Implants Placed in Cut Laminate	419 *(3.2%)*	385 *(-5.2%)*	----	590 *(-13.6%)*
Optical Fibers Placed Directly in Laminate	----	434 *(7.1%)*	----	604 *(-11.5%)*
Teflon Circuit Chip Placed in Cut Laminate	----	----	616 *(-9.7%)*	----
Teflon PZA Placed in Cut Laminate	----	----	639 *(-6.3%)*	----
Circuit Chip Placed Directly in Laminate	----	----	630 *(-8.7%)*	----
Optical Fibers Placed in Cut Laminate	----	----	----	615 *(-9.8%)*

[a] Percentage Difference From Virgin Specimen Average Ultimate Stress

Table 4.4 Comparison of Failure Stresses in MPa Between Virgin and Implanted Specimens In Layups 3 and 4 When Failure Occurred At or Away From Implant

Implant	Layup			
	3 $[45/0/-45/0/90/-45/0/-45/0/45]_s$		4 $[\pm 45]_{4s}$	
	Failure Away From Implant	Failure At Implant	Failure Away From Implant	Failure At Implant
Virgin Specimens	923	----	157	----
Circuit Chip Implants Placed in Cut Laminate	----	787 *(-14.8%)* [a]	----	159 *(1.2%)*
PZA Implants Placed in Cut Laminate	----	799 *(-13.4%)*	----	166 *(5.7%)*
Optical Fibers Placed Directly in Laminate	820 *(-11.1%)*	757 *(-18.0%)*	----	166 *(5.7%)*

[a] Percentage Difference From Virgin Specimen Average Ultimate Stress

4.2.1 Ultimate Stresses for Implanted Specimens with a Layup 1, $[0/(\pm 45)_2/90/(\pm 45)_2]_S$, Configuration

The average ultimate stresses for the implanted coupons made with the layup 1 orientation, which was $[0/(\pm 45)_2/90/(\pm 45)_2]_S$, varied the least of the four layup configurations and were within 8% of the virgin specimens' average ultimate stress. The specimens with optical fiber implants had a 7% higher average ultimate stress than the virgin samples. This trend was also present for coupons with the chip and PZA implants that did not fail at the implants. These specimens had average ultimate stresses 7.7% and 3.2% higher respectively than the virgin coupons. The specimens with chip and PZA implants that failed at the implant had a 4.1% and 5.2% respectively reduced ultimate stress compared to the virgin specimens.

4.2.2 Ultimate Stresses for Implanted Specimens with a Layup 2, $[0/\pm 45/90]_{2S}$, Configuration

The average ultimate stresses for all the coupons with implants made with the layup 2 orientation were reduced relative to the virgin specimens by 6.3% to 13.6% which corresponds to the specimens with the teflon PZA and actual PZA implants respectively. Recall that layup 2 was defined as having fiber orientations of $[0/\pm 45/90]_{2S}$. The specimens with a teflon chip implant failed with an ultimate stress 3.8% less than

specimens with the actual chip and did not fail at the implant. The specimens with a teflon PZA failed with an average ultimate stress 7.3% less than specimens with the actual PZA and also did not fail at the implant. Recall that the teflon PZA was thinner than the actual PZA because the actual PZA had the polyimide tape coating and the single ply thick lead wires. The average failure stress for all of the specimens with the chip implant placed directly into the laminate was 3% less than the failure stress for all of the specimens with the chip implants placed in a cut laminate. The teflon chip implanted specimens did not have failure occur at the implant. When the actual chip implanted specimens failed at the implant, their failure stress was 2.3% worse than the teflon chips. The optical fiber placed in a cut laminate had a failure stress 1.7% lower than the optical fiber placed directly into the laminate.

4.2.3 Ultimate Stresses for Implanted Specimens with a Layup 3, $[45/0/-45/0/90/-45/0/-45/0/45]_S$, Configuration

The largest reduction in ultimate stress due to the implants occurred for specimens with a layup 3 orientation which was $[45/0/-45/0/90/-45/0/-45/0/45]_S$. The specimens with optical fibers, circuit chips and PZA implants had a reduction of ultimate stress relative to the virgin specimens of 13.4%, 14.8% and 18.0% respectively. One coupon with a PZA implant did not fail at the implant but still had an 11.1% reduction in ultimate stress.

4.2.4 Peak Stresses for Implanted Specimens with a Layup 4, $[\pm 45]_{4S}$, Configuration

Specimens with a layup 4 configuration, $[\pm 45]_{4S}$, were not tested to two-piece failure. A comparison of the peak stress values indicated that the peak stress was not affected by the implants.

4.3 Stress-Strain Curve Results

All of the curves show stress plotted against calculated and experimental longitudinal strain. The calculated strain values were based on the theoretical moduli calculated by classical laminated plate theory and the applied load. The experimental longitudinal strain values were measured at the center of the specimen and also away from the implant for specimens with implants. The exact location of all the strain gages is given in Section 3.3.

Experimental strain values for several coupons in batches 2TP, 2TC, 2PZA, 1CHIP and 1OF may be high by 1.25% because two different strain gages with gage factors that varied by 1.25% were used but the placement of the gages with the higher gage factor were not recorded. This error is noted on the stress-strain plots of any coupons affected by this experimental error.

The stress-strain curves do not always start from the origin because the specimens were tested on two different tensile machines. One machine put the specimen into compression when it was gripped and the other machine put the specimen into tension when it was gripped. The initial data for the coupons that were put into compression

when gripped is not shown in these curves as they all start from the origin.

4.3.1 Stress-Strain Curves for Virgin Specimens

A typical stress-strain plot for the virgin specimens with layup 1 is shown in Figure 4.1 by coupon 1V-E. The theoretical and experimental elastic moduli agreed at stresses below 172 MPa. After this point, the specimens exhibited slightly nonlinear behavior and had a lower modulus value than the theoretical value.

The typical stress-strain plot for a virgin specimen made to layup 2 configuration is given in Figure 4.2 by coupon 2V-A. The experimental strain data was linear up to 138 MPa; however, it was less than the theoretical strain values. After this point, the nonlinear behavior caused a continual decrease in the elastic modulus until failure at 675 MPa.

The stress-strain plots for virgin specimens made to a layup 3 and 4 configuration are given in Figures 4.3 and 4.4 respectively by coupons 3V-B and 4V-A. The specimens with a layup 3 orientation had moduli that varied the least from the theoretical value of all four layup configurations. Figure 4.4 shows the highly nonlinear behavior typical of specimens made with layup 4 ply orientations. This specimen behaved similarly to the theoretical linear prediction only up to a stress of 52 MPa.

The remaining plots for virgin specimens made to layup 1, 2, 3 and 4 are given in Appendix C.

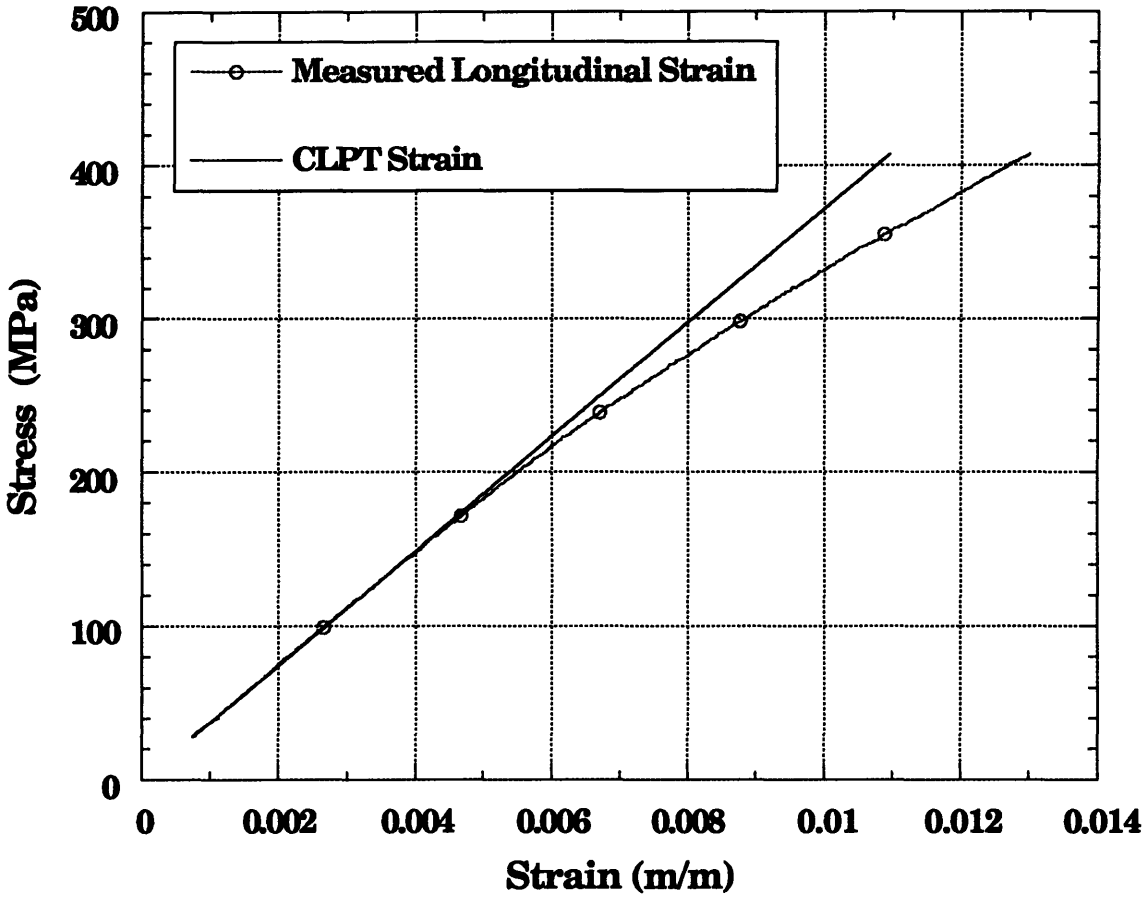

Figure 4.1 Stress-Strain Curves for Virgin Coupon 1V-E with a Layup 1, $[0/(\pm 45)_2/90/(\pm 45)_2]_S$, Configuration Tested to Failure

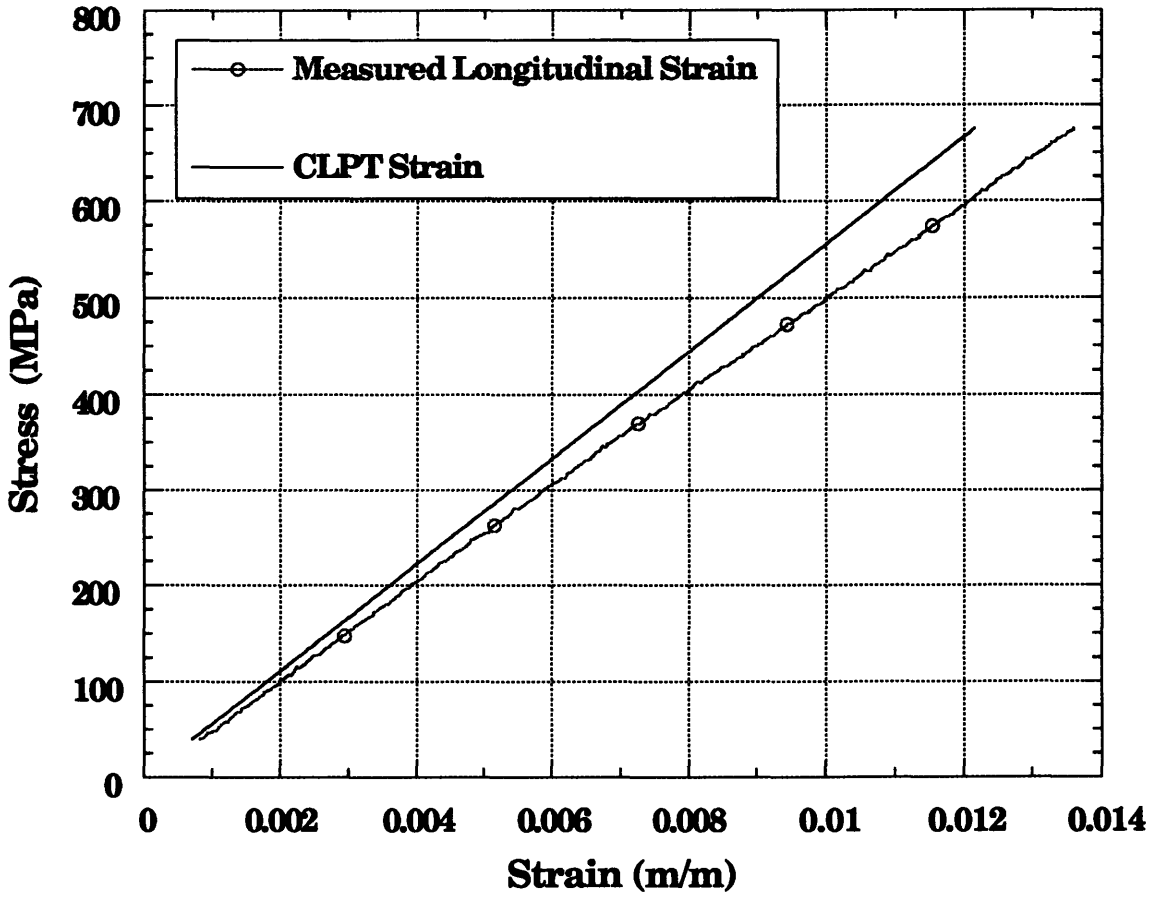

Figure 4.2 Stress-Strain Curves for Virgin Coupon 2V-A with a Layup 2, $[0/\pm45/90]_{2s}$, Configuration Tested to Failure

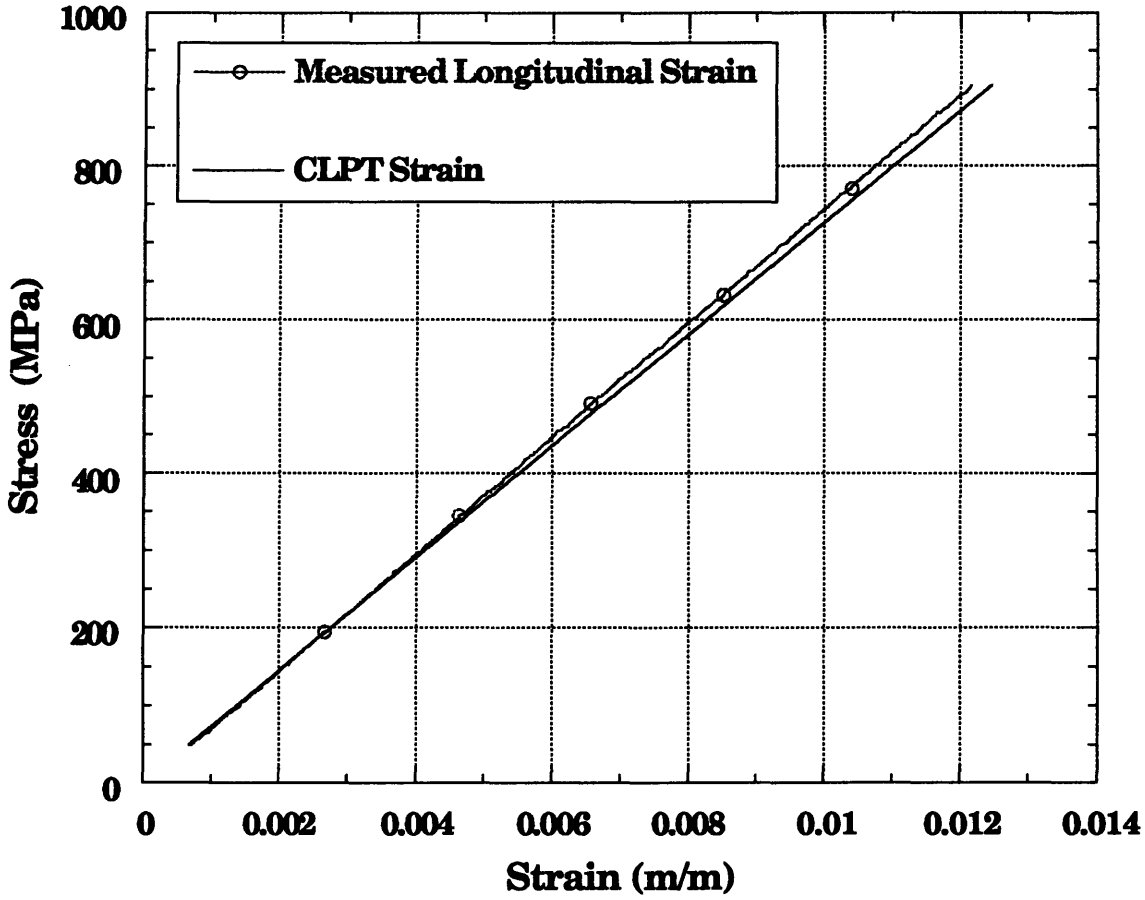

Figure 4.3 Stress-Strain Curves for Virgin Coupon 3V-B with a Layup 3, $[45/0/-45/0/90/-45/0/-45/0/45]_S$, Configuration Tested to Failure

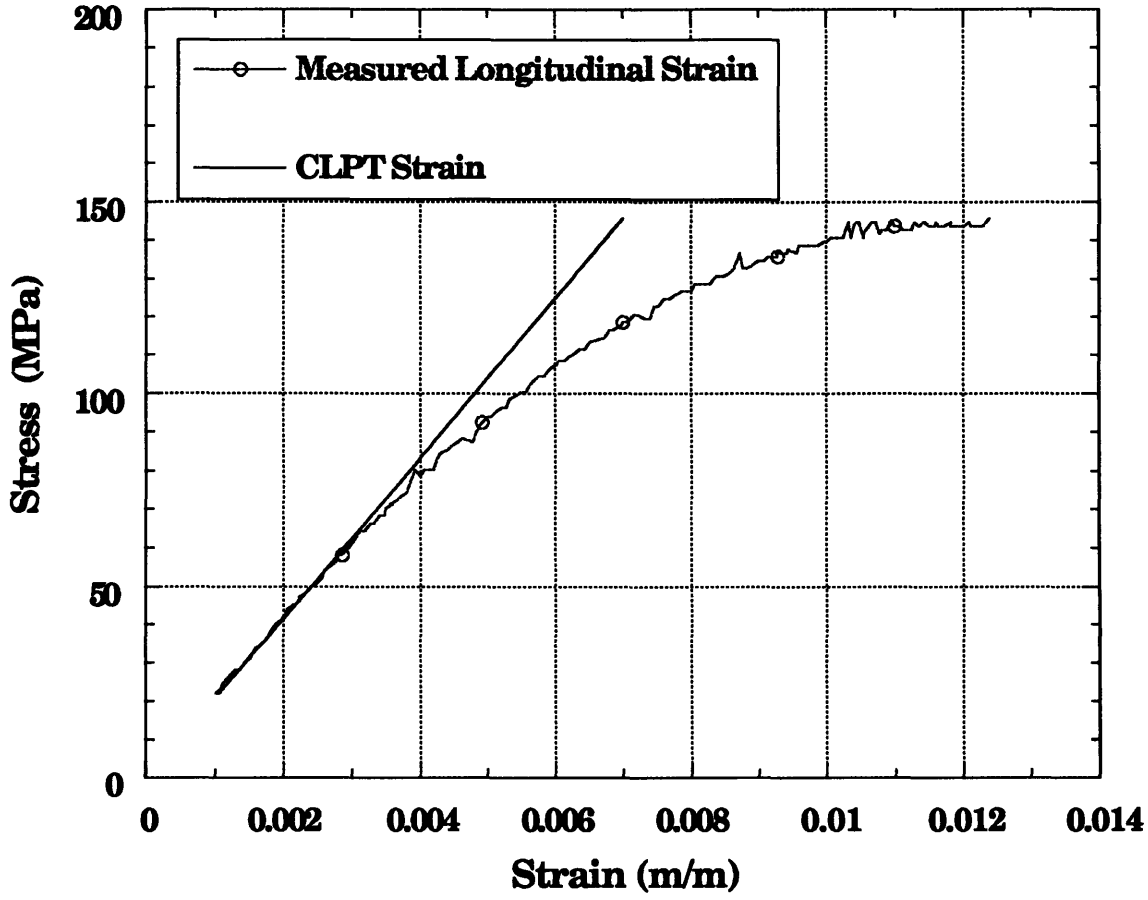

Figure 4.4 Stress-Strain Curves for Virgin Coupon 4V-A with a Layup 4, $[\pm 45]_{4S}$, Configuration Tested to 100% of its Peak Stress

4.3.2 Stress-Strain Curves for Specimens with a Layup 1, $[0/(\pm 45)_2/90/(\pm 45)_2]_S$, Configuration

Typical stress-strain curves for the optical fiber, chip and PZA implants in layup 1 are given in Figures 4.5-4.7 respectively. Similarly to the curves for the virgin specimens, these curves give a comparison between strain derived from the calculated laminated plate theory modulus value and the experimentally determined longitudinal strain directly over and far-field of the implant. Note that the strain gage measured average strain across the area of the gage only. Strain concentrations directly around the implant could not be measured. The gages placed over the optical fibers were especially insensitive to the small area around the optical fiber. The strain gages over the implant typically measured an increased strain due to the implant versus the far-field strain. All experimental strain values were less than the theoretical strain. The strains also deviated from the theoretical values earlier in the testing than did the virgin specimens. The curves for the remaining specimens with implants and a layup 1 ply orientation are given in Appendix D.

4.3.3 Stress-Strain Curves for Specimens with a Layup 2, $[0/\pm 45/90]_{2S}$, Configuration

Typical stress-strain curves for specimens with a layup 2 orientation with the optical fiber, chip, PZA, teflon chip and teflon PZA

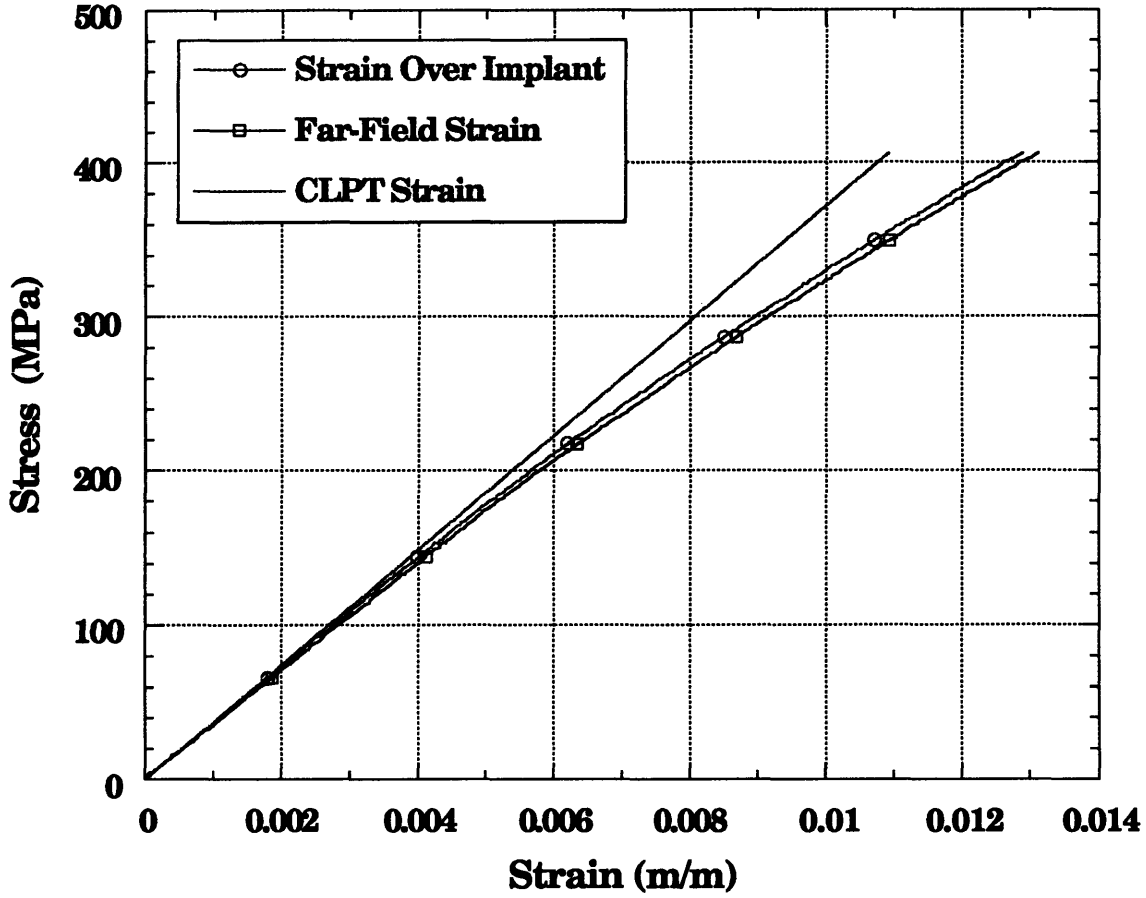

Figure 4.5 Stress-Strain Curves for Coupon 10F-D with a Layup 1, $[0/(\pm 45)_2/90/(\pm 45)_2]_S$, Configuration Tested to 95% of its Ultimate Stress

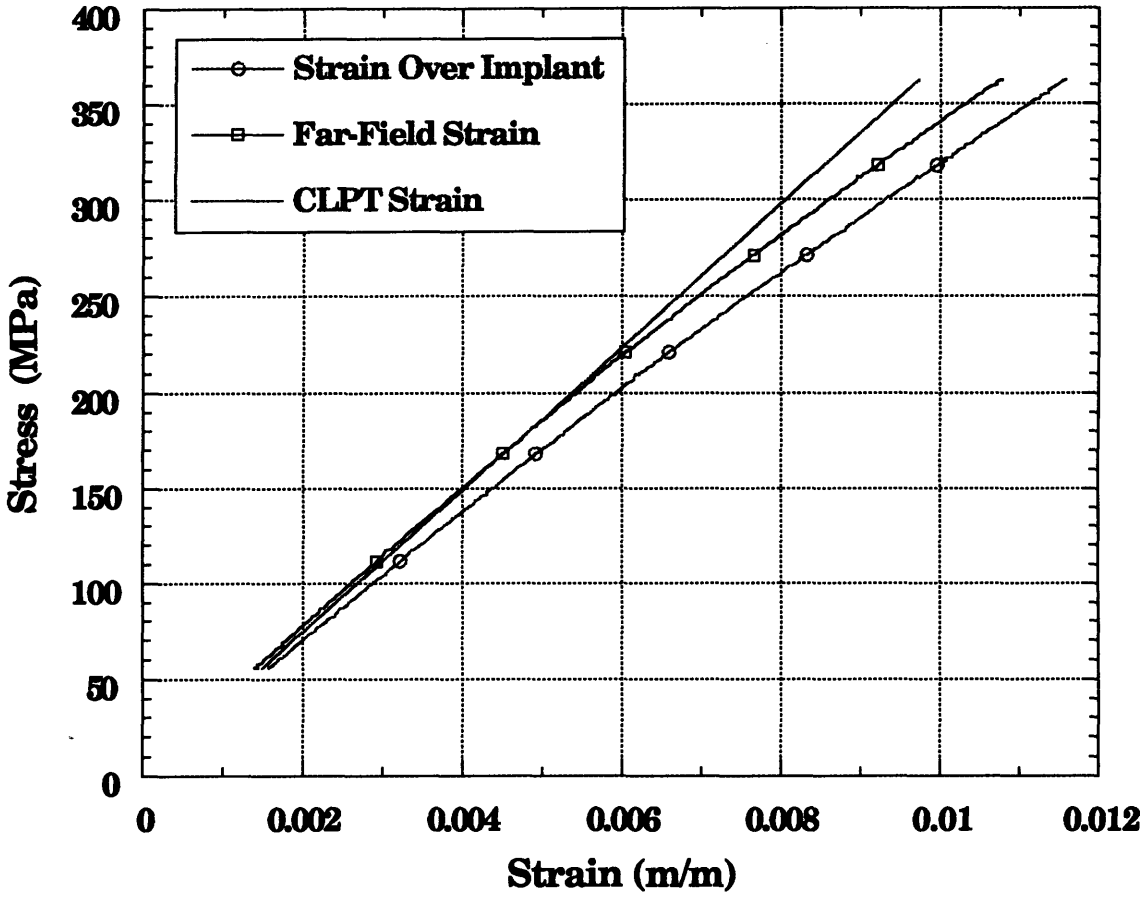

Figure 4.6 Stress-Strain Curves for Coupon 1CHIP-D with a Layup 1, $[0/(\pm 45)_2/90/(\pm 45)_2]_S$, Configuration Tested to Failure

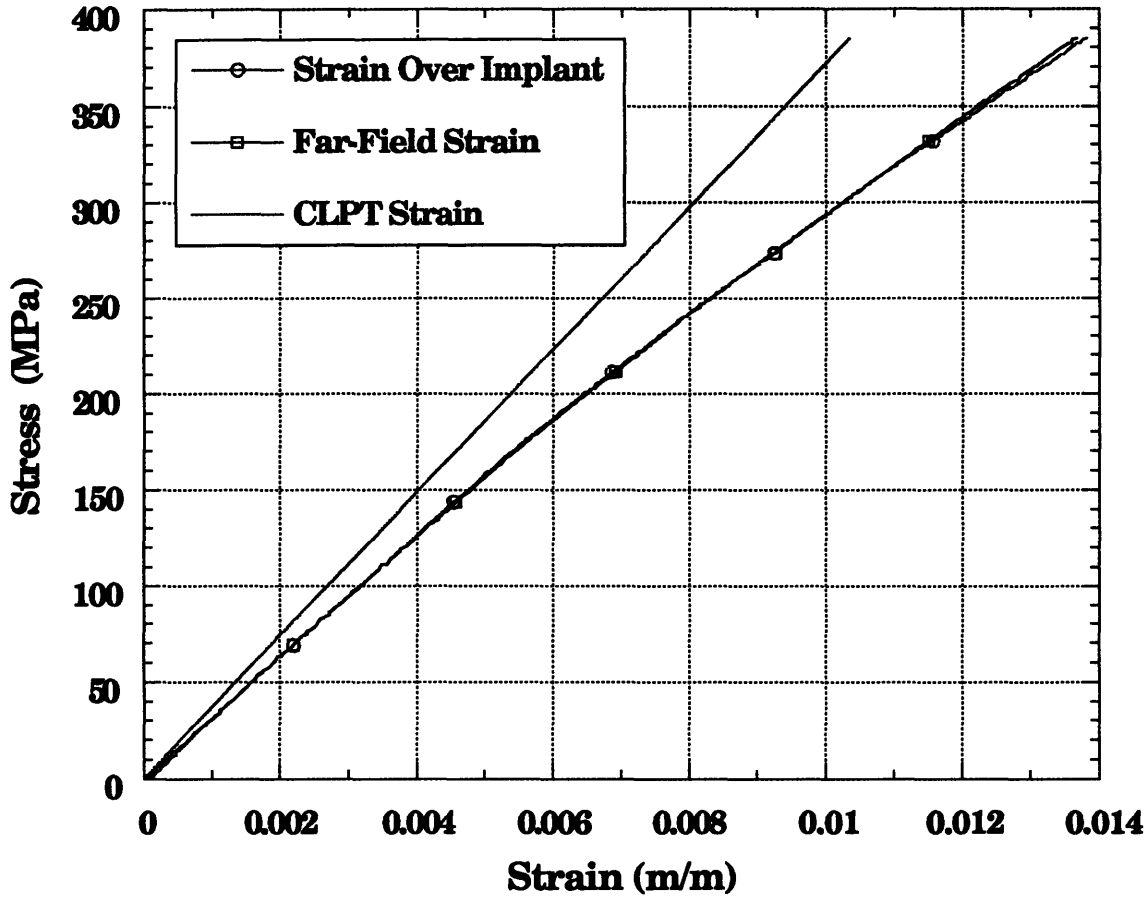

Figure 4.7 Stress-Strain Curves for Coupon 1PZA-E with a Layup 1, $[0/(\pm 45)_2/90/(\pm 45)_2]_S$, Configuration Tested to 90% of its Ultimate Stress

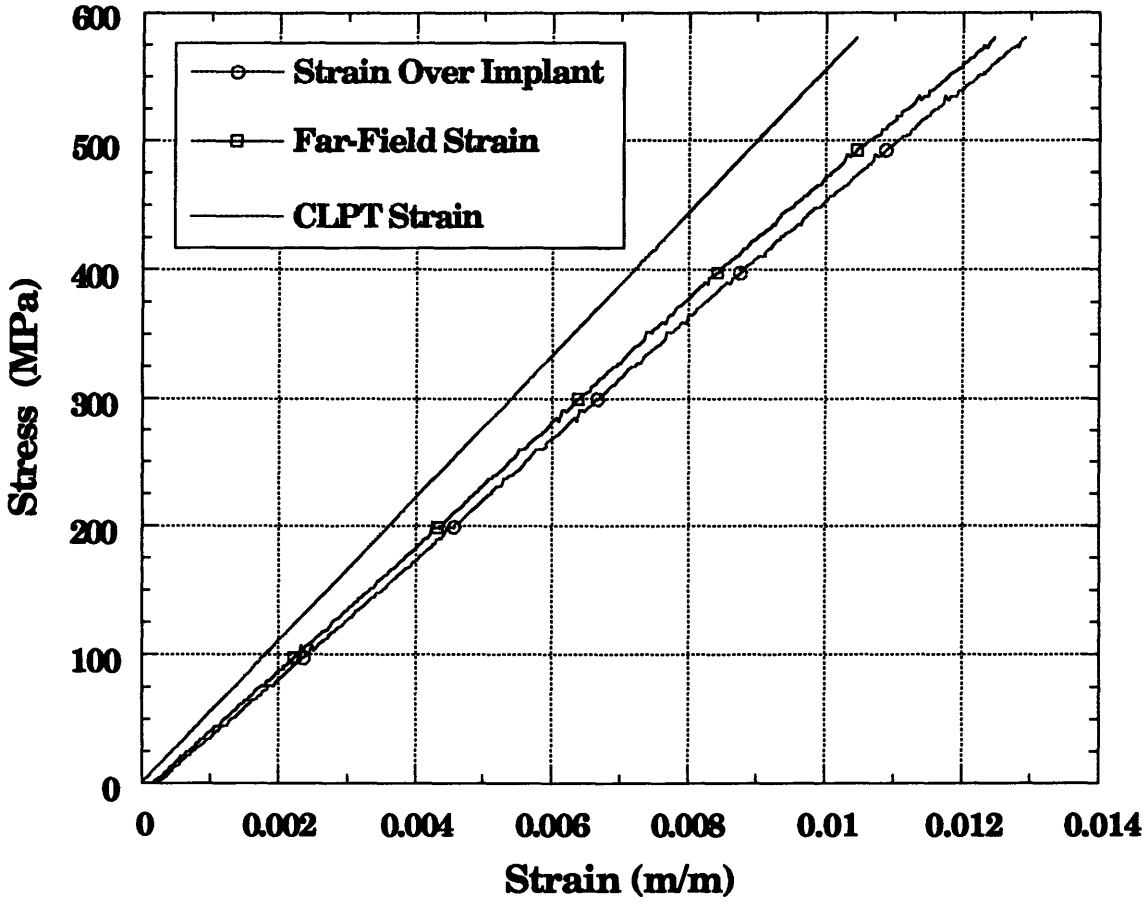

Figure 4.8 Stress-Strain Curves for Coupon 2OF-E with Optical Fiber Placed Directly in Laminate with a Layup 2, $[0/\pm45/90]_{2s}$, Configuration Tested to Failure

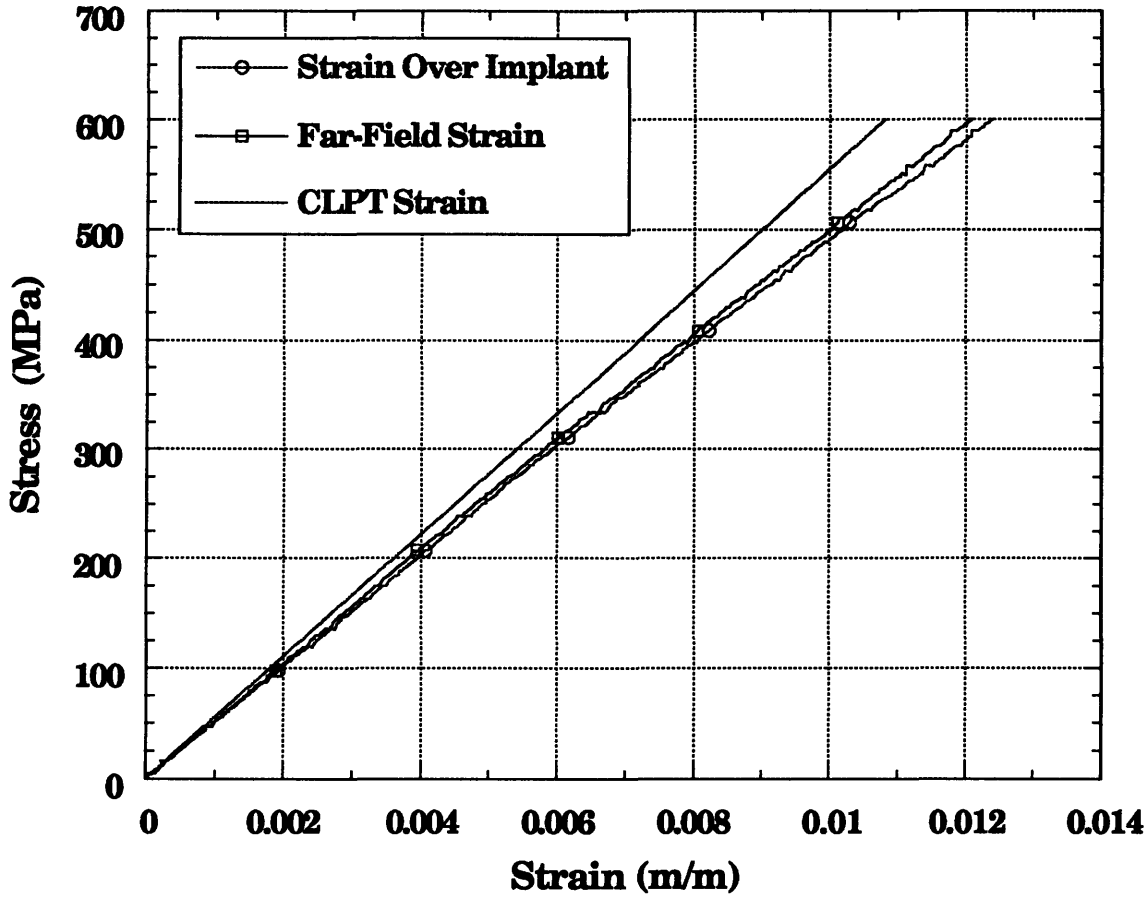

Figure 4.9 Stress-Strain Curves for Coupon 2CHIP-A Tested to Failure with Chip Placed in Cut Laminate with a Layup 2, $[0/\pm45/90]_{2S}$, Configuration

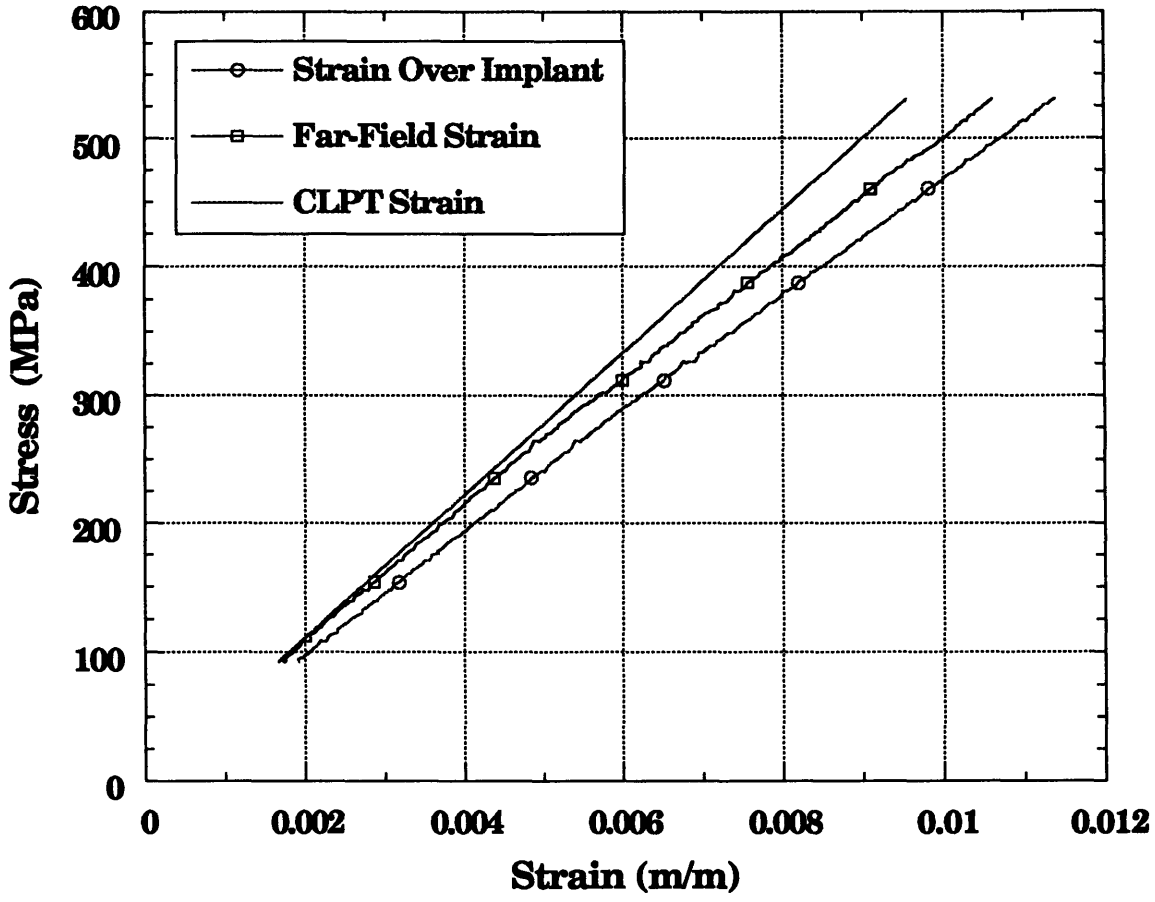

Figure 4.10 Stress-Strain Curves for Coupon 2PZA-E with a Layup 2, $[0/\pm45/90]_{2s}$, Configuration Tested to 90% of its Ultimate Stress

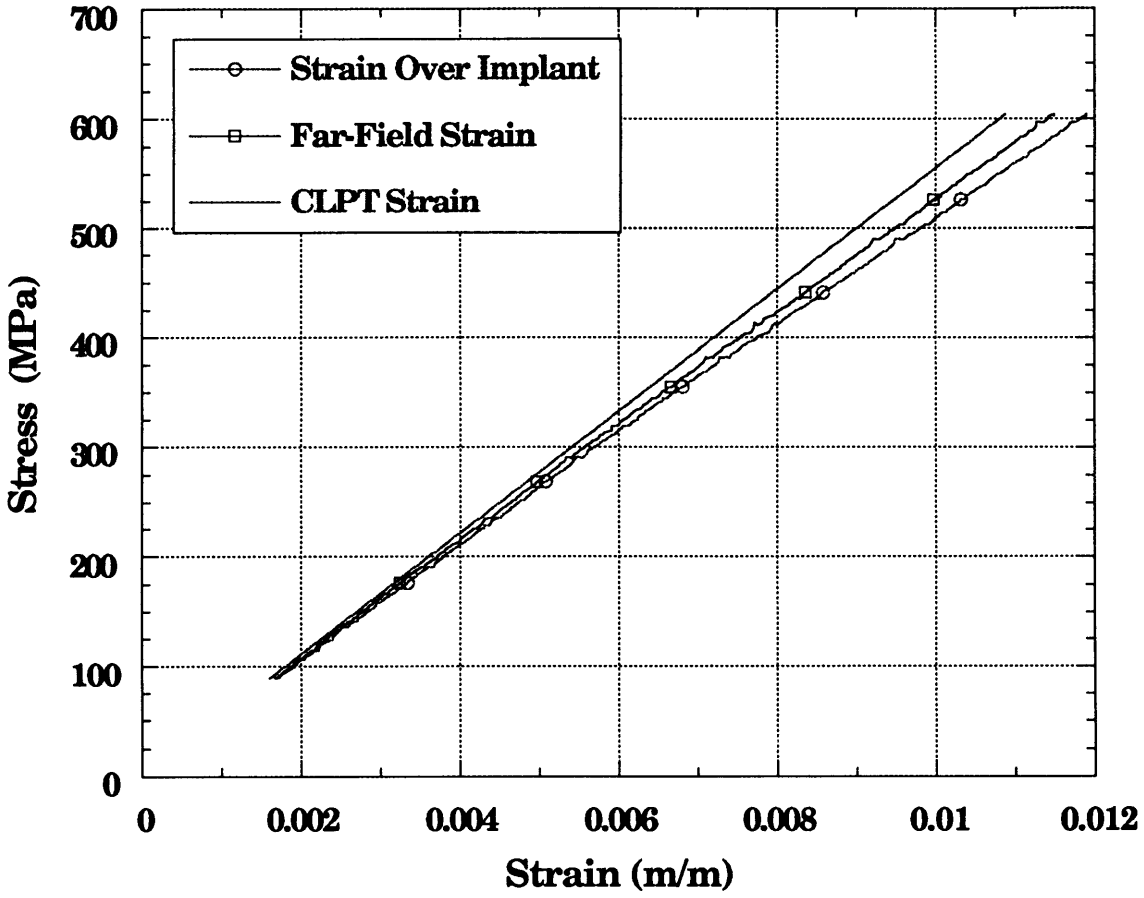

Figure 4.11 Stress-Strain Curves for Coupon 2TC-C with a Layup 2, $[0/\pm45/90]_{2s}$, Configuration Tested to 90% of its Ultimate Stress

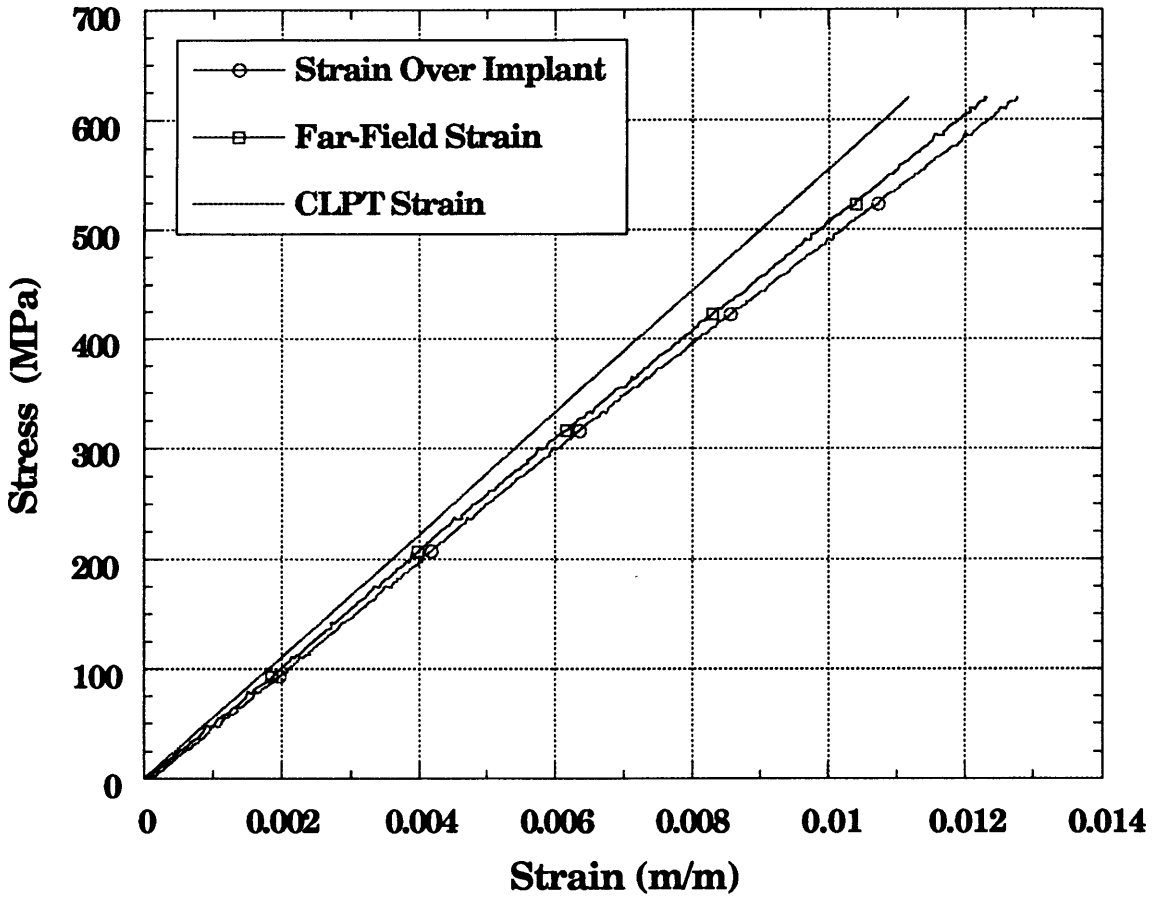

Figure 4.12 Stress-Strain Curves for Coupon 2TP-E with a Layup 2, $[0/\pm45/90]_{2s}$, Configuration Tested to 95% of its Ultimate Stress

implants are given in Figures 4.8-4.12 respectively. Curves for specimens with the chip placed directly into the laminate and the optical fiber that was placed in a cut-out area are given in Figures 4.13 and 4.14 respectively. Similarly to the specimens with implants of layup 1 orientation, the strain values directly over the implant were greater than the strain values away from the implant at the same loading condition. Both experimental strain values were greater than the theoretical values even at low stresses. This deviation from theoretical prediction at low stresses was also seen for the virgin specimens. Curves for the remaining specimens with implants made to a layup 2 configuration are given in Appendix E.

4.3.4 Stress-Strain Curves for Specimens with a Layup 3, $[45/0/-45/0/90/-45/0/-45/0/45]_S$, Configuration

The typical stress-strain curves for specimens with a layup 3 configuration with the optical fiber, chip and PZA implants are given in Figures 4.15-4.17 respectively. The specimen with the optical fiber implant strained more than the virgin specimen at all stress levels. The strain over the optical fiber was less than the far-field strain by 5% which was unusual for most implanted specimens. This difference was within the experimental error of the gages especially since the optical fiber was small relative to the strain gage. Unlike the virgin specimen, the specimen with the chip implant also strained more than the virgin specimens but behaved linearly. The specimen with the PZA implant had a longitudinal strain away from the implant that corresponded

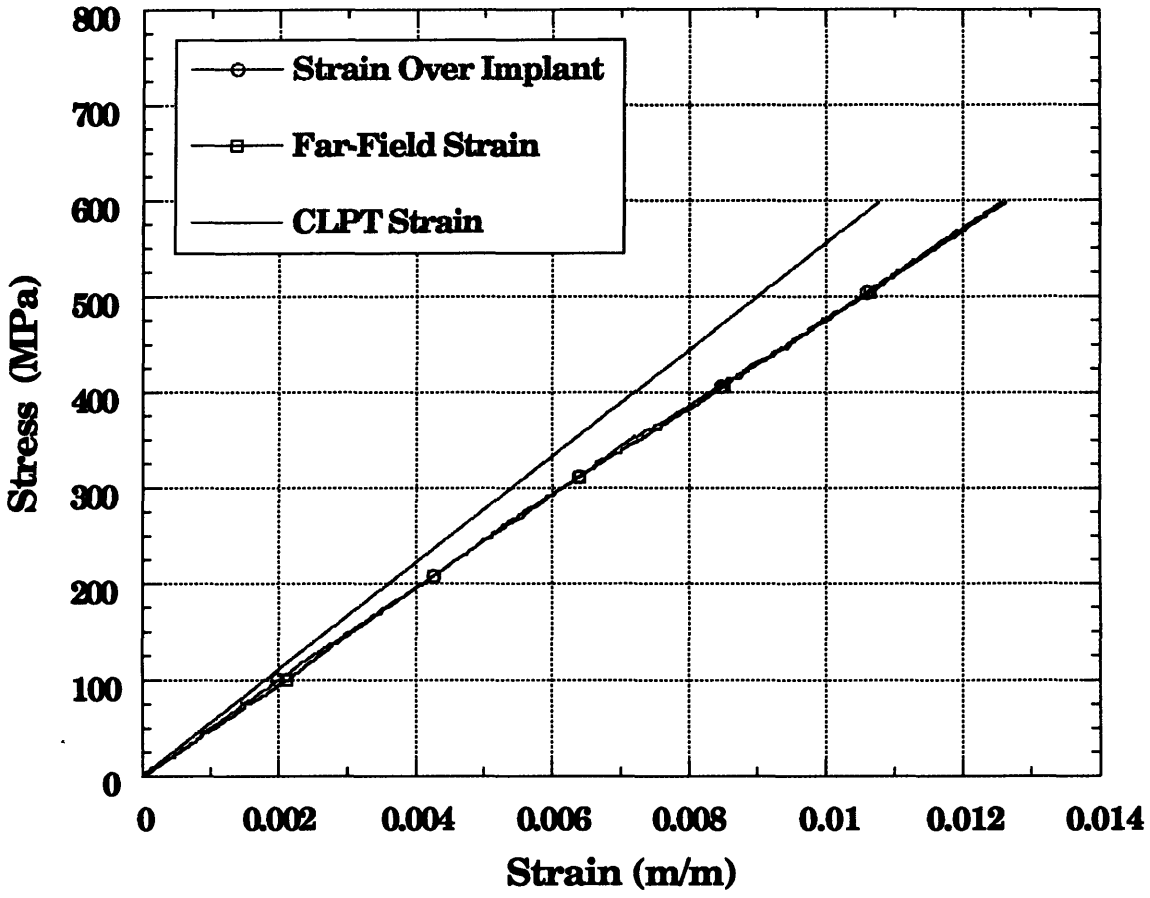

Figure 4.13 Stress-Strain Curves for Coupon 2CHIP-A Tested to 90% of its Ultimate Stress with Chip Placed Directly in Laminate with a Layup 2, $[0/\pm45/90]_{2s}$, Configuration

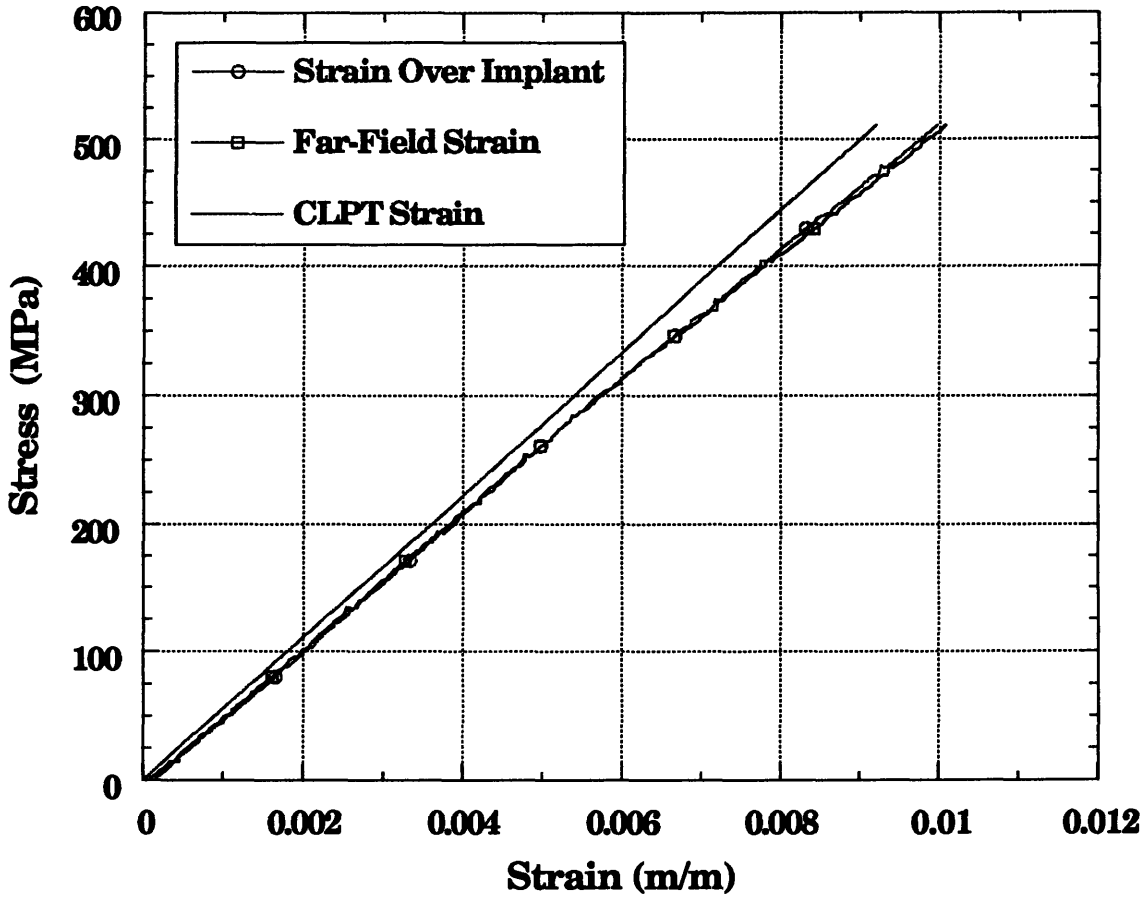

Figure 4.14 Stress-Strain Curves for Coupon 2OF-C Tested to 90% of its Ultimate Stress with Optical Fiber Placed in Cut Laminate with a Layup 2, $[0/\pm45/90]_{2s}$, Configuration

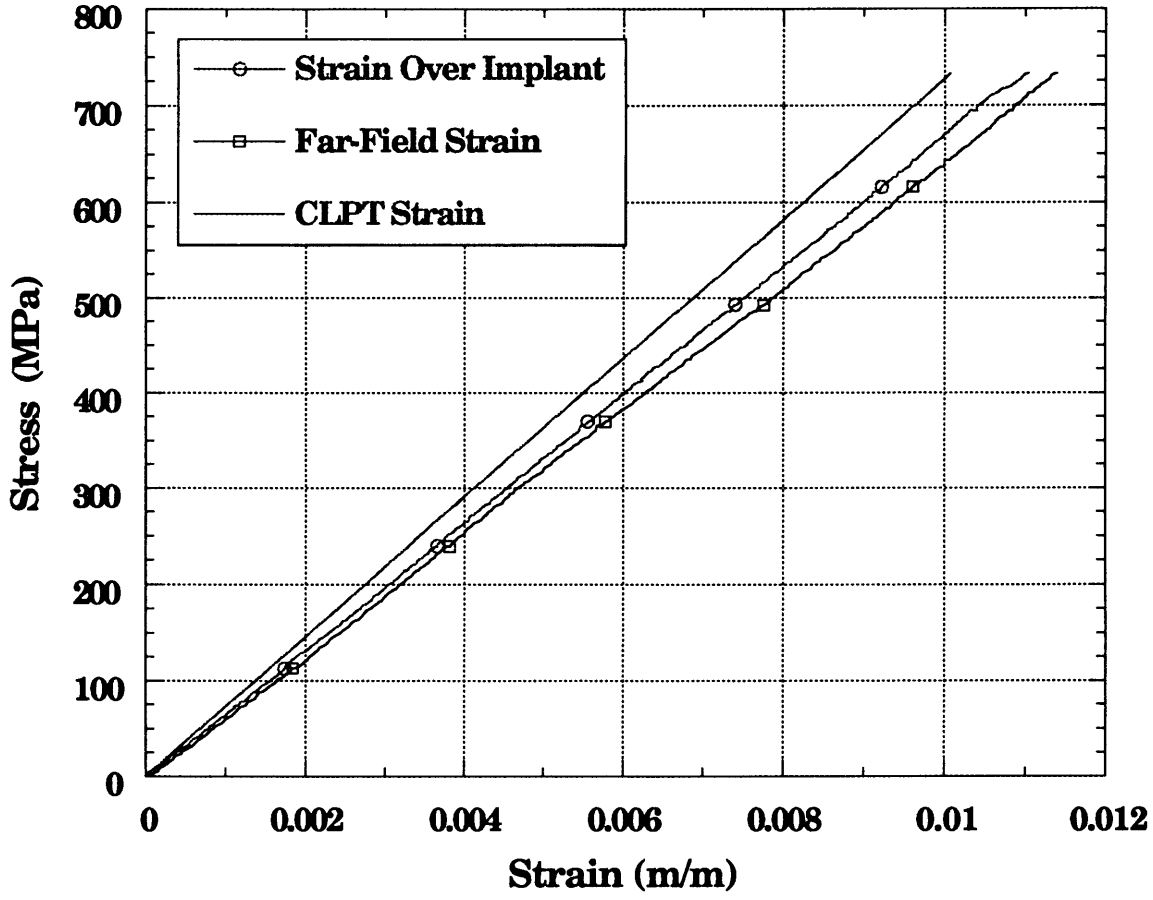

Figure 4.15 Stress-Strain Curves for Coupon 3OF-E with a Layup 3, $[45/0/-45/0/90/-45/0/-45/0/45]_S$, Configuration Tested to Failure

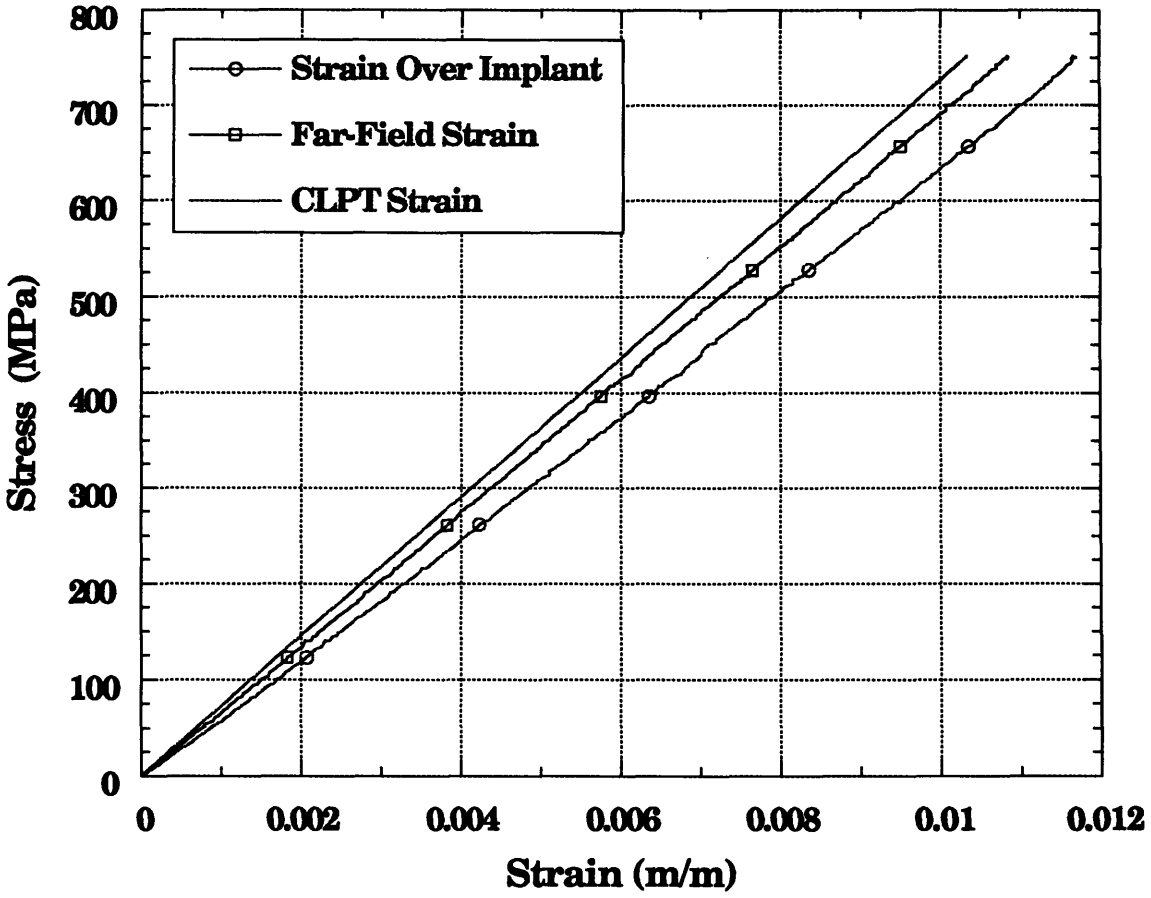

Figure 4.16 Stress-Strain Curves for Coupon 3CHIP-E with a Layup 3, $[45/0/-45/0/90/-45/0/-45/0/45]_S$, Configuration Tested to 95% of its Ultimate Strength

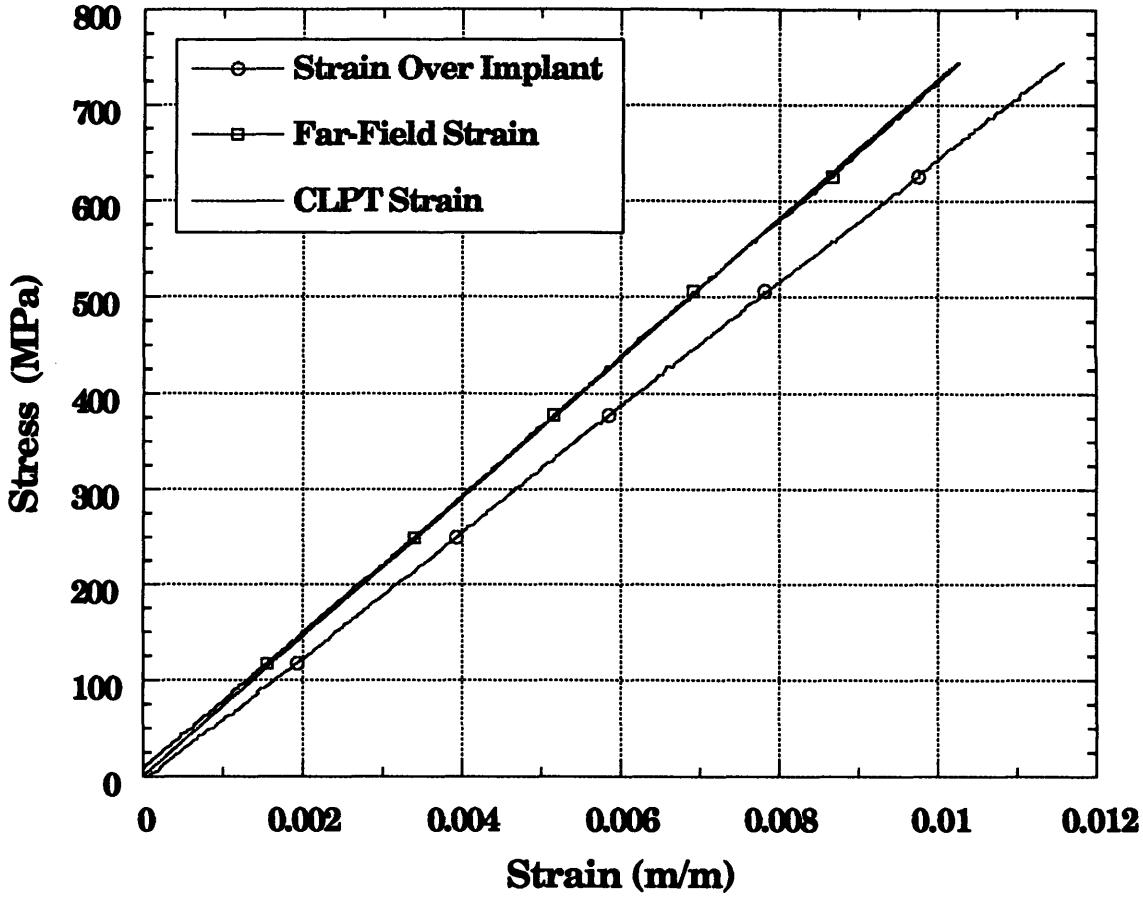

Figure 4.17 Stress-Strain Curves for Coupon 3PZA-D with a Layup 3, $[45/0/-45/0/90/-45/0/-45/0/45]_S$, Configuration Tested to Failure

closely to the theoretical strain value. The strain over the PZA implant was higher than the strain away from the implant indicating the strain concentration due to the implant. The remaining stress-strain plots for all coupons with a layup 3 configuration are given in Appendix F.

4.3.5 Stress-Strain Curves for Specimens with a Layup 4, $[\pm 45]_{4S}$, Configuration

Typical stress-strain curves for specimens with a layup 4 configuration with optical fiber, chip and PZA implants are given in Figures 4.18-4.20 respectively. The strain far-field of the implants behaved similarly to the virgin specimens by following the theoretical prediction up to 52 MPa before behaving nonlinearly. The measured strain directly over the implant was higher than the predicted strain from the beginning of the test and continued to increase relative to the far-field stress by up to 40% at the peak stress value. The remaining curves for specimens with implants are given in Appendix G.

4.4 Failure Modes

The mode of failure for the specimens with implants often varied from the failure mode of the virgin specimens. A general description of the failure modes for the virgin specimens with a particular layup configuration is presented followed by a description of the failure modes for the specimens with implants. The descriptions include differences in the location of failure, amount of delamination, amount of fiber splitting on the upper plies, and orientation of the break due to the

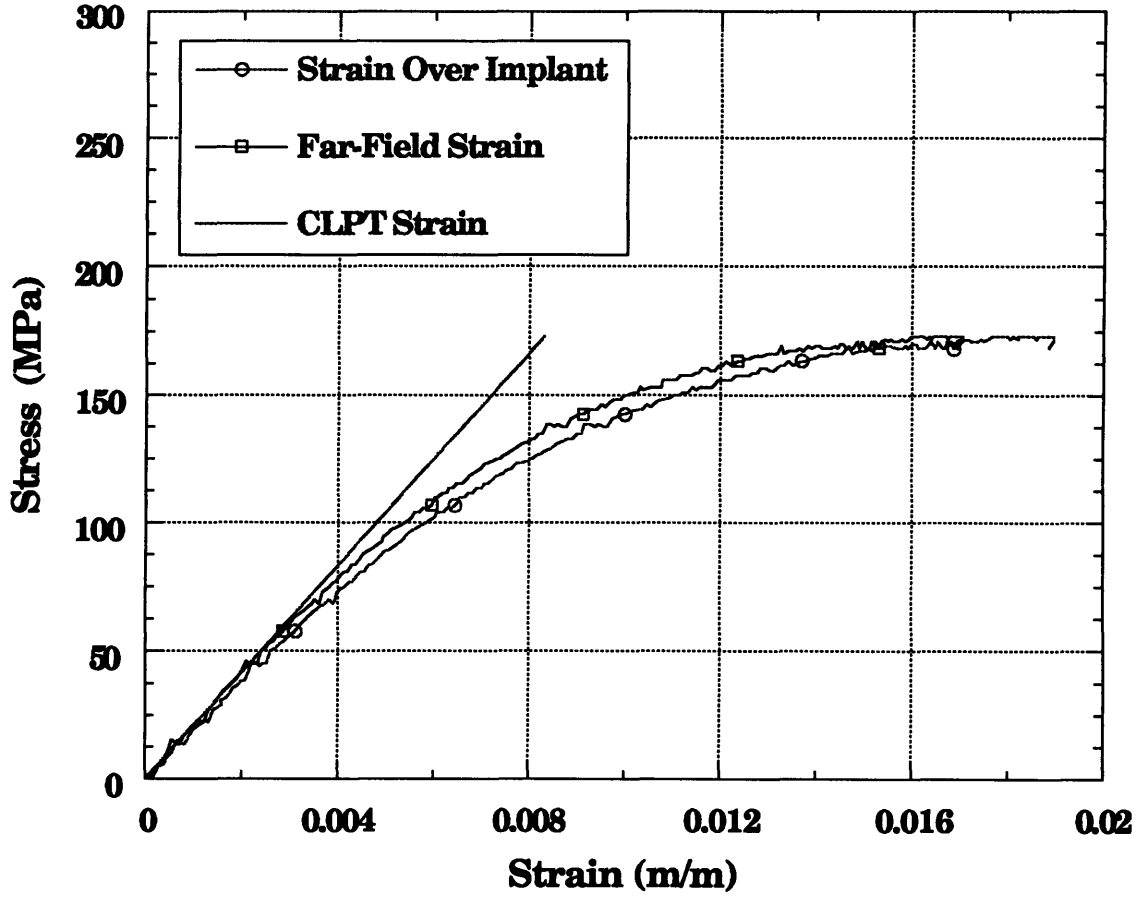

Figure 4.18 Stress-Strain Curves for Coupon 4OF-D with a Layup 4, $[\pm 45]_{4S}$, Configuration Tested to 100% of its Peak Stress

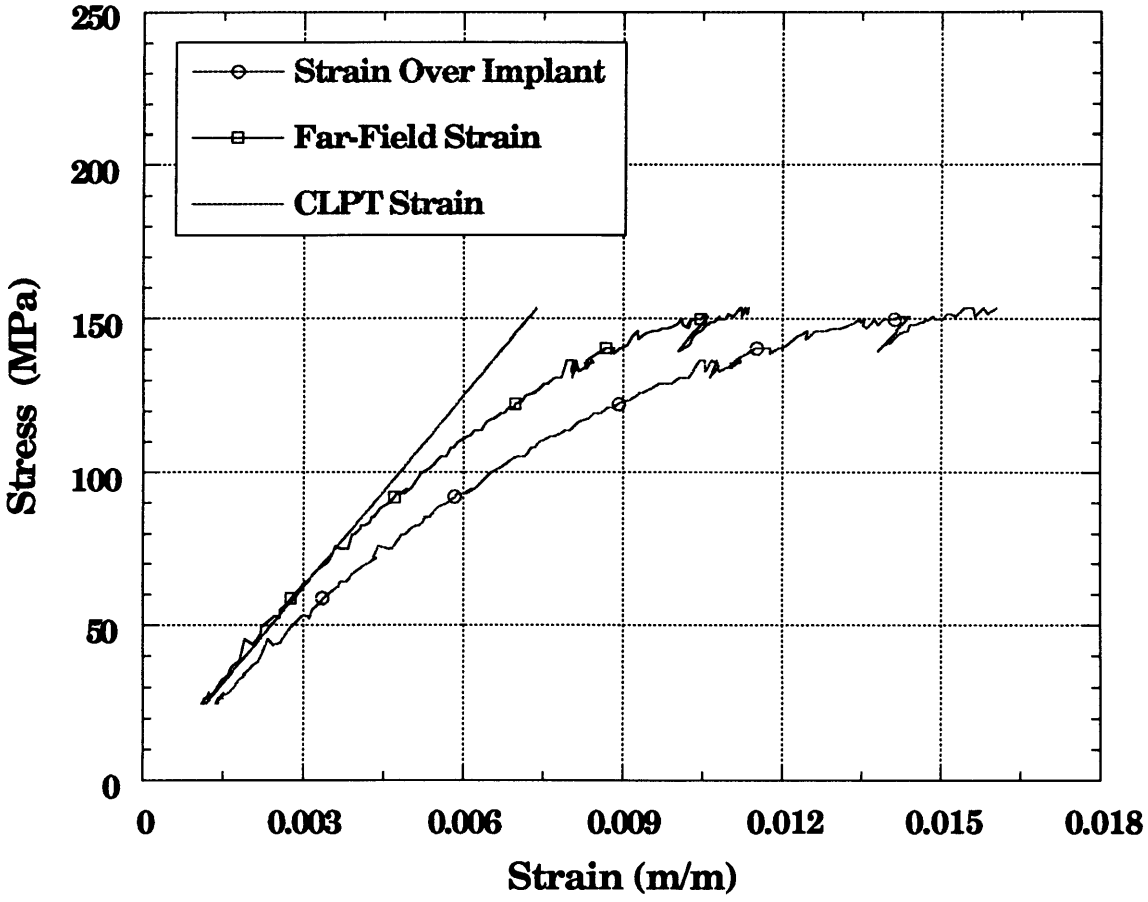

Figure 4.19 Stress-Strain Curves for Coupon 4CHIP-E with a Layup 4, $[\pm 45]_{4S}$, Configuration Tested to Failure

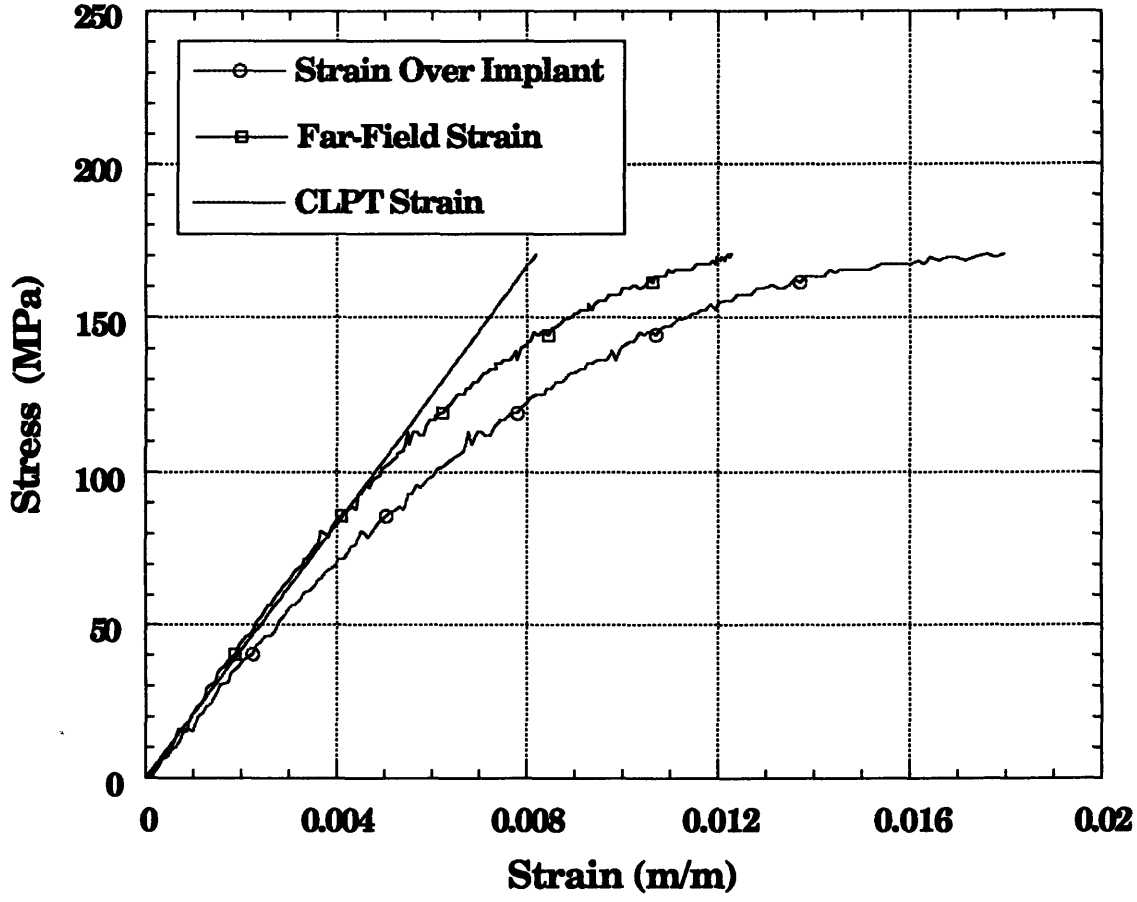

Figure 4.20 Stress-Strain Curves for Coupon 4PZA-D with a Layup 4, $[\pm 45]_{4S}$, Configuration Tested to 100% of its Peak Stress

implants. Descriptions of the failure modes of specimens with a layup 4 orientation are not given because the testing of these specimens did not result in two-piece failure. A discussion is presented describing how failure was defined for the specimens with a layup 4 configuration.

Positions around the implant are described frequently in the following sections. The top and bottom edges of the implant, the sides of the implant and the position over the implant as described are shown in Figure 4.21.

4.4.1 Layup 1, $[0/(\pm 45)_2/90/(\pm 45)_2]_S$, Failure Modes

Photographs of the failure modes for virgin specimens made using a layup 1, $[0/(\pm 45)_2/90/(\pm 45)_2]_S$, are shown in Figure 4.22. Four out of the five failed specimens had a 45° angled break. Often, the coupons would have a 5 mm 90° break on one or both ends of the primary 45° break. One side of the specimen always had a clean break with sections of fibers breaking evenly along the length of the break as shown by the picture of specimen 1V-C. The other side had uneven fiber breaks along the length of the main break as shown by the picture of specimen 1V-D. The side with the even fiber breaks had sections of the upper 0° oriented fibers breaking apart and splitting along the coupon length for up to 25 mm. The picture of coupon 1V-E shows this type of ply splitting that occurred across the width of the specimen. The side with the uneven fiber breaks had sections of the upper 0° oriented fibers breaking apart and splitting along the coupon length for 50 mm up to the entire length of the specimen. The longer ply splitting is shown by the picture of

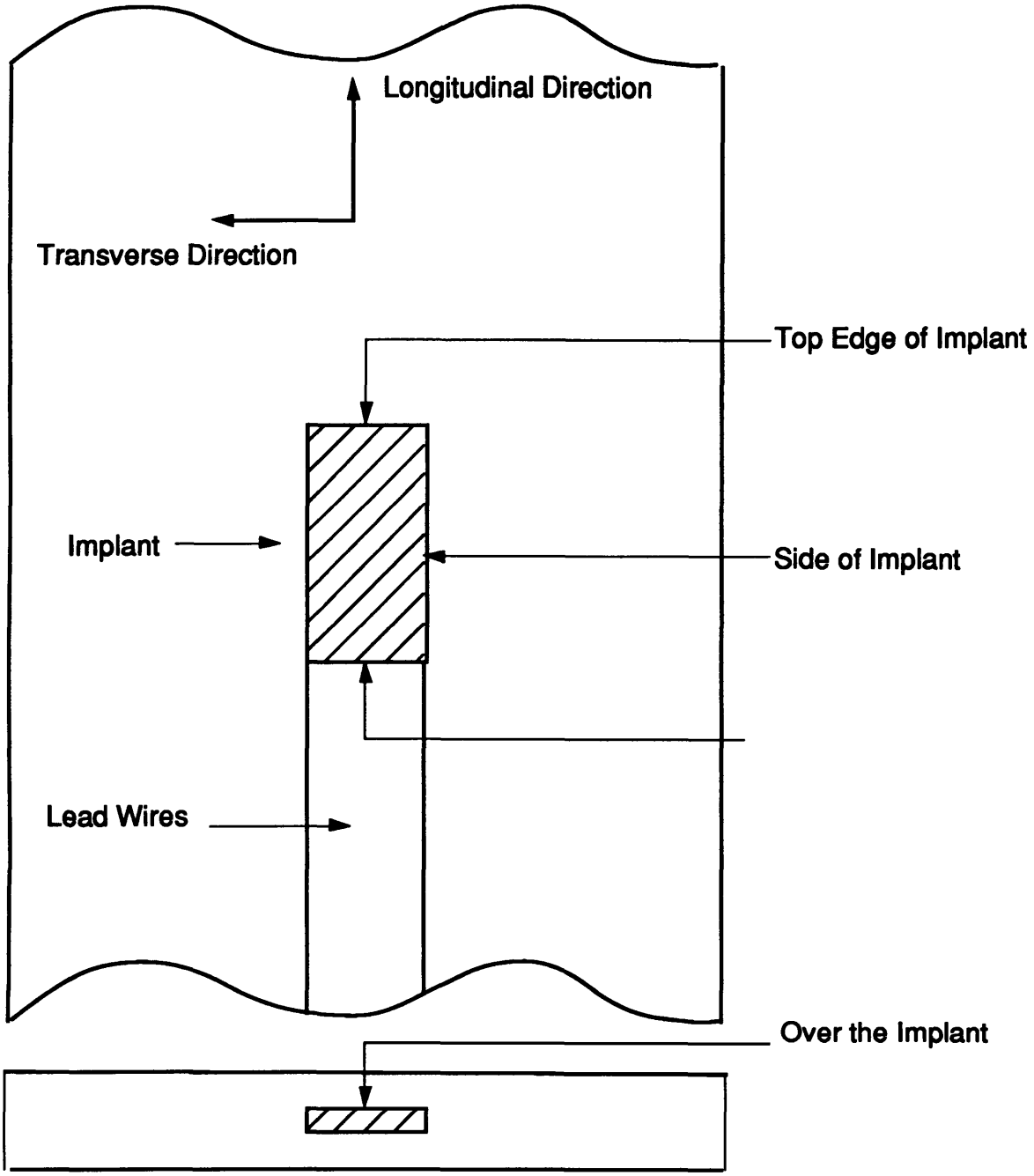

Figure 4.21 Nomenclature Describing Locations Around the Implant

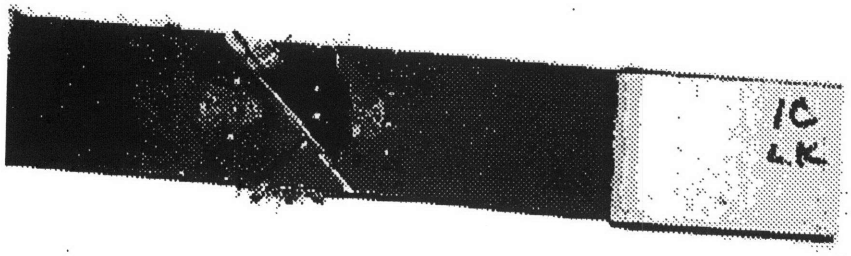

Photograph of Coupon 1V-C

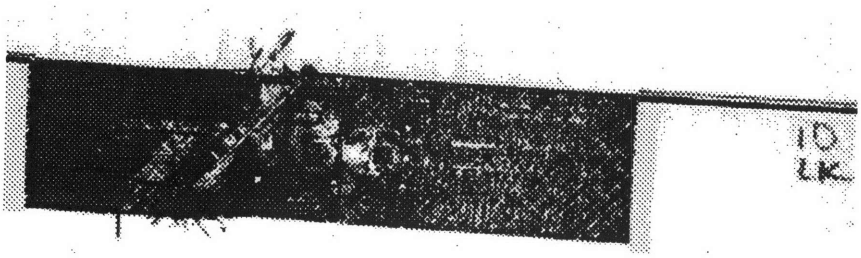

Photograph of Coupon 1V-D

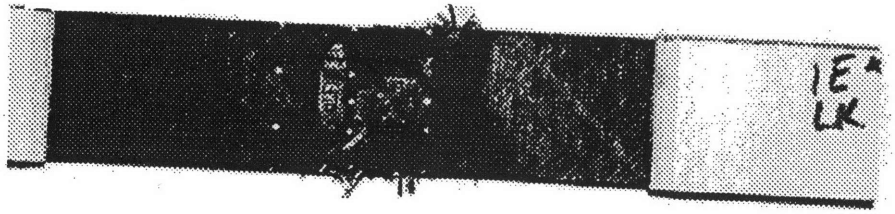

Photograph of Coupon 1V-E

Figure 4.22 Photographs of Failure Modes of Virgin Specimens with a Layup 1, $[0/(\pm 45)_2/90/(\pm 45)_2]_S$, Configuration

coupon 1V-E. The 45° angled layer underneath the upper and lower 0° layers also exhibited ply splitting at 45°. This could be seen because the outer 0° layers delaminated across the coupon width from the 45° ply underneath them. Delamination as seen from a side view of the specimen occurred at both 90° plies emanating from the break and running for up to 100 mm along the length of the specimen.

Two of the three failed specimens with the chip implant in layup 1 failed at the implant. The failure occurred along the top edge of the implant as shown by a photograph and X-ray of the failures of specimen 1CHIP-C in Figure 4.23. The specimen started to fail at 45° at one side of the specimen but the angular orientation of the break changed to 90° along the top of the implant before returning to the 45° orientation at the opposite side of the implant. The X-ray of 1CHIP-C shows how the failure shattered the main sensor and how the internal fiber breakage occurred at 45° angles to the corners of the chip implant. It also shows how the lead wires remained intact. Unlike the virgin specimens, the one specimen with a chip implant that did not fail at the implant did not have a clean break on either side of the coupon.

One out of three failed specimens with the PZA implant in layup 1 failed through the center of the implant as shown by the photograph of the coupon 1PZA-E and an X-ray of the internal fiber breakage in Figure 4.24. The X-ray shows a 90° break for half the coupon width changing to a 45° break at the center of the implant. This fiber breakage at the center of the implant can not be seen in the photograph in Figure 4.24. The photograph shows a 45° break changing to a 90° break at the upper corner of the PZA opposite from the edge where the lead wires extended out of the coupon. The 90° break extended along the top edge of the PZA

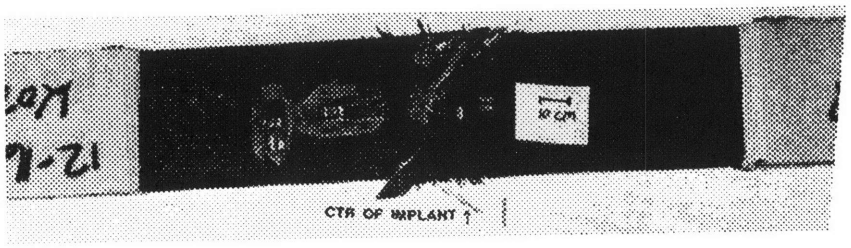

Photograph of Coupon 1CHIP-C

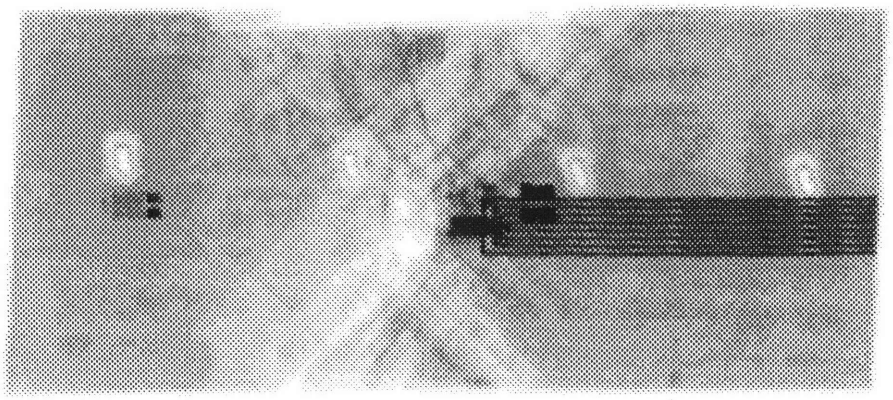

X-Ray of Coupon 1CHIP-C

Figure 4.23 Photograph and X-Ray of Coupon 1CHIP-C with a Layup 1, $[0/(\pm 45)_2/90/(\pm 45)_2]_S$, Configuration Tested to Failure

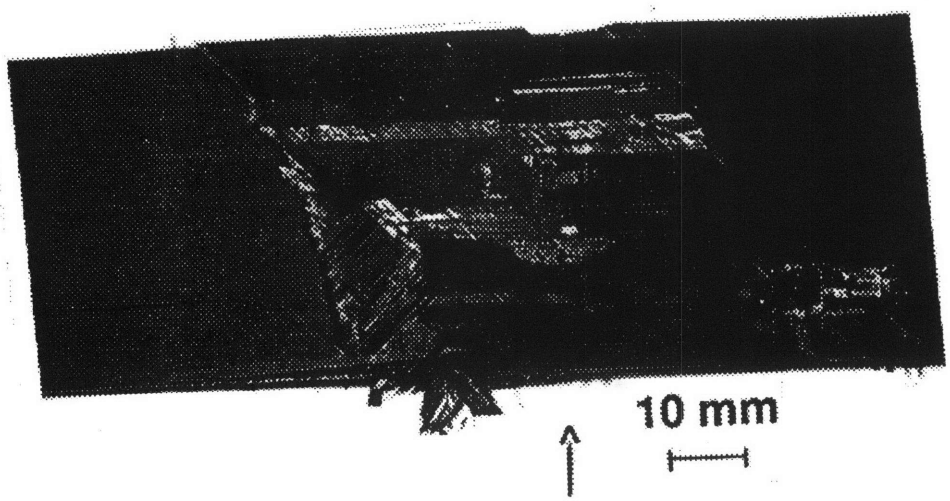

Photograph of Coupon 1PZA-E

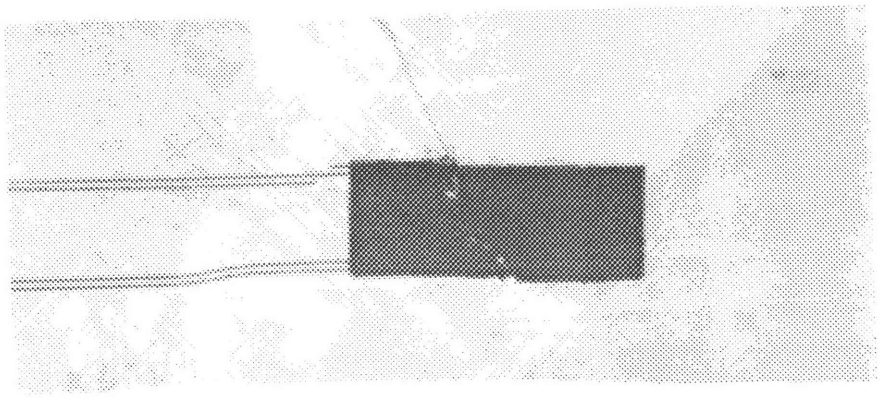

X-Ray of Coupon 1PZA-E

Figure 4.24 Photograph and X-Ray of Coupon 1PZA-E with a Layup 1, $[0/(\pm 45)_2/90/(\pm 45)_2]_S$, Configuration Tested to Failure

and then changed back to a 45° break at the opposite corner of the implant. The exterior view of the coupon shows failure along the top edge of the PZA and more 90° fiber breakage in the outer ply above the center of the PZA for half the coupon width. Unlike the virgin failures, this coupon had uneven fiber breakage on both sides and much more delamination on the upper layers. On one side, a 50 by 50 mm section over the implant was delaminated. Specimen 1PZA-B did not break through the implant but the 90° failure initiated at the same position along the length of the specimen as the top of the PZA and split off at 45 degrees near the corner of the implant as shown by the photograph and X-ray in Figure 4.25. The photograph also shows fiber breakage at 45° for half the coupon width away from the implant above the main break. Specimen 1PZA-C had uneven fiber breakage on both sides and failed 20 mm from the end tab. All coupons had more delamination than the virgin specimens on the upper layer.

The specimens with optical fiber implants had uneven fiber breakage on both sides of the coupon and more delamination then the virgin specimens on the outer layers.

4.4.2 Layup 2, $[0/\pm45/90]_{2s}$, Failure Modes

Photographs of the failure modes for virgin specimens made using layup 2, $[0/\pm45/90]_{2s}$, are shown in Figure 4.26. All virgin coupons failed at 90° with uneven fiber breakage along the break. The upper 0° layer had bundles of fibers splitting in the longitudinal direction for up to 75 mm from the break. This fiber splitting occurred in fiber bundles across the width of the specimen. Two specimens had two piece failures

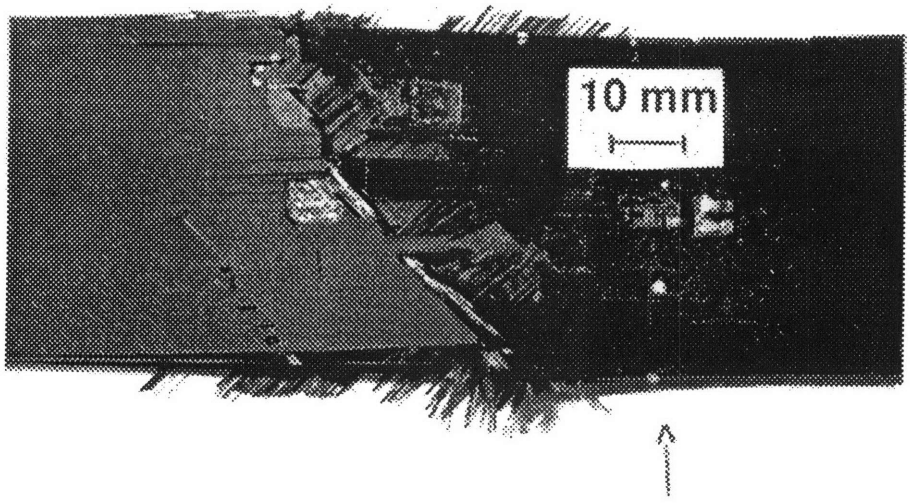

Center of Implant

Photograph of Coupon 1PZA-B

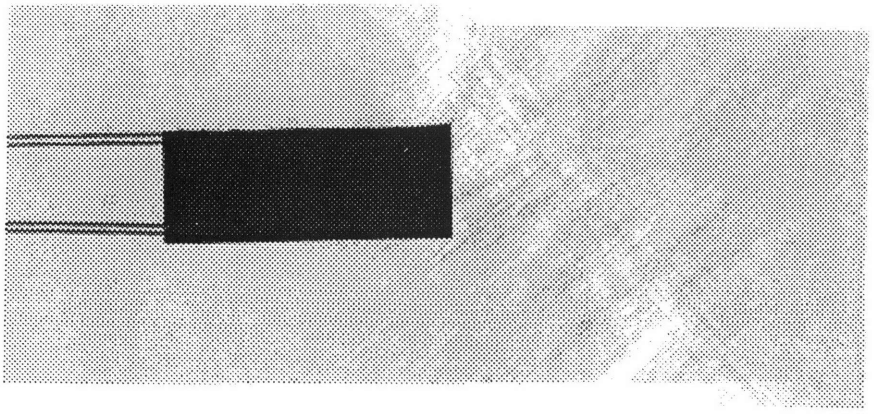

X-Ray of Coupon 1PZA-B

Figure 4.25 Photograph and X-Ray of Coupon 1PZA-B with a Layup 1, $[0/(\pm 45)_2/90/(\pm 45)_2]_S$, Configuration Tested to Failure

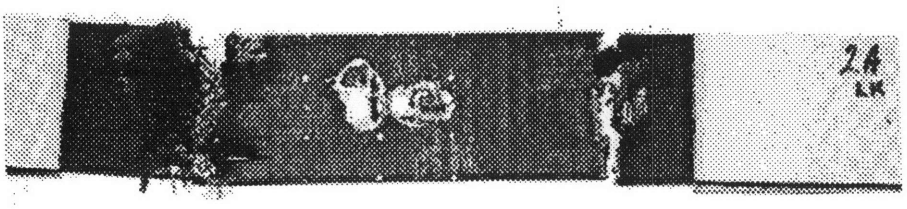

Photograph of Coupon 2V-A

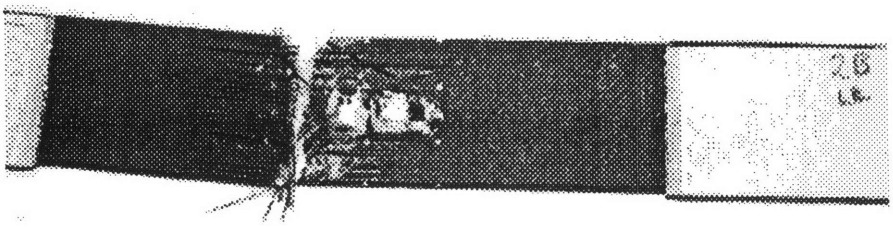

Photograph of Coupon 2V-B

Figure 4.26 Photographs of Typical Failure Modes of Virgin Specimens with a Layup 2, $[0/\pm45/90]_{2s}$, Configuration

and one specimen had a three piece failure. Coupon 2V-E had a two-piece failure and a missing 10 by 15 mm rectangular section at the break. Delamination occurred in all the plies between the outer two 90° plies. This delamination broke through the fibers between the 90° plies. Two out of the three failed specimens had delamination that occurred away from the main break. Coupon 2V-E had all the plies broken through the thickness away from the main failure, including the 0° plies, and the delamination did initiate at the main break.

The most common change in failure mode between the specimens with implants and the virgin specimens was the change from the straight virgin 90° breaks to a combination 90°/45° break. This change did not necessarily occur at the implant. The only other noticeable difference due to the implants was the ragged breaks caused by uneven fiber breakage.

Both coupons with the PZA implant failed at the implant as shown by the photographs of specimens 2PZA-B and 2PZA-D in Figure 4.27. Coupon 2PZA-B broke at 90° 10 mm from the center of the implant across half the coupon width and then the break changed to a 45° orientation. This was unusual compared to the virgin specimens which only exhibited 90° breaks. The fibers of the coupon with the PZA implant broke very unevenly along the failure. Coupon 2PZA-D had three 90° breaks with one of the straight breaks extending along the lower edge of the implant where the lead wires extended out to the end of the coupon.

One out of two failed specimens with the chip implant that was placed in a cut laminate, failed at the implant. Coupon 2CHIP-A failed with 90° damage propagation through the main sensor as shown by the photograph and X-ray in Figure 4.28. The other failed specimen,

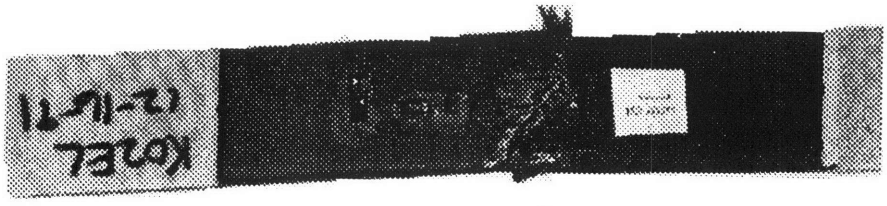

Center of Implant ^

Photograph of Coupon 2PZA-B

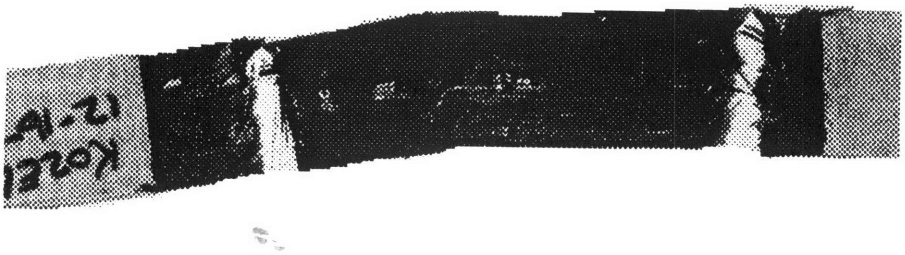

Photograph of Coupon 2PZA-D

Figure 4.27 Photographs of Coupons 2PZA-B and 2PZA-D with a Layup 2, $[0/\pm45/90]_{2S}$, Configuration Tested to Failure

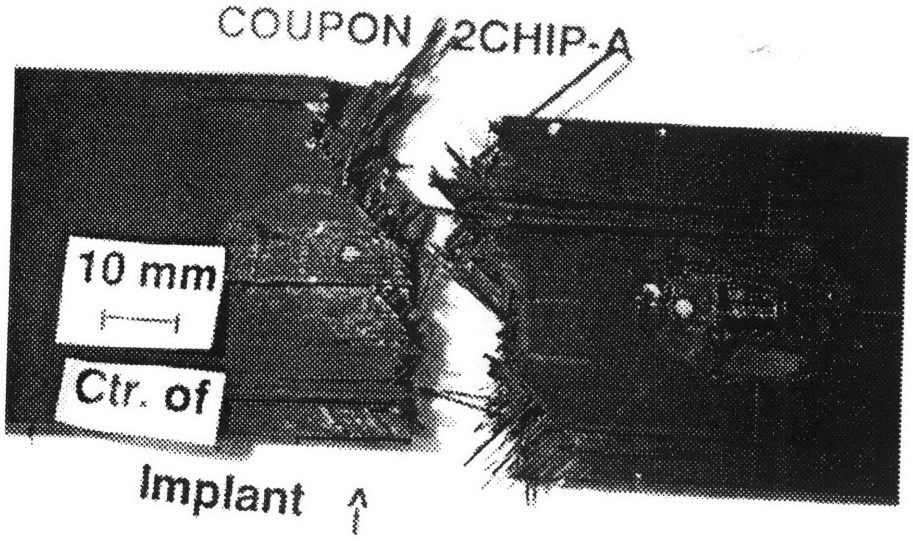

Photograph of Coupon 2CHIP-A

X-Ray of Coupon 2CHIP-A

Figure 4.28 Photograph and X-Ray of Coupon 2CHIP-A Tested to Failure with the Chip Placed in a Cut Laminate with a Layup 2, $[0/\pm45/90]_{2S}$, Configuration

2CHIP-B, had an unusual failure although it did not originate at the implant. It had two 90° breaks that separated the specimen into three sections and two 90° cracks in the outer layers that did not extend across the width of the specimen. None of these cracks or breaks occurred at the implant.

Neither of the two failed coupons with a chip implant placed directly into the center of the laminate had a failure at the implant. Specimen 2CHIP L/O-A had damage propagation at 90° across its width with a failure mode identical to the virgin specimens. Coupon 2CHIP L/O-B had a three-piece failure. One of the breaks occurred at a 90° orientation and the other was at a 45° orientation. A triangular piece having one side coincident with the main 45° break also broke off. Several split fiber bundles extended 10 mm past the main 45° break. This coupon experienced more delamination than the virgin specimens on the upper layers.

The specimens with optical fibers placed directly into the center of the laminate experienced 90° and 45° damage propagation and a three piece failure. The 45° damage propagation interrupted the 90° failure but did not occur across the entire width of the coupon. All of these coupons had fiber bundles that were broken more unevenly across the width than were the virgin specimens. The amount of and location of delamination is similar to the virgin specimens. An example of a typical coupon is shown by a photograph of the failed specimen 2OF-E in Figure 4.29.

Specimens that had the optical fiber placed in two cut plies failed differently than the virgin specimens. The damage propagation did not occur in a clear 90° path like the virgin specimens. The fibers along the

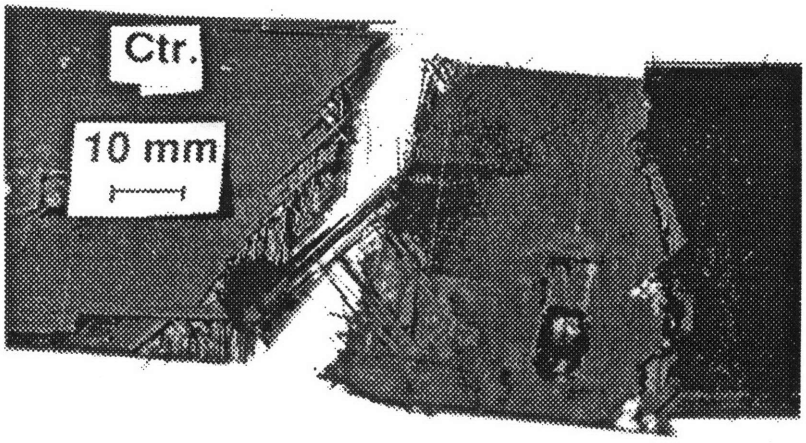

Photograph of Coupon 2OF-E

Figure 4.29 Photograph of Coupon 2OF-E Tested to Failure with the Optical Fiber Placed Directly in a Laminate with a Layup 2, $[0/\pm45/90]_{2s}$, Configuration

break were much more uneven and the implanted specimens had more delamination of the upper layers. A photograph of the failure of 2OF-C/O B is shown in Figure 4.30.

Both coupons with the teflon chip implant failed with a combination 90° and 45° break unlike the typical 90° breaks seen in the virgin coupons. The transition between the two damage orientations occurred roughly along the midline of the coupon. None of the failures occurred at the implant but the teflon implant fell out of a piece that failed 25 mm from the edge of the implant that had a lot of internal delamination. The teflon was intact and there was no evidence it had bonded with the surrounding material.

One coupon with the teflon PZA implant failed identically to the virgin coupons. The other failed coupon had a combination 90° and 45° break similar to the failures of the specimens with the teflon chip implant. The number of delaminations that occurred through the thickness was similar to that for the virgin specimens.

4.4.3 Layup 3, $[45/0/-45/0/90/-45/0/-45/0/45]_s$, Failure Modes

Photographs of the failure modes for virgin specimens made using layup 3, $[45/0/-45/0/90/-45/0/-45/0/45]_s$, are shown in Figure 4.31. There was 45° fiber splitting on the top layer with delamination throughout the upper layers on the surface of the specimen. The direction of damage propagation varied between a 90° and a 45° break for all five specimens. None of the coupons had a 90° break along the entire width of the coupon. Coupons 3V-B and 3V-D had breaks with a 45°

Photograph of Coupon 2OF C/O-B

Figure 4.30 Photograph of Coupon 2OF C/O-B Tested to Failure with the Optical Fiber Placed in a Cut Laminate with a Layup 2, $[0/\pm45/90]_{2s}$, Configuration

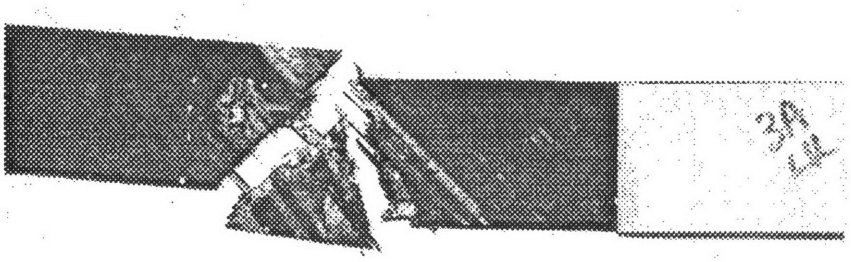

Photograph of Coupon 3V-A

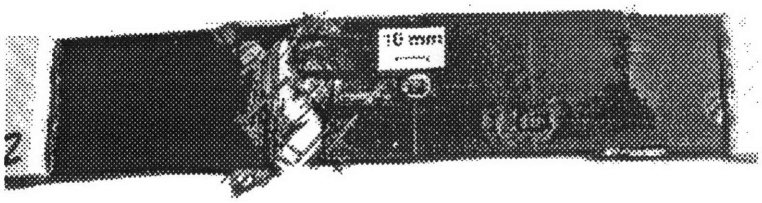

Photograph of Coupon 3V-B

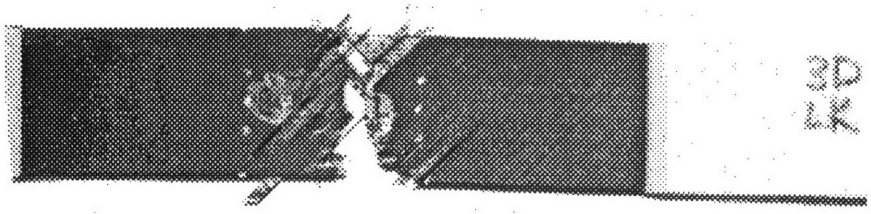

Photograph of Coupon 3V-D

Figure 4.31 Photographs of Typical Failure Modes of Virgin Specimens with a Layup 3, $[45/0/-45/0/90/-45/0/-45/0/45]_s$, Configuration

orientation changing to a 90° orientation and then back to 45°. These 45° breaks occurred within 10 mm of the edge. Coupon 3AV had a 45° break with even fiber breakage and a 90° break initiating from the same point. The photograph shows the triangular section that was broken out of this coupon. Coupon 3V-E also had a triangular section broken out but the 45° break only extended for half the width of the coupon. Coupon 3V-C had three piece failure with one 45° break and a 90° break. Three of the five tested coupons had three piece failures. There was some delamination at the 90° plies but the delamination did not extend along the entire length of the specimen.

Both coupons with the chip implant failed at the implant. Figures 4.32 and 4.33 show a photograph of the failure and X-ray of coupons 3CHIP-B and 3CHIP-C respectively. Coupon 3CHIP-B failed at the main sensor with no damage to the leads. The failure sheared the coupon as shown in Figure 4.32. The break occurred at 90° for 25 mm at the same longitudinal position as the center of the implant before changing to a 45° orientation. Coupon 3CHIP-C also failed at the main sensor and, in addition, the lead wires were pulled apart. This specimen had 90° breaks for about 10 mm on both sides of the coupon with a 45° connecting the two. The fibers were broken so unevenly that the shape of the break had to be determined by examining the X-ray.

Two out of three failed specimens with the PZA implant failed at the center of the implant as shown by a photograph and X-ray of the failures of coupons 3PZA-B and 3PZA-D in Figures 4.34 and 4.35 respectively. The X-ray of specimen 3PZA-B in Figure 4.34 also indicates damage propagation at 45° through the point where one of the lead wires was soldered to the PZA. The photograph of the specimen shows a

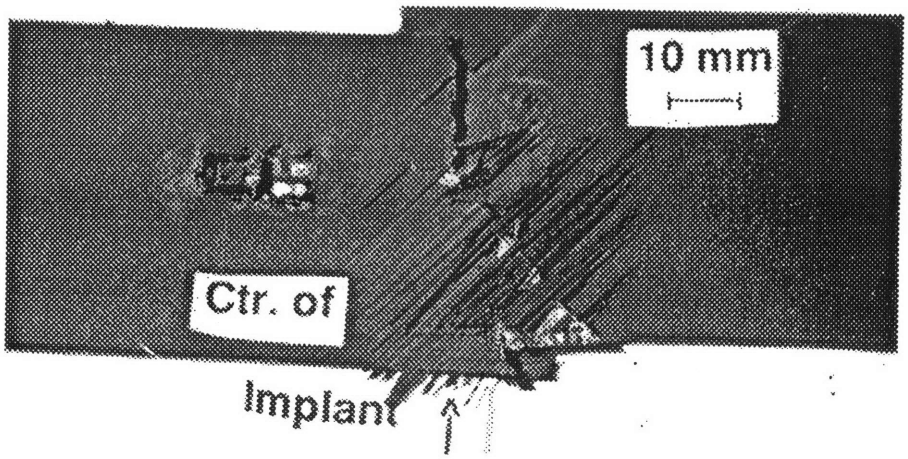

Photograph of Coupon 3CHIP-B

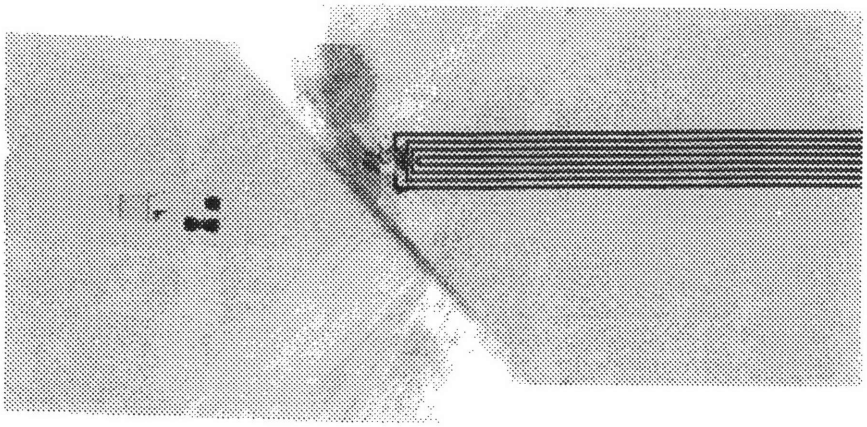

X-Ray of Coupon 3CHIP-B

Figure 4.32 Photograph and X-Ray of Coupon 3CHIP-B with a Layup 3, $[45/0/-45/0/90/-45/0/-45/0/45]_S$, Configuration Tested to Failure

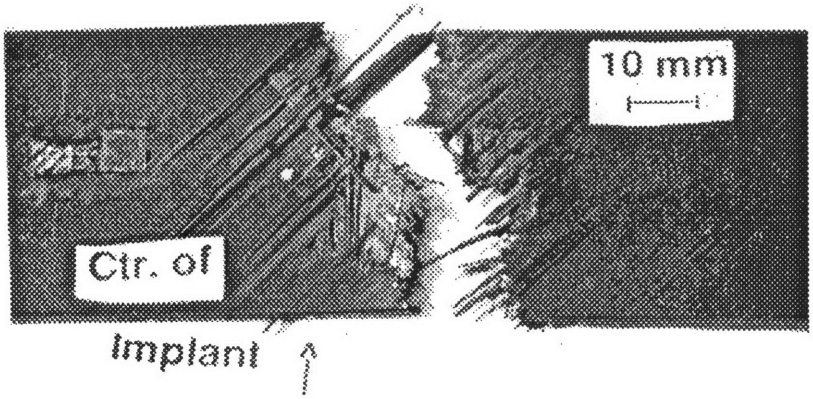

Photograph of Coupon 3CHIP-C

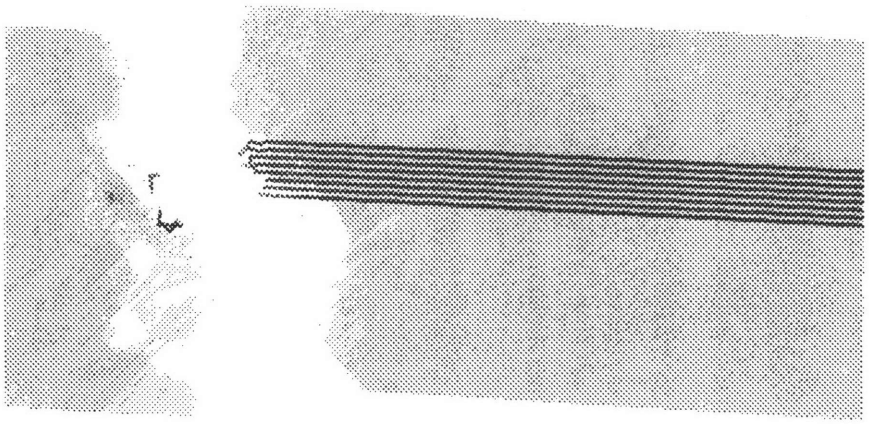

X-Ray of Coupon 3CHIP-C

Figure 4.33 Photograph and X-Ray of Coupon 3CHIP-C with a Layup 3, $[45/0/-45/0/90/-45/0/-45/0/45]_S$, Configuration Tested to Failure

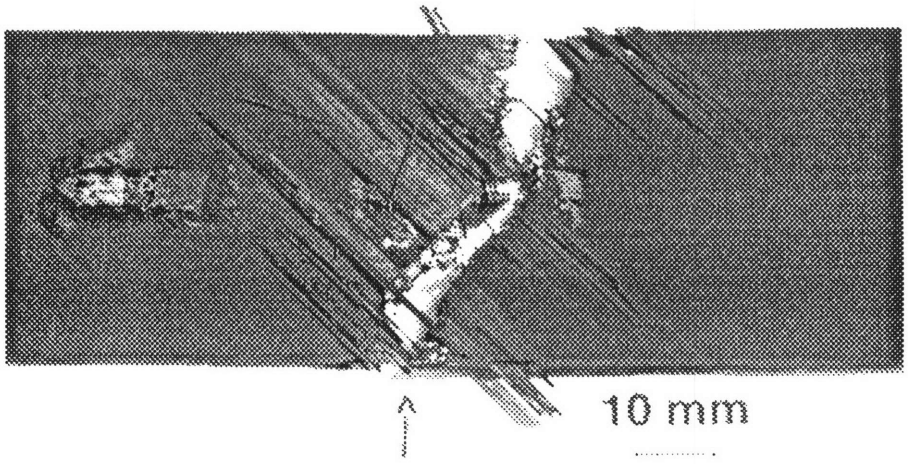

Center of Implant

Photograph of Coupon 3PZA-B

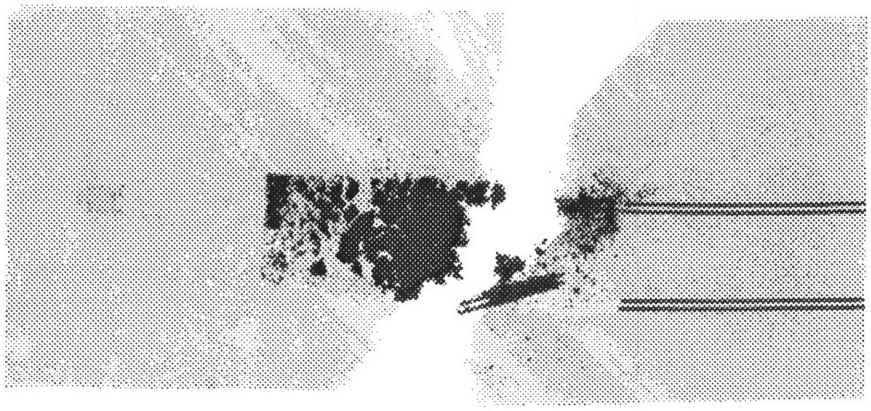

X-Ray of Coupon 3PZA-B

Figure 4.34 Photograph and X-Ray of Coupon 3PZA-B with a Layup 3, $[45/0/-45/0/90/-45/0/-45/0/45]_S$, Configuration Tested to Failure

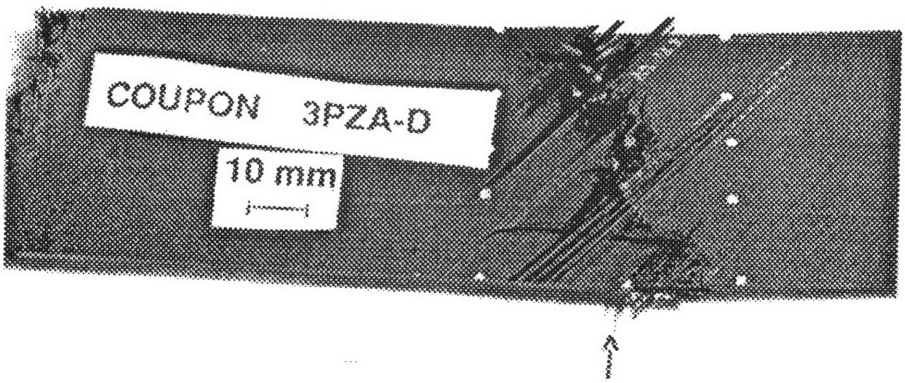

Center of Implant

Photograph of Coupon 3PZA-D

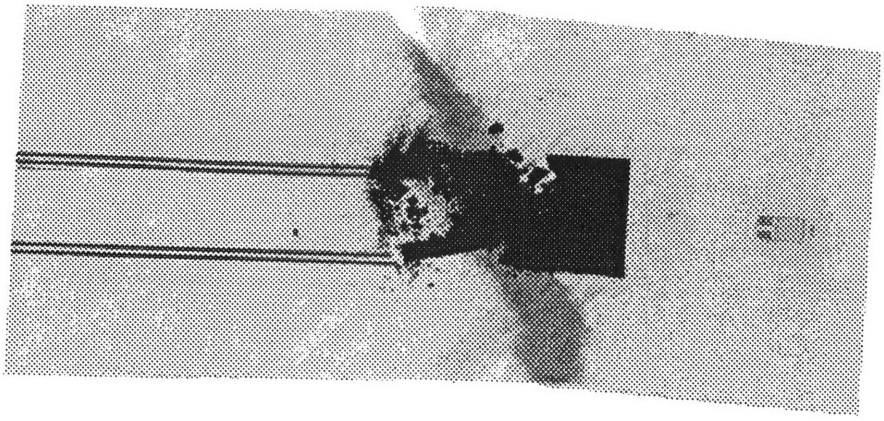

X-Ray of Coupon 3PZA-D

Figure 4.35 Photograph and X-Ray of Coupon 3PZA-D with a Layup 3, [45/0/-45/0/90/-45/0/-45/0/45]s, Configuration Tested to Failure

90°/45°/90° failure path with one of the 90° sections originating at the same longitudinal position as the center of the PZA. The 90° orientation of the failure changed to a 45° 10 mm into the specimen and changed back to 90° at the center of the coupon. Both specimens had a significant amount of 45° fiber splitting on the outer layers of the coupon as was the case for the virgin specimens.

Coupon 3PZA-D had a failure at a 45° orientation that passed through the location where one of the lead wires was soldered onto the PZA. After passing through the PZA, this damage propagation changed to 90° at the side edge of the implant. Although the X-ray of this specimen shown in Figure 4.35 shows the failure occurring through the center of the implant, the fiber breakage on the outer plies shows the damage following the contour of the PZA. The damage propagated at a 90° direction to the edge of the implant parallel to the longitudinal axis. It then followed this edge which is in the 0° laminate direction and turned back to a 90° orientation along the top edge of the implant. The break changed to a 45° orientation at the corner of the PZA and extended out the side of the coupon. This coupon appeared as if it had been shoved together and had fibers sticking out perpendicular to the coupon surface. This could have happened during removal from the tensile machine if the upper crosshead fell slightly while the coupon was gripped before rising away from the specimen; however, experimental procedure dictated opening the upper grip first to prevent this type of post-testing damage. Coupon 3PZA-A also had a three piece failure with a 90° and a 45° break which occurred 15-20 mm away from the end tabs.

All three optical fiber implanted specimens failed similarly to the virgin specimen 3V-E with triangular sections broken as shown by a

photograph of specimen 3OF-B in Figure 4.36. These coupons did not experience any difference in delamination or damage propagation relative to the virgin specimens.

4.4.4 Layup 4, $[\pm 45]_{4S}$, "Failure" Modes

The specimens made to the layup 4 configuration, $[45/-45]_{4S}$, behaved differently than the specimens with layup 1, 2 or 3 orientations. During testing, these coupons reached a load/stress plateau as shown in Figure 4.19 and continued to strain without any increase in stress as determined from far field load divided by the original cross-sectional area. The peak stress or 100% load value for this case was defined as the value of the stress at the stress plateau, whereas for the other specimens, the 100% load or peak stress was equivalent to two-piece failure. The coupons manufactured to a layup 4 orientation were considered failed when they were strained well into the stress plateau region.

During the testing of the specimens made to the layup 4 configuration, drops in stress occurred in conjunction with increased strain throughout testing. X-rays indicated very little matrix cracking within the specimens until they had been loaded to the peak stress value and held there for several seconds. The partial loading testing method for the specimens with the layup 4 configuration was developed after one specimen with a chip and one specimen with a PZA implant were tested in an effort to determine when the matrix cracking initiated. Table 3.6 shows how the coupon with the chip implant was originally tested to 80% of the maximum stress. An X-ray of this specimen showed no

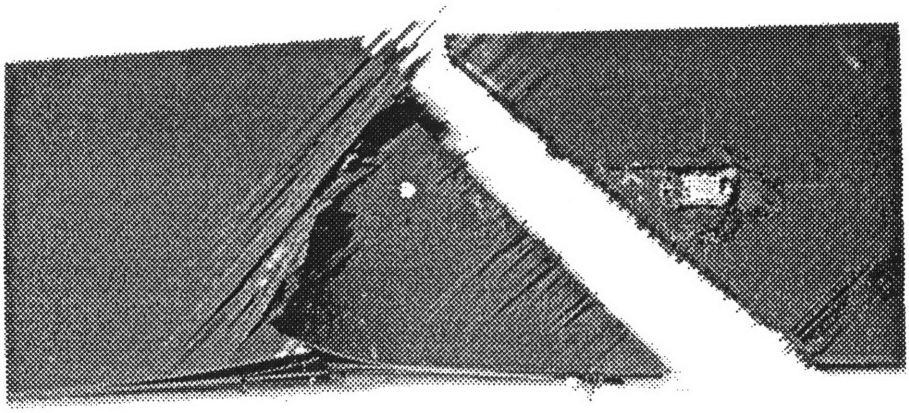

Photograph of Coupon 3OF-C

Figure 4.36 Photograph of Coupon 3OF-C with a Layup 3, $[45/0/-45/0/90/-45/0/45/0/45]_S$, Configuration Tested to Failure

matrix cracking; therefore, it was reloaded to 90% and X-rayed again. It was then loaded to 100% of its peak stress. Matrix cracks were detected only at 100% loading. One specimen with the PZA implant was loaded to 80% of the peak stress value, X-rayed, and then reloaded to the 100% of the maximum stress value. An X-ray of the specimen loaded to 80 and 100% verified that coupons with the PZA implant also required testing to 100% of the maximum stress before matrix cracking occurred. Note that testing to 100% for specimens with the layup 4 configuration was 100% of the peak stress, not the failure stress. Failure occurred after straining at the peak stress for over a minute. At 100% peak load there was no visible physical difference in behavior between the virgin and implanted specimens.

4.5 X-Ray Detection of Damage at the Implant

X-rays were taken of the specimens prior to and after testing. 1,4-Diiodobutane (DIB) X-ray enhancer was applied to the coupon edges either prior to, during or after testing for at least 15 minutes. X-ray data is not available for most specimens from the 2TPZA, 2TC, 2PZA, 1OF and 1CHIP sets. These specimens had DIB applied but the correct X-ray settings which would show the matrix cracks were not discovered until after testing and sectioning of most of these specimens. The settings on the X-ray machine that produced quality X-rays were 30 kV for 105 seconds. The only coupons that were still available for X-raying with the quality settings were 2TPZA-E and 2TPZA-B and 2PZA-E. The following summarizes any unusual matrix cracking or delaminations observed at

the implants. Note that X-rays give an integrated picture through the thickness of any damage present in the laminate.

4.5.1 X-Ray Damage Detection at Implants for Specimens with a Layup 1, $[0/(\pm 45)_2/90/(\pm 45)_2]_S$, Configuration

Specimen 1PZA-D was loaded to 90% of its ultimate stress and had extensive ±45° microcracking around the implant but not directly over or far-field from it. The matrix cracking concentration at the implant was identical to those specimens with a layup 4 configuration as shown by a sketch of the X-ray for specimen 4PZA-D in Figure 4.44 with the exception of the delamination shown on the side of the PZA. The optical fibers created no discontinuity in the usual matrix cracking. X-rays for 1CHIP and 1OF coupons are not available.

4.5.2 X-Ray Damage Detection at Implants for Specimens with a Layup 2, $[0/\pm 45/90]_{2S}$, Configuration

Specimens with a layup 2 configuration all exhibited 90° matrix cracking across the width of the specimen. Coupon 2CHIP-D which was loaded to 95% of its ultimate stress and had the chip placed in a cut laminate, had fiber curvature near the implant as shown by a sketch of the X-ray in Figure 4.37. This may have been induced during manufacturing by differences in the thermal expansion coefficients of the graphite/epoxy and the chip implant. Small ±45° matrix cracking

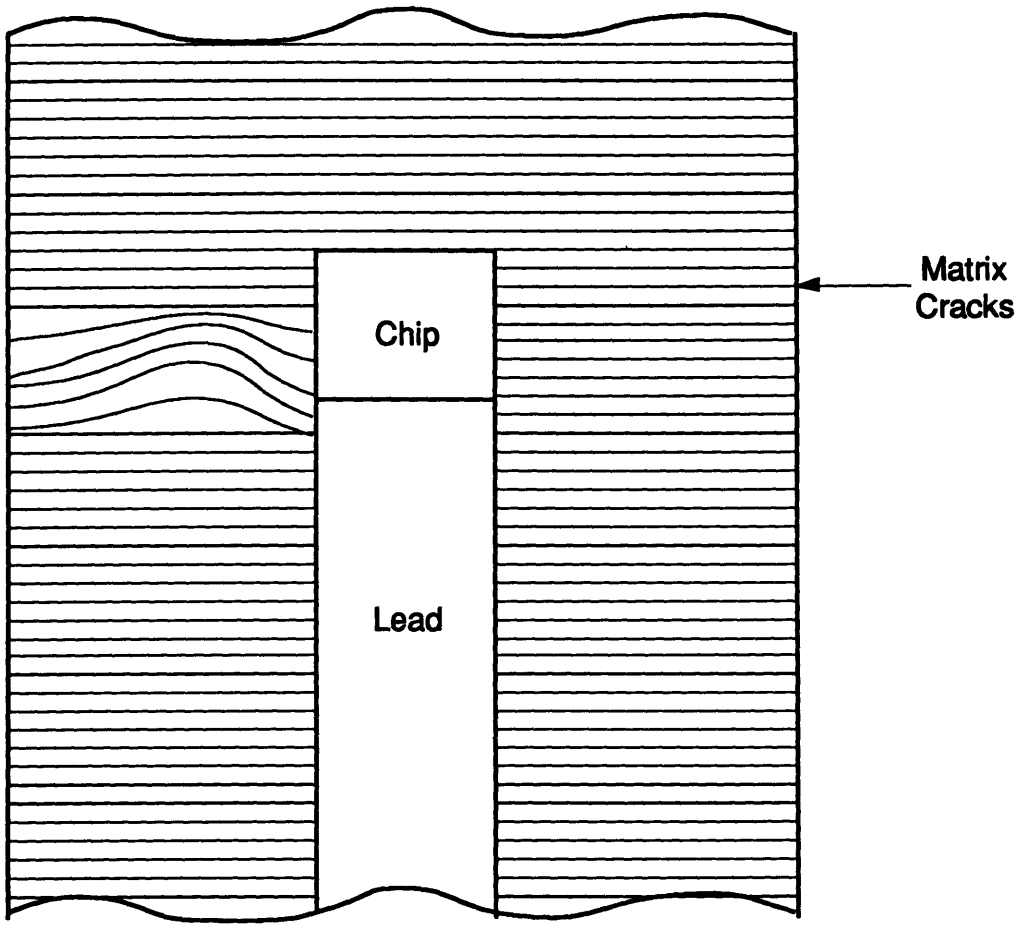

Figure 4.37 Sketch of X-Ray Results for Coupon 2CHIP-D Tested to 95% of its Ultimate Stress with Chip Placed in Cut Laminate with a Layup 2, $[0/\pm45/90]_{2S}$, Configuration

could be seen only at the side of the chip in the X-rays of the failed specimens 2CHIP-B and 2CHIP-E as shown by a sketch of the X-rays in Figure 4.38. Out of the set with the chips placed directly into the composite, the only unusual matrix cracking occurred in specimen 2CHIP L/O-D which was loaded to 95% of its ultimate stress. The 90° matrix cracks were larger at the sides of the implant than far-field of the implant as shown by a sketch of the X-ray in Figure 4.39.

Coupons with optical fibers demonstrated unusual fiber bending at the optical fibers which may be due to the differences in the coefficients of thermal expansion of the optical fibers and graphite/epoxy. This fiber bending was observed for specimens with the optical fiber placed directly into the laminate or placed in a cut laminate. Figure 4.40 shows a sketch of the fiber curvature for the 90% loaded coupons 2OF-D, which had the optical fiber placed directly into the laminate. This sketch also applies to coupon 2OF C/O-C, which had the optical fiber placed in a cut-out area of the laminate. The only other unusual matrix cracking seen for specimens with optical fiber implants was ±45° cracking directly over the optical fibers. Failed coupons 2OF C/O-A and 2OF C/O-B with optical fibers placed in cut laminates, exhibited this behavior. Sketches of the X-rays for these specimens is shown in Figure 4.41.

Two specimens with teflon PZA implants exhibited 90° microcracking everywhere except directly over and next to the implant where ±45° microcracking occurred. One of these specimens had been failed and one had been loaded to 95% of its ultimate stress. A sketch of these X-rays is shown in Figure 4.42.

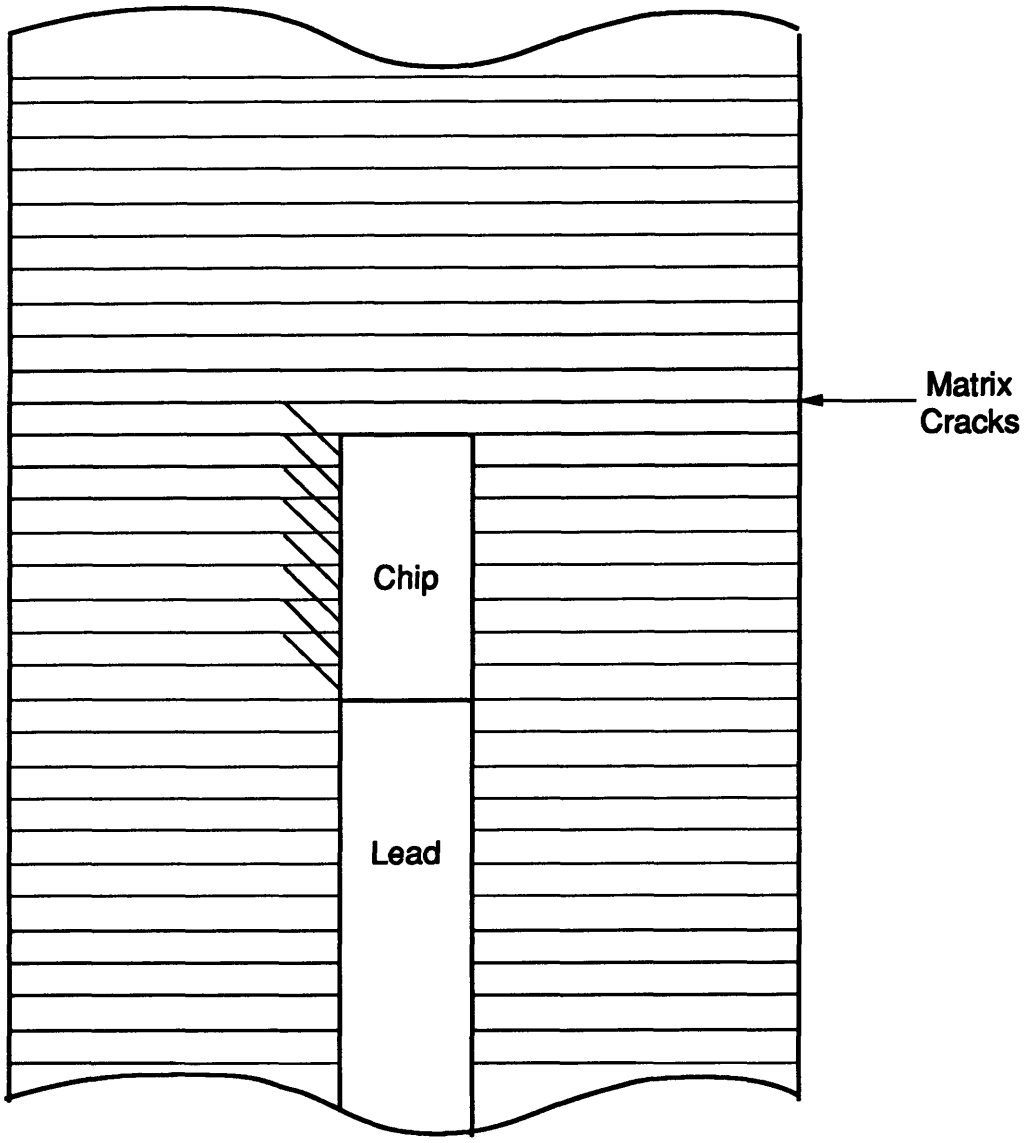

Figure 4.38 Sketch of X-Ray Results for Failed Coupon 2CHIP-B with Chip Placed in Cut Laminate with a Layup 2, $[0/\pm45/90]_{2s}$, Configuration

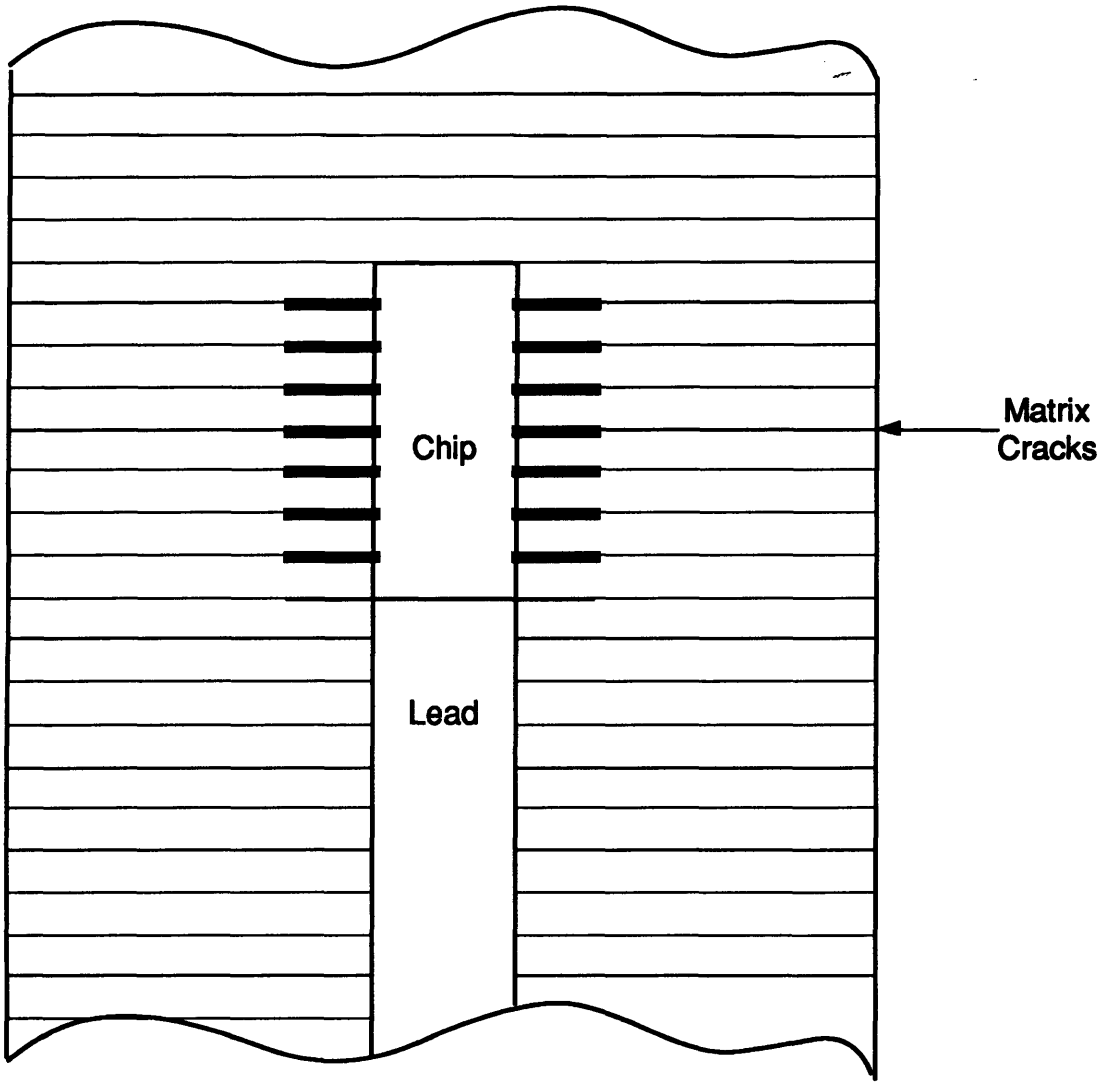

Figure 4.39 Sketch of X-Ray Results for Coupon 2CHIP-D Tested to 95% of its Ultimate Stress with Chip Placed Directly in Laminate with a Layup 2, $[0/\pm45/90]_{2s}$, Configuration

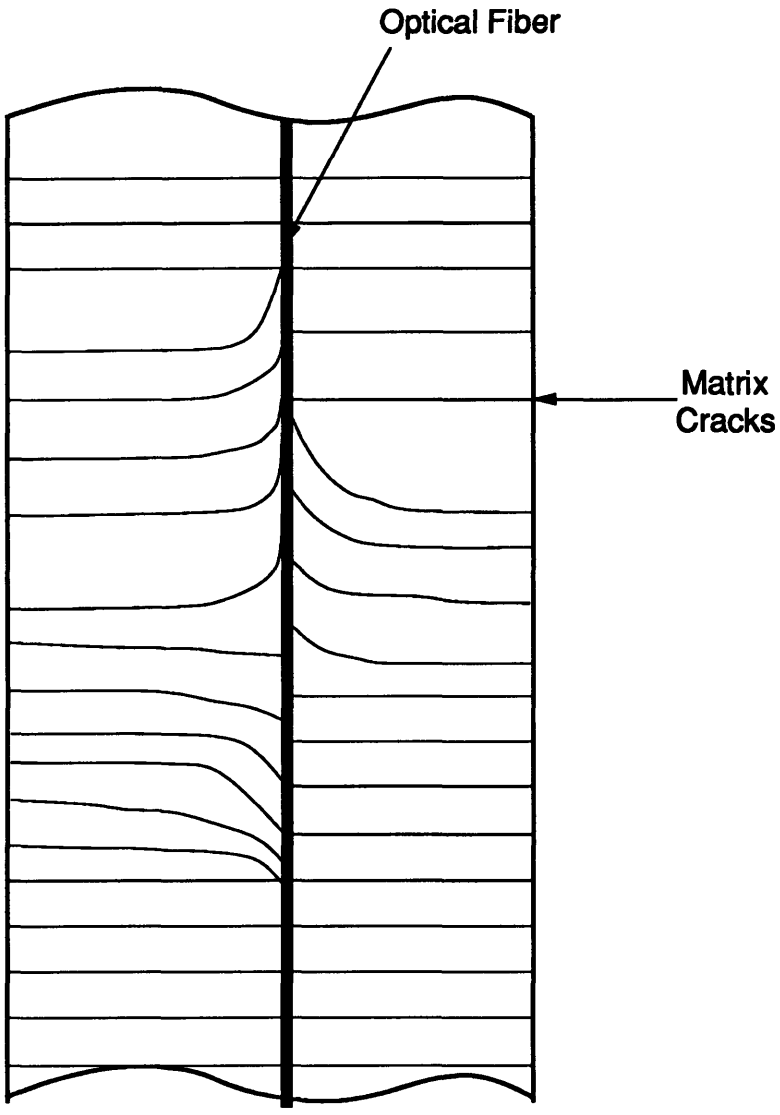

Figure 4.40 Sketch of X-Ray Results for Coupon 2OF-D Tested to 90% of its Ultimate Stress with Optical Fiber Placed Directly in Laminate with a Layup 2, $[0/\pm45/90]_{2S}$, Configuration

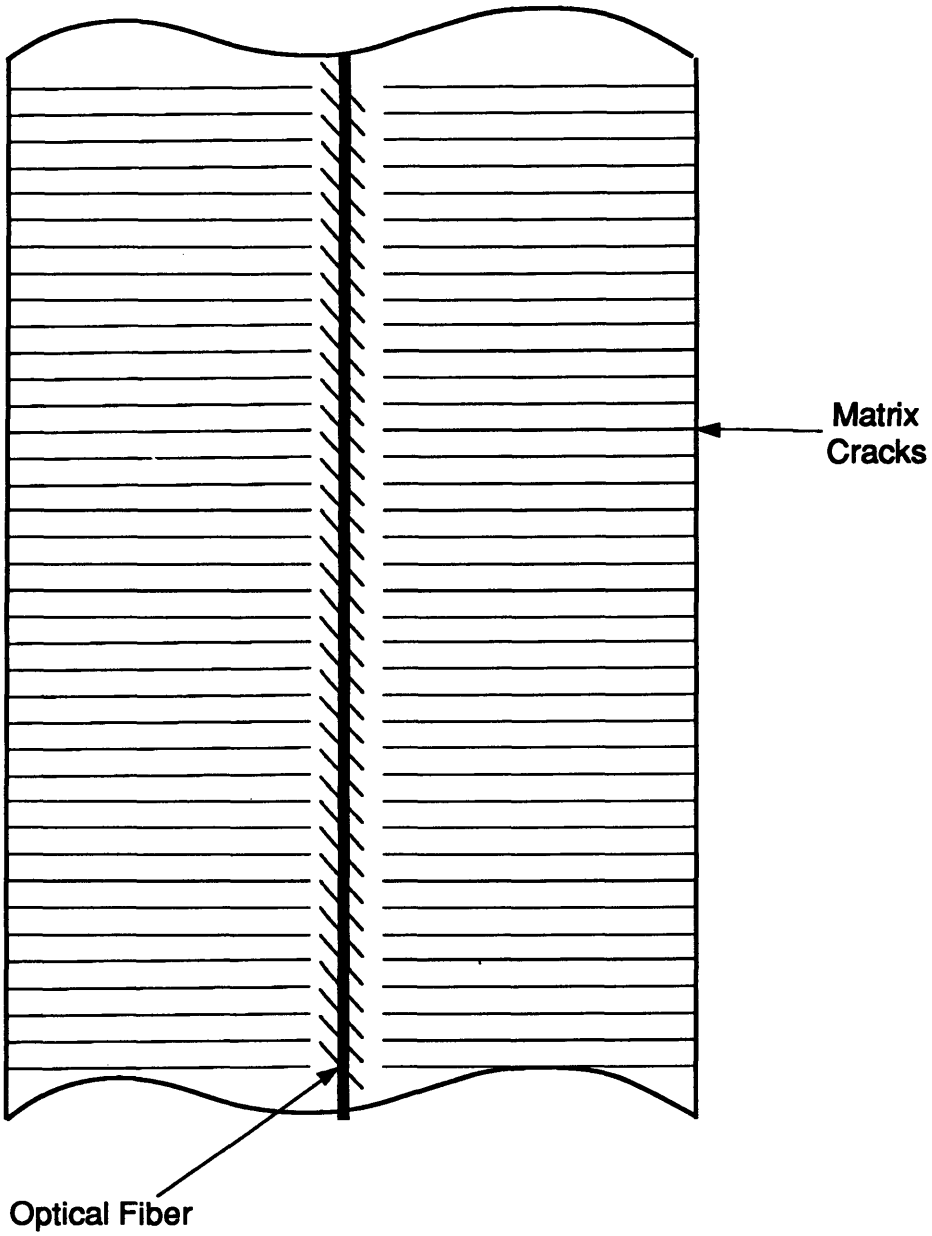

Figure 4.41 Composite Sketch of X-Ray Results for Failed Coupons 2OF C/O-A and 2OF C/O-B with Optical Fibers Placed in Cut Laminates with a Layup 2, $[0/\pm45/90]_{2S}$, Configuration

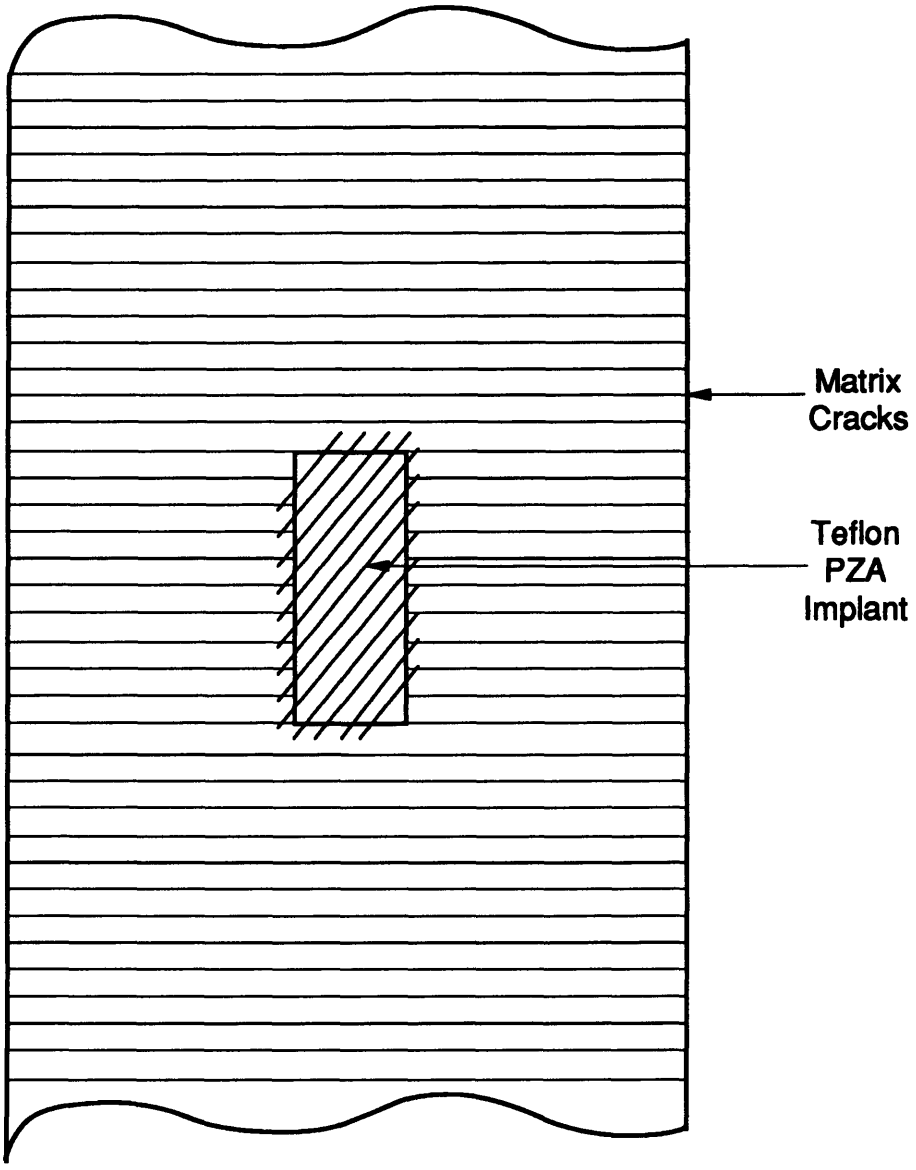

Figure 4.42 Composite Sketch of X-Ray Results for Coupon 2TPZA-E Tested to 95% of its Ultimate Stress and for Failed Coupon 2TPZA-B both with Laminates having a Layup 2, $[0/\pm45/90]_{2s}$, Configuration

The X-ray of specimen 2PZA-E that was loaded to 90% of its ultimate stress showed unusual ±45° matrix cracking at the bottom of the implant where the lead wires extended out and also showed how the matrix cracking did not extend to the side of the implant. A sketch of the X-ray for this specimen is shown in Figure 4.43.

4.5.3 X-Ray Damage Detection at Implants for Specimens with a Layup 3, $[45/0/-45/0/90/-45/0/45/0/45]_s$, Configuration

All specimens made using layup 3 exhibited very little visible matrix cracking. These specimens also had the lowest percentage of 90° plies at 10%. There was some ±45° cracking visible but these cracks were discontinuous and barely observable. No unusual indications could be seen around any of the implants with the layup 3 configuration.

4.5.4 X-Ray Damage Detection at Implants for Specimens with a Layup 4, $[\pm 45]_{4s}$, Configuration,

All specimens with a layup 4 ply orientation exhibited significant ±45° matrix cracking after reaching the peak stress level.

All specimens from the set with PZA implants showed considerable ±45° matrix cracking at the implant and its leads but not directly over or far-field of the implant. Both specimens 4PZA-D and

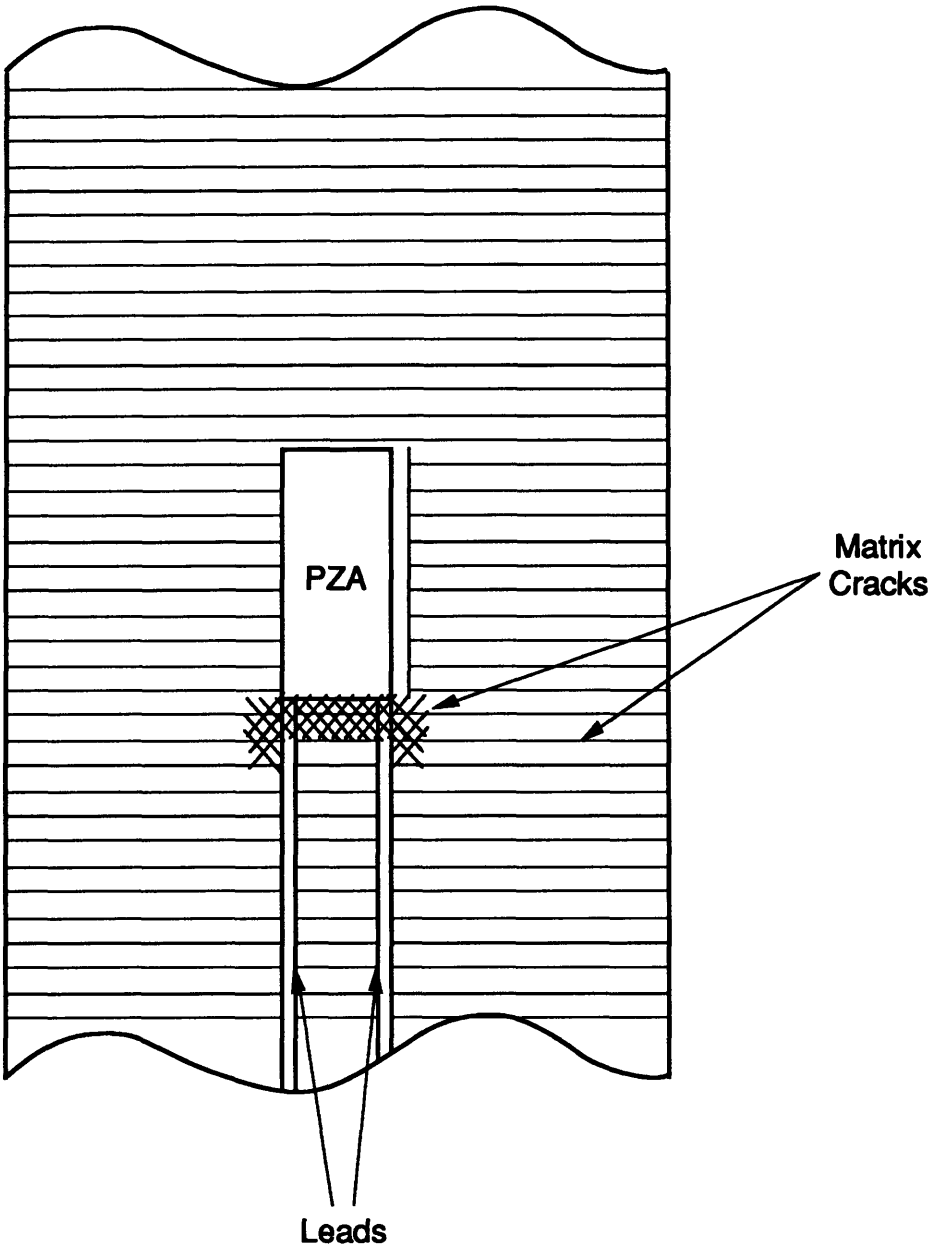

Figure 4.43 Sketch of X-Ray Results for Coupon 2PZA-E with a Layup 2, $[0/\pm45/90]_{2s}$, Configuration Tested to 90% of its Ultimate Stress

4PZA-C also showed delaminations occurring at the side of the implant as shown in Figure 4.44.

The specimens with chip implants also had significant ±45° matrix cracking at the implant and leads but not directly over or far-field to the implant. None of the chip specimens had any obvious delaminations at the side of the implant but there was often more obvious ±45° cracks at the edge of the chip.

The specimens with optical fibers made using layup 4 exhibited ±45° matrix cracking but the cracks were not deformed or enlarged at the optical fiber.

4.6 Sectioning Results of Tensile Specimens

Sectioning was performed with the milling machine to determine if damage occurred through the thickness which the X-rays, which gave an integrated picture of the damage through the thickness, could not detect. The specimens with the chip or teflon chip implants were sectioned into 5 mm slices at the top, middle and bottom of the implant and into 10 mm slices far-field of both ends. The specimens with the PZA or teflon PZA implants were sectioned into 10 mm slices and also sectioned far-field of both ends of the PZA.

Observations of matrix cracking, fiber breakage, delamination and bonding of the implant with the surrounding material in specimens with either the chip or optical fiber implants did not vary with the particular layup configuration. Photographs of selected specimens are presented which represent all of the tested specimens. Some of the specimens were tested to failure and some were tested to a percentage of

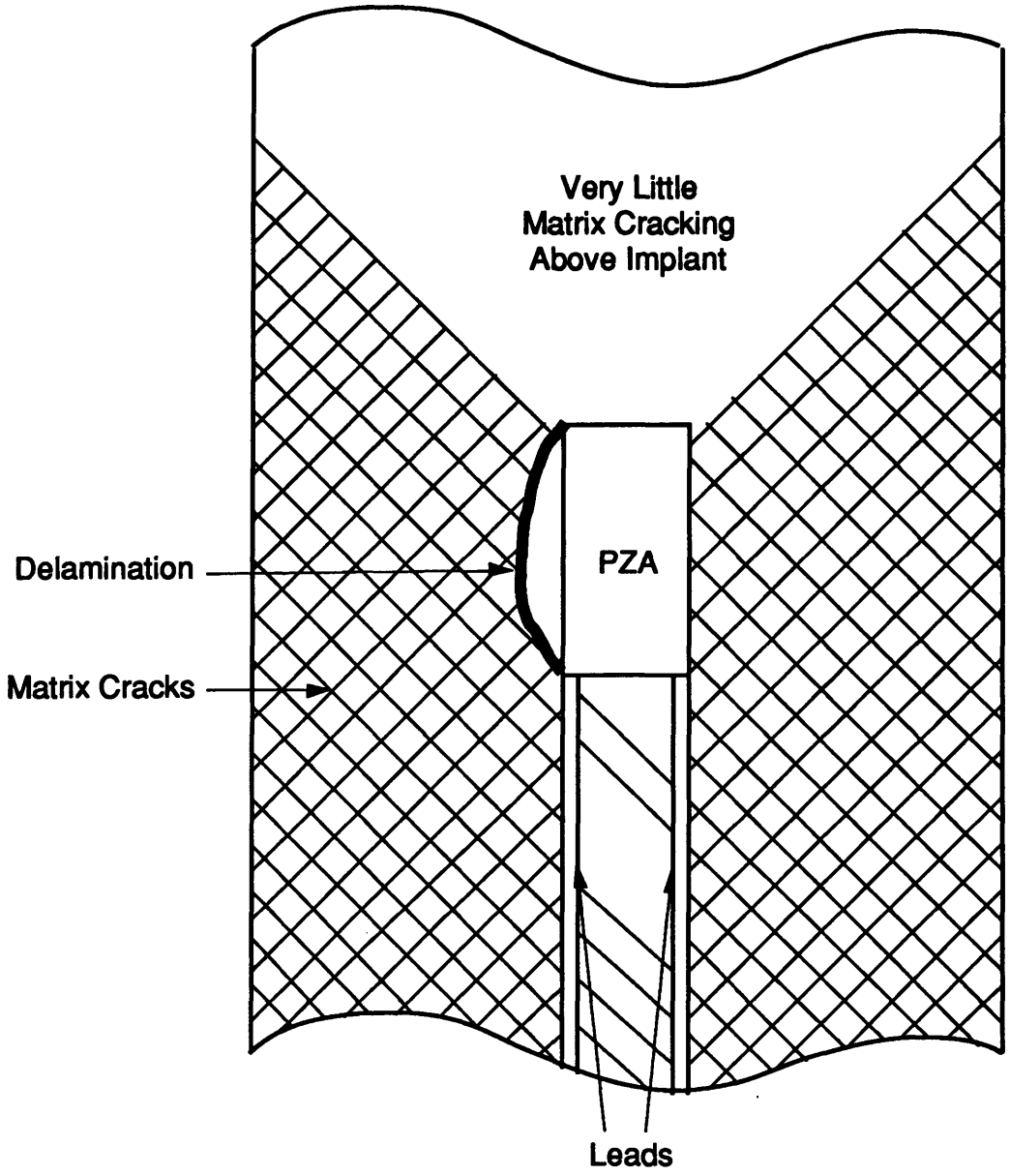

Figure 4.44 Composite Sketch of X-Ray Results for Coupons 4PZA-D and 4PZA-C with Layup 4, $[\pm 45]_{4S}$, Configurations Tested to 100% of their Peak Stresses

their ultimate stress. There was no observed damage at the implant for either of these two cases.

Damage at the PZA implant was observed for specimens with a layup 4 configuration but not for specimens with layup 1, 2 or 3 configurations.

4.6.1 Sectioning Results for Specimens with Chip Implants

Resin rich areas occurred at the top edge of the chip implant. This can be seen in the photograph of the untested specimen 1CHIP-A shown in Figure 4.45. A typical cross-section of the implanted chip and leads is shown in the photograph of the failed coupon 1CHIP-B in Figure 4.46. Note that the resin pockets at the side of the implant should not be mistaken for cracks emanating from the upper and lower edges of the chip. Many specimens had misaligned fibers at the side of the implant as shown by a photograph of the untested coupon 1CHIP-A in Figure 4.47. No obvious delaminations at the implants were observed for any of the specimens with chip implants.

4.6.2 Sectioning Results for Specimens with PZA Implants

Specimens with PZA implants had resin rich pockets between the lead wires at the edge where they extended past the main PZA implant. The resin rich areas are shown in Figure 4.48 by the photographs of a section from the failed specimen 2PZA-D and the specimen 2PZA-C,

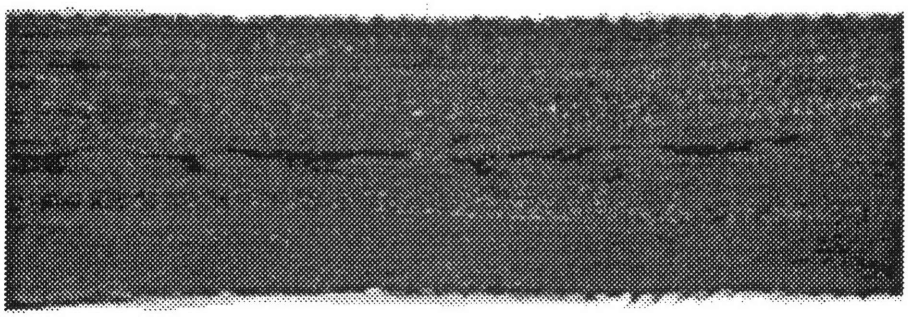

Only local section at top edge of chip shown, not the entire width of the specimen. Height shown is full laminate thickness. Dark areas are resin rich areas.

Figure 4.45 Photograph of Section of Untested Coupon 1CHIP-A with a Layup 1, $[0/(\pm 45)_2/90/(\pm 45)_2]_S$, Configuration Showing Resin Rich Areas at the Top Edge of the Chip Implant

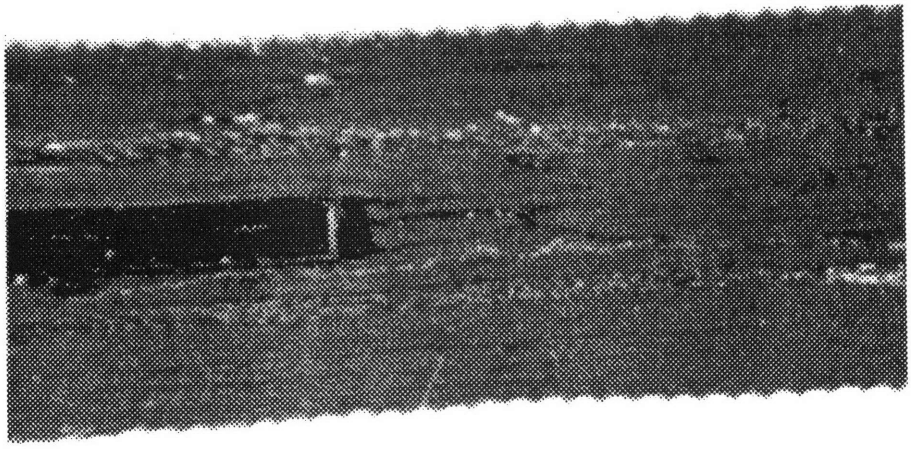

Dark area on left is part of the chip implant. The height is the full laminate thickness; however, only a local section of the specimen width is shown. Dark lines to right of implant are resin rich areas.

Figure 4.46 Photograph of Section of Coupon 1CHIP-B with a Layup 1, $[0/(\pm 45)_2/90/(\pm 45)_2]_S$, Configuration Showing Typical Adhesion to Composite

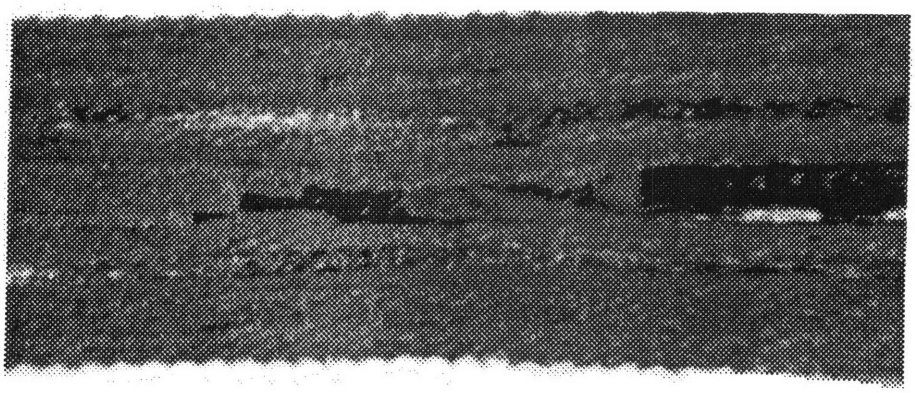

Dark area on right is part of the chip implant. The height is the full laminate thickness; however, only a local section of the specimen width is shown. Dark areas to left of implant are resin rich areas.

Figure 4.47 Photograph of Section of Untested Coupon 1CHIP-A with a Layup 1, $[0/(\pm 45)_2/90/(\pm 45)_2]_s$, Configuration Demonstrating Misalignment of Fibers Adjacent to Implant

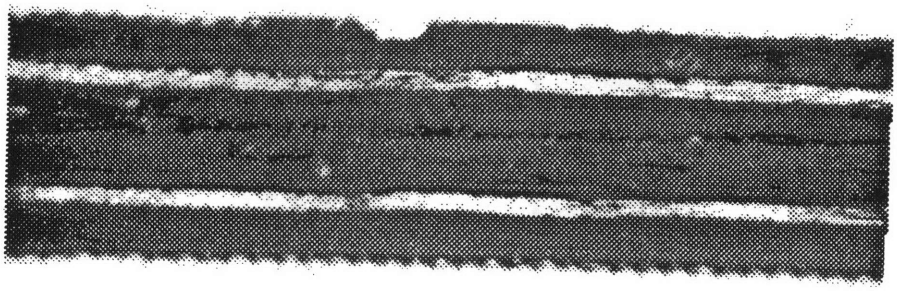

Large dark area on left is part of the PZA implant with a lead wire on top. The height is the full laminate thickness; however only a local section of the specimen width is shown. Dark lines to right of implant are resin rich area.

Photograph of Coupon 2PZA-D

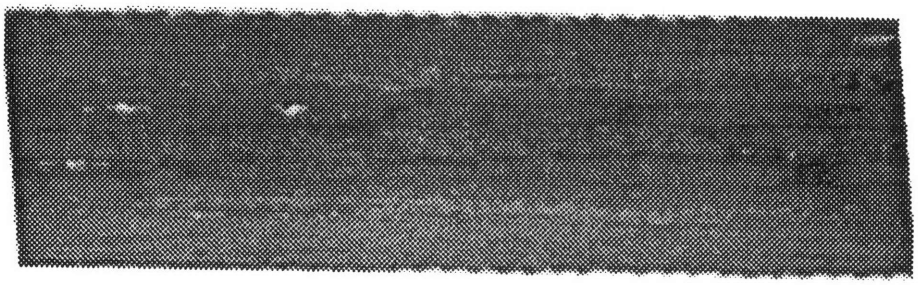

The height is the full laminate thickness; however, only a local section of the width between the two lead wires is shown. Dark areas are resin pockets.

Photograph of Coupon 2PZA-C

Figure 4.48 Photograph of Section of Failed Coupon 2PZA-D and Coupon 2PZA-C Which was Tested to 90% of its Ultimate Stress with a Layup 2, $[0/\pm45/90]_{2s}$, Configuration Showing Damage Between Lead Wires

which was tested to 90% of its ultimate stress. A photograph of the untested specimen 2PZA-A is shown in Figure 4.49 and demonstrates how the PZA implants bonded in the laminate. Fiber misalignment resulting in resin rich areas was also observed at the side of the PZA implants parallel to the loading direction as shown by a photograph of the failed coupon 2PZA-D in Figure 4.50. The misalignment of the fibers was not as pronounced as that seen next to the chip implants.

The only damage that was detected for any of the implants in any of the layup configurations occurred at the side of the PZA in the layup 4 configuration. This delamination is shown by a photograph of the 100% loaded specimen 4PZA-D in Figure 4.51.

4.6.3 Sectioning Results for Specimens with Optical Fiber Implants

A typical resin pocket in the shape of an eye around the optical fiber is shown by a photograph of coupon 1OF-E in Figure 4.52. This specimen was tested to 90% of its ultimate stress. There was no matrix cracking or delamination at the optical fiber in any of the layup configurations.

The resin pocket was largest for specimens with a layup 2 configuration where the optical fiber was placed perpendicular to two 90° plies. The optical fiber was placed between two 45° plies for the remaining layup configurations.

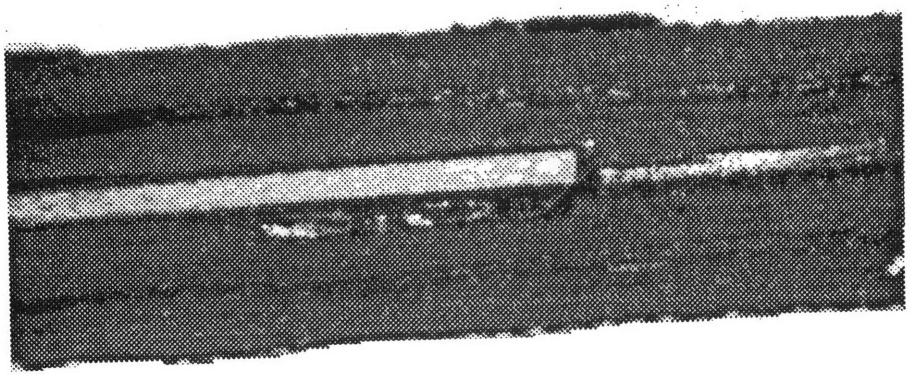

Light area on left is part of the PZA implant with a lead wire on its lower right side. The height shown is the full laminate thickness; however only a local section of the specimen width is shown.

Figure 4.49 Photograph of Section of Untested Coupon 2PZA-A with a Layup 2, $[0/\pm45/90]_{2s}$, Configuration Showing Typical Adhesion in Composite

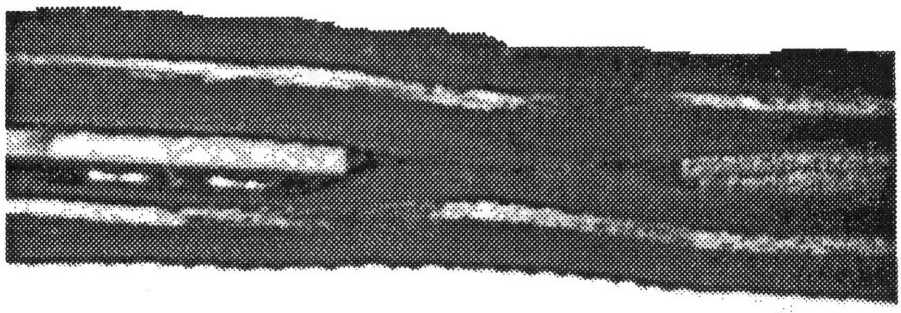

Light area on left is part of the PZA Implant with a lead wire attached on its lower right side. The height shown is the full laminate thickness; however, only a local section of the specimen width is shown.

Figure 4.50 Photograph of Section of Failed Specimen 2PZA-D with a Layup 2, $[0/\pm45/90]_{2s}$, Configuration Showing Misalignment of Fibers Adjacent to Implant

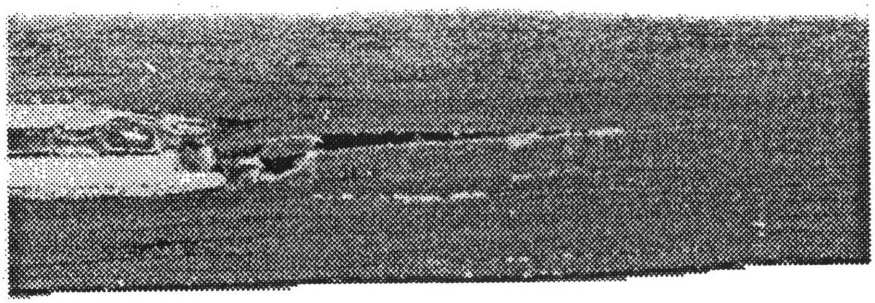

Light area on left is part of the PZA implant with a lead wire attached on its upper right side. Dark area to right of implant is delamination. The height shown is the full laminate thickness; however, only a local section of the specimens width is shown.

Figure 4.51 Photograph of Section of Specimen 4PZA-B Tested to its Peak Stress Value with a Layup 4, $[\pm 45]_{4S}$, Configuration Showing Delamination at Side of Implant

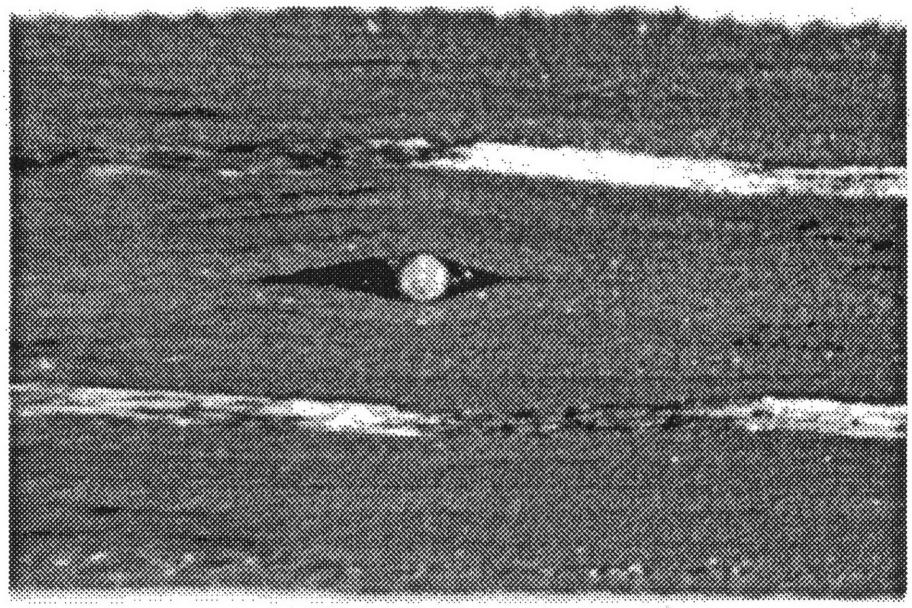

The optical fiber is the light round object in the center of the photograph. The surrounding dark areas is the resin pocket. The height is the full laminate thickness; however, only a local section of the specimen width is shown.

Figure 4.52 Photograph of Section of Coupon 1OF-E Tested to 90% of its Ultimate Stress with a Layup 1, $[0/(\pm 45)_2/90/(\pm 45)_2]_S$, Configuration Showing a Typical Resin Pocket Surrounding the Optical Fiber

4.6.4 Sectioning Results for Specimens with Teflon Implants

A typical bond for specimens with teflon chip implants is shown by a photograph of specimen 2TC-C which was tested to 90% of its ultimate stress in Figure 4.53. Note the resin rich areas at the upper and lower corners of the implant. The fiber misalignment that was present next to the actual chip implants was also visible next to the teflon implants as shown by a photograph of the untested specimen 2TC-A in Figure 4.54.

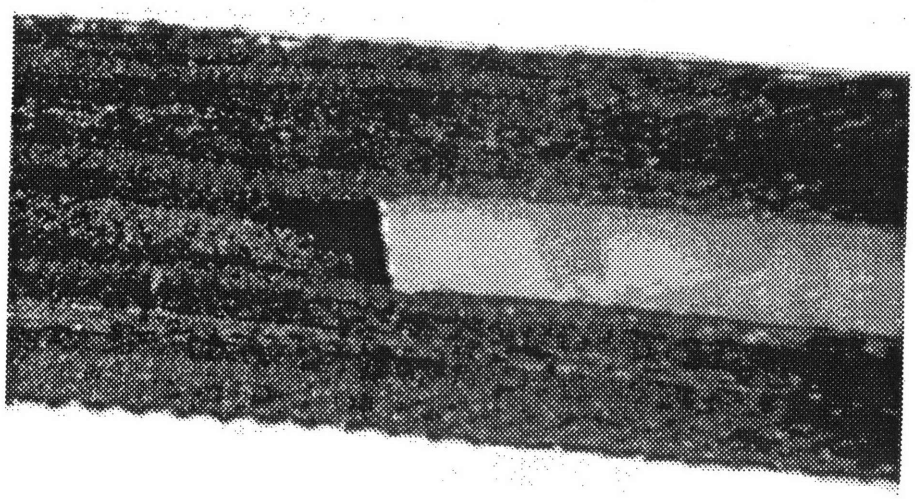

Light area on right is part of the teflon implant. The height shown is the full laminate thickness; however, only a local section of the specimen width is shown. The dark areas to the left of the implant are resin pockets.

Figure 4.53 Photograph of Coupon 2TC-C Tested to 90% of its Ultimate Stress with a Layup 2, $[0/\pm45/90]_{2s}$, Configuration Showing a Typical Bond and the Resin Rich Areas at the Upper and Lower Corners of the Implant

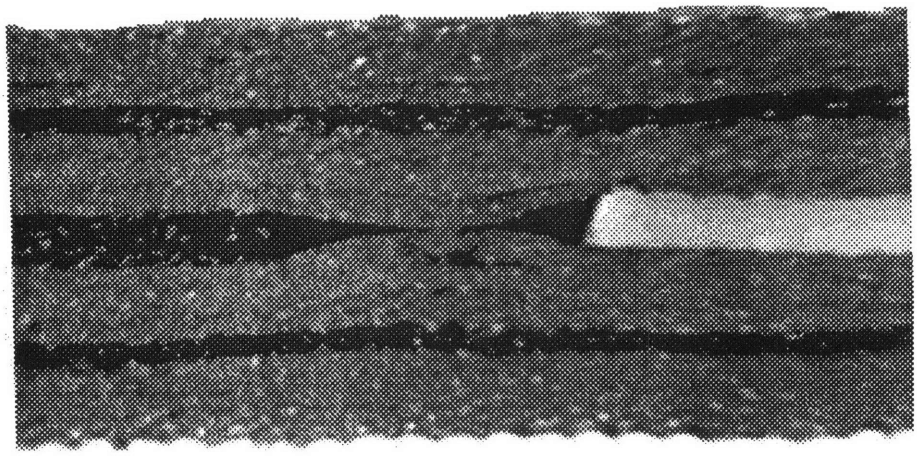

The light area on right side is part of the teflon implant. The height is the full laminate thickness; however, only a local section of the specimen width is shown.

Figure 4.54 Photograph of Untested Coupon 2TC-A with a Layup 2, $[0/\pm45/90]_{2S}$, Configuration Showing Misalignment of Fibers Adjacent to Implant

CHAPTER 5

Discussion

In this chapter, a discussion of the experimental results is presented. The discussion includes the effects of the implant on tensile stress and failure mode of graphite/epoxy tensile coupons with circuit chip, PZA, optical fiber, and teflon chip and PZA implants.

5.1 Prediction of Ultimate Stress Reduction and Overview of Results

As expected, average ultimate stress for the tested laminates was found to be dependent on the percentage of 0°, 45° and 90° plies. Layup 3 had 40% 0° plies which was the highest percentage of all tested layups and virgin specimens with this configuration had the highest ultimate stress of 922 MPa. This was more than twice that of specimens made to the layup 1 configuration that had 10% 0° plies.

Classical laminated plate theory can be used to analyze the load carrying capability of each ply in a laminate with respect to the laminate axes due to an applied load in the laminate longitudinal axis. The percentage of load carrying capability of a ply can be determined by the

ratio of the load carrying capability of that ply with respect to the laminate axes to the sum of the load carrying capability of all the plies with respect to the laminate axes. If, for example, several plies are cut, the percentage of load carrying capability lost can be calculated in a straightforward manner. The following discussion compares predicted losses in ultimate stress due to the cut plies for the implants to the experimentally determined reductions in ultimate stress. Tables 5.1 and 5.2 tabulate the predicted and experimental reductions in ultimate stress due to the implants. Table 5.1 includes percent reductions for all specimens made to a layup 1 or 2 configuration. Table 5.2 includes percent reductions in ultimate stress from the virgin ultimate stresses for all specimens made to a layup 3 or 4 configuration.

All the data presented is for sample sizes of five specimens or less which is too small to perform any comprehensive statistical analysis. The coefficient of variation, however, was presented with all the ultimate stress data in Chapter 4 in Table 4.3 and with the exception of the case with the teflon chip implant, the variation in experimental data was within 10% and often much better.

The variation in ultimate stress data was much smaller if the failure stresses were averaged for failures at and failures away from the implant as shown in Tables 4.4 and 4.5. Failure at the implant was defined as fiber breakage either through or on the edge of an implant. Failure away from the implant was defined when there was no damage to the implant and no fiber breakage on the edge of the implant. When failure occurred at the implant, the ultimate failure stress was up to 12% less than the same implanted specimen that failed away from the

Table 5.1 Comparison of Predicted and Experimentally Determined Reductions in Ultimate Strength Due to Cut Plies for Specimens with a Layup 1 or 2 Configuration

Implant	Layup			
	1 $[0/(\pm45)_2/90/(\pm45)_2]_s$		2 $[0/\pm45/90]_{2s}$	
	Actual % Decrease in Ultimate Stress	Predicted % Decrease in Ultimate Stress	Actual % Decrease in Ultimate Stress	Predicted % Decrease in Ultimate Stress
Chip Implants Placed in Cut Laminate	-.2%	-15.0%	-6.0%	-10.0%
Teflon Chip Implants Placed in Cut Laminate	_____	_____	-10.0%	-10.0%
Chip Implants Placed Directly Into Laminate	_____	_____	-9.0%	_____
PZA Implant Placed in Cut Laminate	+.2%	-15.0%	-14.0%	-14.0%
Teflon PZA Placed in Cut Laminate	_____	_____	-6.0%	-6.0%
Optical Fibers Placed in Cut Laminate	_____	_____	-10.0%	-2.0%
Optical Fibers Placed Directly Into Laminate	+7.0%	_____	-12.0%	_____

Table 5.2 Comparison of Predicted and Experimentally Determined Reductions in Ultimate Strength Due to Cut Plies for Specimens with a Layup 3 or 4 Configuration

Implant	Layup			
	3 $[45/0/-45/0/90/-45/0/-45/0/45]_s$		4 $[\pm 45]_{4s}$	
	Actual % Decrease in Ultimate Stress	Predicted % Decrease in Ultimate Stress	Actual % Decrease in Ultimate Stress	Predicted % Decrease in Ultimate Stress
Circuit Chip Implants Placed in Cut Laminate	-14.8%	-23.7%	+1.2%	-25.0%
PZA Implants Placed in Cut Laminate	-15.7%	-25.9%	+5.7%	-31.2%
Optical Fibers Placed Directly in Laminate	-13.4%	-----	+5.7%	-----

implant. The failure stress data for each specimen given in Appendix B shows that all specimens that failed at the implant with a layup 2 or 3 configuration had failure stresses well below the range of the failure stresses of the virgin specimens with a similar layup configuration. The remaining specimens with a layup 2 or 3 configuration, with the exception of one 2CHIP and one 2TC specimen, also had failure stresses below the range of the virgin specimens' failure stresses although the difference was not as pronounced.

Even though all specimens with a layup 2 or 3 configuration had a decrease in ultimate stress, damage initiation did not always occur at the implant. The comparison of longitudinal moduli given in Table 4.1 indicates that in some cases, the implant can degrade the modulus far-field of the implant.

The strain measured directly over the implant was higher than the strain measured away from the implant for almost all specimens tested. The strain concentration indicated that the load redistribution around the implant was a 3-D phenomenon and depended on the angular orientation of the plies above and below the implant as well as those in the implant plane. The specimens were only tested unidirectionally, whereas in actual application, loading could occur in multiple directions. In the design of actual structures, the load carrying capacity of the plies that were cut for the implant and that surround the implant would change depending on the applied load and their relative orientation to it. The design of smart structures must therefore take all these conditions into consideration.

5.2 Effect of Implants in Specimens with a Layup 1, $[0/(\pm 45)_2/90/(\pm 45)_2]_S$, Configuration

The implants put into specimens with a layup 1 configuration did not have a significant effect on ultimate tensile strength; however, the implants did have an effect on the failure mode. The failure stresses for specimens with chip implants varied from 3% above to 6% below the highest and lowest ultimate stress of the virgin specimens respectively. The implanted specimen with the lowest ultimate stress did fail at the implant. Figure 5.1 shows the variability in the ultimate stress for the virgin and implanted specimens. The large variability is assumed to be due to the limited number of tested specimens; the number of data points are represented by circles on the stress ranges. The horizontal line in the box is the median value for all the data. The top and bottom of the box indicate the maximum and minimum data points. These ranges were based on all failed specimens and do not indicate the difference in ultimate stress that occurred when failure was at the implant. The circles overlaid on the bars indicate where the actual data fell within the range.

Layup 1 had 10% 0° plies, 80% ±45° plies and 10% 90° plies. The 16 ±45° plies carried over 60% of the total longitudinal stress along the laminate loading axis for this particular layup. Only ±45 plies were cut for the implants. The cut ±45° plies carried 15% and 14% of the longitudinal stress in the laminate loading axis for the PZA and chip implants respectively as shown in Table 5.1. These percentages also

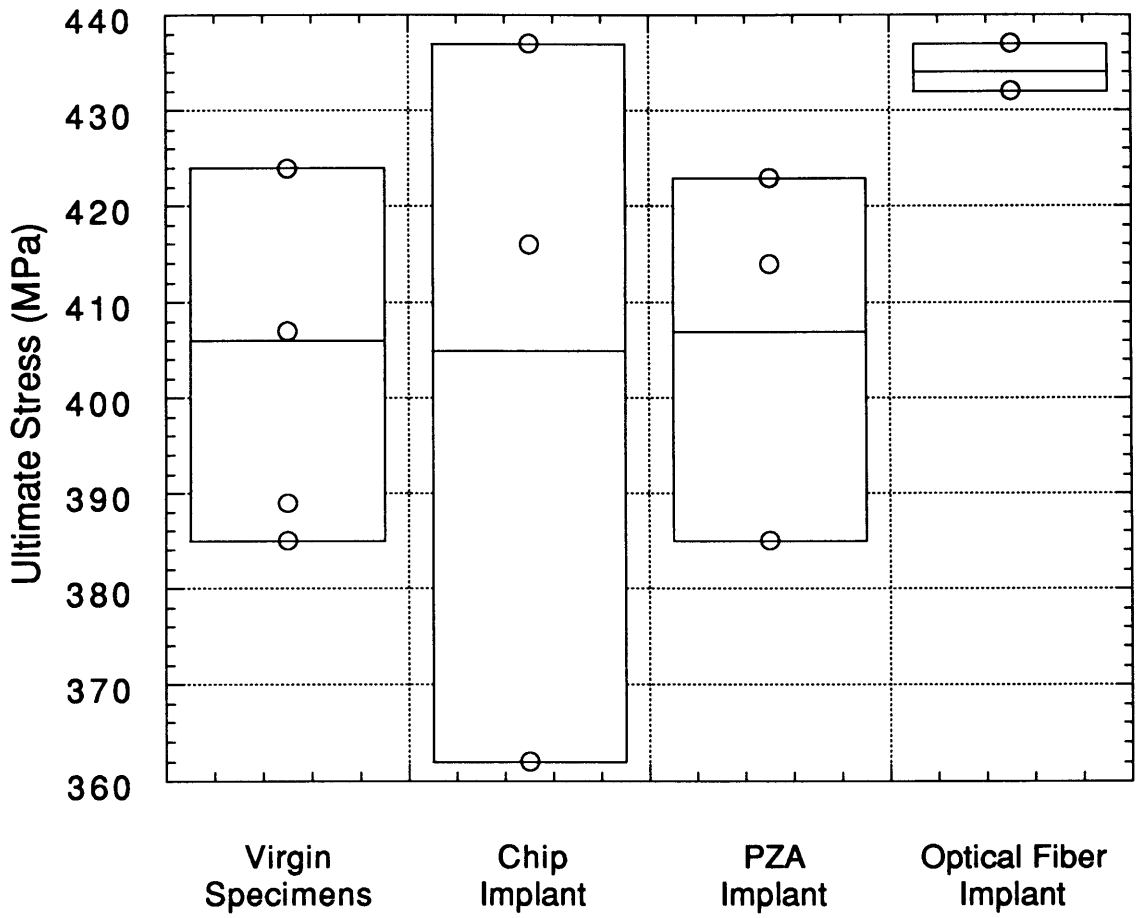

° = Actual specimen data

Figure 5.1 Range of Ultimate Stress Values For Specimens With a Layup 1, $[0/(\pm 45)_2/90/(\pm 45)_2]_S$, Configuration

assumed that the ply was cut along the entire width whereas in reality, the cut extended over a fraction of the entire width. Despite the discrepancy in the amount of cut material, the percentage of load carrying capability should provide some correlation to a decrease in ultimate stress if those plies are cut.

The experimental data showed that the ultimate stress was actually impacted by less than 1% by the presence of the chip and PZA implants. There is no obvious explanation for this result. One possible reason was that the high percentage of ±45° plies caused greater load transfer around the implant and increased the nonlinear constitutive behavior of the material. The 7% increase in average ultimate stress for specimens with optical fiber implants in the layup 1 configuration may be due to variability in material properties between different batches of prepreg material. The difference between the highest ultimate stress of all the virgin specimens and the highest ultimate stress of all the specimens with an implanted optical fiber was only 3%. The small sample sizes may also factor into the discrepancy but the coefficient of variation for both cases was only 4.6% and 8.3% respectively.

The specimens with implants did not always fail at the implant. When the failure did not occur at the implant, the failure modes were similar to the virgin specimens as noted in Chapter 4. The orientation of the damage propagation was altered in the specimens that did fail at the implant. For both the PZA and chip implants, a 45° fracture was changed to 90° along the upper edge of the implant and then returned to a 45° for the remainder of the coupon width. Damage propagation along the upper edge of the implant was not surprising since resin rich areas were present in the sectioned coupons at the top and bottom edges of the

implants. These resin pockets were evident in both tested and untested specimens; therefore, it was assumed to be a result of the manufacturing process. The PZA implant caused a failure through the center of the implant where the lead wires were attached. This type of failure for PZA implanted specimens was observed for all layup configurations and indicated how important it was to have a smooth transition between the leads and the implants. The packaging of the circuit chip and its leads resulted in a lower stress concentration at the corners where the leads were attached relative to the higher stress concentration seen at the opposite corners. Examination of the sectioned specimens that were tested to 95% of the ultimate stress or were failed indicated no signs of delamination at the implants prior to failure.

5.3 Effect of Implants in Specimens with a Layup 2, $[0/\pm45/90]_{2S}$, Configuration

Layup 2 was quasi-isotropic and had 25% 0°, 25% 90° plies and 50% ±45° plies. The specimens with implants in this layup configuration had between a 6% to 14% decrease in ultimate stress versus the virgin specimens. Figure 5.2 shows the variability of the failure stress data for all specimens with the layup 2 configuration. Table 5.1 summarizes the actual and predicted loss of load carrying capability for all specimens with a layup 2 configuration. Embedding the chip implant required that two 90° and two -45° plies be cut. These plies carried 10% of the total longitudinal stress in the laminate loading axes. The specimens with actual and teflon chip implants had average failure stresses 10% and 6% lower than the virgin specimen's average

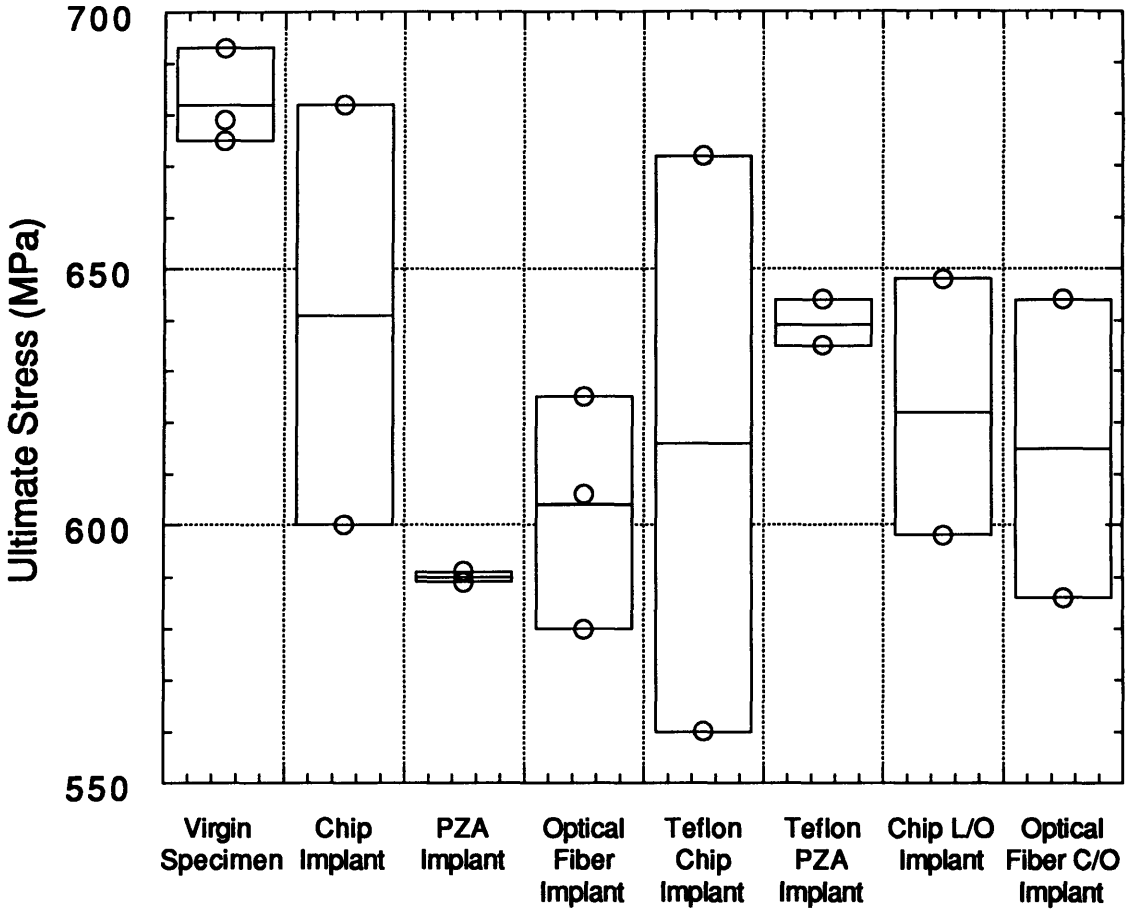

° = Actual specimen data

Figure 5.2 Range of Ultimate Stress Values For Specimens With a Layup 2, $[0/\pm45/90]_{2S}$, Configuration

ultimate stress respectively. Note that the reduction in ultimate stress correlated closely with the predicted value for specimens with the teflon chip implants. The specimens with the chip that was placed directly into the laminate also had a 9% reduction in the ultimate stress even though no plies were cut. This failure was probably due to an increase in interlaminar stresses. It is assumed that another failure mechanism such as delamination must drive this type of failure although no signs of delamination were observed at the implant.

The optical fiber placed directly into the laminate and also into a cut laminate resulted in ultimate stress degradations of 12% and 10% respectively. The predicted loss of strength was only 2% based on the loss of load carrying capability of the two cut plies. The shape and smaller size of the optical fiber may exclude it from the predictions applicable to the larger rectangular implants because different types of failure mechanisms may be occurring. The average ultimate stresses for the two cases was based on a small sample size and the data for both cases did overlap as shown by Figure 5.2. The limited data suggested that there was not a significant difference between laying the optical fiber directly into the laminate or placing it between two cut plies. In this layup, the optical fiber was placed directly between two 90° plies which caused the largest resin pocket and therefore, the largest stress concentration. This might explain the unexpectedly high stress degradation versus the prediction based on the load carrying capacity of the cut plies. Previous research discussed in Chapter 2 suggests that the optical fiber should be placed parallel to the adjacent plies and parallel to the loading direction to minimize any strain concentrations. The placement of the optical fiber parallel to the surrounding plies

would significantly reduce the resin pocket and would be an improvement over cutting the plies.

Two 90° and one -45° plies had to be cut to embed the teflon PZA implants which had no lead wires. These plies carried 6% of the total longitudinal load in the laminate loading axes; however, the actual PZA also required that additional +45° and -45° plies be cut for the leads which should decrease the load carrying capability from the virgin specimens by 14%. This decrease in load carrying capability for both the teflon and actual PZA implants correlated closely with the experimental results for specimens with PZA implants. The teflon and actual PZA specimens had an average ultimate stress 6% and 14% lower than the virgin specimen's average ultimate stress respectively as shown in Table 5.1.

The trend between predicted and actual decreases in ultimate stress due to the cut plies in the layup 2 configuration was much more accurate than for the specimens with the layup 1 configuration. The high percentage of ±45° plies in layup 1 increased the nonlinear load-strain response of the material as seen by the slope in the stress/strain curves for specimens with a layup 1 configuration. It is hypothesized that in general, the experimental ultimate stresses should be higher than those predicted by assuming the ultimate stress decreased proportionally to the percentage of lost load carrying capability of the cut plies. The implanted specimens did not have the plies cut across the entire width and would, therefore, have been capable of some load carrying capability. The 6% actual decrease in ultimate stress for the chip implanted specimens was less than the predicted 10% and supported this hypothesis. The fact that the measured stress of

specimens with teflon chip implants agreed well with the predicted value may be due to the fact that they cannot carry as much load as the actual chip implants. Using the same assumptions, however, the specimens with the PZA implants should also have had greater load carrying capability than the predicted 14% decrease. In this case, the additional stress concentrations at the lead wire attachment to the PZA may have contributed to the low experimental failure stresses. Teflon PZA implants did not have lead wires so the lead wire attachment site could not be the factor that decreased the ultimate stress of these specimens. Similar to the reasoning used for the low ultimate stresses of specimens with teflon chip implants, the teflon PZA was not capable of carrying as much load as the actual specimen and therefore could contribute to the reduced ultimate strength.

The chip and PZA implants also had an affect on the failure mode. Both specimens with PZA implants failed at the implant. The PZA implant had one failure where the implant altered the orientation of the failure from a 90° to a 45° break at the center of the implant, and one failure that occurred along the lower edge of the PZA. Similar to the PZA implants in layup 1, the location where the lead wires were soldered to the PZA was a weak link in the structure. Although the ±45° plies surrounded the implant as for layup 1, their ability to transfer the longitudinal load around the implant was apparently not as effective. The ±45° plies primarily carry shear stress and were not the primary longitudinal load carriers for this layup configuration.

The chip implant did not alter the orientation of the failure although the 90° failure was associated with the upper edge of the implant as defined by Figure 4.21. Sectioned specimens revealed resin

rich areas at this location in both the tested and untested specimens. An X-ray of this specimen indicated that the main sensor in the chip implant was shattered without any damage to the lead wires. This experimental evidence supports finite element work done by Chow [17] which concluded that the lead wires for the dielectric circuit chip implant were not a significant site for strain concentrations due to the smooth transition between the chip and lead wires.

Neither of the specimens with the chip placed directly into the laminate failed at the implant although their ultimate stresses were within the range of the specimens with the chips placed in a cut-out area. The failure modes for these specimens were identical to those seen for the virgin specimens. The limited amount of data suggests that placement of the chip implant directly into the laminate minimized the effect of the implant on the failure mode of the laminate.

None of the specimens with teflon sized to the chips and PZA implants failed at the implant; however, both had failures where the damage propagation occurred at 45° and 90° which deviated from the typical 90° direction.

5.4 Effect of Implants in Specimens with a Layup 3, $[45/0/-45/0/90/-45/0/-45/0/45]_S$, Configuration

This layup was composed of 40% 0° plies, 50% ±45° plies and 10% 90° plies. The specimens with implants in this layup configuration had between a 13% and 18% decrease in ultimate stress for the specimens with optical fiber and PZA implants respectively versus the virgin

specimens. Cutting the 0° plies, which were the primary longitudinal load carriers, had a significant affect on the ultimate stress of all implanted specimens. Figure 5.3 shows the variability in the ultimate stress ranges for all the virgin and implanted specimens.

Table 5.2 summarizes the actual and predicted loss of load carrying capability for all specimens with a layup 3 configuration. Embedding the chip implant required that two 45° and two 0° plies be cut which carry 23.7% of the total longitudinal load of the specimen. The actual reduction in ultimate stress was only 15%. The predicted reduction in ultimate stress for the specimens with PZA implants was 25.9% compared to the actual reduction of 16%. This layup had the largest percentage of 0° plies which may be able to pick up more of the redirected longitudinal stress than the previous layup configuration which was only composed of 25% 0° plies. The 0° plies may not help redistribute the interlaminar stresses induced by the cut plies as effectively as the ±45° plies. In both layup 2 and 3, the plies that surrounded the implant were of a 45° and 0° orientation. Laminates with a layup 3 configuration were composed of 20 plies versus the 16 ply laminates with a layup 2 configuration. The thicker laminate could also have helped the three dimensional load transfer around the implant.

The optical fiber reduced the ultimate stress by 13.4%. These optical fibers were placed between two 45° plies which reduced the size of the resin pocket compared to the optical fibers in specimens with the layup 2 configuration that were placed between two 90° plies. If the size of the resin pocket was the only factor contributing to the stress concentration at the optical fiber, the specimens with a layup 3 configuration with optical fibers should have degraded the stress less

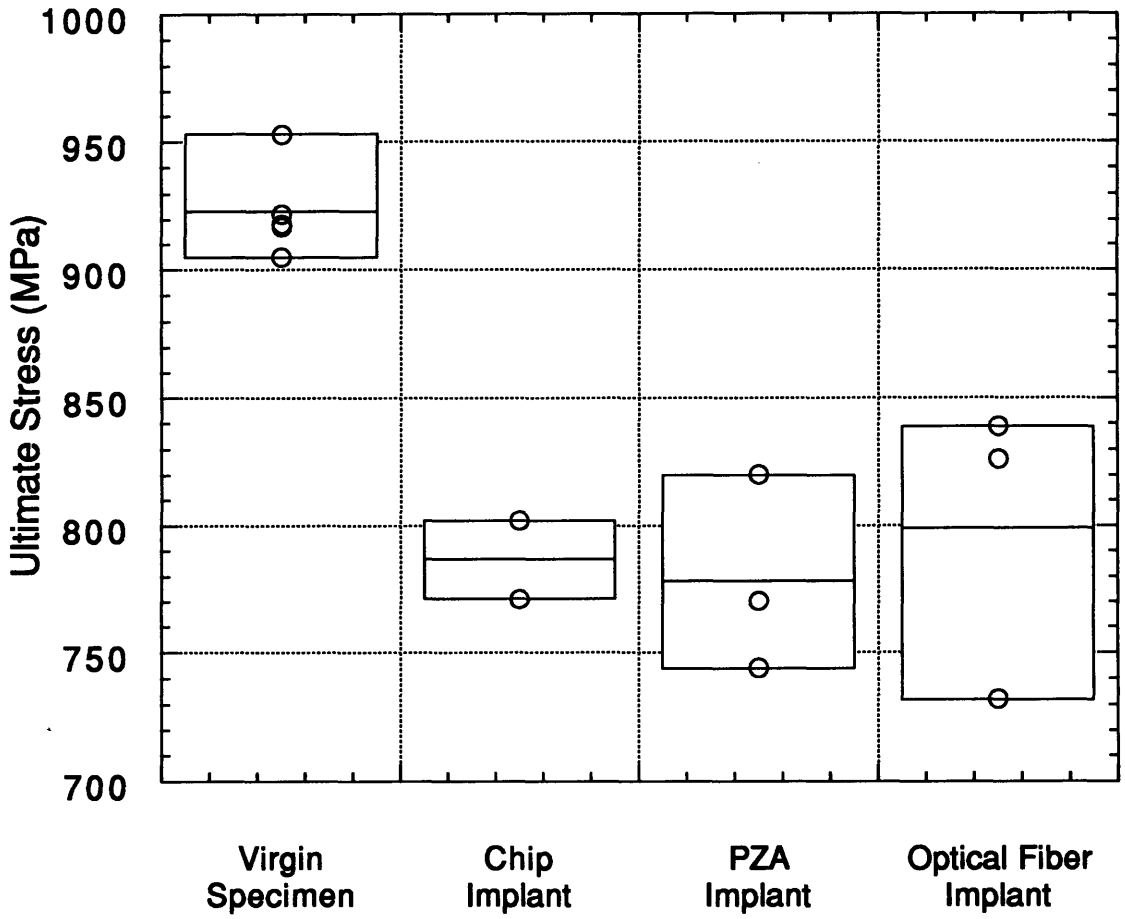

° = Actual specimen data

Figure 5.3 Range of Ultimate Stress Values For Specimens With a Layup 3, $[45/0/-45/0/90/-45/0/-45/0/45]_S$, Configuration

than specimens with a layup 2 configuration. This was not the case however, because the 90° plies surrounding the optical fiber in the specimens with a layup 2 configuration exhibited matrix cracking as shown by the X-rays in Figure 4.43. These matrix cracks limited if not totally destroyed the load carrying capability of the 90° plies; therefore, the induced stress concentrations of the optical fibers were less important than when the optical fibers were between load-carrying plies in layup 3.

The failure modes of specimens were affected by the presence of the chip and PZA implants. The effect of the PZA on failure mode was similar to that seen for the PZA in layups 1 and 2. The failure path for both failed specimens with the PZA implant was through the center of the PZA where the lead wires were attached. The implant also altered the orientation of the failure which followed the outer contour of the implant. This result reinforced the assumption that the edges of the implant were a site for strain concentrations.

Both failed specimens with chip implants showed damage propagation through the implant which shattered the main sensor. The site where the lead wires extended past the main chip out of the laminate did not appear to be a location with a strain concentration since no specimens with any of the four layup configurations failed at this location. Failures along the top edge of the chip implant were at the same location as the resin rich areas observed after sectioning the specimen. The resin pockets were assumed to result from the difference in thermal expansion coefficients between the chip and surrounding graphite/epoxy material. A similar phenomenon was observed in the

form of misaligned fibers adjacent to the chip implant as shown in Figure 4.38.

5.5 Effect of Implants in Specimens with a Layup 4, $[\pm 45]_{4S}$, Configuration

Layup 4 contained 100% ±45° plies. The implants did not affect the stress plateau seen during loading of specimens made with this layup configuration. Table 5.2 shows a comparison of the predicted decrease in ultimate stress to the actual decrease in ultimate stress. Each ply carried 6.2% of the total stress in the laminate loading direction. Embedding the circuit chip required that four plies be cut which was the equivalent of 25% of the load carrying capability of the laminate. Implanting the PZA required five plies be cut which was the equivalent of 31% of the entire load carrying capability of the laminate. The tested specimens actually had an increase of +1.2%, +5.7% and +5.7% of the peak stress for the specimens with chip, PZA, and optical fiber implants respectively. This trend was similar to that seen for implants with a layup 1 configuration that had 80% ±45° plies. These specimens strained very nonlinearly with the applied load. All of the specimens had peak stress values that overlapped into the data for the virgin specimens.

Although the implants did not affect the peak stress for these specimens, the PZA exhibited extensive delamination along its side. By the time the X-rays were taken, it was impossible to determine where the delamination initiated.

It was apparent that matrix cracking for all specimens with a layup 4 configuration was centered around the implant. Although the peak stress was not affected by the implants, this particular configuration would not be recommended due to the extensive delamination that occurred at the implant.

CHAPTER 6

Conclusions and Recommendations

6.1 Conclusions

The following conclusions were made based on the experimental work:

- Implants had the ability to significantly reduce the laminate ultimate stress although the implants were not necessarily the site of failure.

- Failure modes could be significantly altered by the presence of the implant even when the failure did not occur at the implant.

- No evidence of delaminations near any of the implants in the layup 1, 2 or 3 configurations was observed when the specimens were tested to 90 or 95% of their ultimate stress. Delamination was present at the side of the PZA implant in specimens with a layup 4 configuration

that were tested to their peak stress value. Matrix cracking was observed in all four layup configurations.

- Cutting out 0° or primary load path plies for implant placement caused the most severe degradation in ultimate stress, up to 16%.

- Cutting ±45° plies in a laminate with a high (>80%) percentage of ± 45° plies did not cause a significant reduction in ultimate or peak stress; however, the implant could become the site for delamination.

- There was no significant difference in ultimate stress for specimens having the chip or optical fiber placed into a cut-out area or directly into the laminate; however, placing the chip directly into the laminate appeared to prevent failure at the implant but had little affect on failure mode.

- For laminates with less than 50% ±45° plies, the degradation in ultimate stress due to implants could be predicted by a calculation of the decrease in load carrying capacity due to the cut plies. This prediction also worked for the chip placed directly into the laminate. This prediction did not appear appropriate for optical fiber implants which, in some cases, had a more severe affect than predicted.

- The teflon implants had an affect on ultimate stress similar to the actual implants.

- The center of the PZA where the lead wires were attached was the site of many failures.

- Damage propagation in specimens with chip implants often occurred along the top edge of the chip. Resin rich areas were observed at this location in the sectioned specimens.

- The location where the leads extended past the main chip was not a significant site for strain concentrations and subsequent failure.

- The strain concentrations over the implant indicated that there was 3-D load transfer around the implant. The relative size of the implant compared to the total laminate thickness contributed to the load redistribution around the implant.

- Variations in the thermal coefficient of expansion between the implants and surrounding graphite/epoxy appeared to be the cause of fiber misalignment and resin rich pockets around the implant.

6.2 Recommendations

The following are recommendations for further work to evaluate the effect of implants on the structural integrity of composite materials:

- Future experimental and analytical work should attempt to determine the affect of different stacking sequences as well as different

ply orientations on the failure stress and modes of laminates with implants.

- Future experimental and analytical work should attempt to isolate the type of load transfer occurring around the implant which may be dependent on the orientation of the cut and surrounding plies to the load direction.

- A method should be established for predicting the degradation of strength for any combination of implant and laminate.

- Experiments should be conducted to determine the effects of implants on the fatigue characteristics of these laminates.

- The effect of different thermal environments on the interaction between the implant and the laminate should be investigated.

- The effect of implants on the structural integrity of laminates subjected to gradient stress fields and multiaxial loading should be investigated.

References

1. Ahmad, I., "'Smart' Structures and Materials," U.S. Army Research Office Workshop on Smart Materials, Structures, and Mathematical Issues, Blacksburg, Virginia, September, 1988, pp. 13-16.

2. Rogers, C.A., Barker, D.K., and Jaeger, C.A., "Introduction to Smart Materials and Structures," U.S. Army Research Office Workshop on Smart Materials, Structures, and Mathematical Issues, Blacksburg, Virginia, September, 1988, pp. 17-28.

3. Smith, H., "Smart Structures for Combat Aircraft," Advances in Instrumentation and Control, Proceedings of ISA 90 Int'l Conference and Exhibition, New Orleans, LA, October, 1990, pp. 1659-1665.

4. Gerardi, T., "Health Monitoring Aircraft," U.S.-Japan Workshop on Smart/Intelligent Materials and Systems, 1990, pp. 82-91.

5. Talat, K., "Smart Skins and Fiber-Optic Sensors Application and Issues," Fiber Optic Smart Structures and Skins III, Proceedings of the SPIE, San Jose, CA, 1990, pp. 103-114.

6. Rogers, C., "Intelligent Material Systems and Structures," U.S.-Japan Workshop on Smart/Intelligent Materials and Systems, 1990, pp. 11-33.

7. Turner, F. Valis, T. Hogg, W. and Measures, R., "Fiber-Optic Strain Sensors for Smart Structures," Journal of Intelligent Material Systems and Structures, Vol. 1, January, 1990, pp. 26-48.

8. Wood, L., "Design and Fabrication Considerations for Composite Structures with Embedded Fiber Optic Sensors," Fiber Optic Smart Structures and Skins II, Proceedings of the SPIE, Vol. 1170, 1989, pp. 160-170.

9. Claus, R., and Bennett, K., "Smart Skins, Structures, and Materials Instrumentation," Advances in Instrumentation and Control, Proceedings of ISA 90 Int'l Conference and Exhibition, New Orleans, LA, October, 1990, pp. 1649-1657.

10. Sirkis, J., Dasgupta, A., Haslach, H., Chopra, I., Singh, H., Wan, Y., Mathews, C. and Whipple, K., "Smart Structures Mechanics Research at the University of Maryland," Fiber Optic Smart Structures and Skins III, Proceedings of the SPIE, San Jose, CA, 1990, pp. 88-102.

11. Dasgupta, A., Wan, Y. Sirkis, J., and Singh, H., "Micro-Mechanical Investigation of an Optical Fiber Embedded in a Laminated Composite," Fiber Optic Smart Structures and Skins III, Proceedings of the SPIE, San Jose, CA, 1990, pp. 119-128.

12. Salehi, A., Tay, A. Wilson, D., and Smith, D., "Strain Concentrations Around Embedded Optical Fibers by FEM and Moire' Interferometry," Design and Manufacturing of Advanced Composites, Proceedings of the Fifth Annual ASM/ESD Advanced Composites Conference, Dearborn, MI, September, 1989, pp. 11-18.

13. Dasgupta, A. Sirkis, J. and Liu, C., "The Importance of Coatings to Structurally Embedded Optical Fiber Sensors," Advances in Instrumentation and Control, Proceedings of ISA 90 Int'l Conference and Exhibition, New Orleans, LA, October, 1990, pp. 1673-1693.

14. Jensen, D., and Pascual, J., "Performance of Graphite/Bismaleimide Laminates with Embedded Optical Fibers. Part I: Uniaxial Tension," Smart Materials and Structures, Vol. 1, Number 1, March, 1992, pp. 24-30.

15. Measures, R. Glossop, N., Lymer, J., Leblanc, J., West, J., Dubois, S., Tsaw, W. and Tennyson, R., " Structurally Integrated Fiber Optic Damage Assessment System for Composite Materials," Applied Optics, Vol. 28, No. 13, July 1989, pp. 2626-2633.

16. Crawley, E., and de Luis, J., "Use of Piezoelectric Actuators as Elements of Intelligent Structures," AIAA Journal, Vol. 25, No. 10, 1987, pp. 1373-1385.

17. Warkentin, D., and Crawley, E., "Embedded Electronics for Intelligent Structures," 32nd Structures, Structural Dynamics and Materials Conference, AIAA/ASME/ASCE/AHS, New York, NY, 1991.

18. Chow, W., and Graves, M., "Stress Analysis of a Rectangular Implant in Laminated Composites Using 2-D and 3-D Finite Elements," 33rd Structures, Structural Dynamics and Materials Conference, AIAA/ASME/ASCE/AHS, Dallas, TX, April 13-15, 1992, pp. 848-861.

19. Lagace, P., Brewer, J., and Varnerin, C., "TELAC Manufacturing Class Notes," TELAC Report 88-4, MIT, Cambridge, MA 1988.

20. Vizzini, A., "An Efficient Algorithm to Characterize Stress/Strain Data Using Piecewise Linear Curves," Journal of Testing and Evaluation, Vol. 20, No. 2, March, 1992, pp. 126-131.

Appendix A

Thickness and Width Measurements of all Tested Specimens

Thicknesses of Specimens with a Layup 1, $[0/(\pm 45)_2/90/(\pm 45)_2]_S$ Configuration

Specimen	T_1 mm	T_2 mm	T_3 mm	T_4 mm	T_5 mm	T_6 mm	T_7 mm	T_8 mm	T_9 mm	T_{avg} mm
1V-A	2.57	2.60	2.59	2.62	2.57	2.62	2.53	2.57	2.58	2.583
1V-B	2.64	2.67	2.63	2.67	2.63	2.68	2.63	2.66	2.62	2.648
1V-C	2.64	2.68	2.63	2.54	2.58	2.67	2.60	2.60	2.61	2.617
1V-D	2.68	2.54	2.60	2.62	2.62	2.63	2.62	2.60	2.60	2.612
1V-E	2.66	2.62	2.66	2.67	2.59	2.62	2.64	2.65	2.62	2.637
1 CHIP-A	2.65	2.65	2.66	2.73	2.76	2.72	2.73	2.70	2.70	2.70
1CHIP-B	2.77	2.72	2.73	2.73	2.79	2.74	2.76	2.76	2.74	2.75
1CHIP-C	2.69	2.73	2.76	2.72	2.73	2.78	2.76	2.74	2.80	2.75
1CHIP -D	2.77	2.77	2.78	2.71	2.74	2.72	2.75	2.71	2.74	2.74
1CHIP-E	2.71	2.68	2.68	2.64	2.65	2.66	2.67	2.67	2.65	2.67
1OF-A	2.73	2.66	2.69	2.70	2.75	2.78	2.68	2.72	2.72	2.71
1OF-B	2.72	2.72	2.74	2.77	2.73	2.77	2.75	2.75	2.74	2.74
1OF-C	2.72	2.70	2.73	2.74	2.77	2.78	2.72	2.72	2.73	2.74
1OF-D	2.75	2.82	2.83	2.80	2.82	2.77	2.77	2.76	2.77	2.79
1OF-E	2.79	2.69	2.77	2.76	2.73	2.74	2.82	2.69	2.72	2.75
1PZA-B	2.81	2.86	2.83	2.86	2.89	2.85	2.81	2.8	2.8	2.83
1PZA-C	2.9	2.88	2.9	2.8	2.85	2.86	2.7	2.8	2.85	2.84
1PZA-D	2.84	2.9	2.96	2.85	2.85	2.85	2.88	2.85	2.82	2.87
1PZA-E	2.83	2.89	2.92	2.88	2.9	2.84	2.8	2.88	2.87	2.87

Widths of Specimens with a Layup 1, $[0/(\pm 45)_2/90/(\pm 45)_2]_S$ Configuration

Specimen	W_1 mm	W_2 mm	W_3 mm	W avg mm	A avg mm^2
1V-A	51.54	51.56	51.66	51.58	133.2
1V-B	51.64	51.66	51.68	51.64	136.7
1V-C	51.72	51.72	51.70	51.71	135.3
1V-D	74	70	68	51.71	135.1
1V-E	51.86	51.8	51.7	51.8	136.6
1CHIP-A	50.2	50.3	50.40	50.3	135.8
1CHIP-B	50.26	50.24	50.23	50.24	138.2
1CHIP-C	50.1	50.1	50.18	50.13	137.9
1CHIP-D	49.9	49.75	49.6	49.75	136.3
1CHIP-E	50.24	50.24	50.24	50.24	134.1
1OF-A	50.24	50.24	50.28	50.25	136.2
1OF-B	50.3	50.28	50.32	50.3	137.8
1OF-C	50.29	50.3	50.35	50.31	137.8
1OF-D	50.32	50.34	50.36	50.34	135.9
1OF-E	50.96	50.8	50.7	50.82	139.8
1PZA-B	50.12	50.12	50.1	50.11	142.0
1PZA-C	50.08	50.12	50.12	50.11	142.2
1PZA-D	50.08	50.08	50.08	50.08	143.6
1PZA-E	50.14	50.1	50	50.08	143.6

Thicknesses of Specimens with a Layup 2, $[0/\pm45/90]_{2S}$ Configuration

Specimen	T_1 mm	T_2 mm	T_3 mm	T_4 mm	T_5 mm	T_6 mm	T_7 mm	T_8 mm	T_9 mm	T_{avg} mm
2V-A	2.11	2.08	2.11	2.06	2.09	2.11	2.09	2.06	2.09	2.09
2V-B	2.13	2.12	2.13	2.17	2.17	2.13	2.18	2.13	2.16	2.09
2V-D	2.22	2.15	2.16	2.09	2.07	2.09	2.15	2.26	2.14	2.15
2V-E	2.13	2.13	2.12	2.14	2.14	2.14	2.15	2.16	2.17	2.14
2TP-A	2.16	2.16	2.18	2.14	2.15	2.17	2.14	2.15	2.19	2.16
2TP-B	2.22	2.23	2.25	2.23	2.27	2.26	2.25	2.22	2.26	2.24
2TP-C	2.27	2.22	2.27	2.25	2.24	2.21	2.25	2.25	2.26	2.25
2TP-D	2.21	2.25	2.21	2.24	2.23	2.27	2.23	2.25	2.27	2.24
2TP-E	2.17	2.19	2.22	2.17	2.18	2.19	2.21	2.16	2.21	2.19
2CHIP-A	2.17	2.17	2.15	2.19	2.16	2.18	2.20	2.16	2.19	2.17
2CHIP-B	2.21	2.23	2.22	2.27	2.27	2.25	2.26	2.22	2.22	2.24
2CHIP-C	2.21	2.19	2.24	2.24	2.28	2.28	2.21	2.19	2.24	2.23
2CHIP -D	2.27	2.22	2.25	2.28	2.29	2.25	2.25	2.23	2.23	2.25
2CHIP-E	2.24	2.20	2.20	2.22	2.21	2.17	2.19	220	2.20	2.20
2TC-A	2.20	2.13	2.16	2.16	2.25	2.16	2.14	2.11	2.15	2.16
2TC-B	2.23	2.25	2.25	2.26	2.31	2.27	2.25	2.22	2.23	2.25
2TC-C	2.26	2.25	2.26	2.27	2.32	2.25	2.25	2.24	2.22	2.26
2TC-D	2.23	2.21	2.22	2.21	2.29	2.22	2.21	2.25	2.25	2.23
2TC-E	2.13	2.13	2.17	2.17	2.19	2.17	2.20	2.16	2.20	2.17
2PZA-E	2.19	2.18	2.20	2.26	2.29	2.28	2.21	2.22	2.33	2.24
2PZA-B	2.27	2.24	2.27	2.31	2.31	2.29	2.36	2.26	2.26	2.29
2PZA-A	2.27	2.26	2.18	2.26	2.25	2.23	2.25	2.26	2.31	2.25
2PZA-D	2.25	2.17	2.29	2.16	2.20	2.24	2.20	2.18	2.23	2.21
2PZA-C	2.30	2.26	2.24	2.28	2.26	2.29	2.31	2.26	2.20	2.27
2OF-B	2.29	2.28	2.28	2.32	2.33	2.34	2.31	2.27	2.3	2.3
2OF-C	2.36	2.33	2.35	2.38	2.3	2.3	2.37	2.31	2.27	2.33
2OF-D	2.27	2.25	2.29	2.33	2.32	2.31	2.37	2.28	2.22	2.29
2OF-E	2.2	2.16	2.25	2.25	2.22	2.27	2.22	2.21	2.24	2.22
2CHIP-A L/O	2.2	2.26	2.21	2.23	2.43	2.23	2.16	2.3	2.27	2.25
2CHIP-B L/O	2.24	2.23	2.22	2.23	2.38	2.25	2.29	2.26	2.28	2.26
2CHIP-C L/O	2.29	2.29	2.3	2.25	2.4	2.28	2.3	2.31	2.28	2.30
2CHIP-D L/O	2.28	2.26	2.26	2.28	2.4	2.25	2.28	2.34	2.26	2.29
2OF-A C/O	2.14	2.17	2.15	2.1	2.15	2.11	2.16	2.13	2.11	2.14
2OF-B C/O	2.12	2.2	2.23	2.16	2.16	2.18	2.16	2.17	2.2	2.18
2OF-C C/O	2.23	2.22	2.2	2.25	2.25	2.21	2.23	2.17	2.2	2.22
2OF-D C/O	2.17	2.17	2.2	2.16	2.17	2.2	2.17	2.2	2.23	2.19

Widths of Specimens with a Layup 2, $[0/\pm45/90]_{2S}$ Configuration

Specimen	W_1 mm	W_2 mm	W_3 mm	W_{avg} mm	A_{avg} mm^2
2V-A	50.46	50.42	50.42	50.43	105.3
2V-B	50.4	50.4	50.4	50.4	105.4
2V-D	50.48	50.46	50.42	50.46	108.4
2V-E	50.1	50.12	50.2	50.15	107.3
2TP-A	49.88	49.94	49.98	49.93	107.9
2TP-B	50.20	50.24	50.24	50.23	112.5
2TP-C	50.12	50.18	50.20	50.17	112.9
2TP-D	50.18	50.20	50.21	50.20	112.4
2TP-E	50.10	50.22	50.34	50.22	110.0
2CHIP-A	50.10	50.02	50.00	50.04	108.6
2CHIP-B	50.22	50.14	50.12	50.16	112.4
2CHIP-C	50.00	50.06	50.16	50.07	111.7
2CHIP -D	50.22	50.18	50.16	50.19	112.9
2CHIP-E	50.36	50.56	50.78	50.57	111.3
2TC-A	50.44	50.62	50.74	50.60	109.3
2TC-B	50.22	50.20	50.22	50.21	113.0
2TC-C	50.17	50.20	50.22	50.20	113.5
2TC-D	50.08	50.12	50.18	50.13	111.8
2TC-E	50.08	50.07	50.09	50.08	108.7
2PZA-E	50.39	50.4	50.38	50.39	112.9
2PZA-B	50.18	50.24	50.26	50.23	115.0
2PZA-A	50.64	50.64	50.8	50.69	114.1
2PZA-D	50.28	50.28	50.28	50.28	111.1
2PZA-C	50.38	50.37	50.34	50.36	114.3
2OF-B	50.1	50.2	50.21	50.17	115.4
2OF-C	50.4	50.28	50.24	50.31	117.2
2OF-D	50.22	50.2	50.18	50.20	115.0
2OF-E	51.12	51.13	51.14	51.13	113.5
2CHIP-A L/O	50.06	50.2	50.2	50.15	112.8
2CHIP-B L/O	50.34	50.52	50.52	50.46	114.0
2CHIP-C L/O	50.4	50.5	50.56	50.49	116.1
2CHIP-D L/O	50.1	50.2	50.2	50.17	114.9
2OF-A C/O	50.34	50.32	50.33	50.33	107.7
2OF-B C/O	50.3	50.3	50.3	50.30	109.7
2OF-C C/O	50.4	50.4	50.38	50.39	111.9
2OF-D C/O	50.44	50.44	50.38	50.42	110.4

Thicknesses of Specimens with a Layup 3, $[45/0/-45/0/90/-45/0/-45/0/45]_s$, Configuration

Specimen	T_1 mm	T_2 mm	T_3 mm	T_4 mm	T_5 mm	T_6 mm	T_7 mm	T_8 mm	T_9 mm	T_{avg} mm
3V-A	2.49	2.51	2.51	2.53	2.55	2.56	2.54	2.56	2.56	2.53
3V-B	2.65	2.65	2.66	2.63	2.65	2.63	2.65	2.66	2.66	2.65
3V-C	2.68	2.68	2.65	2.65	2.65	2.66	2.66	2.63	2.65	2.66
3V-D	2.64	2.64	2.61	2.68	2.65	2.61	2.65	2.65	2.64	2.64
3V-E	2.57	2.59	2.57	2.60	2.60	2.60	2.61	2.64	2.64	2.60
3CHIP-B	2.7	2.63	2.65	2.72	2.8	2.81	2.72	2.84	2.8	2.74
3CHIP-C	2.77	2.73	2.82	2.8	2.79	2.79	2.76	2.8	2.82	2.79
3CHIP -D	2.75	2.72	2.75	2.72	2.77	2.78	2.75	2.76	2.77	2.75
3CHIP-E	2.71	2.72	2.75	2.67	2.7	2.7	2.72	2.73	2.74	2.72
3OF-A	2.71	2.84	2.9	2.95	2.84	2.79	2.77	2.82	2.82	2.83
3OF-B	2.89	2.86	2.96	2.95	2.90	2.91	2.87	2.89	2.89	2.90
3OF-C	2.95	2.91	2.95	2.97	2.95	2.97	3012	3.02	2.93	2.97
3OF-D	2.95	2.95	2.89	3.05	3.15	2.94	2.91	2.89	2.92	2.96
3OF-E	2.78	2.75	2.73	2.82	2.82	2.82	2.85	2.77	2.77	2.79
3PZA-A	2.6	2.58	2.6	2.64	2.66	2.65	2.67	2.75	2.67	2.65
3PZA-B	2.77	2.73	2.7	2.68	2.75	2.72	2.68	2.68	2.67	2.71
3PZA-C	2.72	2.72	2.71	2.7	2.7	2.67	2.76	2.72	2.74	2.72
3PZA-D	2.69	2.68	2.65	2.75	2.72	2.75	2.75	2.79	2.79	2.73

Widths of Specimens with a Layup 3, $[45/0/-45/0/90/-45/0/-45/0/45]_s$, Configuration

Specimen	W_1 mm	W_2 mm	W_3 mm	Wavg mm	Aavg mm^2
3V-A	50.66	50.6	50.56	50.60	128.2
3V-B	50.56	50.52	50.42	50.50	133.8
3V-C	50.55	50.54	50.54	50.55	134.3
3V-D	50.54	50.54	50.48	50.52	133.4
3V-E	50.44	50.42	50.42	50.43	131.1
3CHIP-B	50	50.2	50	50.07	137.2
3CHIP-C	50.17	50.14	50.05	50.12	139.8
3CHIP -D	50.1	50.08	50	50.06	137.7
3CHIP-E	50.3	50.28	50.25	50.28	136.8
3OF-A	49.9	50.1	50.13	50.04	141.6
3OF-B	49.98	49.88	49.84	49.9	144.7
3OF-C	49.82	49.79	49.79	49.8	147.9
3OF-D	49.9	49.88	49.86	49.88	147.6
3OF-E	49.1	49.12	49.9	49.37	137.7
3PZA-A	50.45	50.46	50.48	50.46	133.7
3PZA-B	50.3	50.3	50.3	50.30	136.3
3PZA-C	50.9	50.12	50.92	50.65	137.8
3PZA-D	49.24	49.25	49	49.16	134.2

Thicknesses of Specimens made to a Layup 4, $[\pm 45]_{4S}$, Configuration

Specimen	T_1 mm	T_2 mm	T_3 mm	T_4 mm	T_5 mm	T_6 mm	T_7 mm	T_8 mm	T_9 mm	T_{avg} mm
4V-A	2.17	2.15	2.14	2.17	2.13	2.21	2.13	2.08	2.06	2.14
4V-B	2.20	2.13	2.17	2.10	2.13	2.17	2.11	2.12	2.11	2.14
4V-C	2.09	2.05	2.14	2.13	2.13	2.14	2.09	2.08	2.08	2.10
4V-D	2.09	2.07	2.09	2.12	2.12	2.08	2.08	2.08	2.10	2.09
4V-E	2.11	2.14	2.14	2.09	2.14	2.15	2.09	2.11	2.12	2.12
4CHIP-B	2.26	2.29	2.3	2.25	2.32	2.3	2.23	2.25	2.28	2.28
4CHIP-C	2.23	2.23	2.3	2.26	2.26	2.26	2.3	2.31	2.31	2.27
4CHIP-D	2.28	2.26	2.27	2.3	2.33	2.32	2.28	2.27	2.3	2.29
4CHIP-E	2.31	2.31	2.33	2.26	2.3	2.32	2.25	2.22	2.24	2.82
4OF-A	2.15	2.2	2.17	2.15	2.23	2.15	2.15	2.23	2.17	2.18
4OF-B	2.2	2.21	2.21	2.24	2.22	2.24	2.22	2.24	2.23	2.22
4OF-C	2.16	2.22	2.17	2.19	2.22	2.19	2.23	2.27	2.2	2.21
4OF-D	2.23	2.25	2.27	2.26	2.24	2.25	2.21	2.24	2.26	2.25
4PZA-A	2.08	2.1	2.12	2.09	2.08	2.11	2.11	2.1	2.07	2.10
4PZA-B	2.11	2.14	2.14	2.17	2.16	2.13	2.12	2.17	2.2	2.15
4PZA-C	2.15	2.15	2.21	2.1	2.12	2.13	2.09	2.17	2.09	2.13
4PZA-D	2.15	2.13	2.17	2.1	2.13	2.11	2.14	2.13	2.14	2.13

Widths of Specimens made to a Layup 4, $[\pm 45]_{4S}$, Configuration

Specimen	W_1 mm	W_2 mm	W_3 mm	W_{avg} mm	A_{avg} mm^2
4V-A	50.55	50.60	50.62	50.59	108.2
4V-B	50.5	50.50	50.48	50.49	107.9
4V-C	50.44	50.44	50.44	50.44	106.1
4V-D	50.34	50.34	50.34	50.34	105.3
4V-E	50.57	50.57	50.56	50.57	107.2
4CHIP-B	50.18	50.22	50.16	50.19	114.4
4CHIP-C	50.02	50.1	50.1	50.07	113.7
4CHIP-D	50.05	50.1	50.25	50.13	114.8
4CHIP-E	50.2	50.28	50.26	50.25	141.7
4OF-A	50.3	50.6	50.7	50.53	110.1
4OF-B	50.2	50.26	50.3	50.25	111.7
4OF-C	50.2	50.34	50.44	50.33	111.0
4OF-D	50.32	50.34	50.28	50.31	113.0
4PZA-A	50.3	50.37	50.4	50.36	105.5
4PZA-B	50.5	50.56	50.7	50.59	108.7
4PZA-C	50.4	50.48	50.54	50.47	107.7
4PZA-D	50.42	50.45	50.52	50.46	107.7

Appendix B

Failure Stresses of All Tested Specimens

Failure Stresses in MPa of All Tested Specimens

Implant	Layup			
	1 $[0/(\pm45)_2/90/(\pm45)_2]_s$	2 $[0/\pm45/90]_{2s}$	3 [45/0/-45/0/90/-45/0/-45/0/45]s	4 $[\pm45]_{4s}$
Virgin Specimens	385 424 389 424 407 C.V. = .046	675 693 679 C.V. = .014	922 905 917 918 953 C.V. = .019	145 159 166 C.V. = .068
Circuit Chip Implants Placed in Cut Laminate	437 416* 362 C.V. = .097	600* 682 C.V. = .090	771* 802* C.V. = .028	152 166 C.V. = .062
PZA Implants Placed in Cut Laminate	414 423 385* C.V. = .052	591* 589* C.V. = .0024	820 770* 744* C.V. = .052	166 166 C.V. = 0
Optical Fibers Placed Directly in Laminate	437 432 C.V. = .0083	606 625 580 C.V. = .037	826 839 732 C.V. = .073	166 166 C.V. = 0
Teflon Circuit Chip Placed in Cut Laminate	—	672 560 C.V. = .129	—	—
Teflon PZA Placed in Cut Laminate	—	635 644 C.V. = .010	—	—
Circuit Chip Placed Directly in Laminate	—	598 648 C.V. = .058	—	—
Optical Fibers Placed in Cut Laminate	—	586 644 C.V. = .067	—	—

* Failure At Implant

Appendix C

Stress-Strain Curves for Virgin Specimens

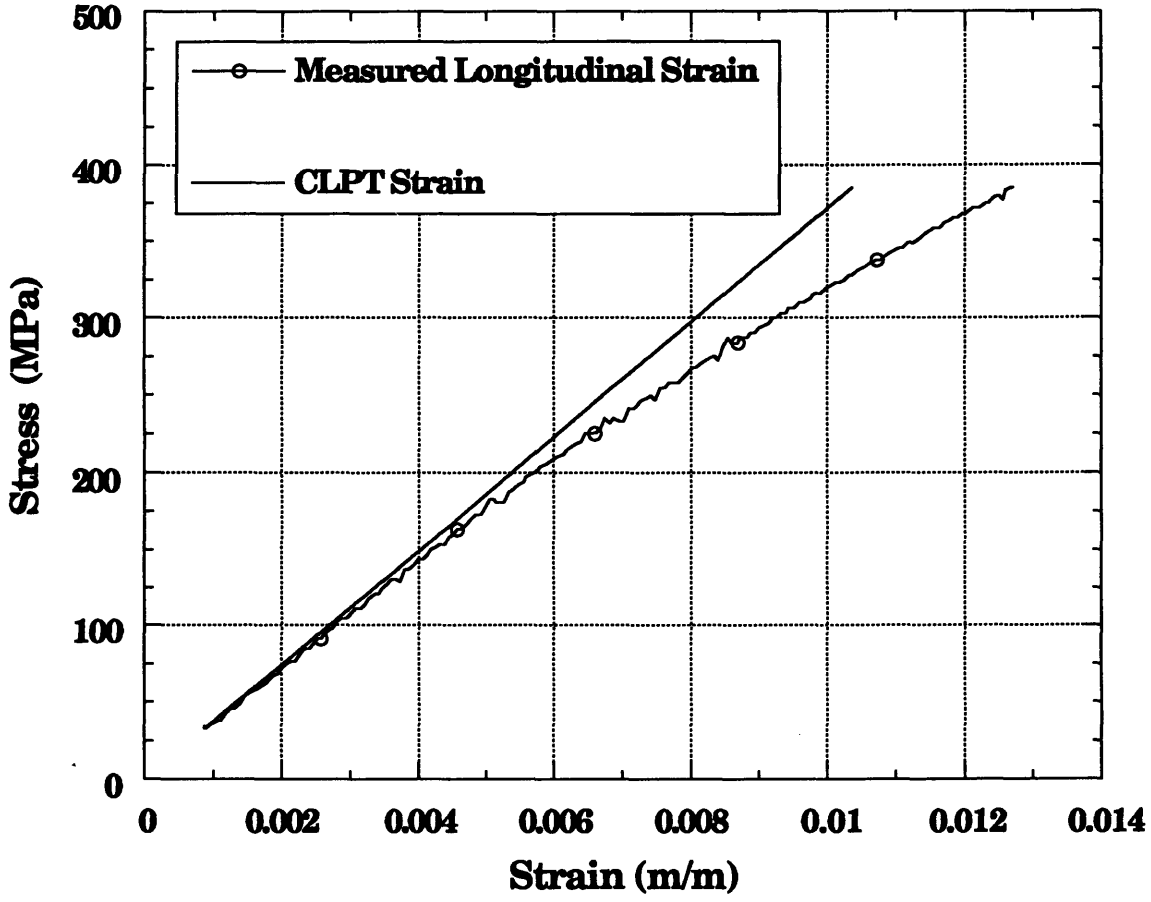

Figure C.1 Stress-Strain Curves for Virgin Coupon 1V-A with a Layup 1, $[0/(\pm 45)_2/90/(\pm 45)_2]_S$, Configuration Tested to Failure

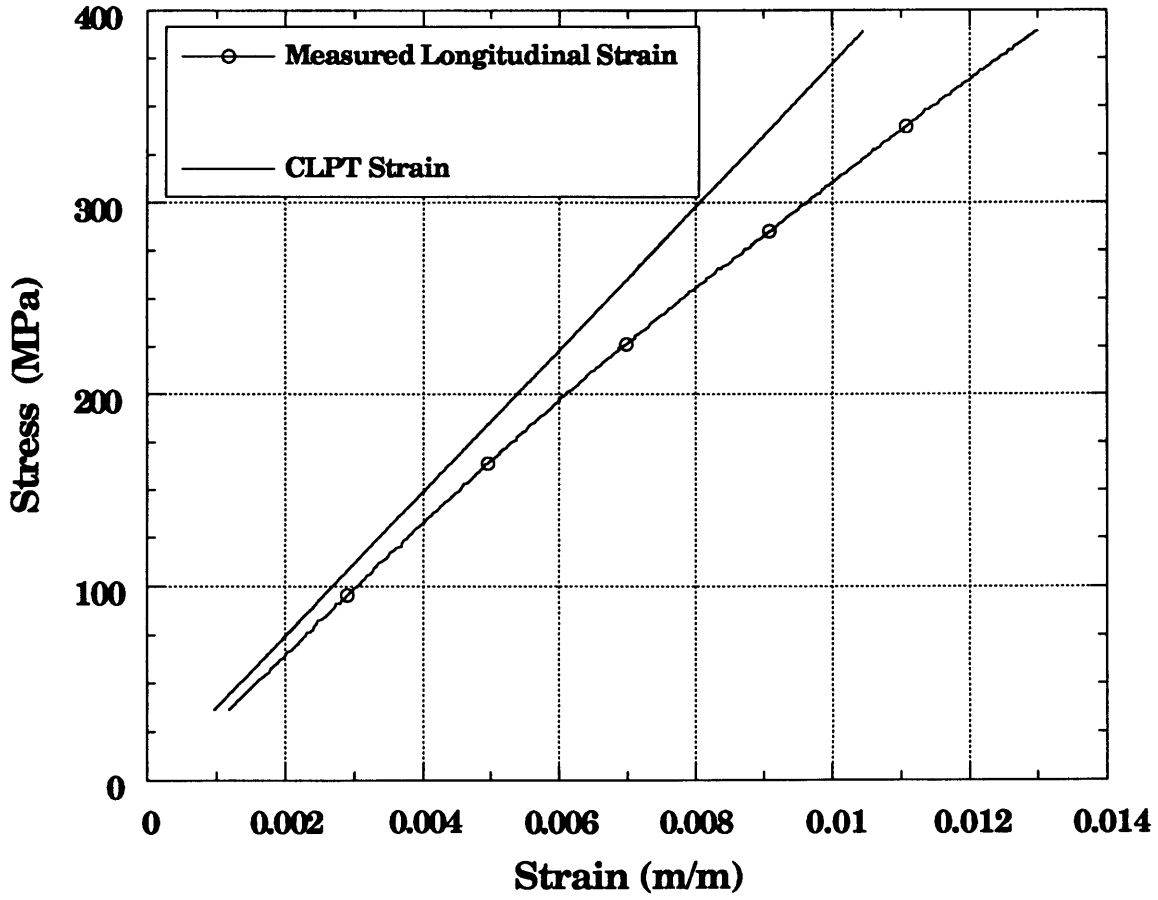

Figure C.2 Stress-Strain Curves for Virgin Coupon 1V-C with a Layup 1, $[0/(\pm 45)_2/90/(\pm 45)_2]_S$, Configuration Tested to Failure

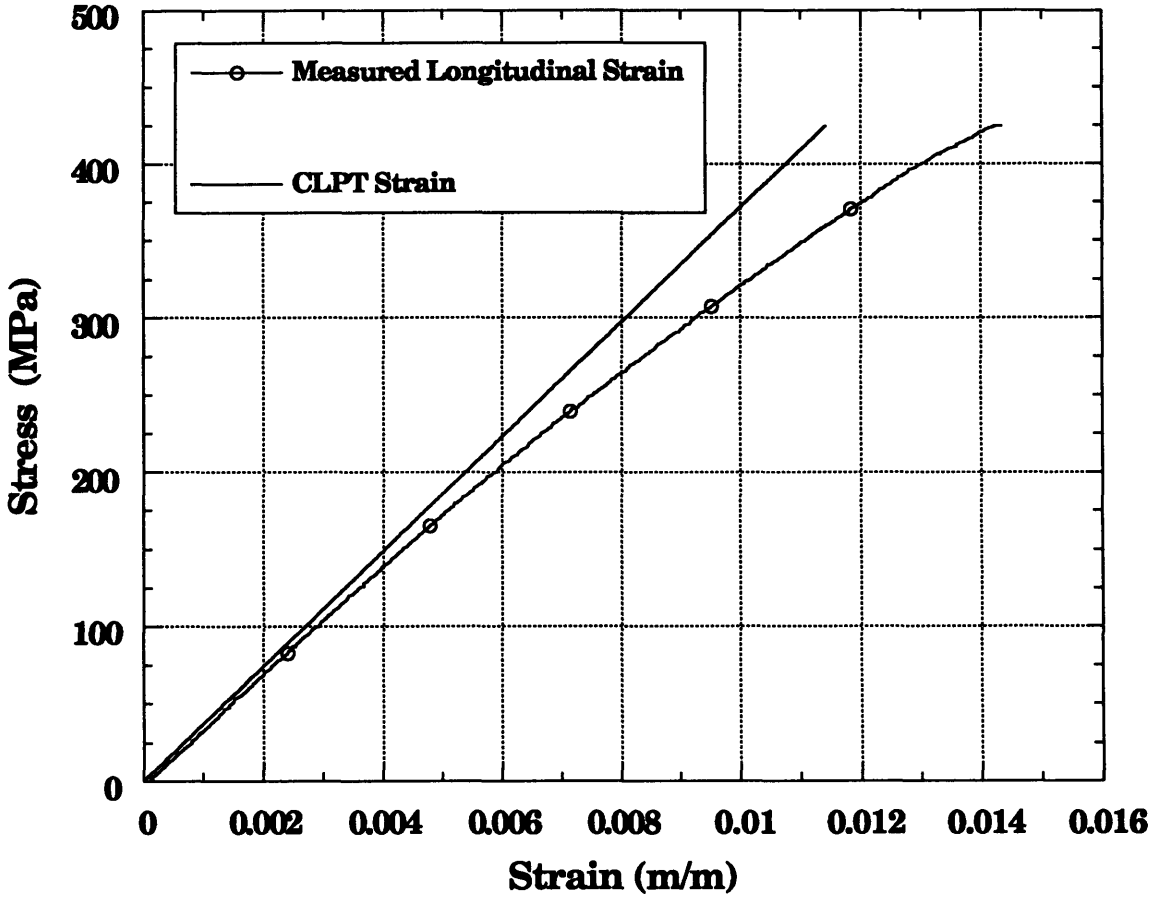

Figure C.3 Stress-Strain Curves for Virgin Coupon 1V-D with a Layup 1, $[0/(\pm 45)_2/90/(\pm 45)_2]_S$, Configuration Tested to Failure

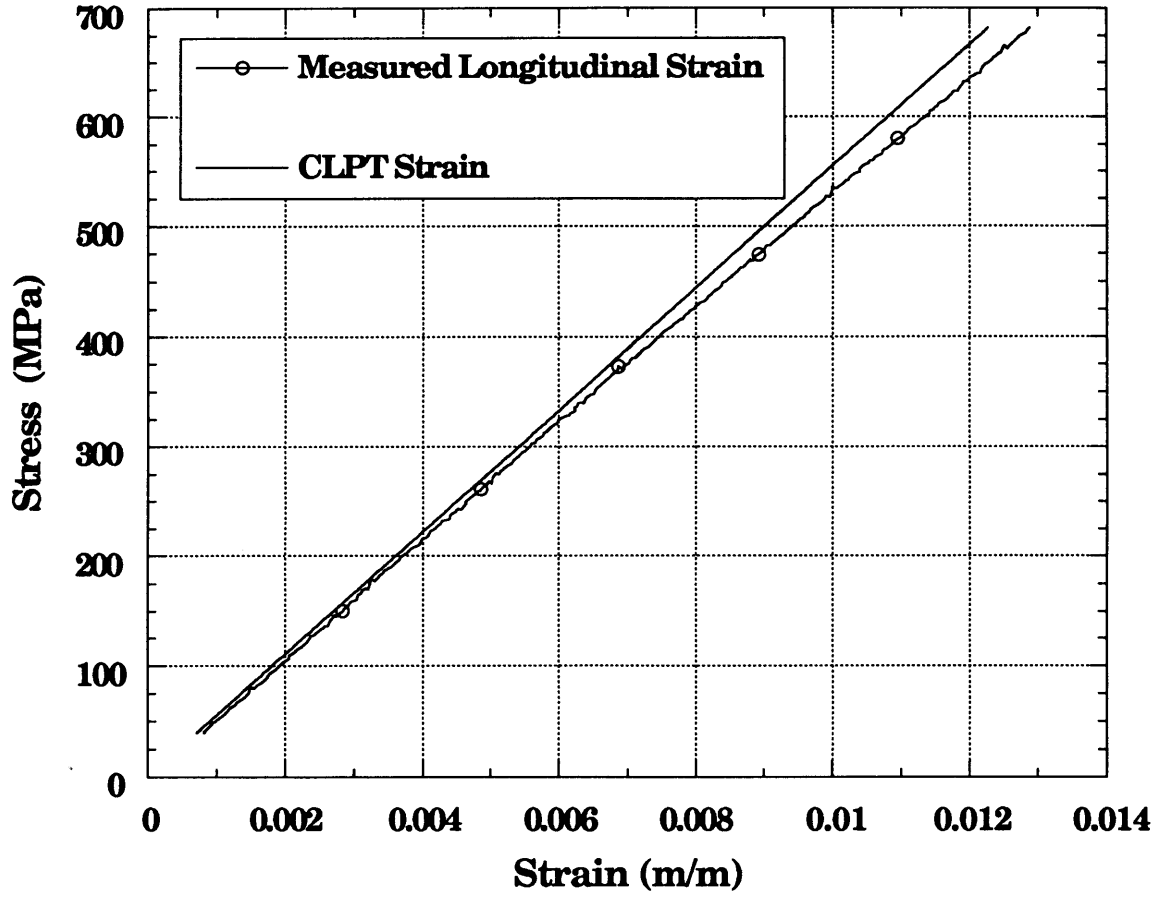

Figure C.4 Stress-Strain Curves for Virgin Coupon 2V-B with a Layup 2, $[0/\pm45/90]_{2s}$, Configuration Tested to Failure

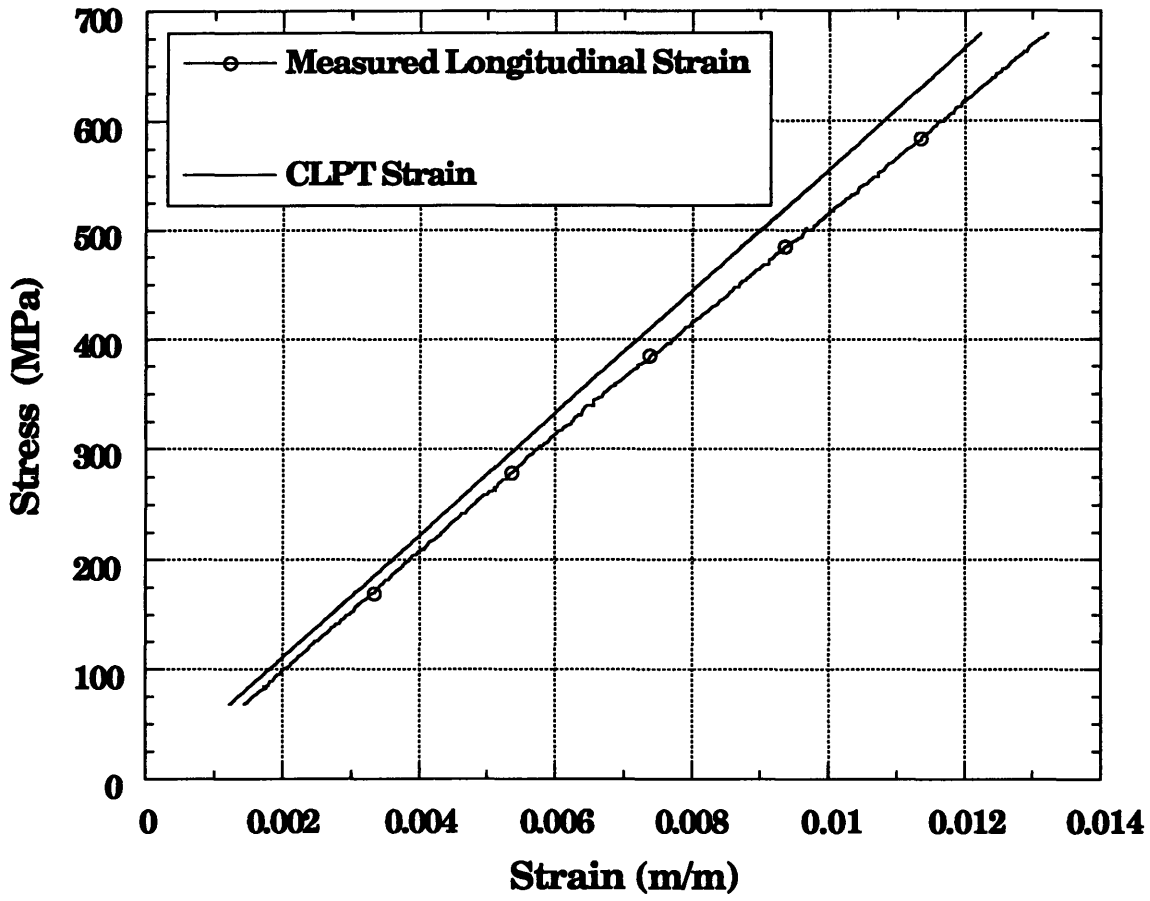

Figure C.5 Stress-Strain Curves for Virgin Coupon 2V-E with a Layup 2, $[0/\pm45/90]_{2S}$, Configuration Tested to Failure

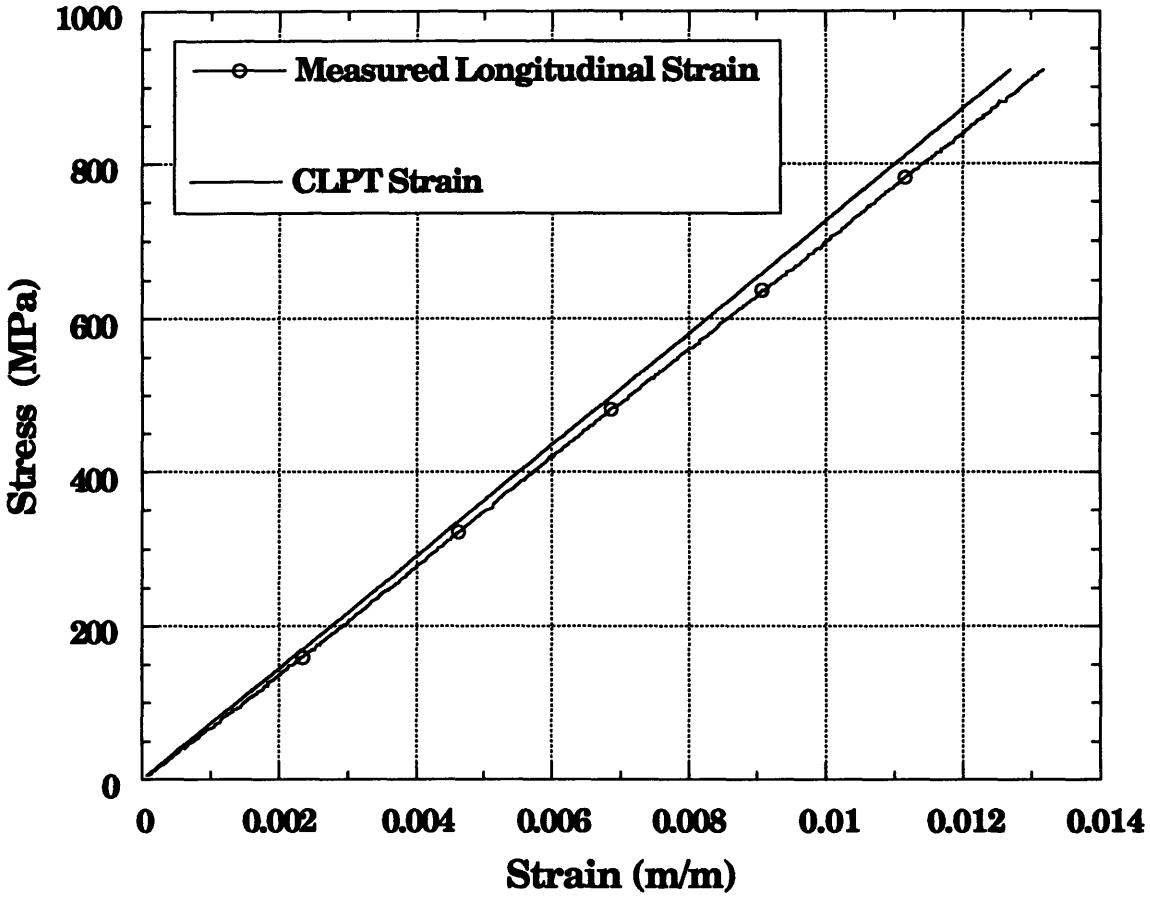

Figure C.6 Stress-Strain Curves for Virgin Coupon 3V-A with a Layup 3, $[45/0/-45/0/90/-45/0/-45/0/45]_S$, Configuration Tested to Failure

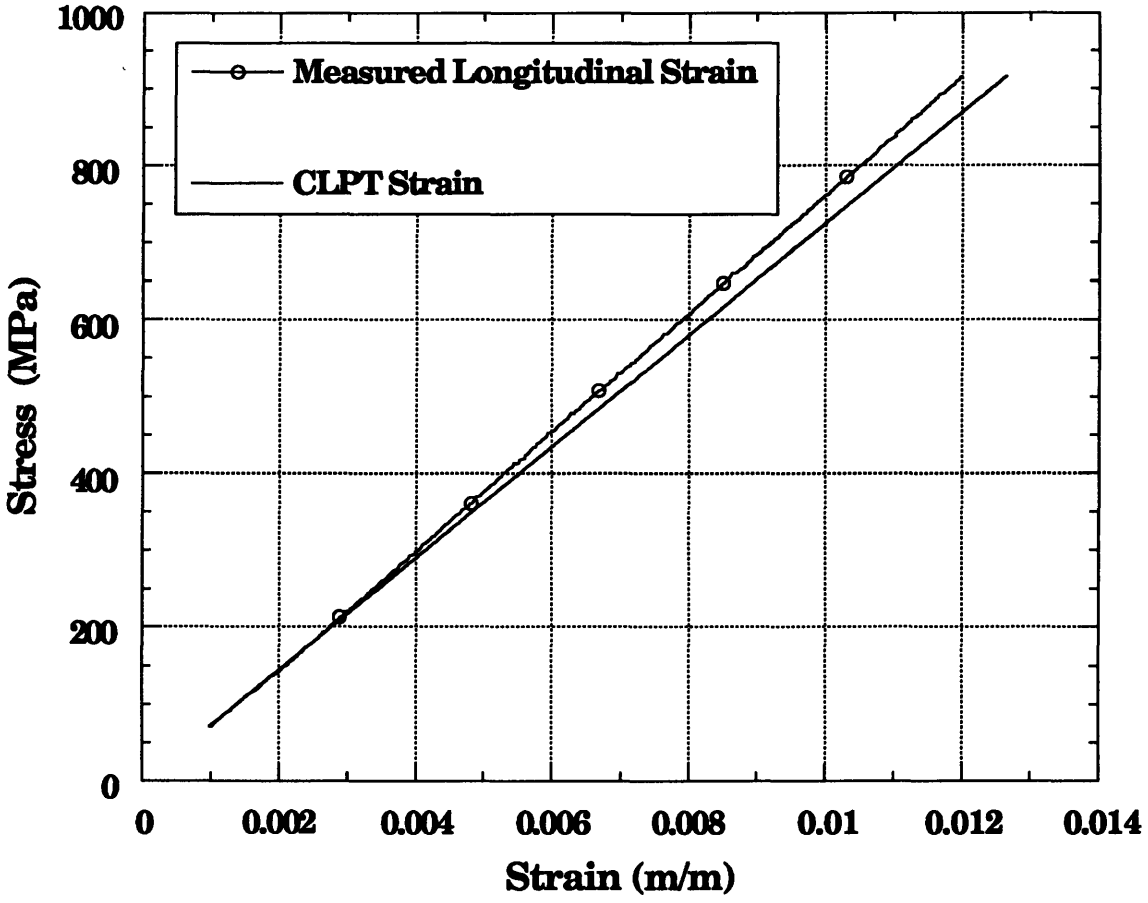

Figure C.7 Stress-Strain Curves for Virgin Coupon 3V-C with a Layup 3, $[45/0/-45/0/90/-45/0/-45/0/45]_S$, Configuration Tested to Failure

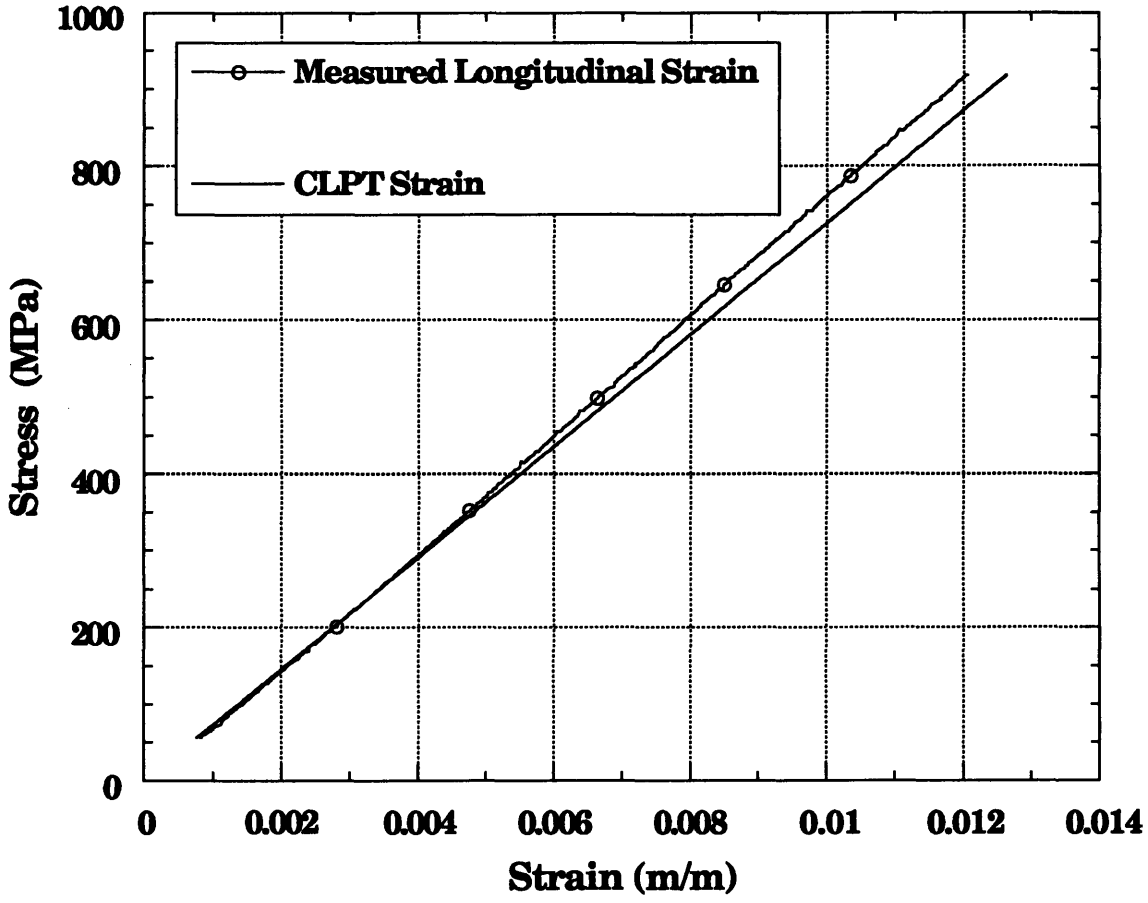

Figure C.8 Stress-Strain Curves for Virgin Coupon 3V-D with a Layup 3, $[45/0/-45/0/90/-45/0/-45/0/45]_S$, Configuration Tested to Failure

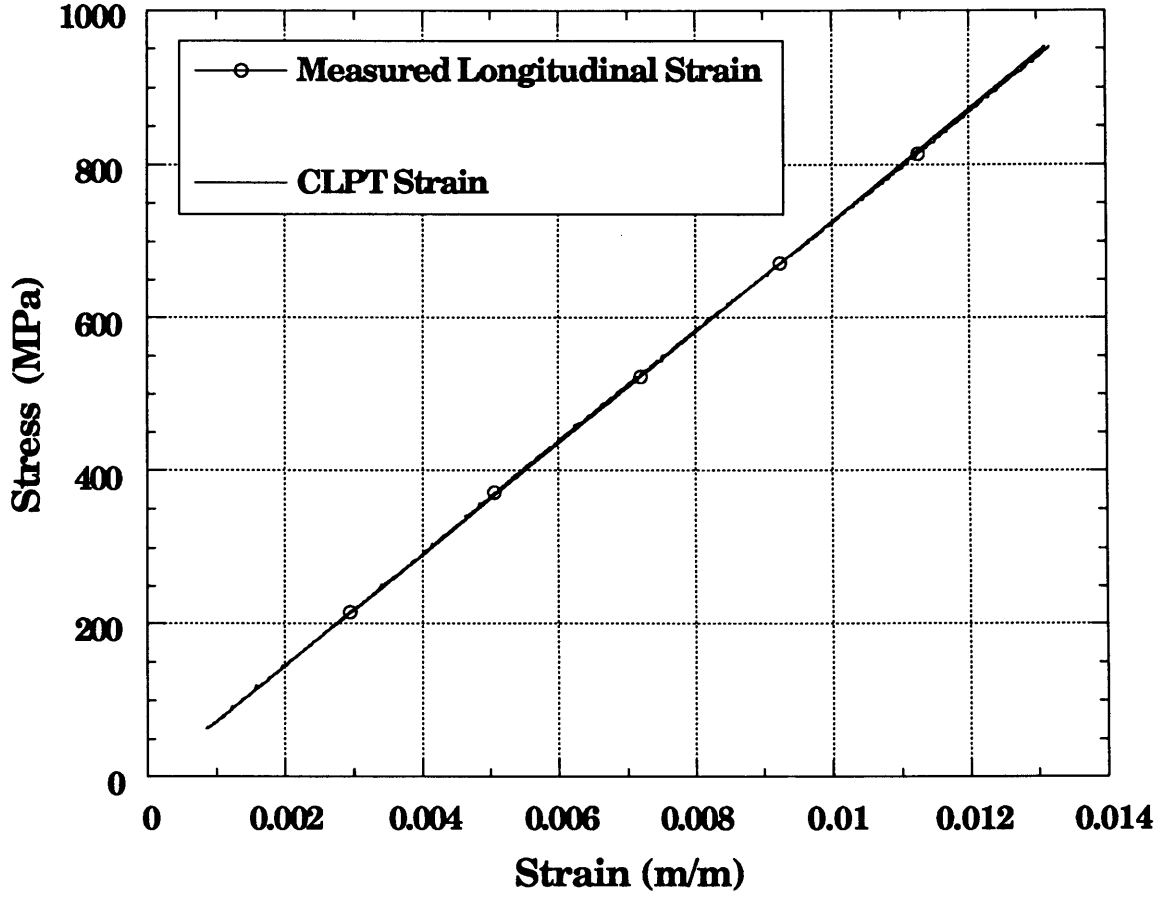

Figure C.9 Stress-Strain Curves for Virgin Coupon 3V-E with a Layup 3, $[45/0/-45/0/90/-45/0/-45/0/45]_S$, Configuration Tested to Failure

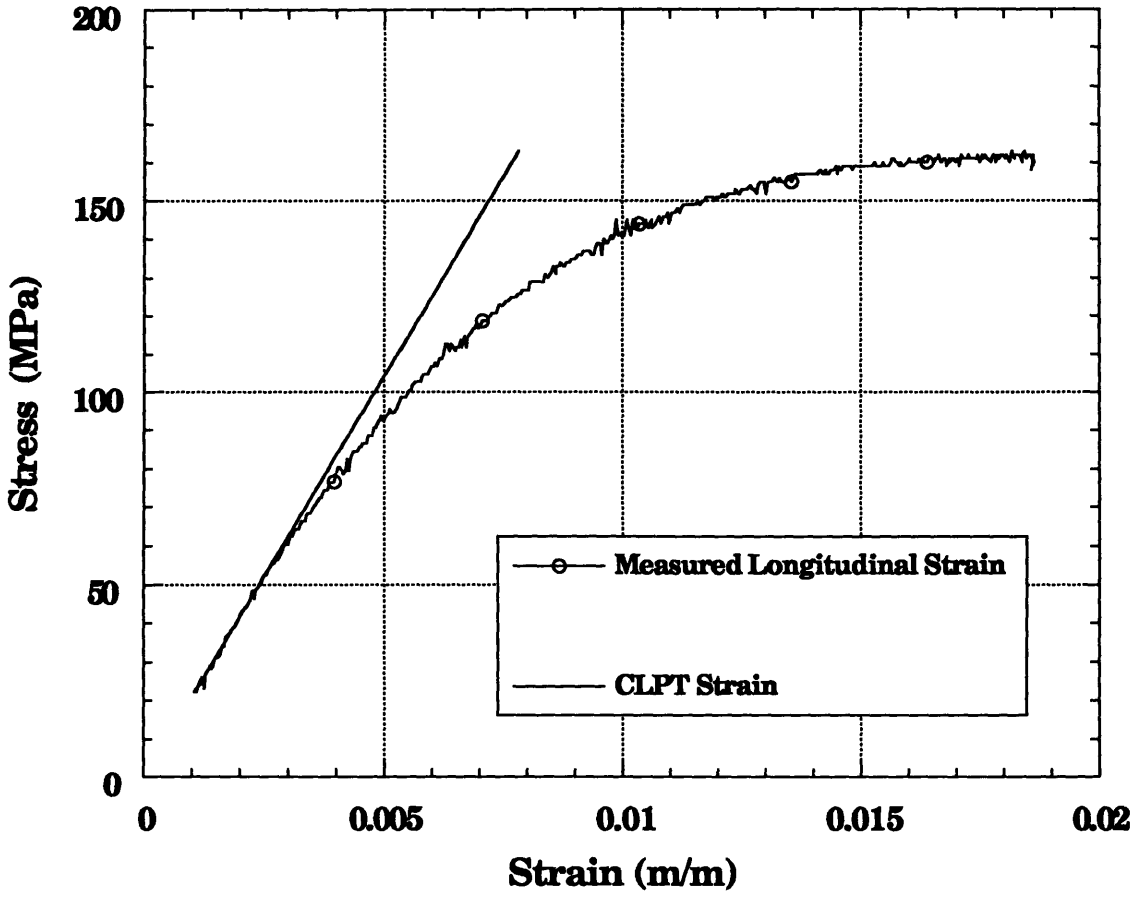

Figure C.10 Stress-Strain Curves for Virgin Coupon 4V-B with a Layup 4, $[\pm 45]_{4S}$, Configuration Tested to Failure

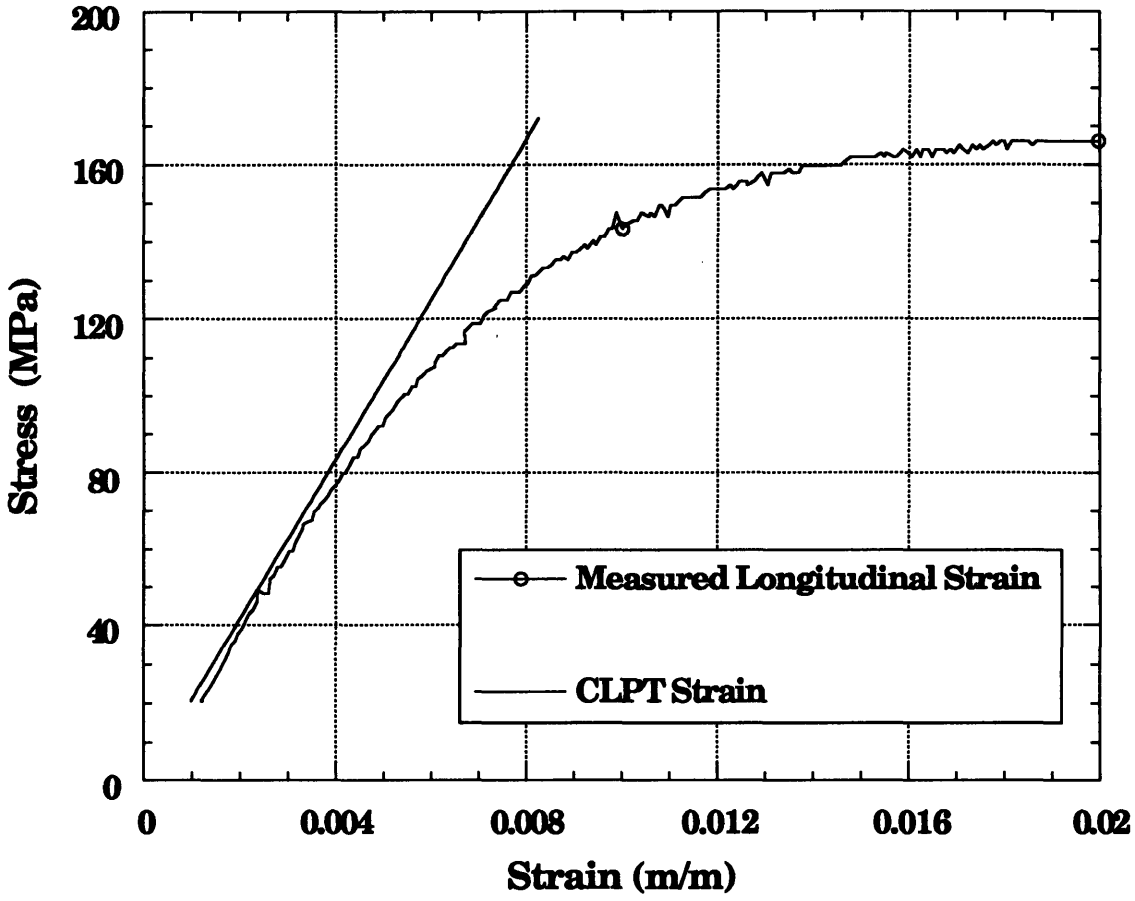

Figure C.11 Stress-Strain Curves for Virgin Coupon 4V-C with a Layup 4, $[\pm 45]_{4S}$, Configuration Tested to Failure

Appendix D

Stress-Strain Curves for Specimens with a Layup 1, $[0/(\pm 45)_2/90/(\pm 45)_2]_s$, Configuration

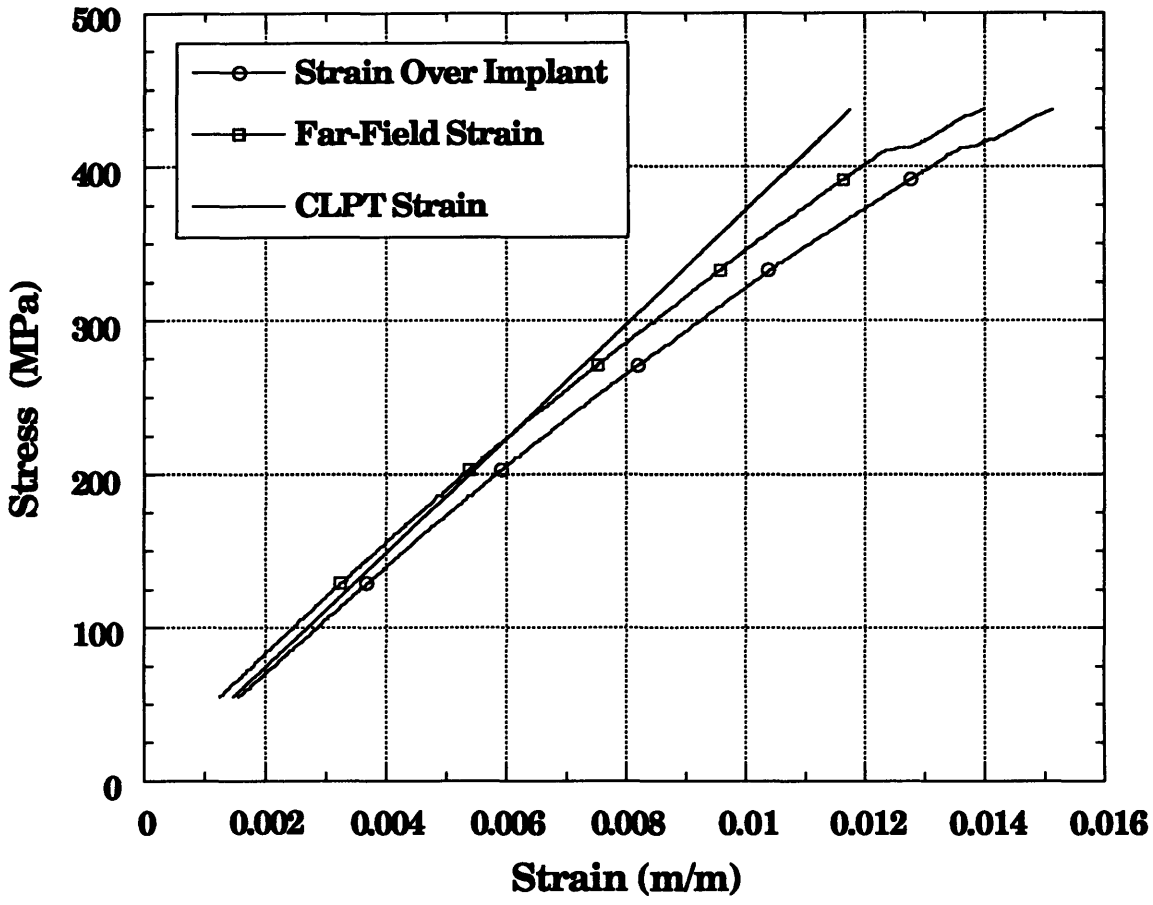

Strain data may have 1.25% error

Figure D.1 Stress-Strain Curves for Coupon 1CHIP-B with a Layup 1, $[0/(\pm 45)_2/90/(\pm 45)_2]_s$, Configuration Tested to Failure

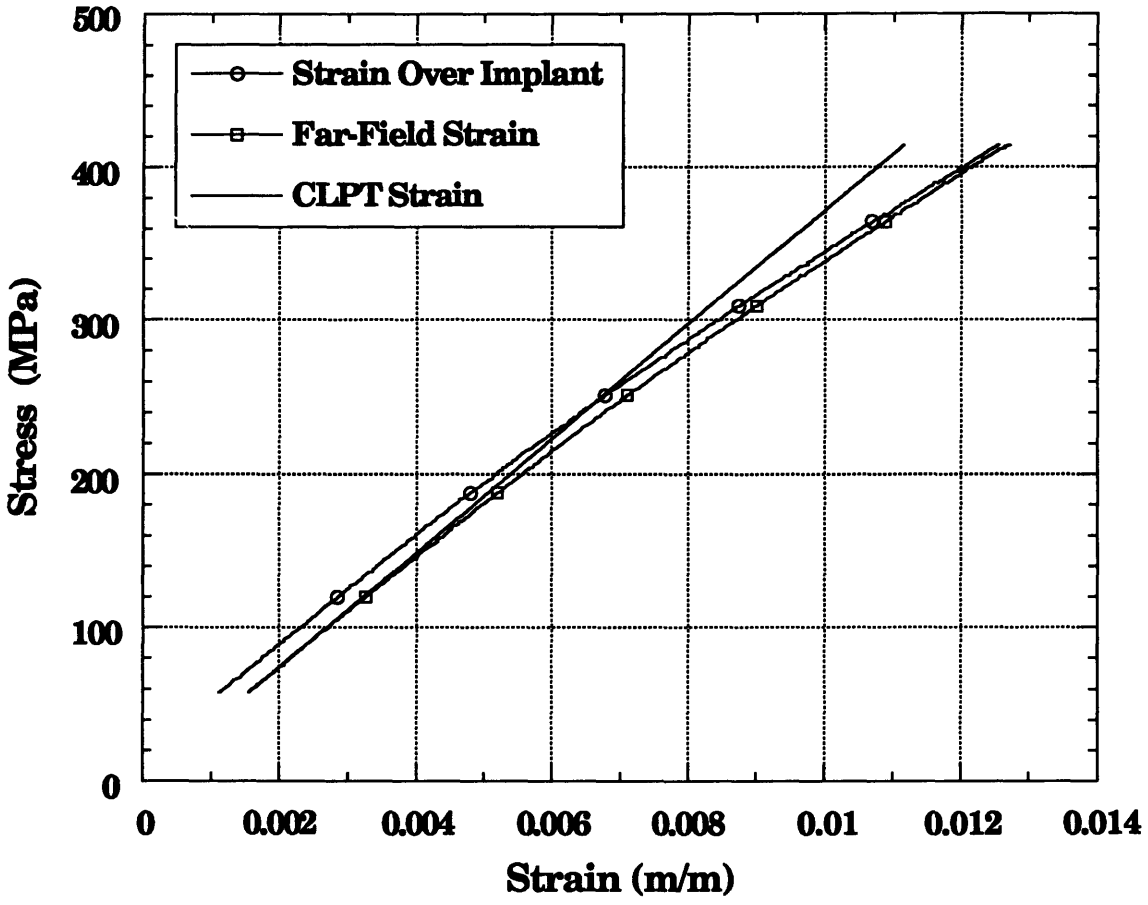

Strain data may have 1.25% error

Figure D.2 Stress-Strain Curves for Coupon 1CHIP-C with a Layup 1, $[0/(\pm 45)_2/90/(\pm 45)_2]_s$, Configuration Tested to Failure

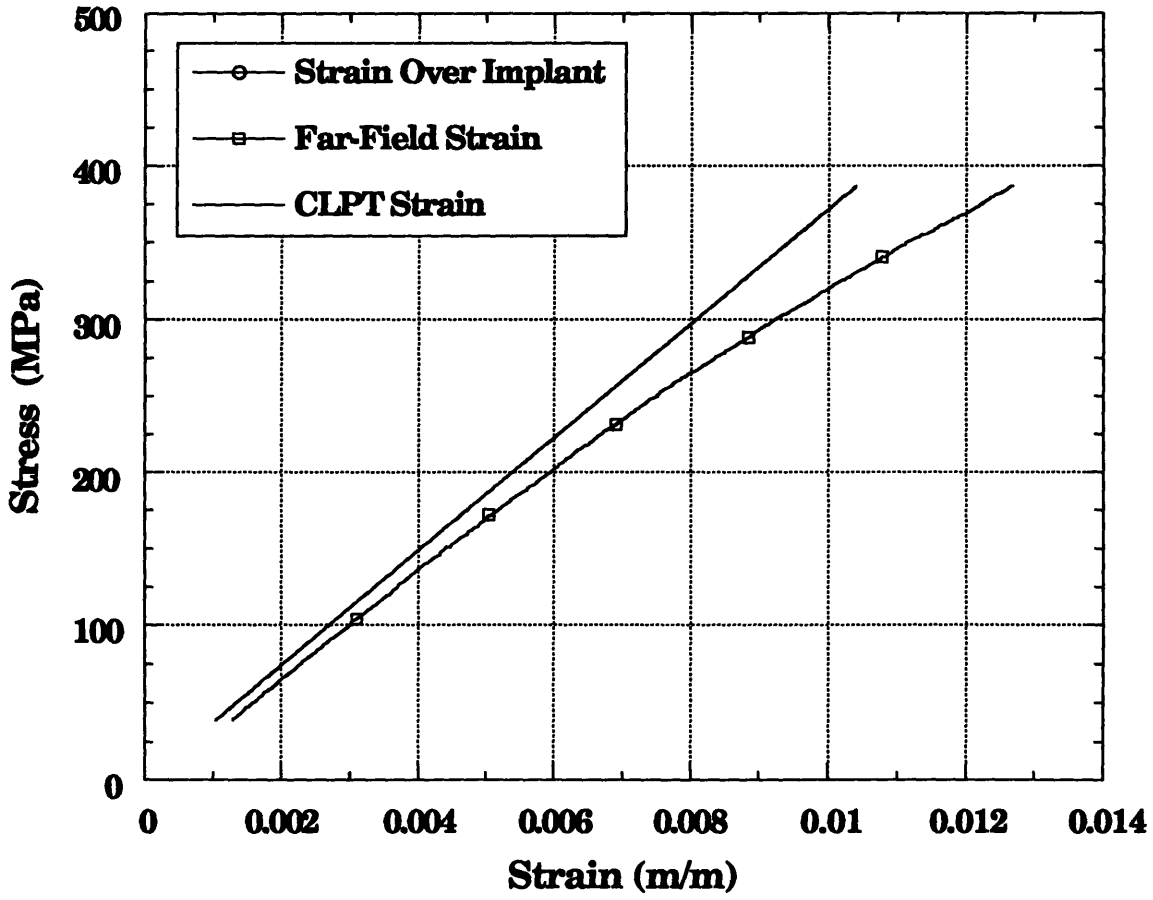

Figure D.3 Stress-Strain Curves for Coupon 1CHIP-E with a Layup 1, $[0/(\pm 45)_2/90/(\pm 45)_2]_s$, Configuration Tested to 90% of its Ultimate Stress

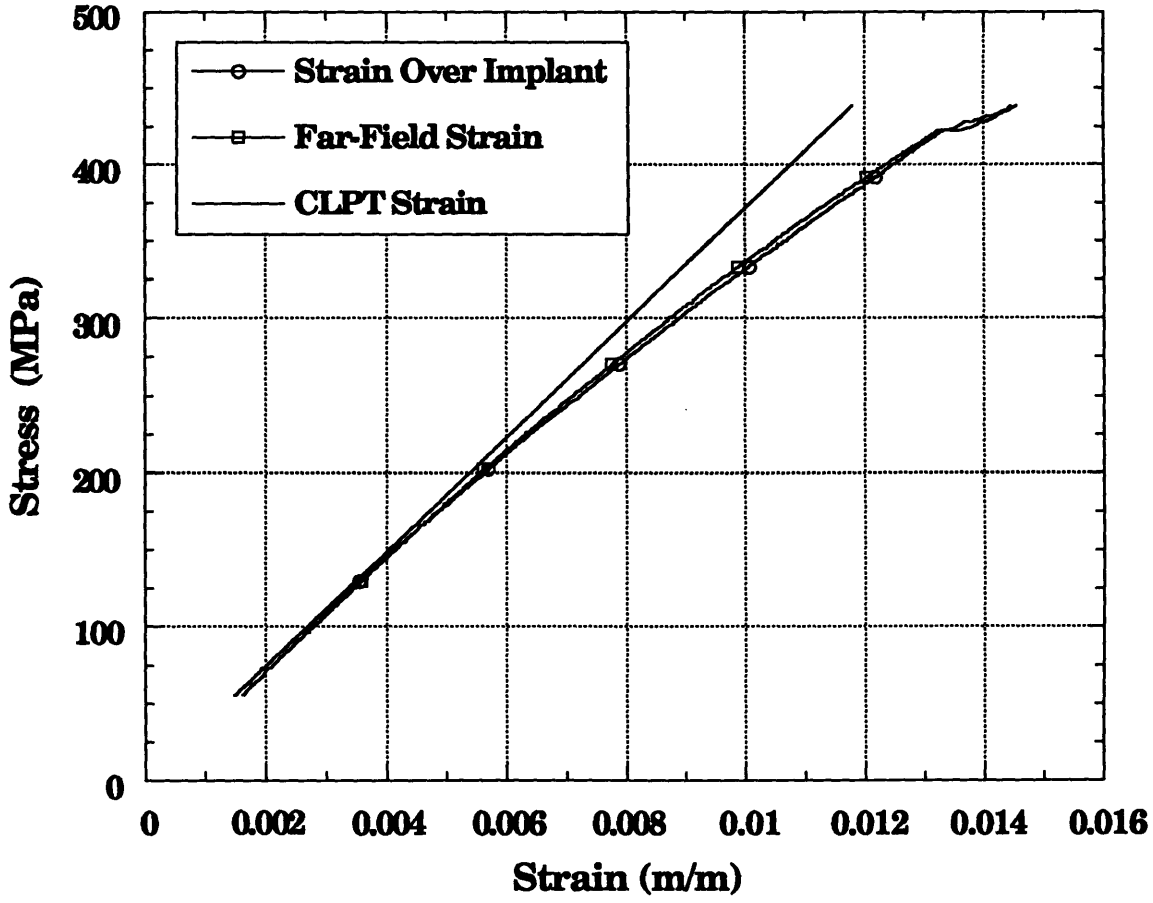

Strain data may have 1.25% error

Figure D.4 Stress-Strain Curves for Coupon 1OF-B with a Layup 1, $[0/(\pm 45)_2/90/(\pm 45)_2]_s$, Configuration Tested to Failure

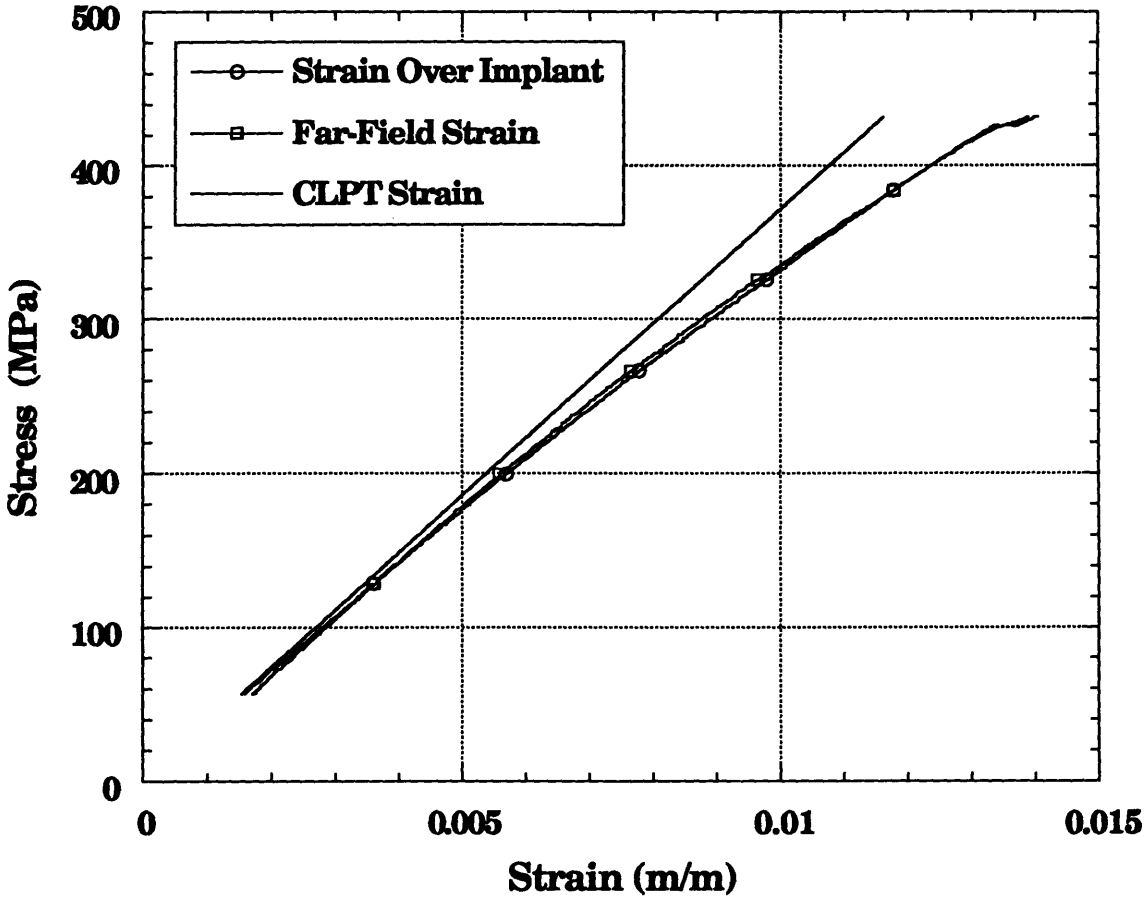

Strain data may have 1.25% error

Figure D.5 Stress-Strain Curves for Coupon 1OF-C with a Layup 1, $[0/(\pm 45)_2/90/(\pm 45)_2]_S$, Configuration Tested to Failure

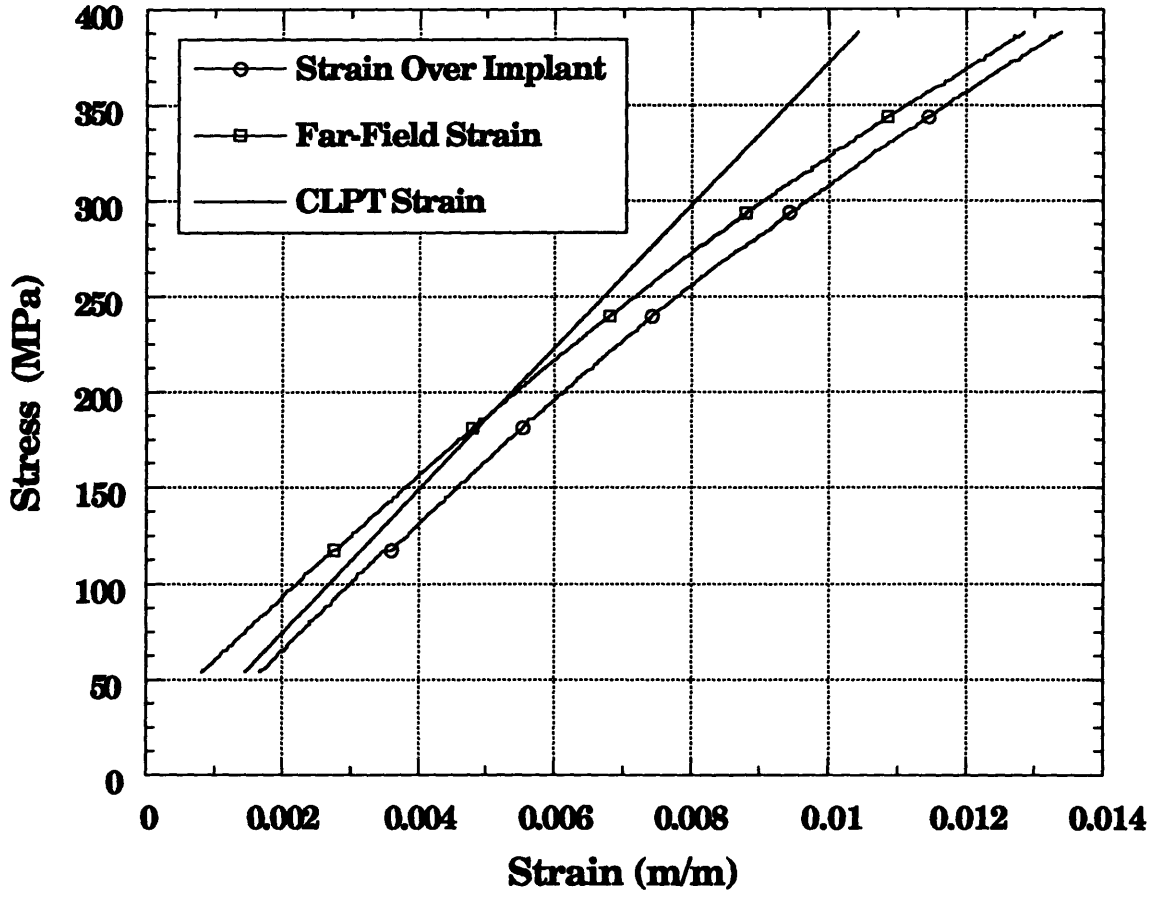

Figure D.6 Stress-Strain Curves for Coupon 1OF-E with a Layup 1, $[0/(\pm 45)_2/90/(\pm 45)_2]_s$, Configuration Tested to 90% of its Ultimate Stress

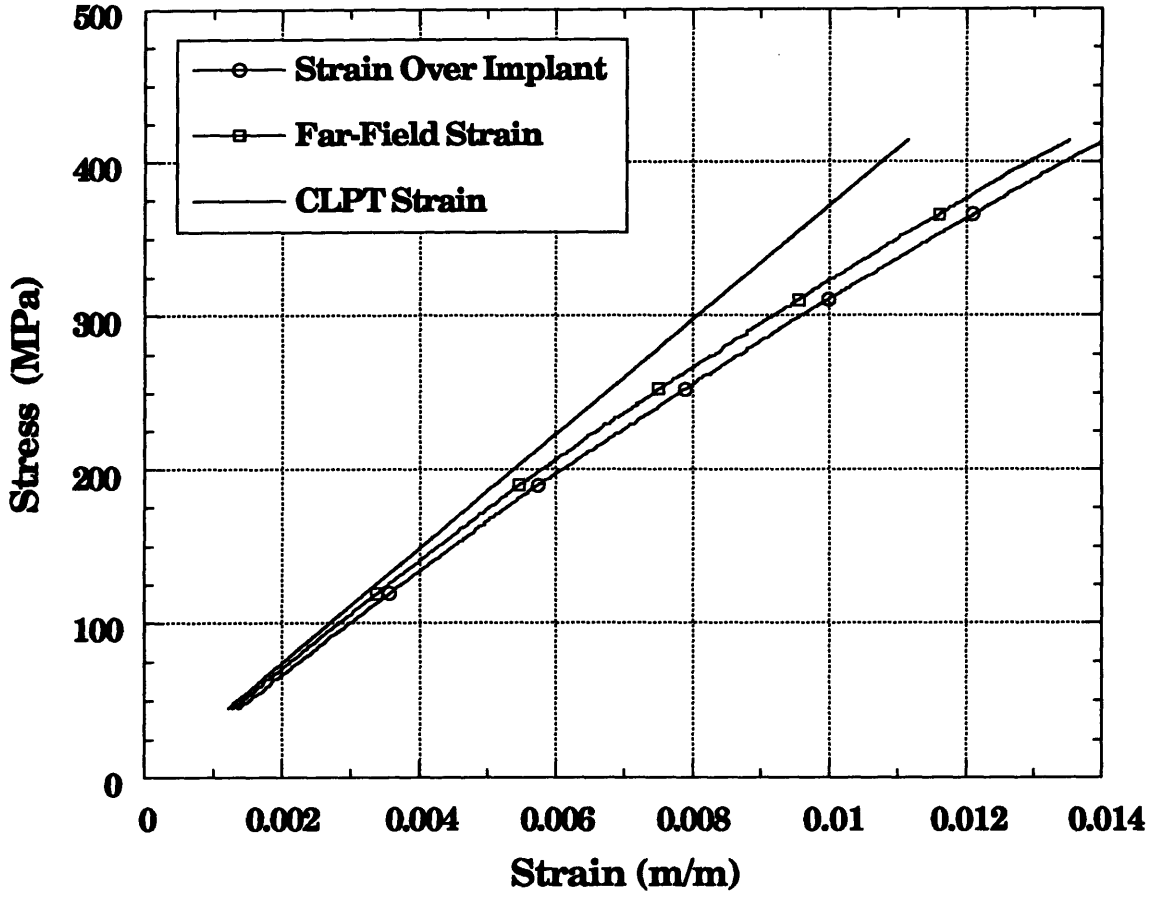

Figure D.7 Stress-Strain Curves for Coupon 1PZA-B with a Layup 1, $[0/(\pm 45)_2/90/(\pm 45)_2]_S$, Configuration Tested to Failure

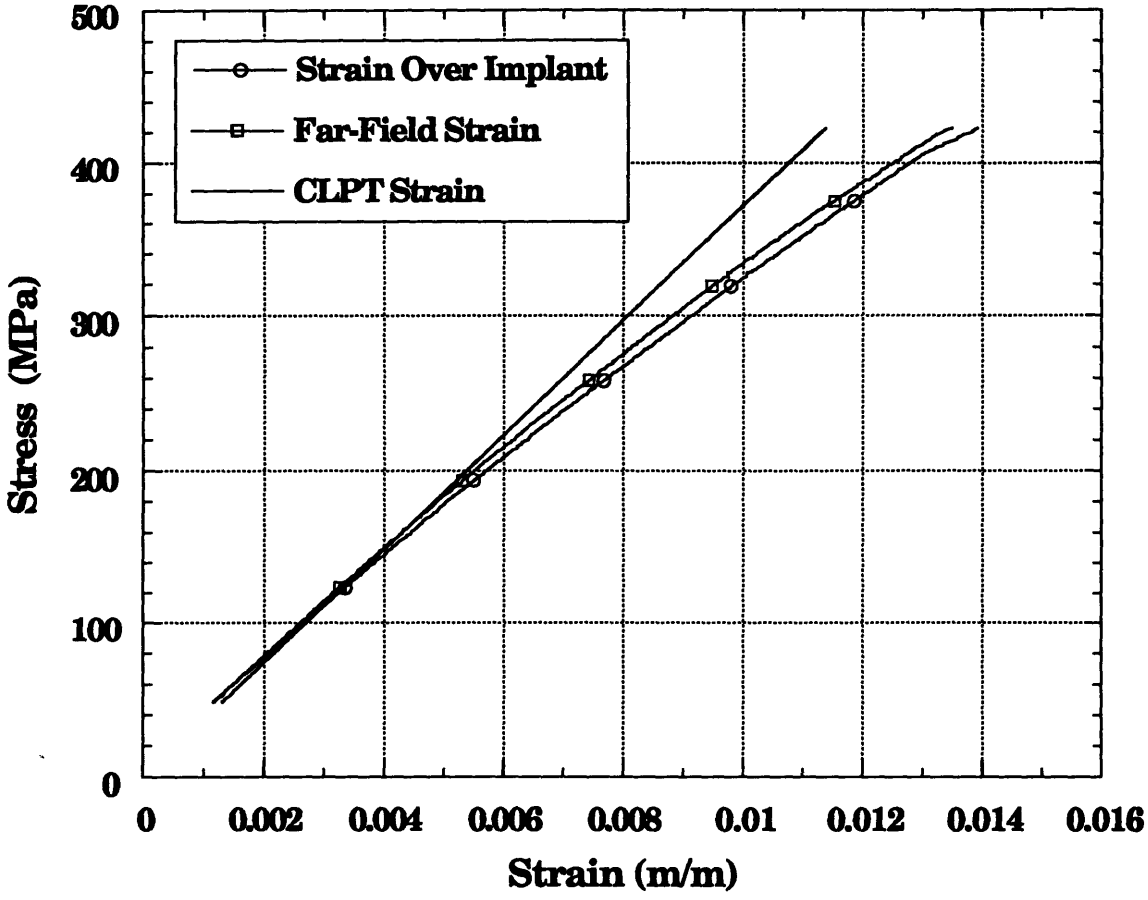

Figure D.8 Stress-Strain Curves for Coupon 1PZA-C with a Layup 1, $[0/(\pm 45)_2/90/(\pm 45)_2]_s$, Configuration Tested to Failure

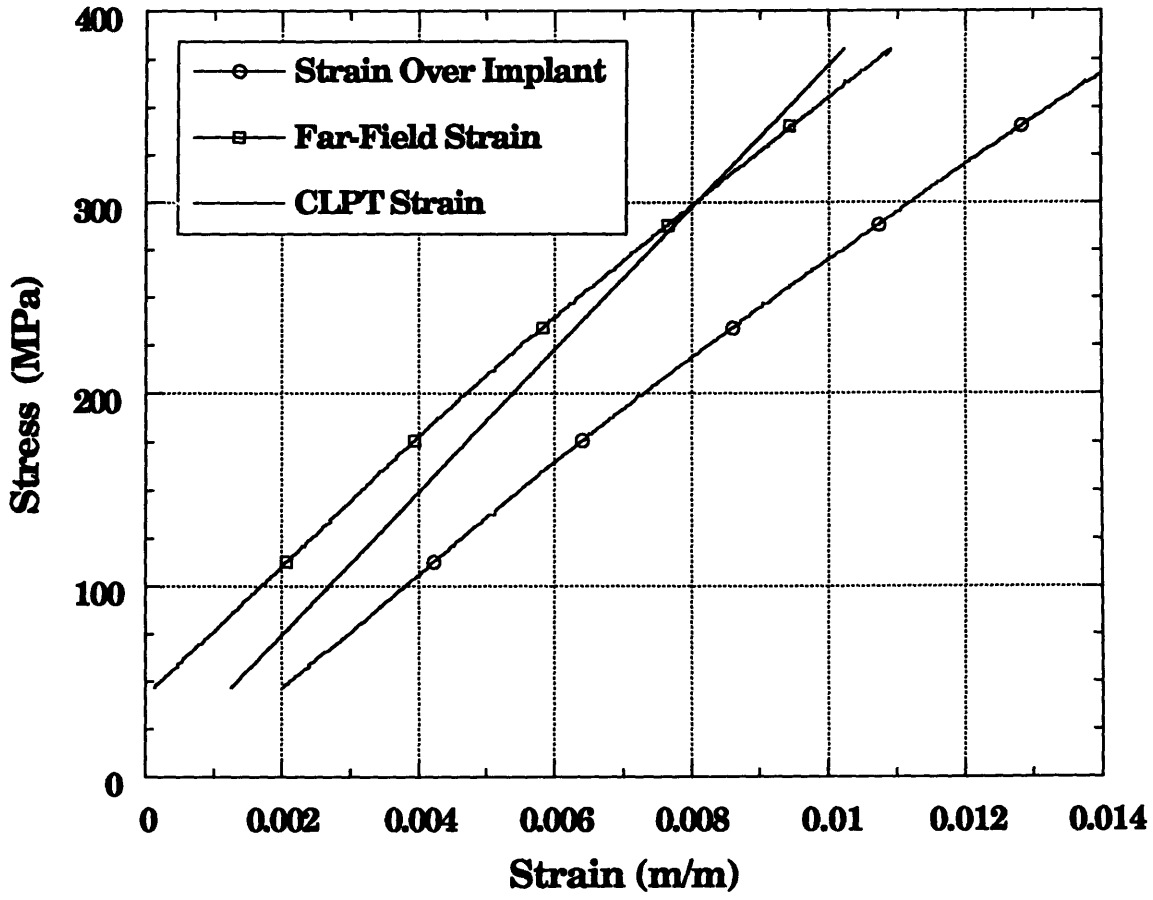

Figure D.9 Stress-Strain Curves for Coupon 1PZA-D with a Layup 1, $[0/(\pm 45)_2/90/(\pm 45)_2]_S$, Configuration Tested to 90% of its Ultimate Stress

Appendix E

Stress-Strain Curves for Specimens with a Layup 2, $[0/\pm45/90]_{2s}$, Configuration

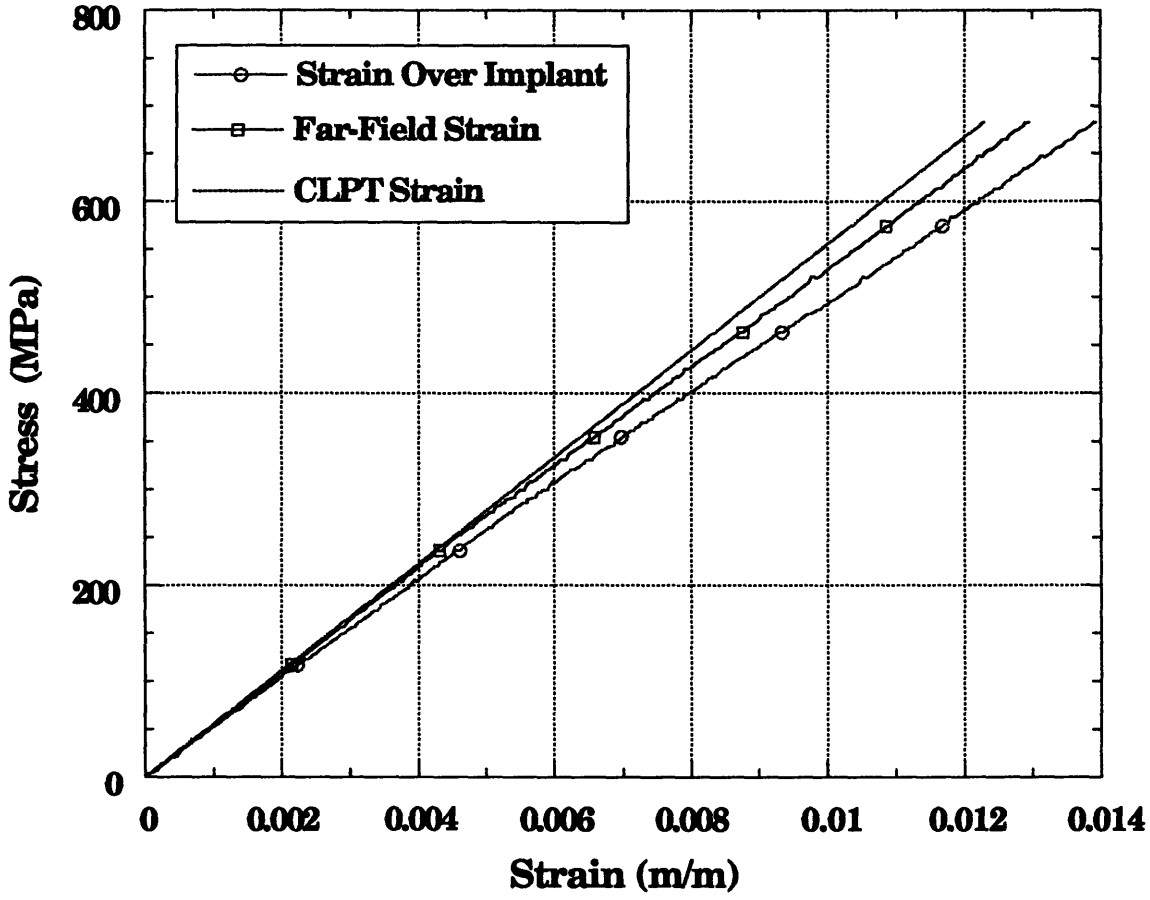

Figure E.1 Stress-Strain Curves for Coupon 2CHIP-B Tested to Failure with Chip Placed in Cut Laminate with a Layup 2, $[0/\pm45/90]_{2s}$, Configuration

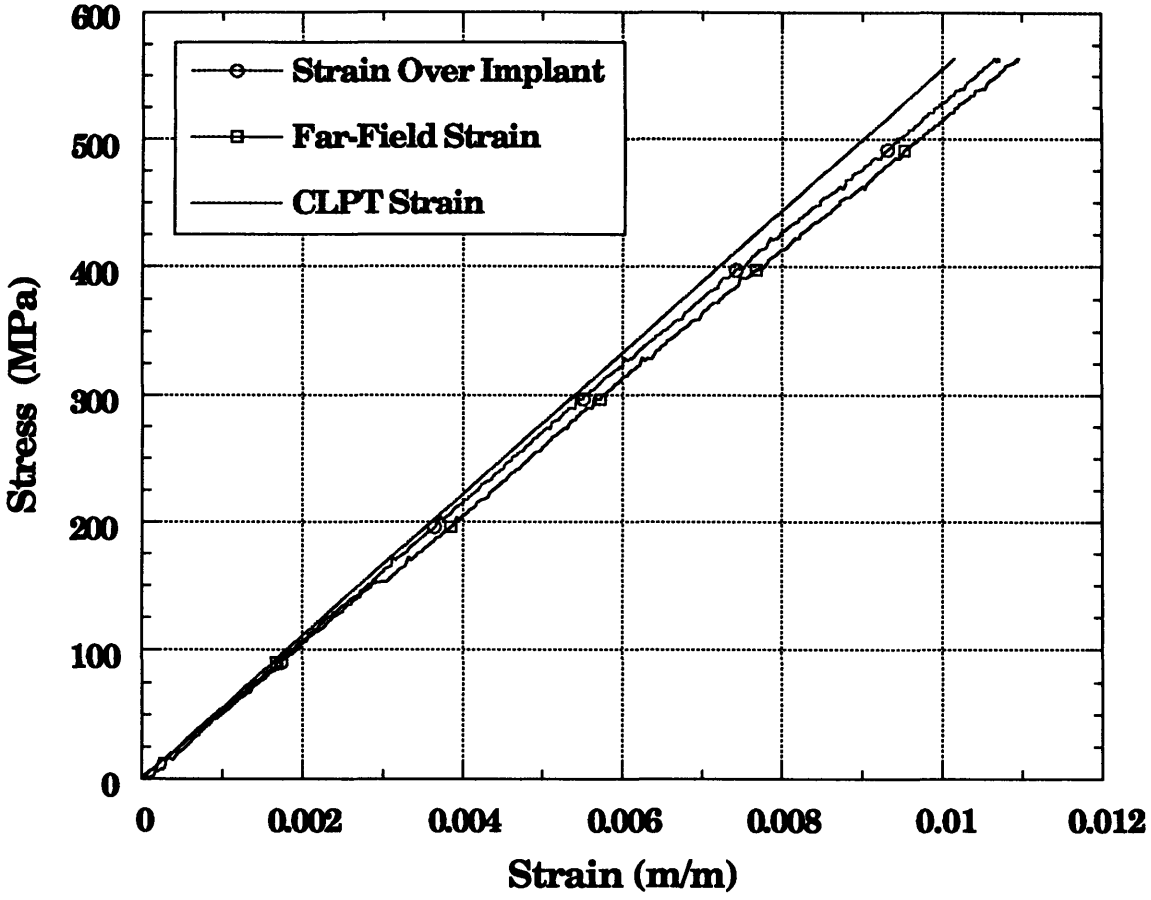

Figure E.2 Stress-Strain Curves for Coupon 2CHIP-C Tested to 90% of its Ultimate Stress with Chip Placed in Cut Laminate with a Layup 2, $[0/\pm45/90]_{2S}$, Configuration

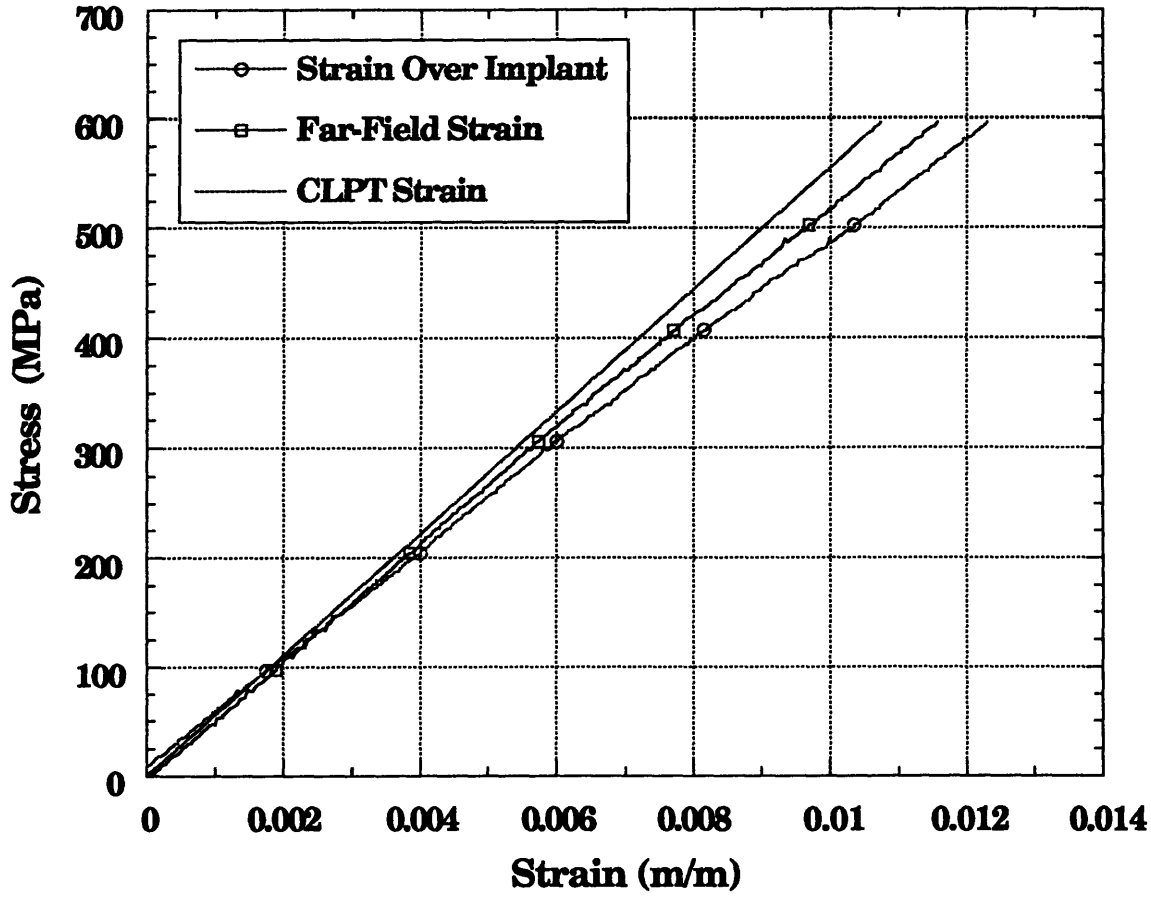

Figure E.3 Stress-Strain Curves for Coupon 2CHIP-D Tested to 95% of its Ultimate Stress with Chip Placed in Cut Laminate with a Layup 2, $[0/\pm45/90]_{2S}$, Configuration

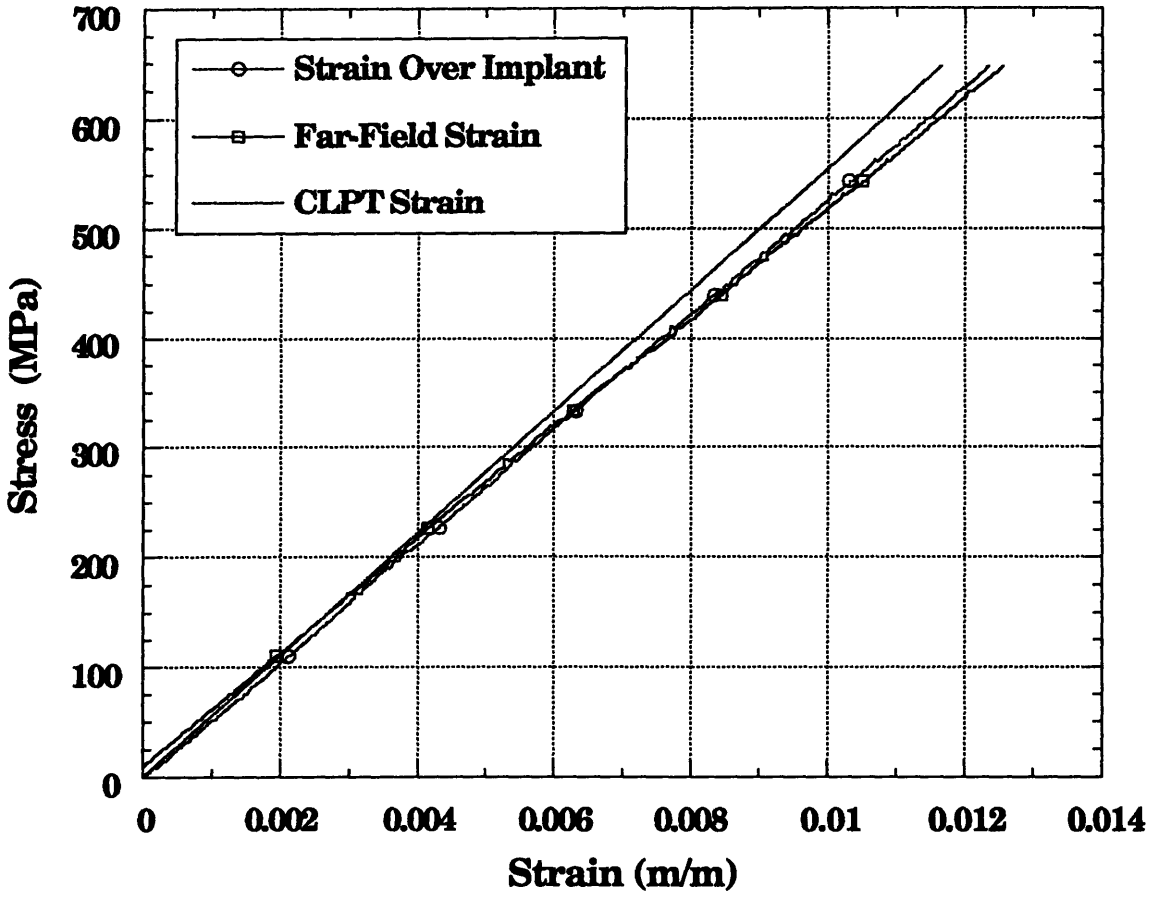

Figure E.4 Stress-Strain Curves for Coupon 2CHIP L/O-B Tested to Failure with Chip Placed Directly in Laminate with a Layup 2, $[0/\pm45/90]_{2s}$, Configuration

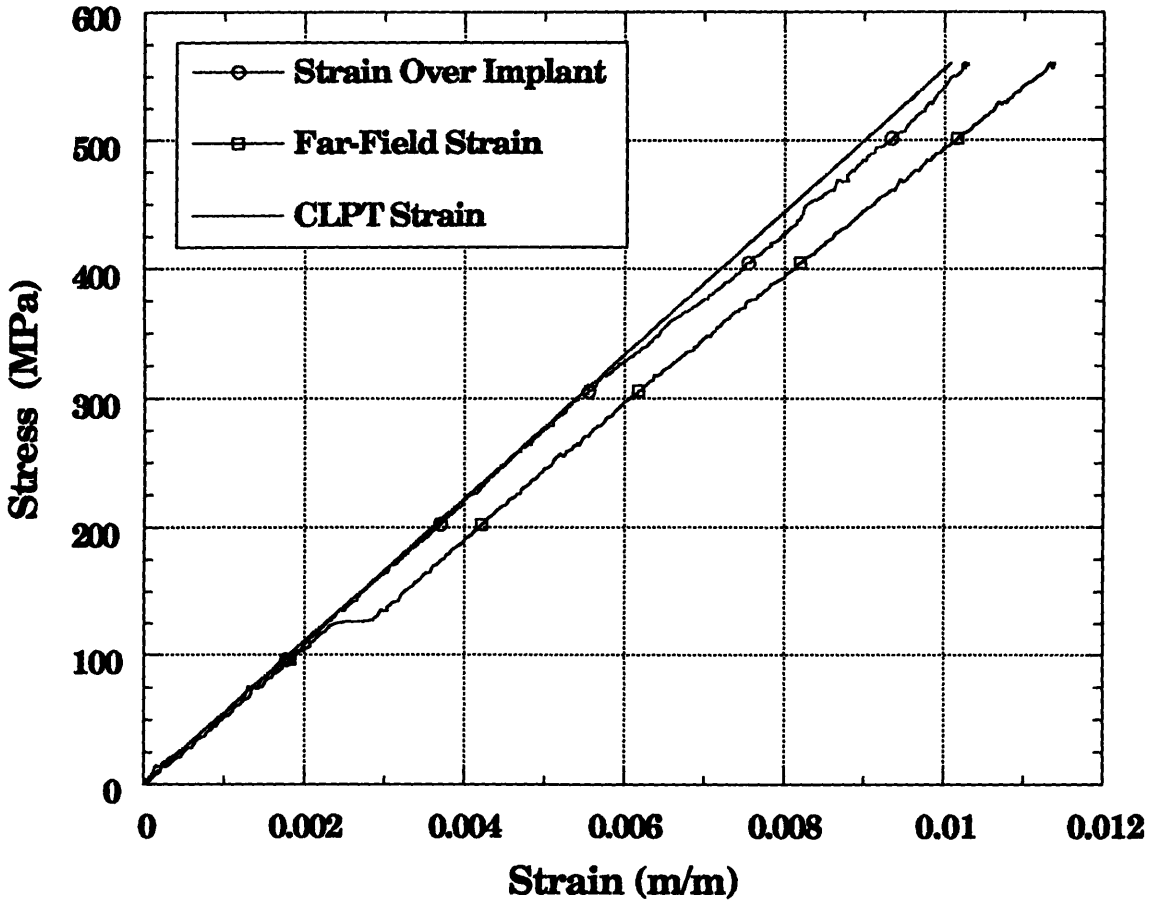

Figure E.5 Stress-Strain Curves for Coupon 2CHIP L/O-D Tested to Failure with Chip Placed Directly in Laminate with a Layup 2, $[0/\pm45/90]_{2S}$, Configuration

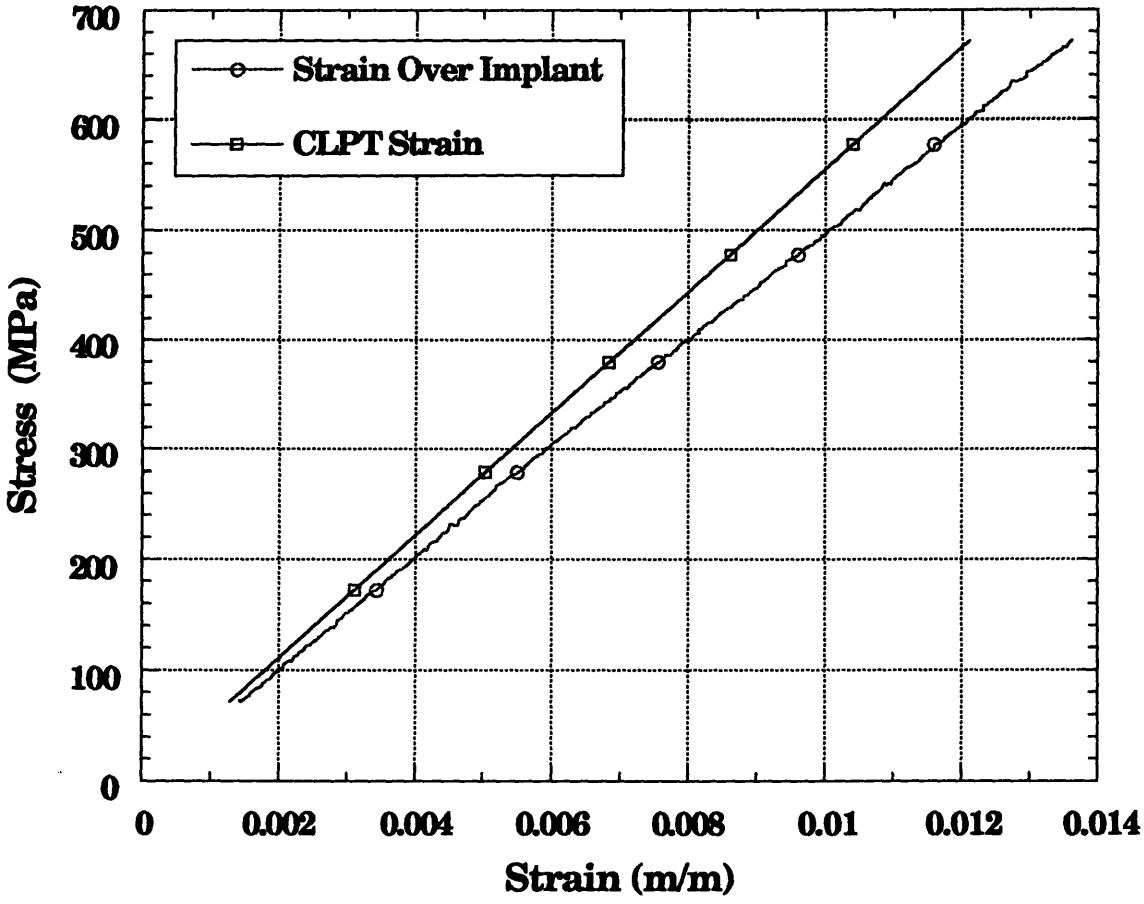

Strain data may have 1.25% error

Figure E.6 Stress-Strain Curves for Coupon 2TC-B with a Layup 2, $[0/\pm45/90]_{2S}$, Configuration Tested to Failure

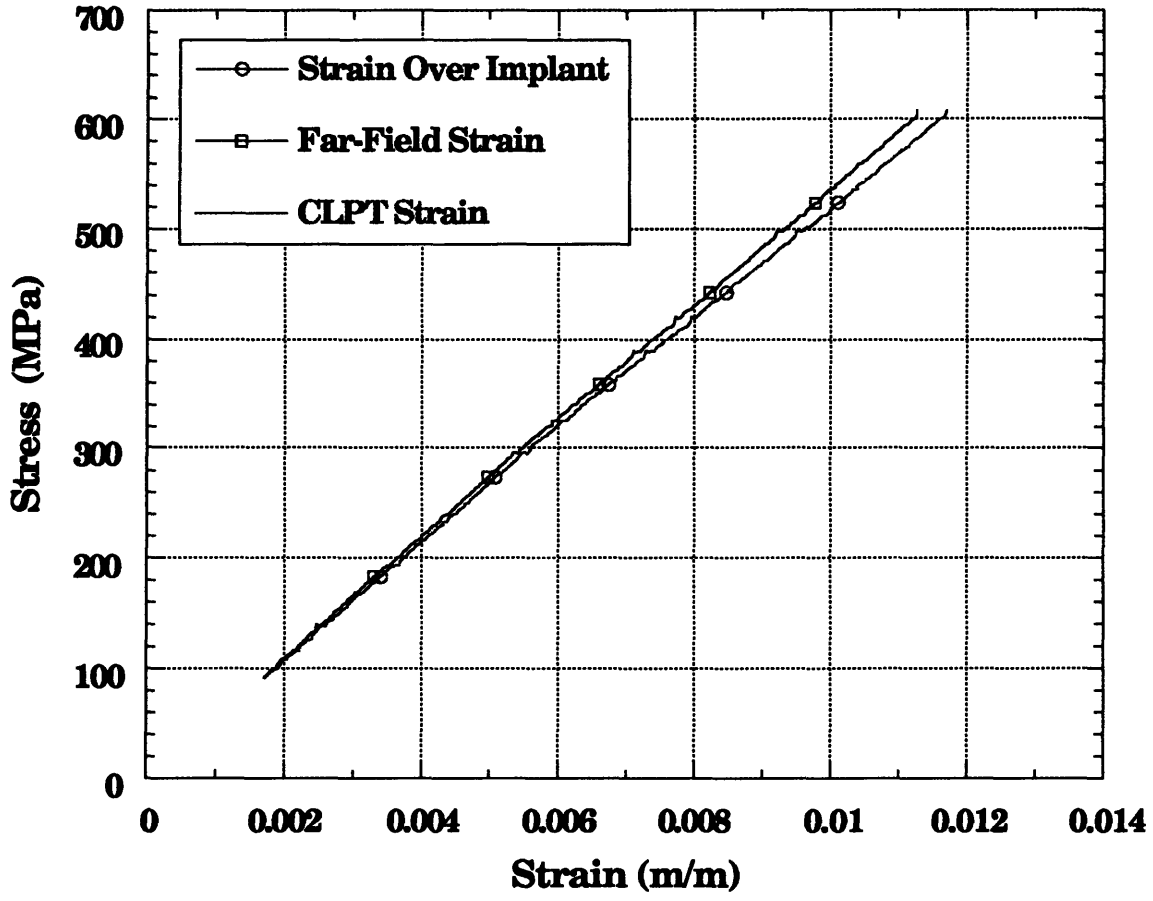

Figure E.7 Stress-Strain Curves for Coupon 2TC-D with a Layup 2, $[0/\pm45/90]_{2s}$, Configuration Tested to 90% of its Ultimate Stress

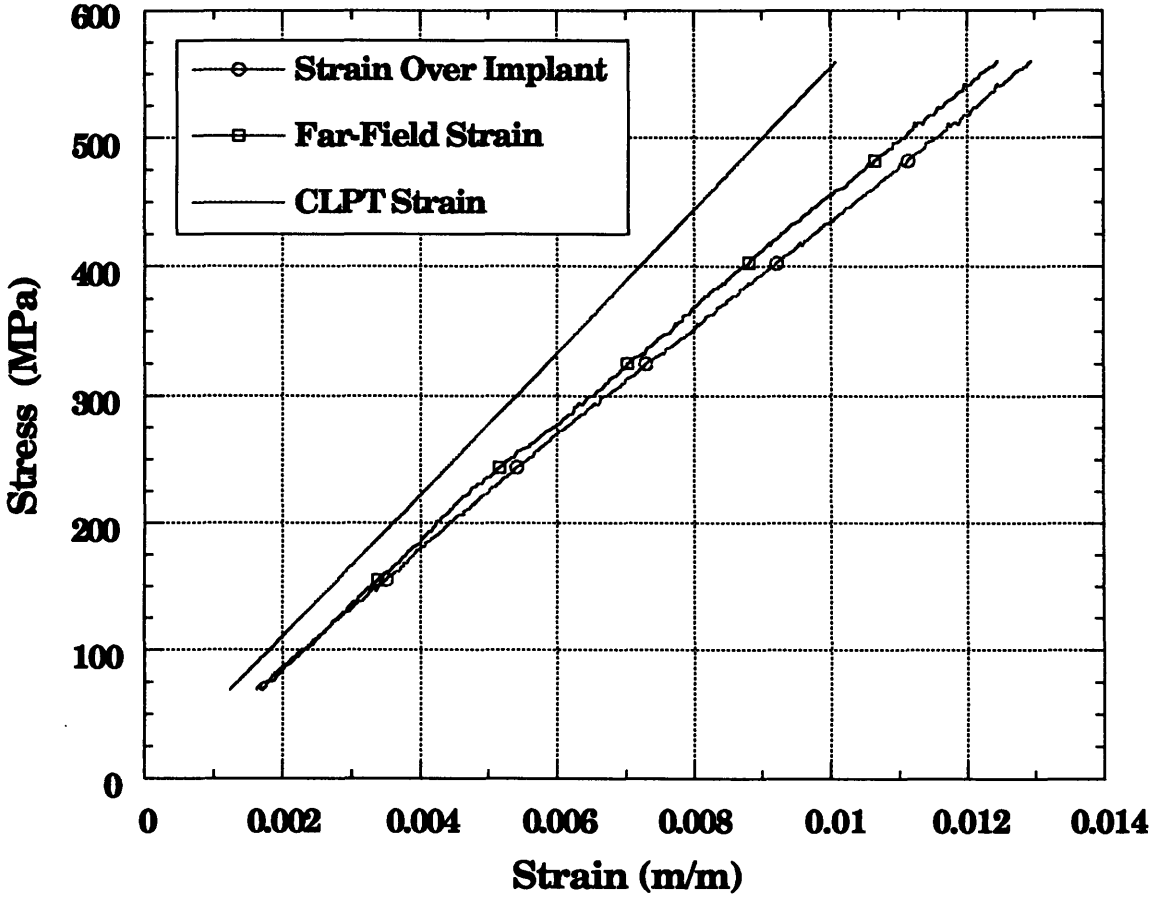

Strain data may have 1.25% error

Figure E.8 Stress-Strain Curves for Coupon 2TC-E with a Layup 2, $[0/\pm45/90]_{2s}$, Configuration Tested to Failure

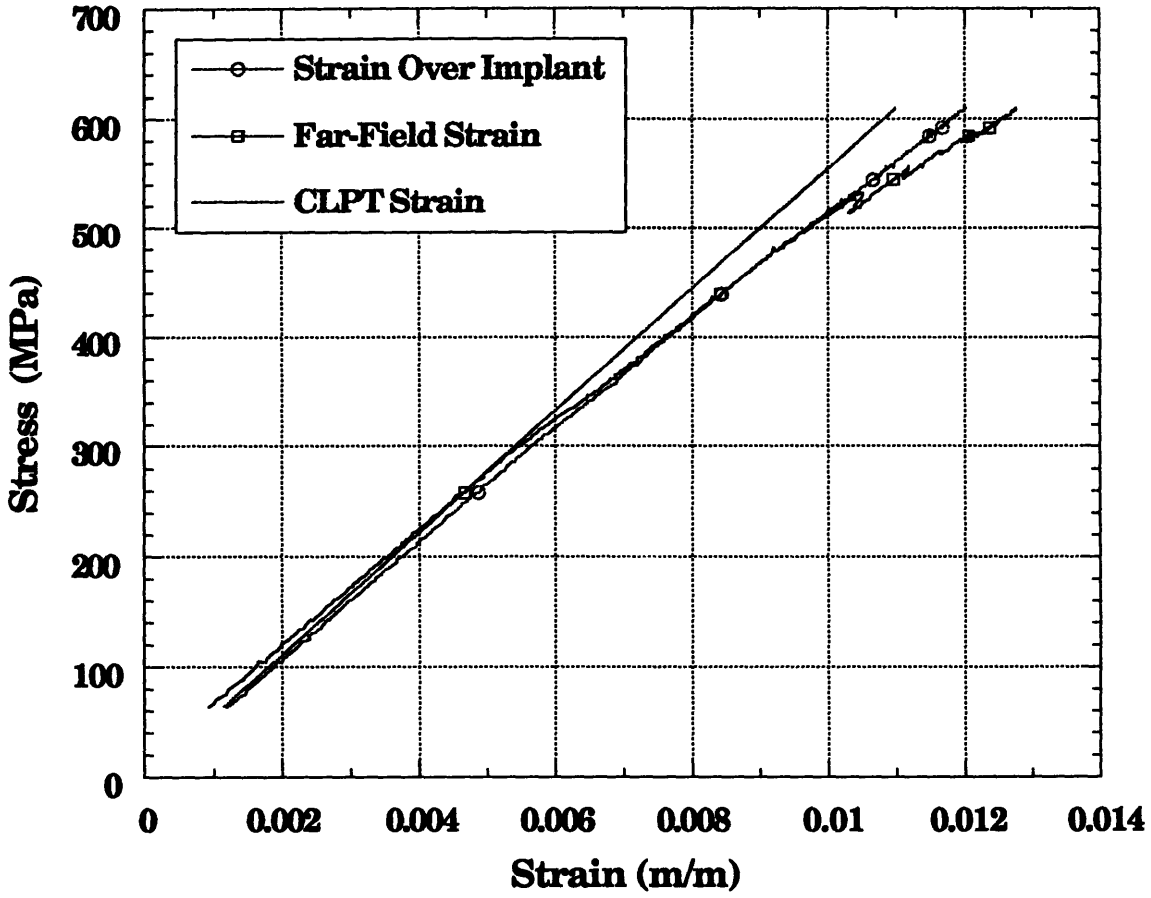

Figure E.9 Stress-Strain Curves for Coupon 2OF-B Tested to Failure with Optical Fiber Placed Directly in Laminate with a Layup 2,$[0/\pm45/90]_{2s}$, Configuration

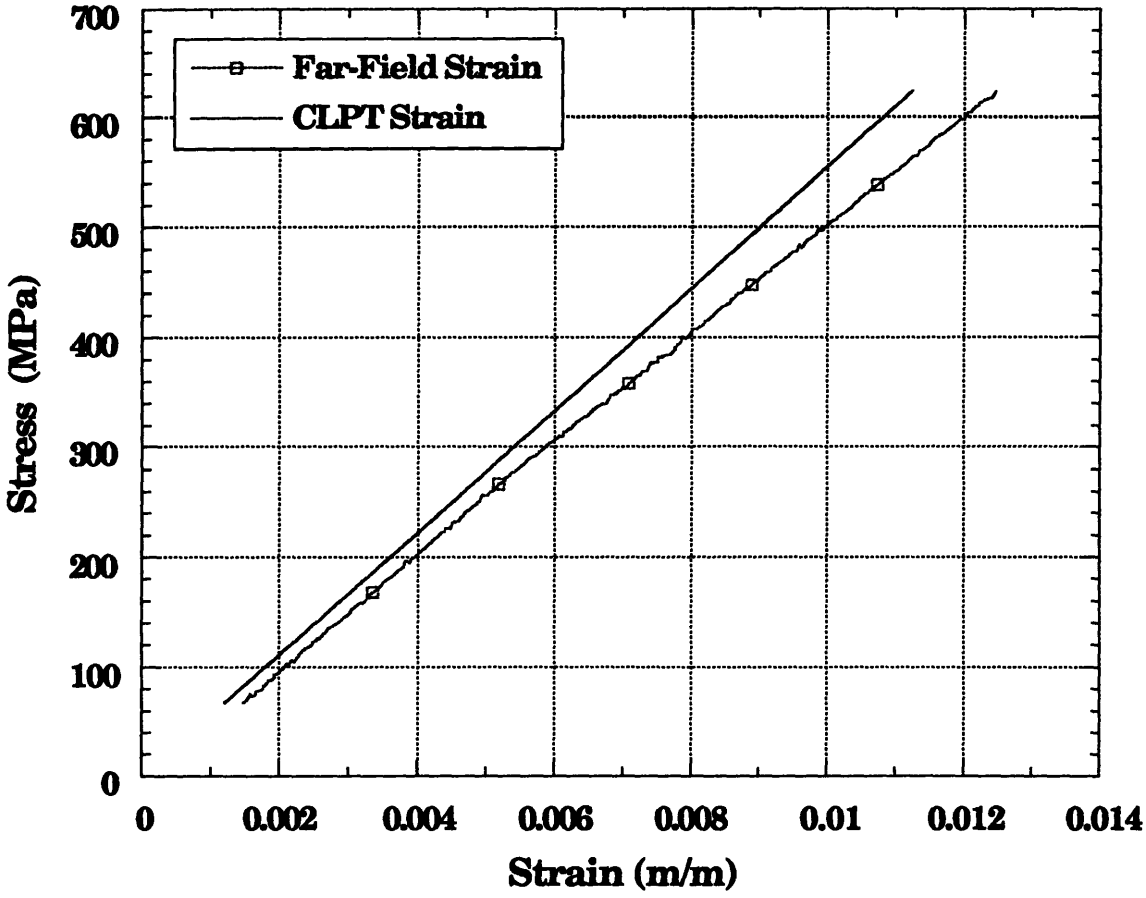

Figure E.10 Stress-Strain Curves for Coupon 2OF-D Tested to Failure with Optical Fiber Placed Directly in Laminate with a Layup 2, $[0/\pm45/90]_{2s}$, Configuration

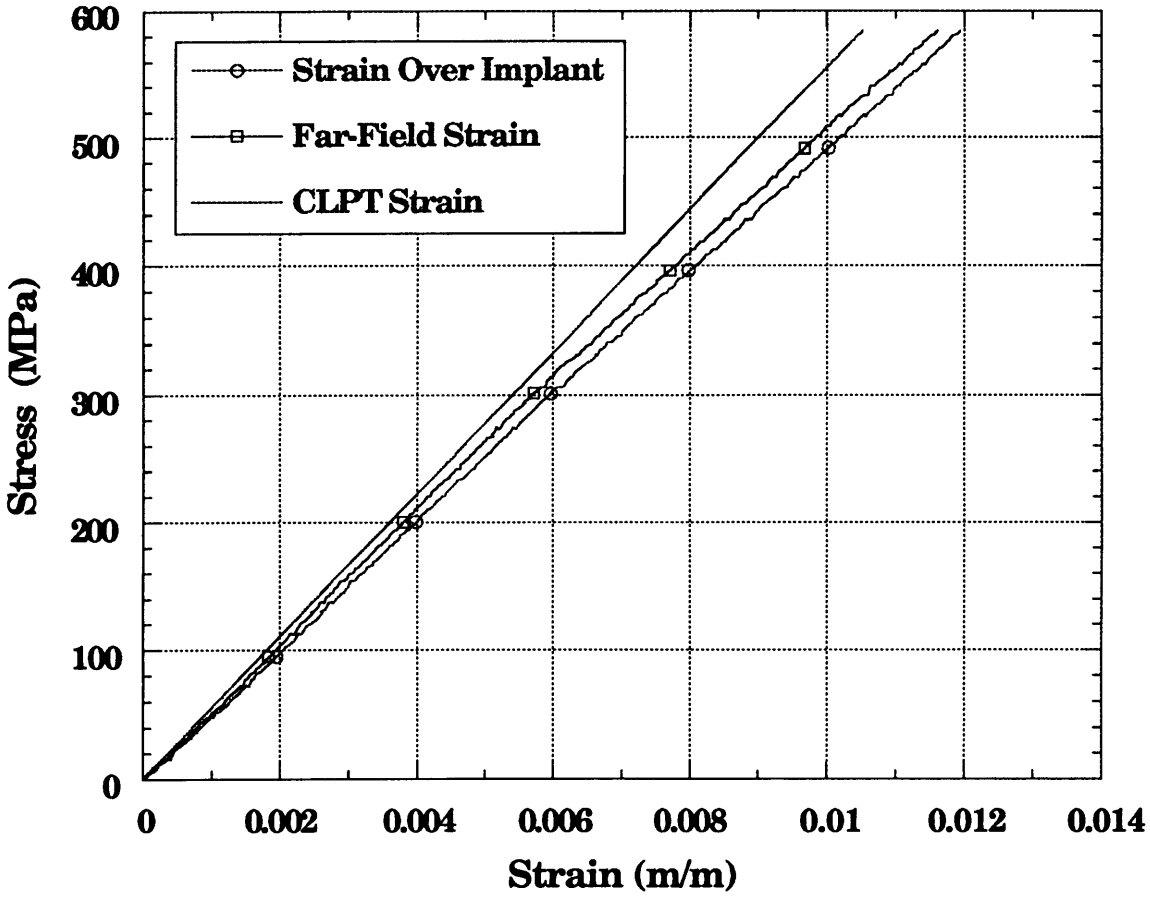

Figure E.11 Stress-Strain Curves for Coupon 2OF C/O-A Tested to Failure with Optical Fiber Placed in Cut Laminate with a Layup 2, $[0/\pm45/90]_{2S}$, Configuration

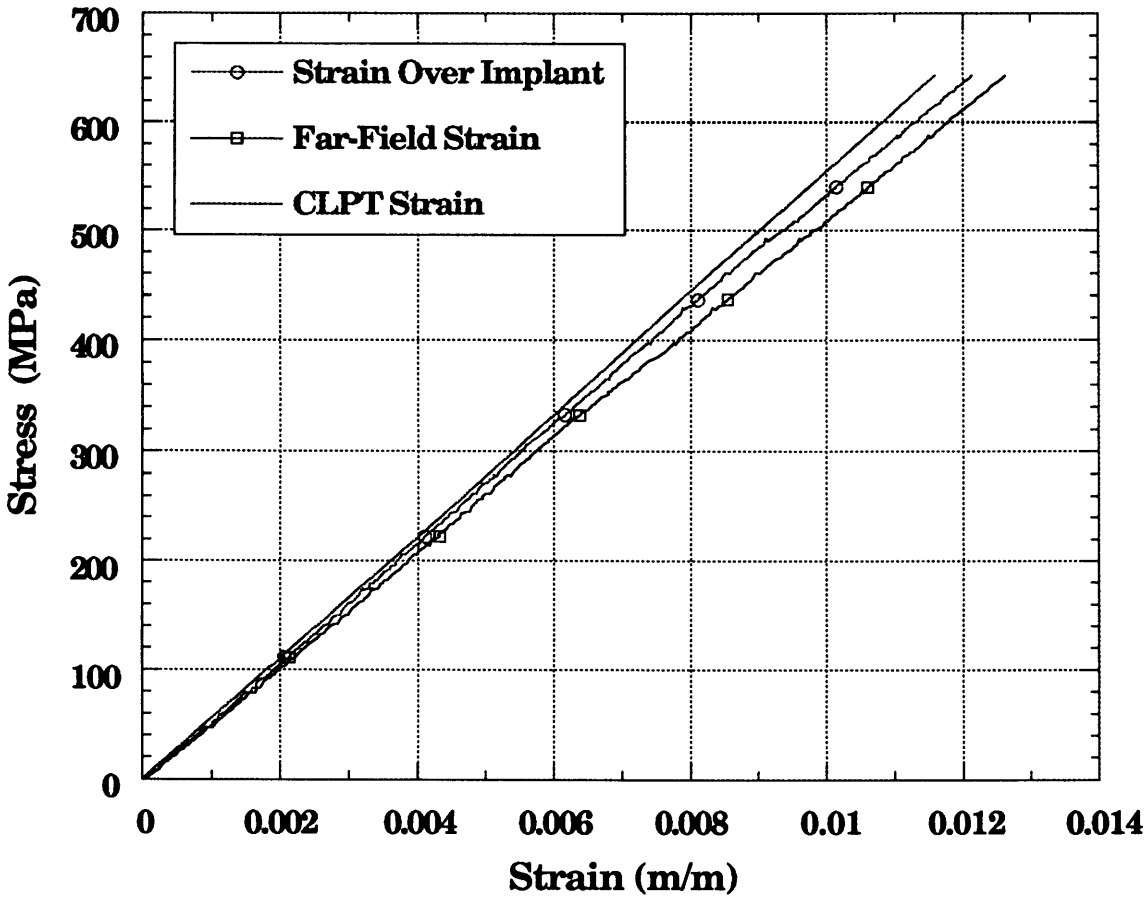

Figure E.12 Stress-Strain Curves for Coupon 2OF C/O-B Tested to Failure with Optical Fiber Placed in Cut Laminate with a Layup 2, $[0/\pm45/90]_{2S}$, Configuration

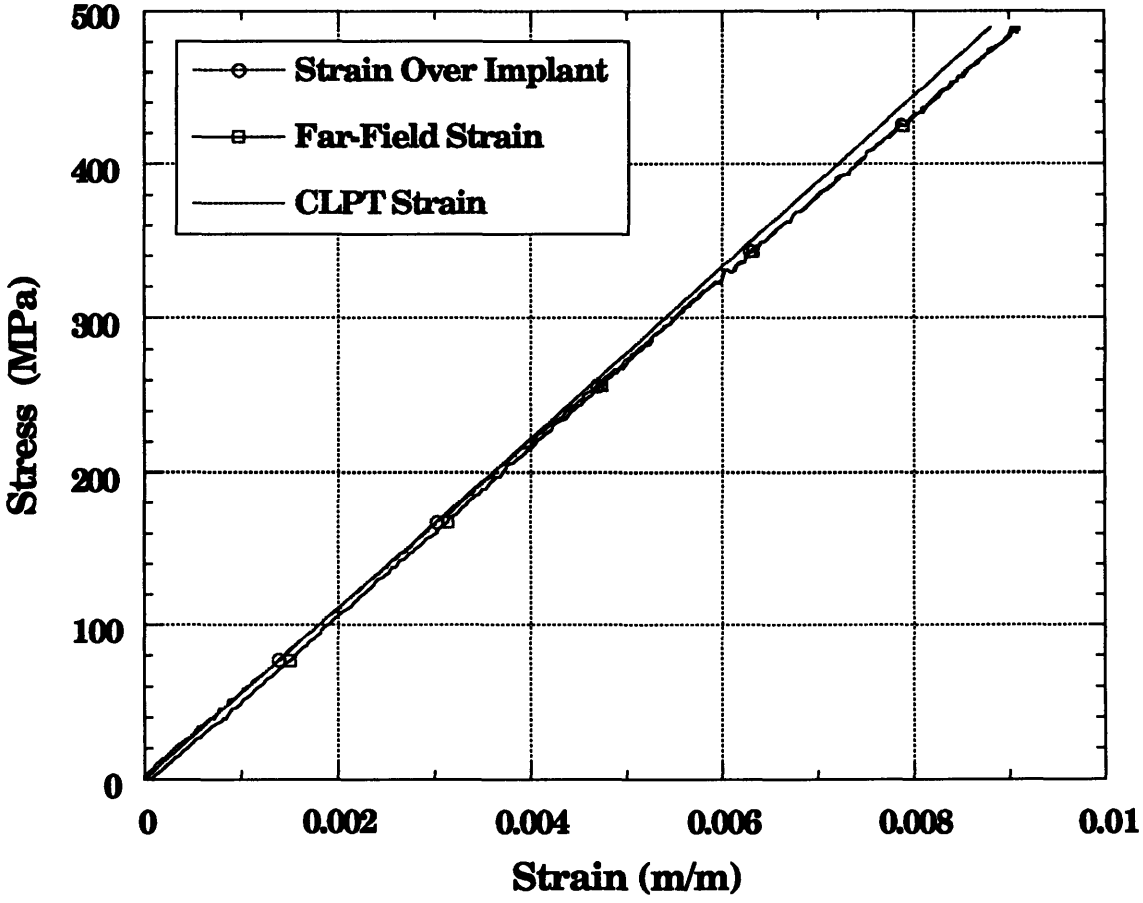

Figure E.13 Stress-Strain Curves for Coupon 2OF C/O-D Tested to 80% of its Ultimate Stress with Optical Fiber Placed in Cut Laminate with a Layup 2, $[0/\pm45/90]_{2S}$, Configuration

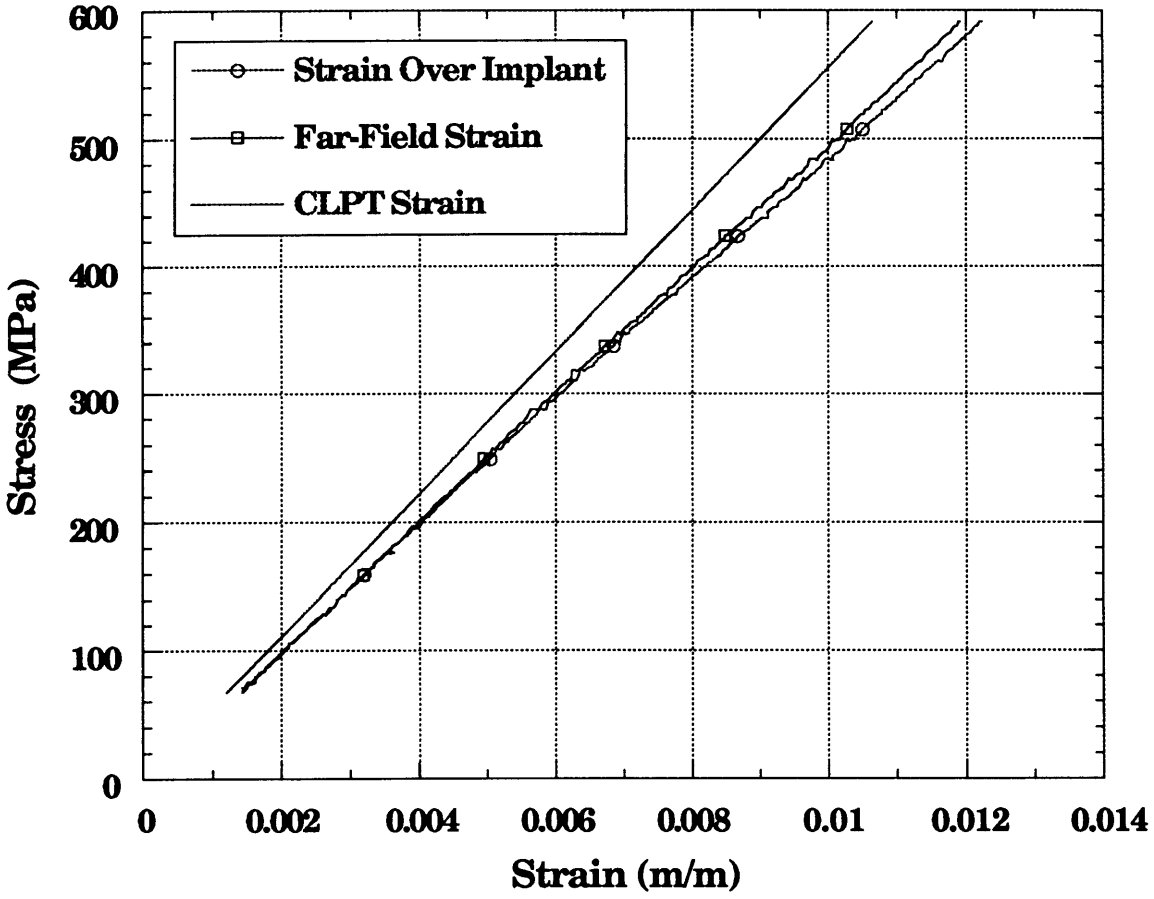

Strain data may have 1.25% error

Figure E.14 Stress-Strain Curves for Coupon 2PZA-B with a Layup 2, $[0/\pm45/90]_{2S}$, Configuration Tested to Failure

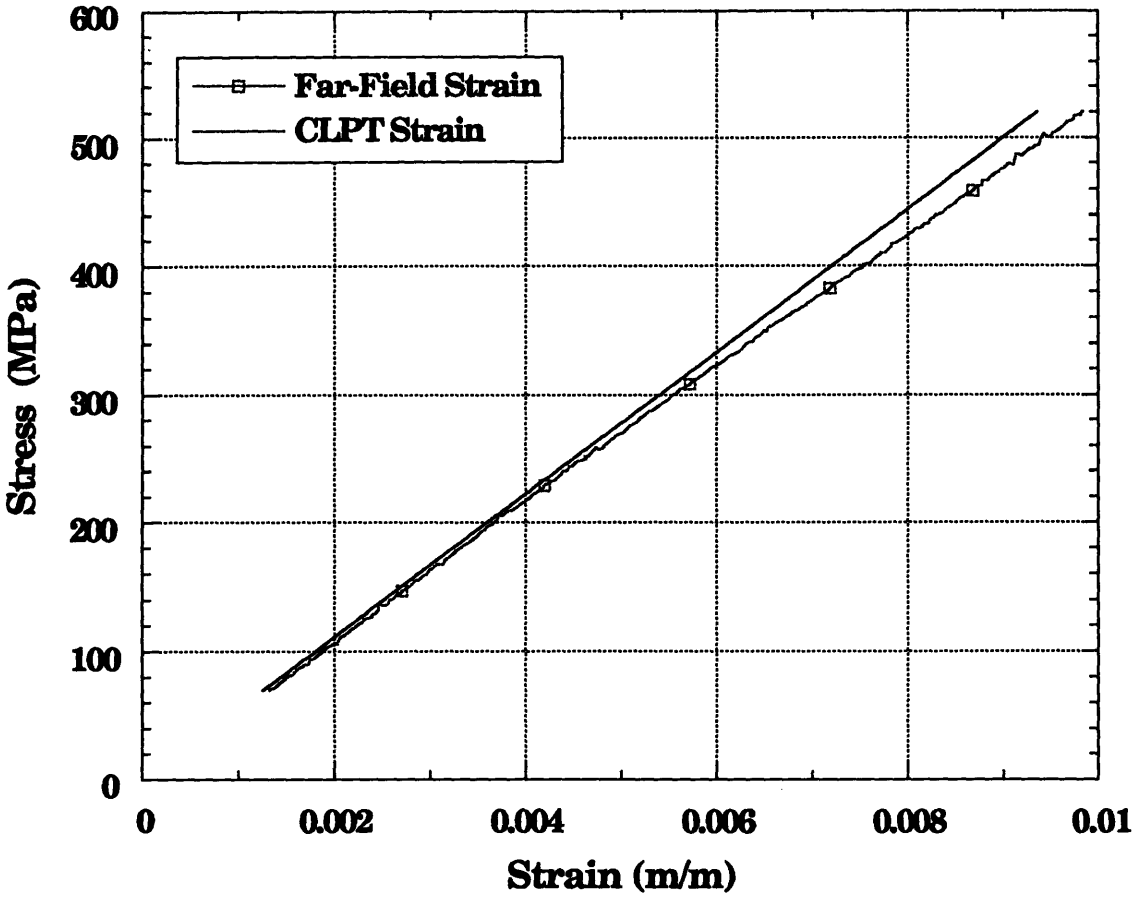

Strain data may have 1.25% error

Figure E.15 Stress-Strain Curves for Coupon 2PZA-C with a Layup 2, $[0/\pm45/90]_{2S}$, Configuration Tested to 90% of its Ultimate Stress

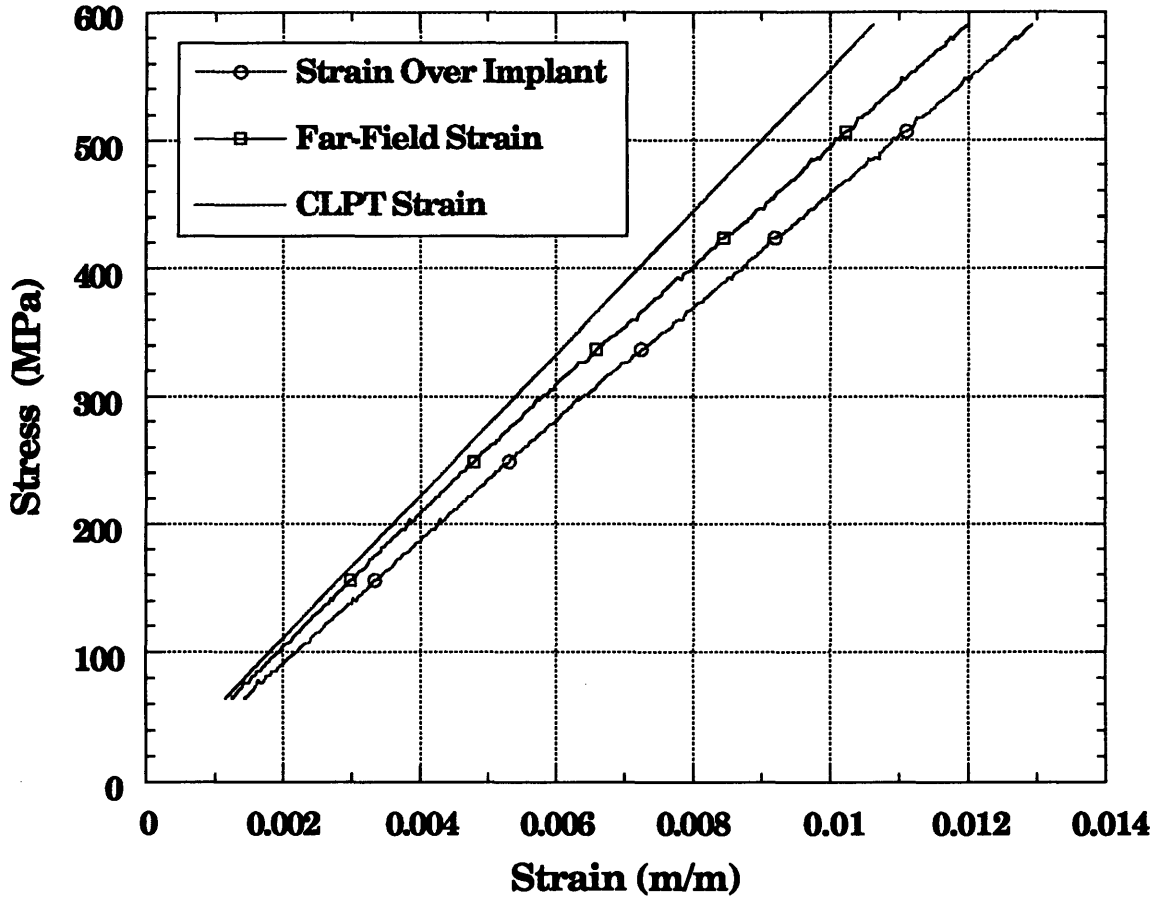

Strain data may have 1.25% error

Figure E.16 Stress-Strain Curves for Coupon 2PZA-D with a Layup 2, $[0/\pm45/90]_{2S}$, Configuration Tested to Failure

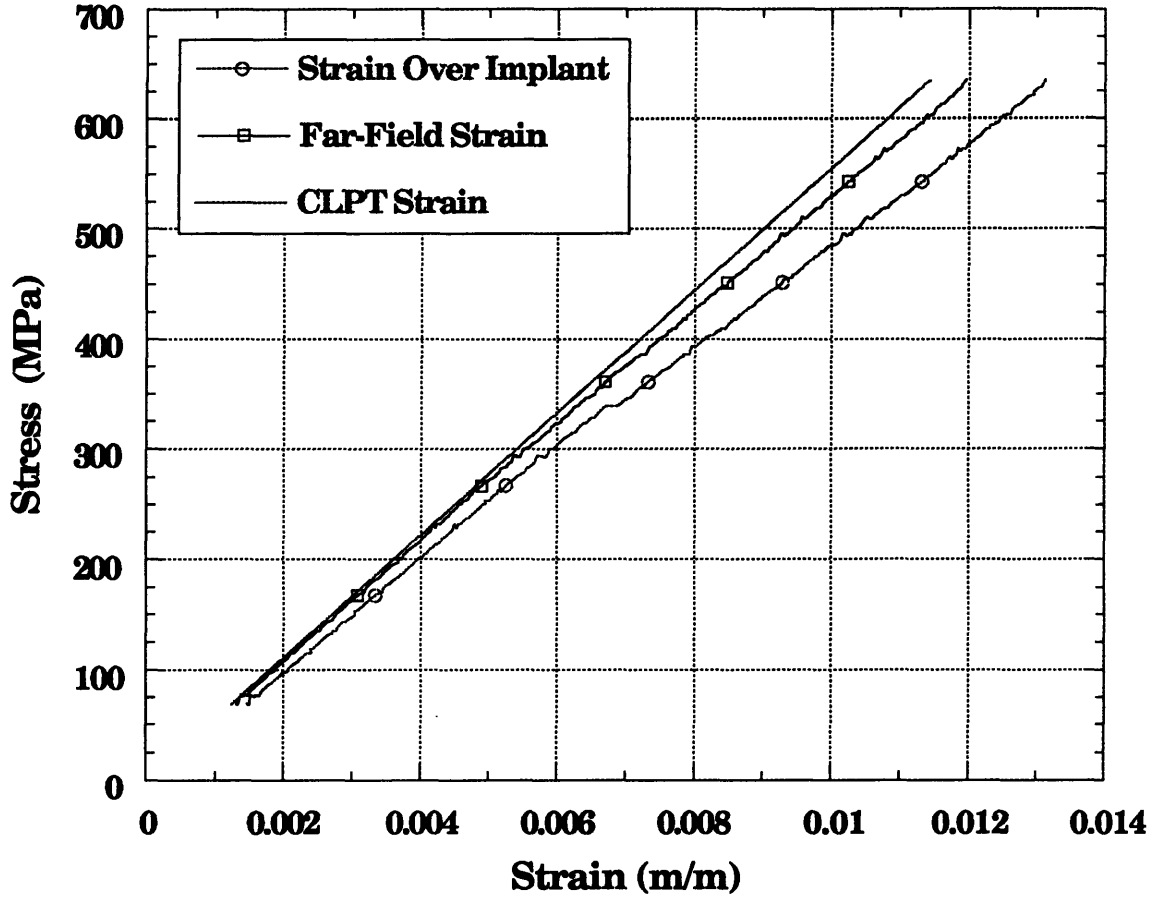

Strain data may have 1.25% error

Figure E.17 Stress-Strain Curves for Coupon 2TPZA-B with a Layup 2, $[0/\pm45/90]_{2S}$, Configuration Tested to Failure

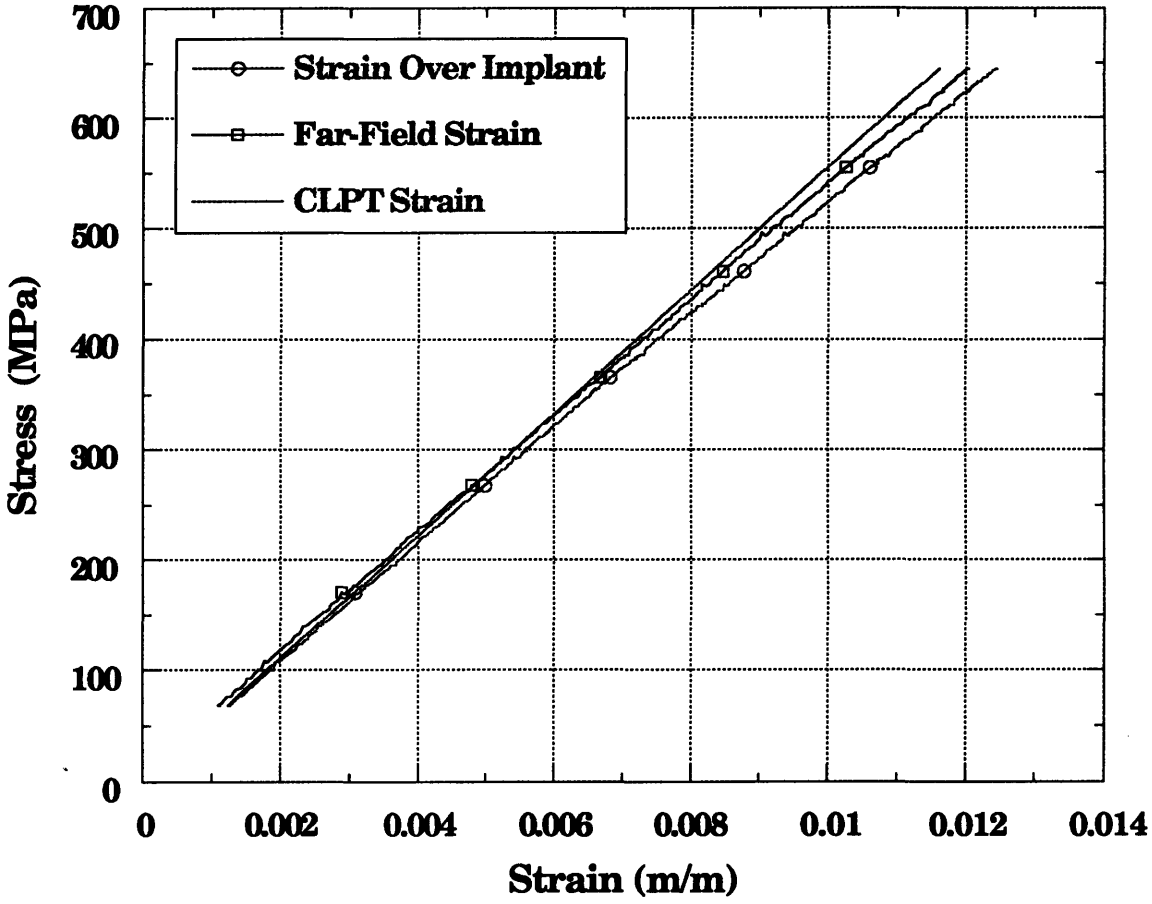

Strain data may have 1.25% error

Figure E.18 Stress-Strain Curves for Coupon 2TPZA-C with a Layup 2, $[0/\pm45/90]_{2S}$, Configuration Tested to Failure

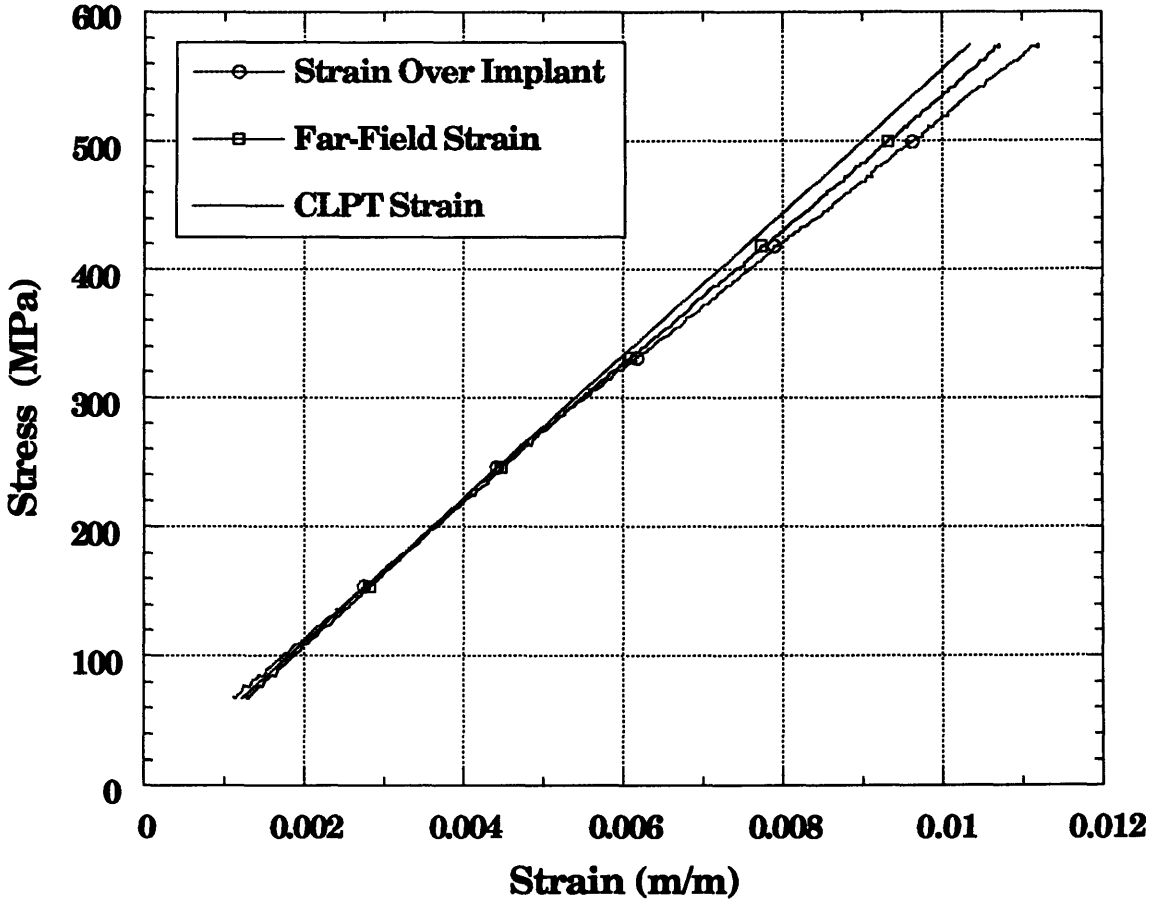

Figure E.19 Stress-Strain Curves for Coupon 2TPZA-D with a Layup 2, $[0/\pm45/90]_{2S}$, Configuration Tested to 90% of its Ultimate Stress

Appendix F

Stress-Strain Curves for Specimens with a Layup 3, $[45/0/-45/0/90/-45/0/-45/0/45]_s$, Configuration

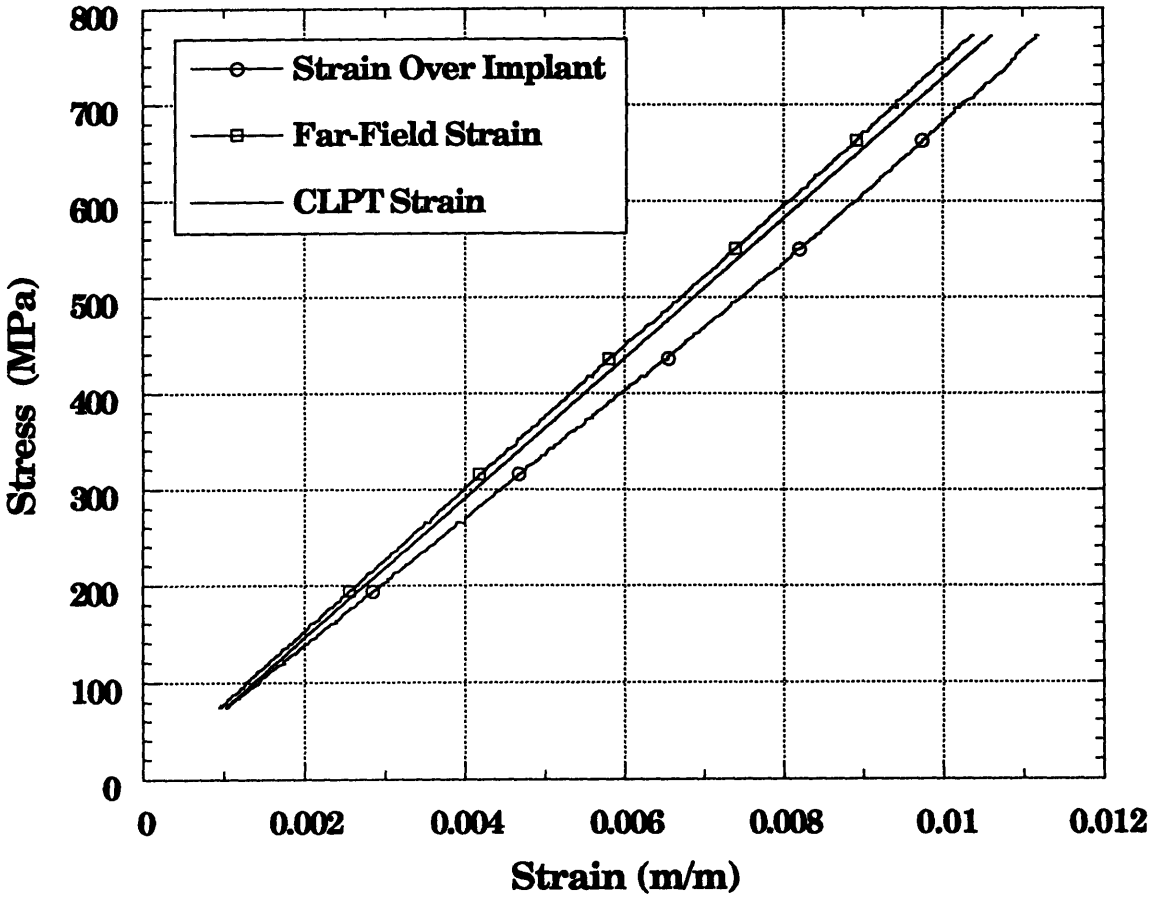

Figure F.1 Stress-Strain Curves for Coupon 3CHIP-B with a Layup 3, $[45/0/-45/0/90/-45/0/-45/0/45]_S$, Configuration Tested to Failure

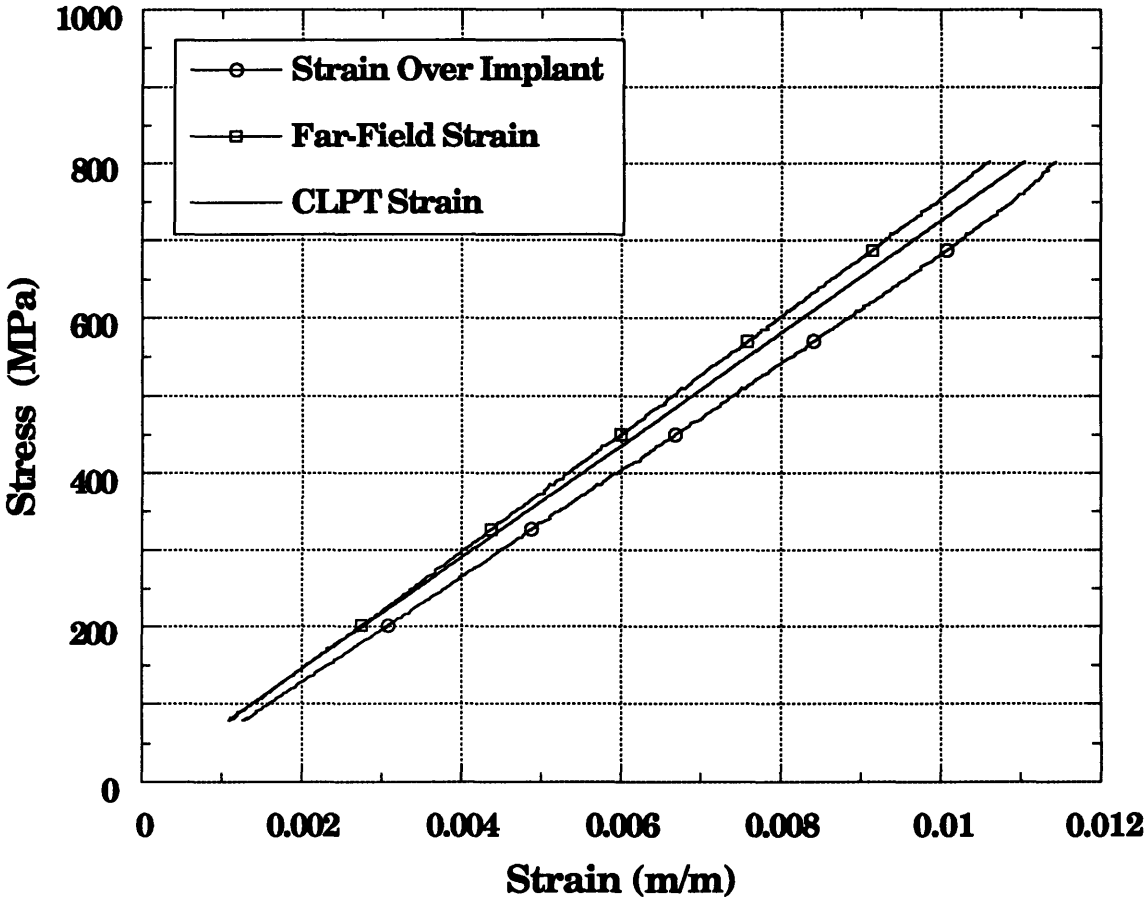

Figure F.2 Stress-Strain Curves for Coupon 3CHIP-C with a Layup 3, $[45/0/-45/0/90/-45/0/-45/0/45]_S$, Configuration Tested to Failure

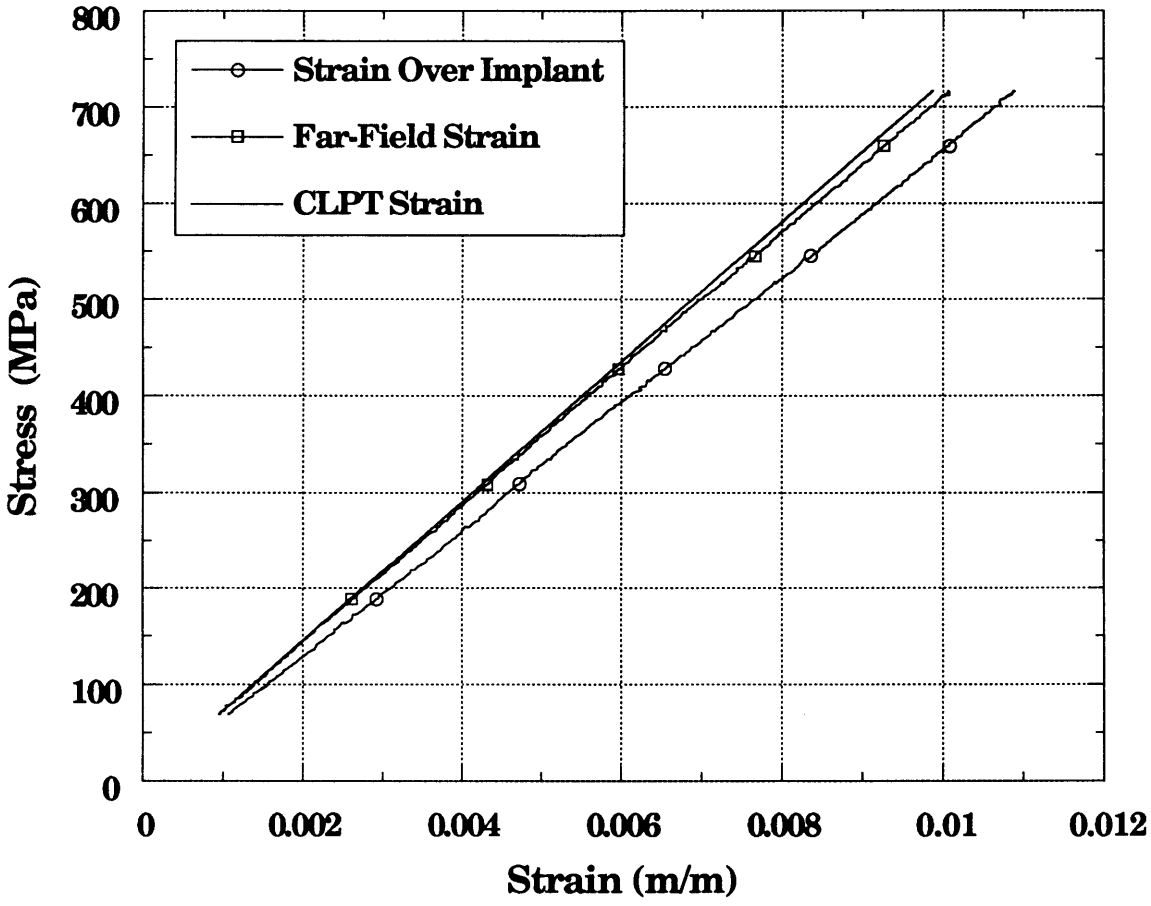

Figure F.3 Stress-Strain Curves for Coupon 3CHIP-D with a Layup 3, $[45/0/-45/0/90/-45/0/-45/0/45]_S$, Configuration Tested to 90% of its Ultimate Stress

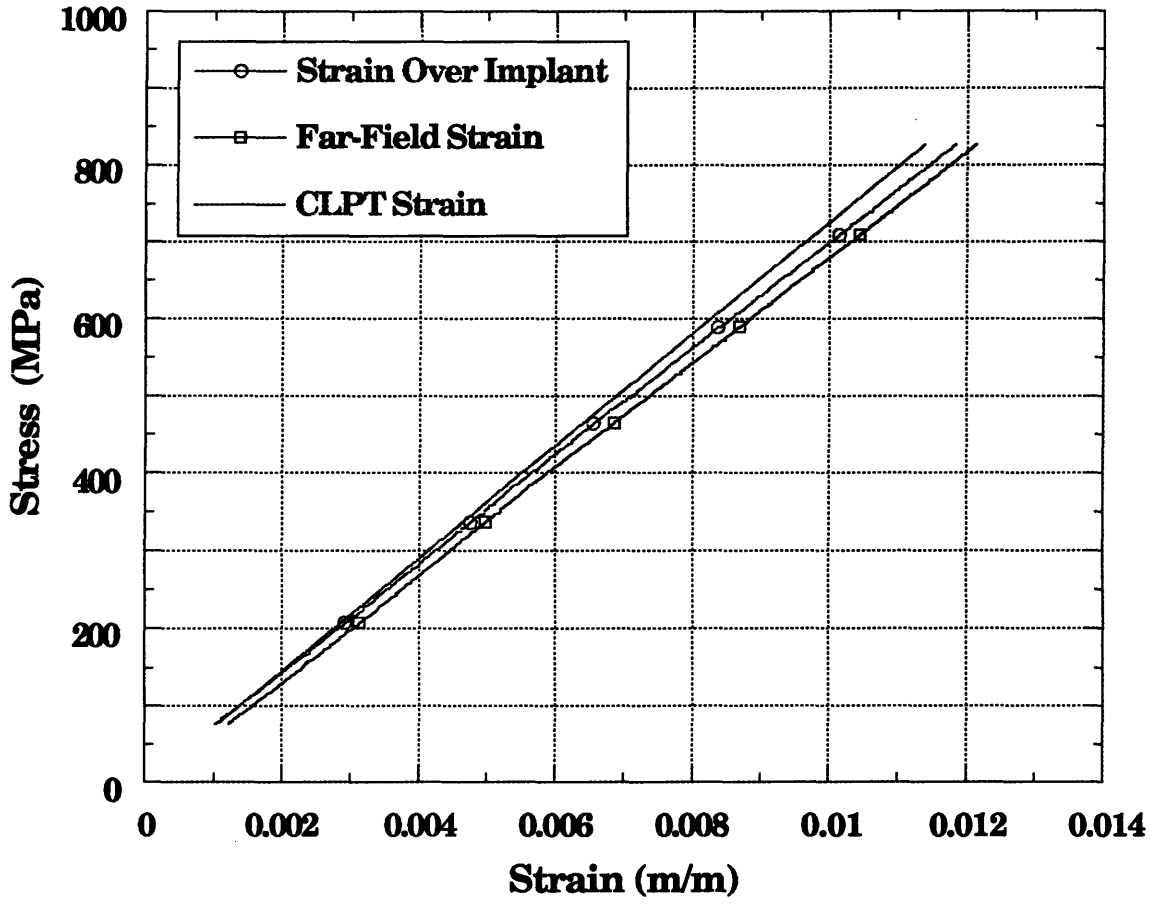

Figure F.4 Stress-Strain Curves for Coupon 3OF-B with a Layup 3, $[45/0/-45/0/90/-45/0/-45/0/45]_S$, Configuration Tested to Failure

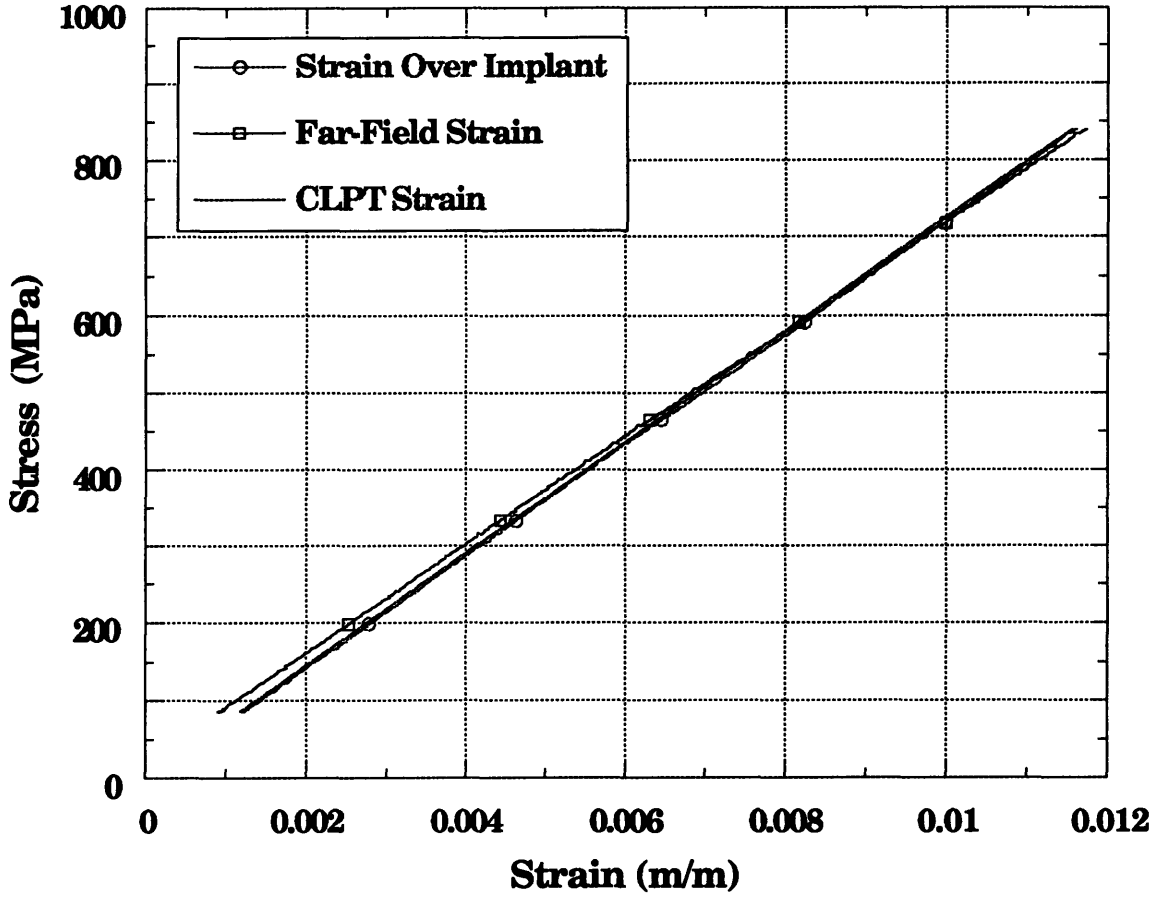

Figure F.5 Stress-Strain Curves for Coupon 3OF-C with a Layup 3, $[45/0/-45/0/90/-45/0/-45/0/45]_S$, Configuration Tested to Failure

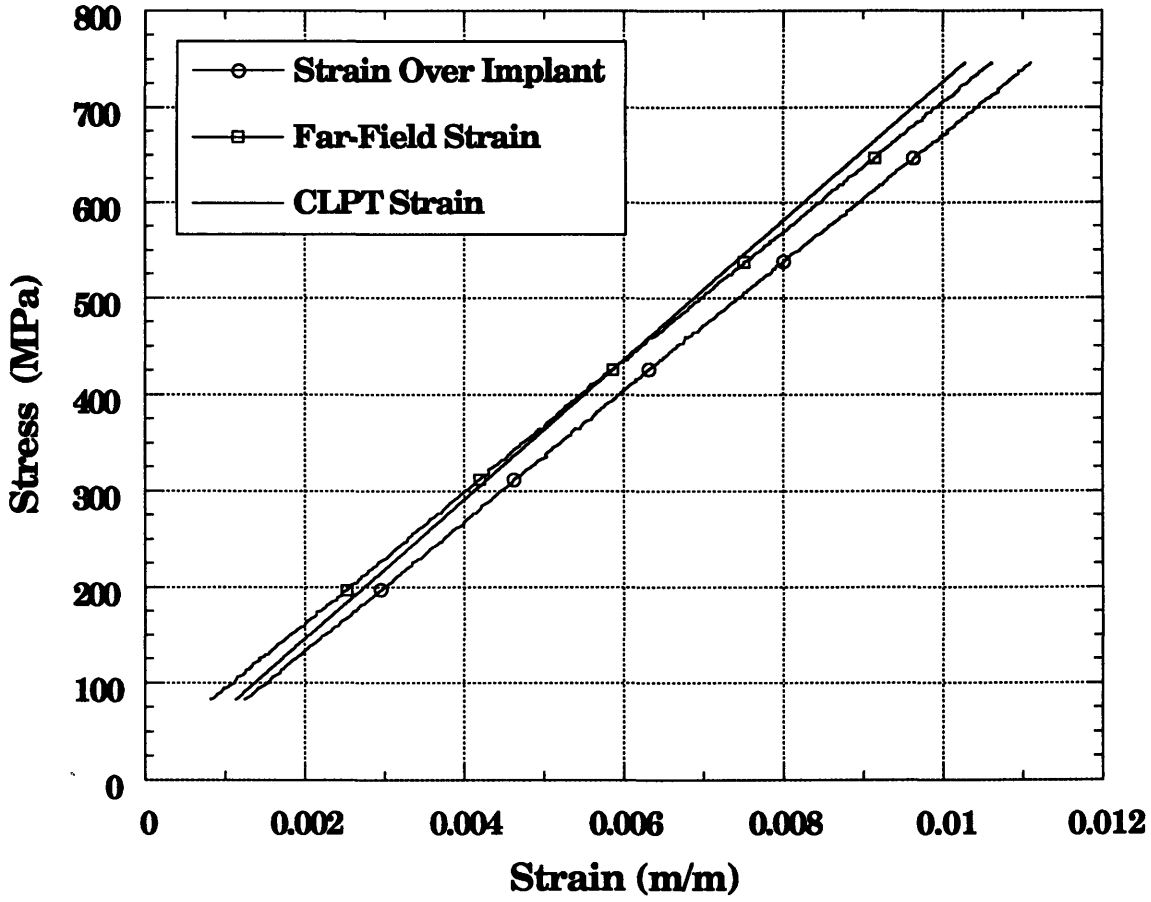

Figure F.6 Stress-Strain Curves for Coupon 3OF-D with a Layup 3, $[45/0/-45/0/90/-45/0/-45/0/45]_S$, Configuration Tested to 90% of its Ultimate Stress

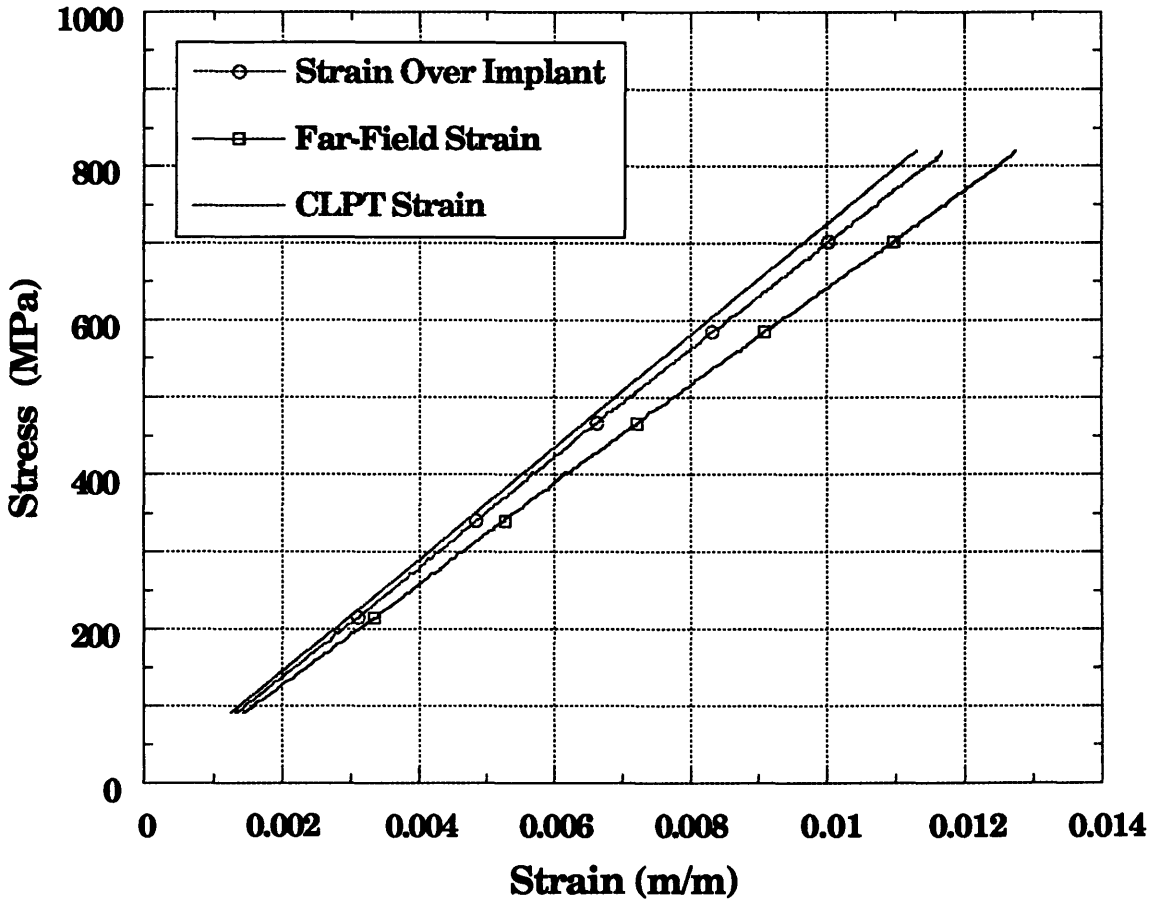

Figure F.7 Stress-Strain Curves for Coupon 3PZA-A with a Layup 3, $[45/0/-45/0/90/-45/0/-45/0/45]_S$, Configuration Tested to Failure

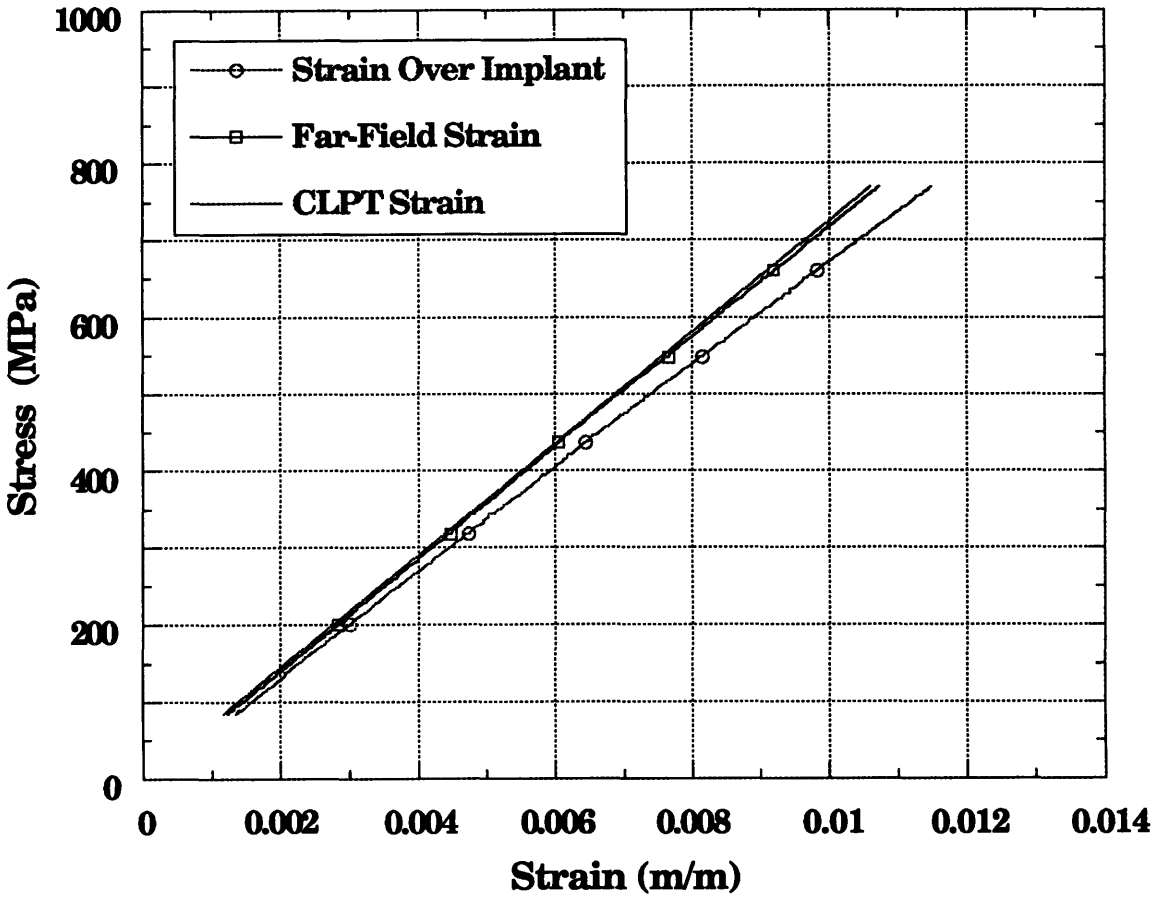

Figure F.8 Stress-Strain Curves for Coupon 3PZA-B with a Layup 3, $[45/0/-45/0/90/-45/0/-45/0/45]_S$, Configuration Tested to Failure

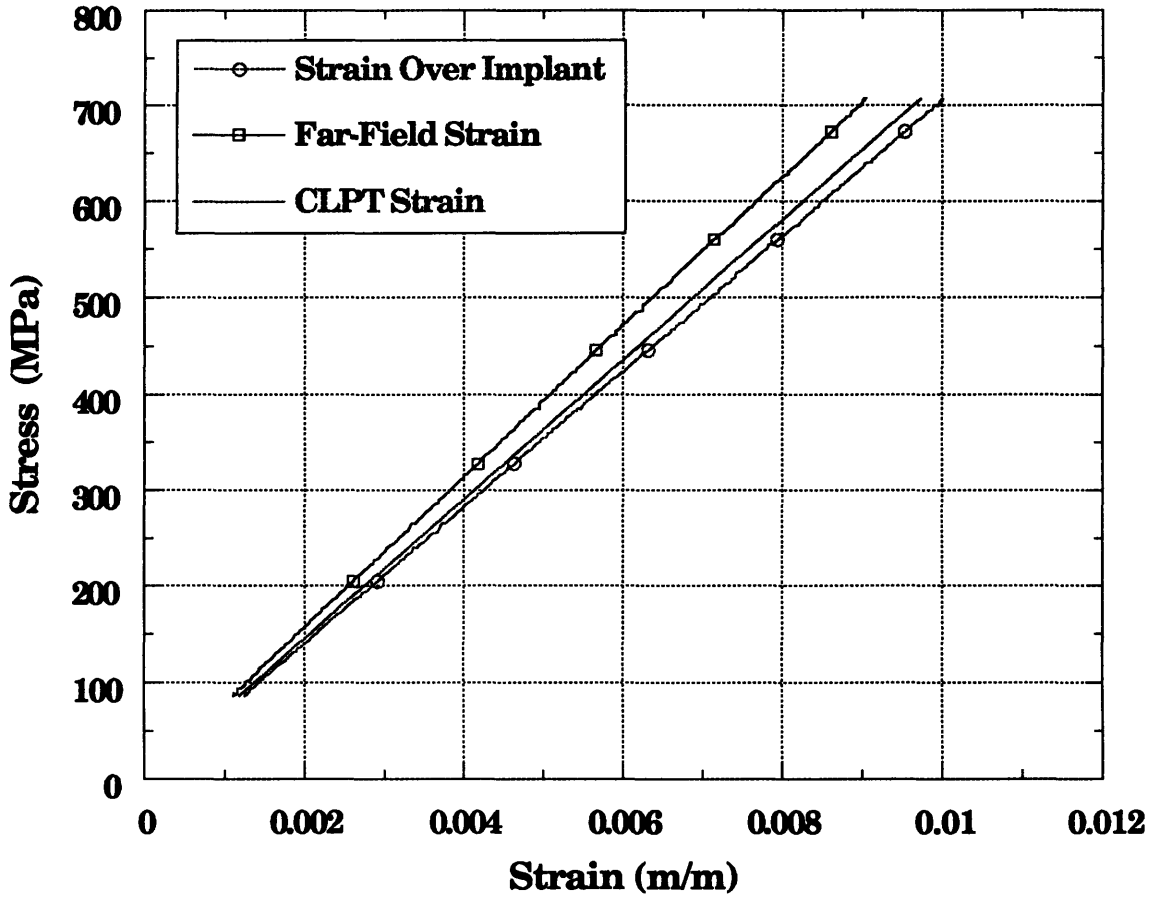

Figure F.9 Stress-Strain Curves for Coupon 3PZA-C with a Layup 3, $[45/0/-45/0/90/-45/0/-45/0/45]_S$, Configuration Tested to 90% of its Ultimate Stress

Appendix G

Stress-Strain Curves for Specimens with a Layup 4, $[\pm 45]_{4s}$, Configuration

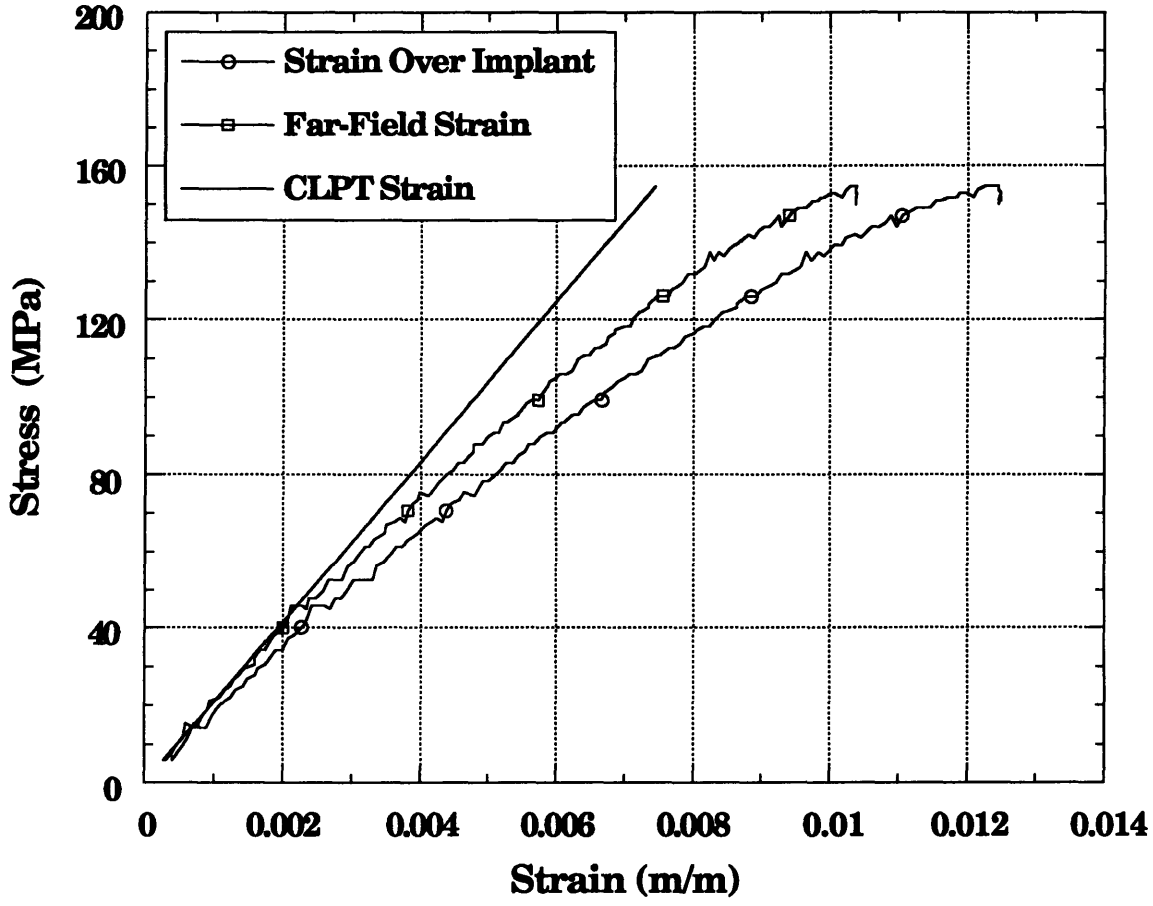

Figure G.1 Stress-Strain Curves for Coupon 4CHIP-C with a Layup 4, $[\pm 45]_{4S}$, Configuration Tested to 100% of its Peak Stress

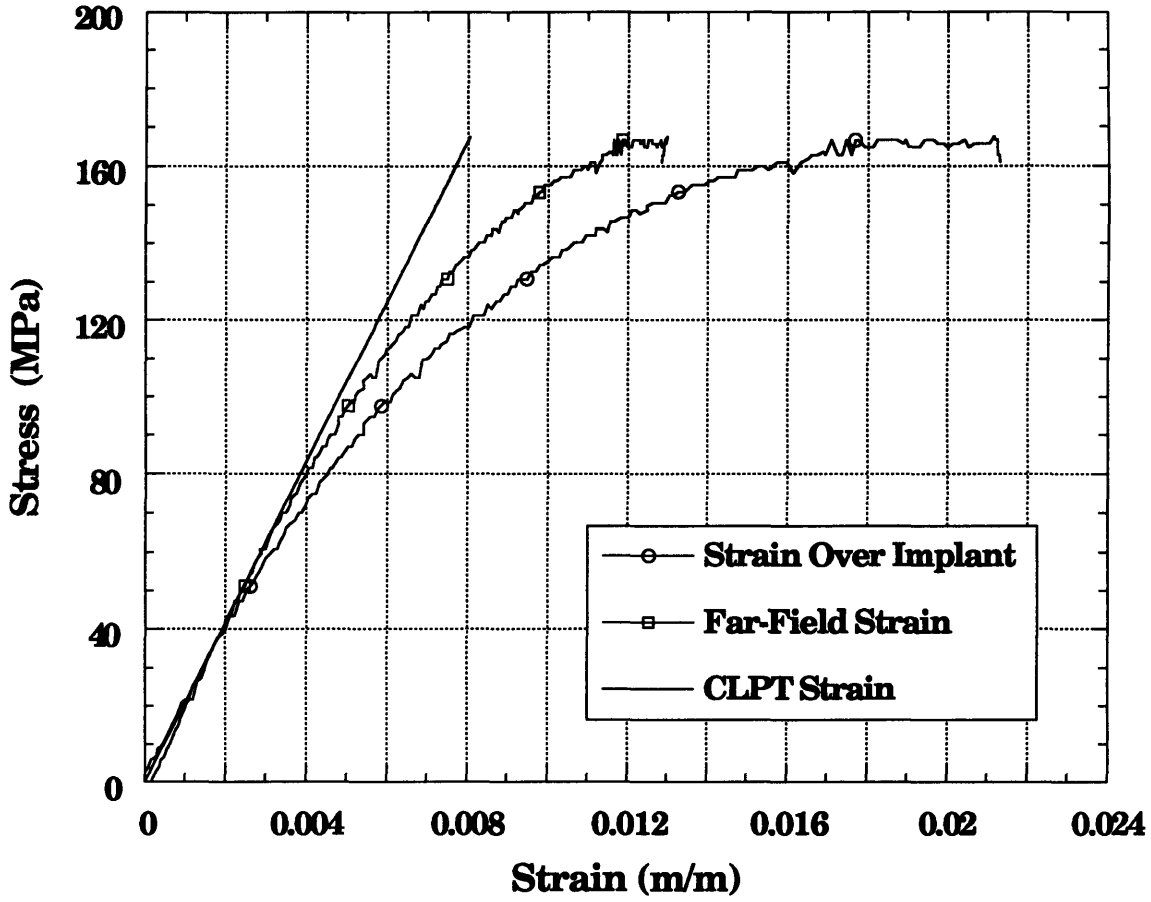

Figure G.2 Stress-Strain Curves for Coupon 4CHIP-D with a Layup 4, $[\pm 45]_{4S}$, Configuration Tested to 100% of its Peak Stress

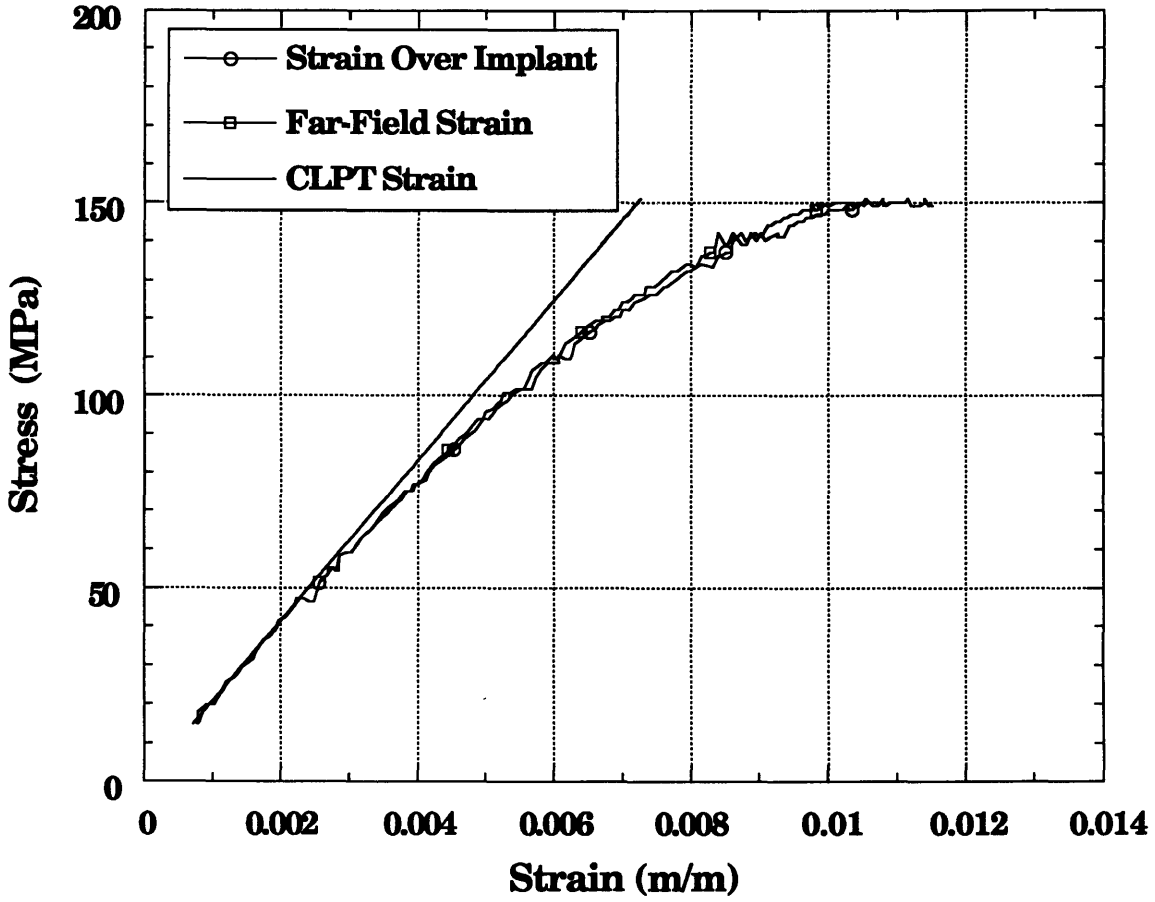

Figure G.3 Stress-Strain Curves for Coupon 4OF-A with a Layup 4, $[\pm 45]_{4S}$, Configuration Tested to 100% of its Peak Stress

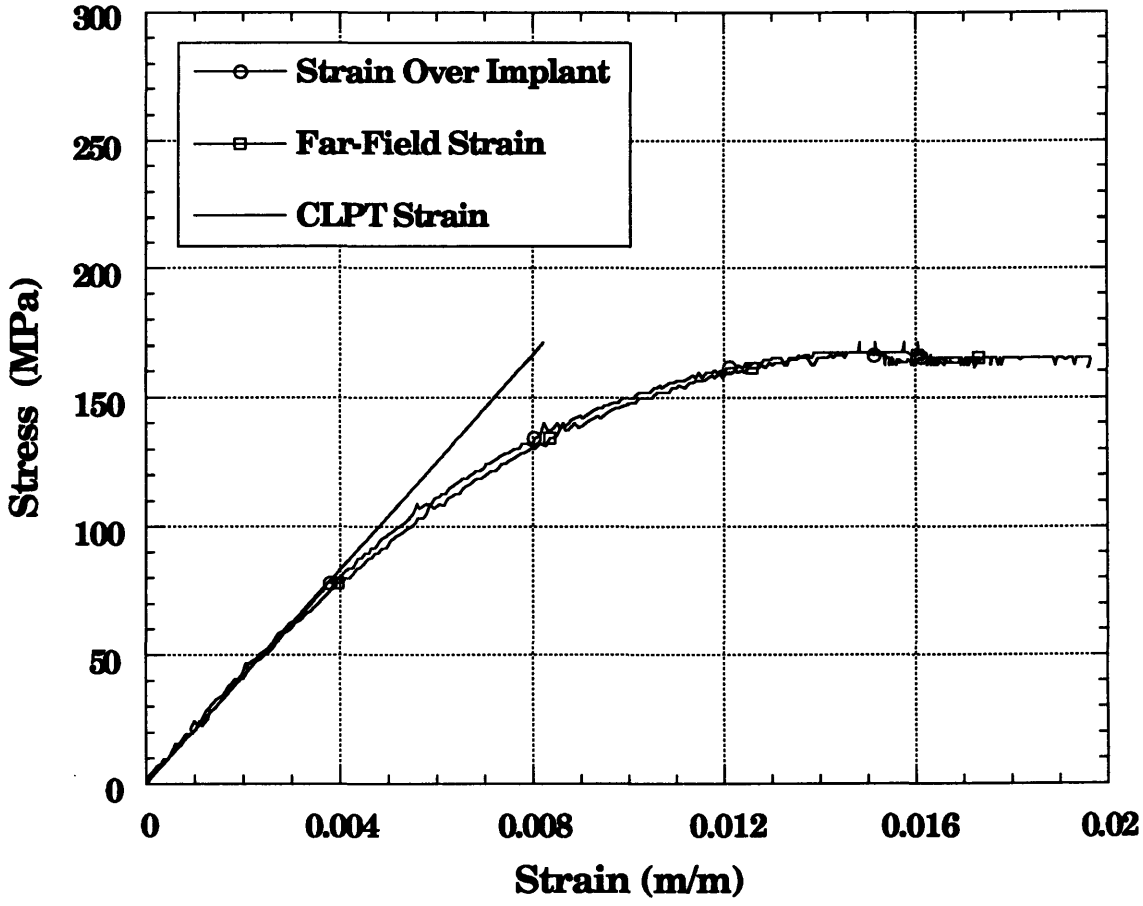

Figure G.4 Stress-Strain Curves for Coupon 4OF-B with a Layup 4, $[\pm 45]_{4S}$, Configuration Tested to 100% of its Peak Stress

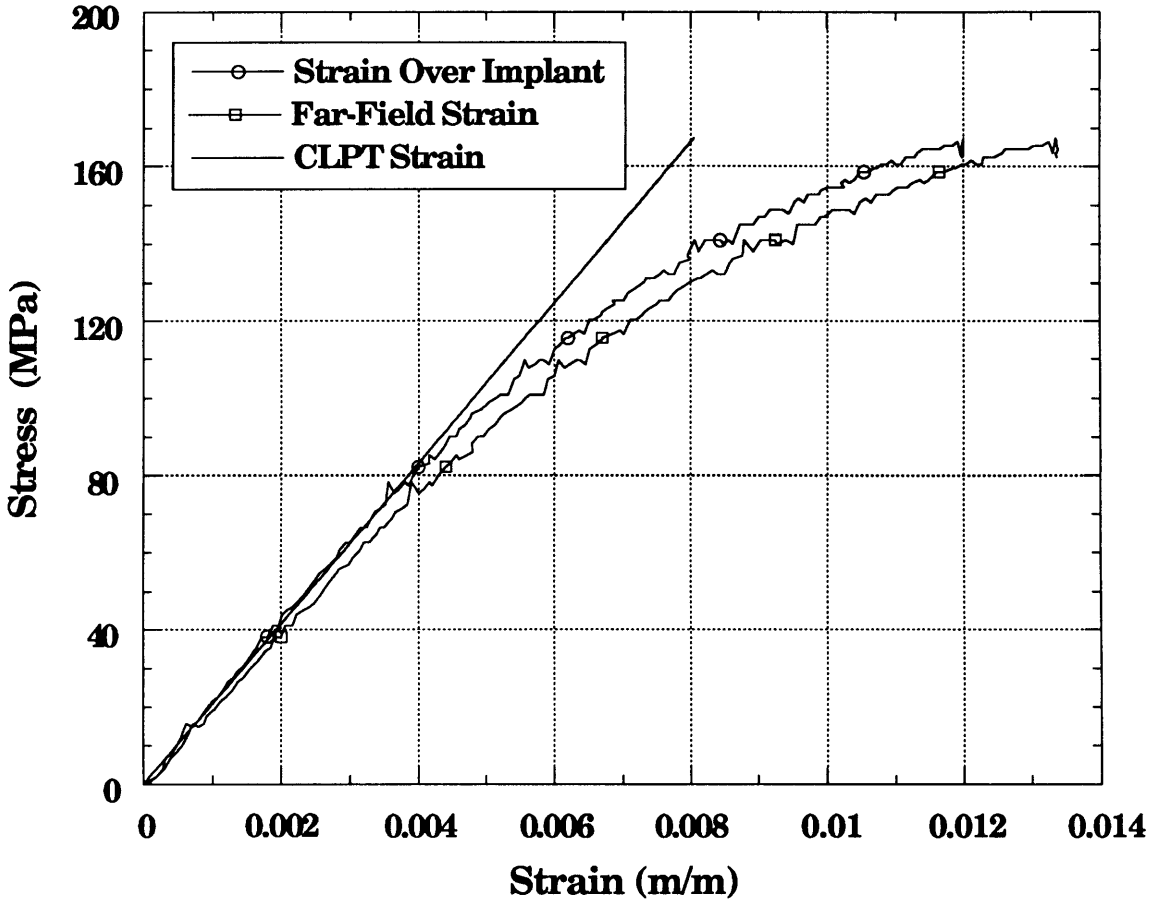

Figure G.5 Stress-Strain Curves for Coupon 4OF-C with a Layup 4, $[\pm 45]_{4S}$, Configuration Tested to 100% of its Peak Stress

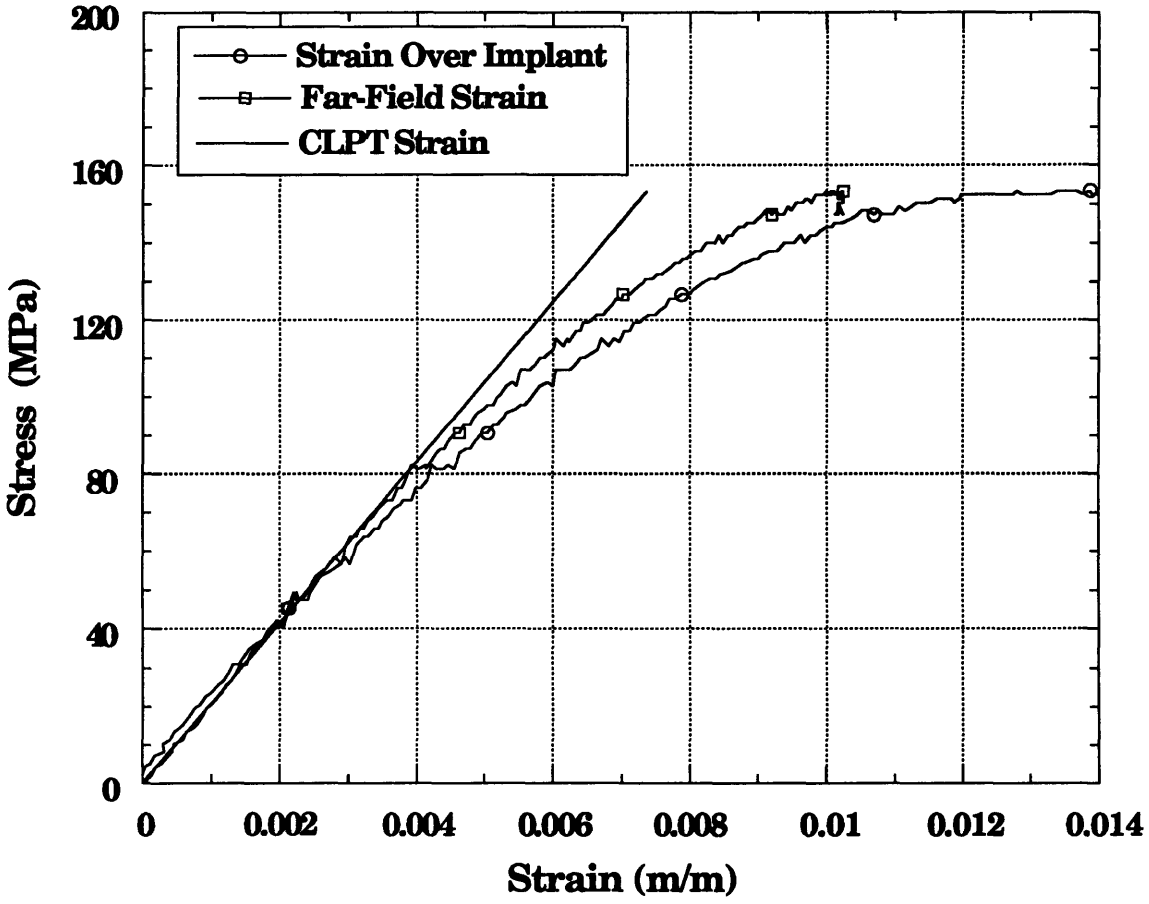

Figure G.6 Stress-Strain Curves for Coupon 4PZA-A with a Layup 4, $[\pm 45]_{4S}$, Configuration Tested to 100% of its Peak Stress

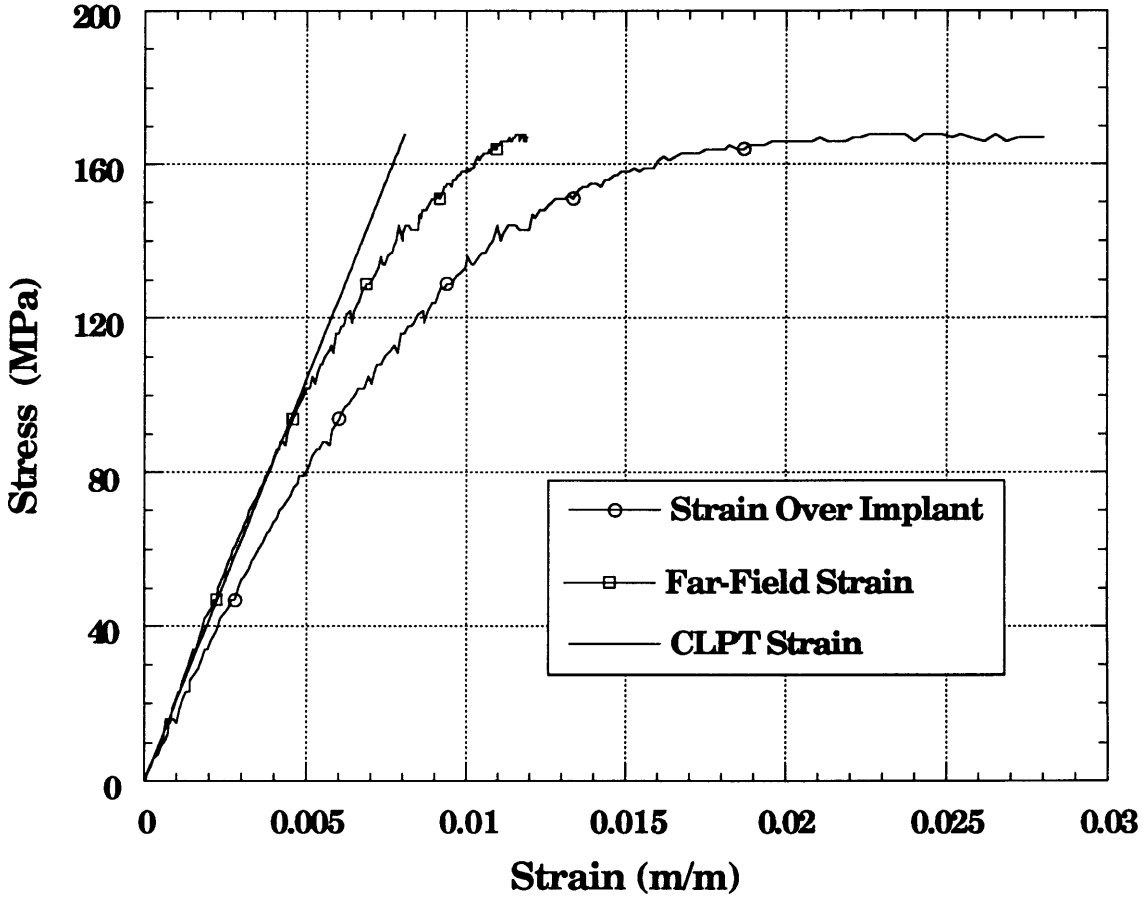

Figure G.7 Stress-Strain Curves for Coupon 4PZA-B with a Layup 4, $[\pm 45]_{4S}$, Configuration Tested to 100% of its Peak Stress

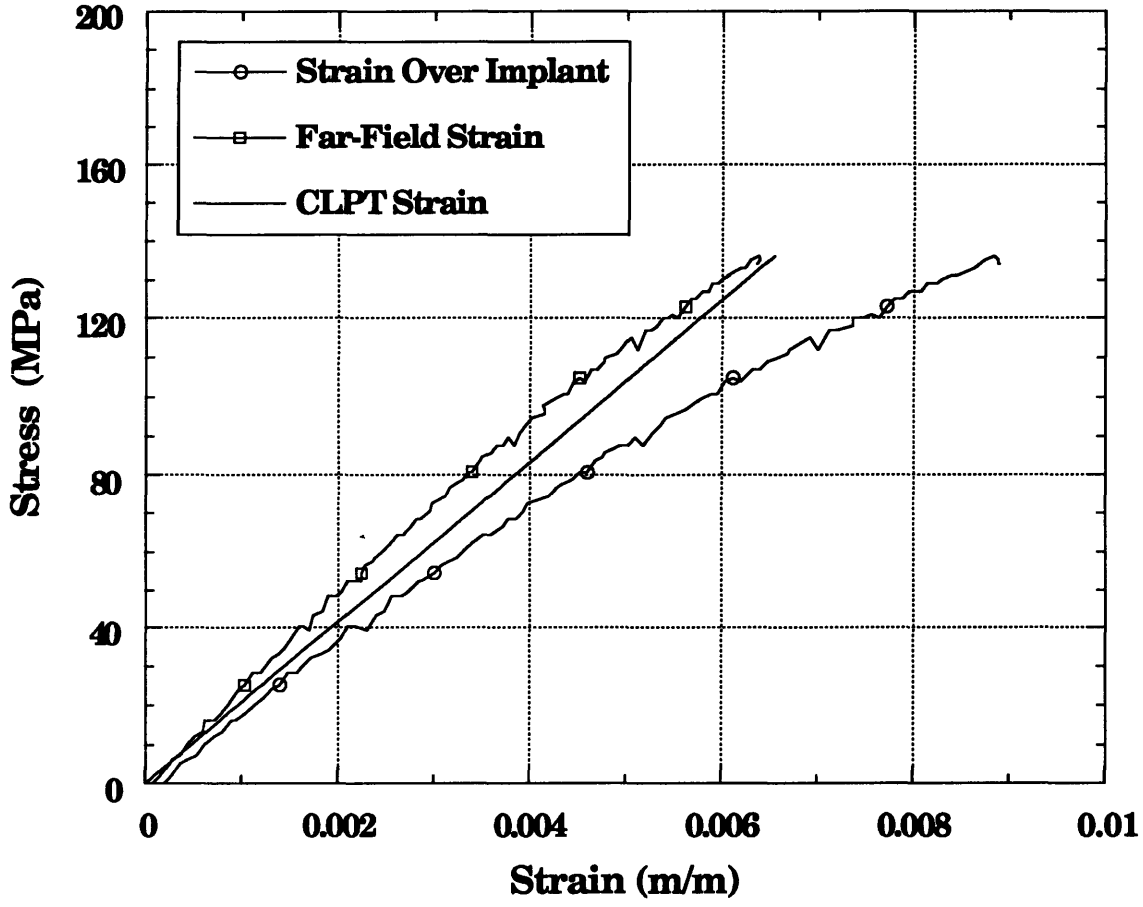

Figure G.8 Stress-Strain Curves for Coupon 4PZA-C with a Layup 4, $[\pm 45]_{4S}$, Configuration Tested to 100% of its Peak Stress